# T-cell responses to influenza virus in pigs

**Katie Tungatt**

School of Medicine

Cardiff University

July 2017

**A thesis submitted to Cardiff University in candidature for the Degree of Doctor of Philosophy.**

**DECLARATION**

This work has not been submitted in substance for any other degree or award at this or any other university or place of learning, nor is being submitted concurrently in candidature for any degree or other award.

Signed …………………………………… (candidate)    Date ………………….………….…………

**STATEMENT 1**

This thesis is being submitted in partial fulfillment of the requirements for the degree of PhD

Signed…………………………………… (candidate)    Date …………………………….…………

**STATEMENT 2**

This thesis is the result of my own independent work/investigation, except where otherwise stated, and the thesis has not been edited by a third party beyond what is permitted by Cardiff University's Policy on the Use of Third Party Editors by Research Degree Students. Other sources are acknowledged by explicit references.  The views expressed are my own.

Signed …………………………………… (candidate)       Date ………………….…………………

**STATEMENT 3**

I hereby give consent for my thesis, if accepted, to be available online in the University's Open Access repository and for inter-library loan, and for the title and summary to be made available to outside organisations.

Signed…………………………………… (candidate)       Date …………………………….…………

**STATEMENT 4: PREVIOUSLY APPROVED BAR ON ACCESS**

I hereby give consent for my thesis, if accepted, to be available online in the University's Open Access repository and for inter-library loans **after expiry of a bar on access previously approved by the Academic Standards & Quality Committee.**

Signed…………………………………… (candidate)       Date ………………………………….………

## Acknowledgments

# Thesis Summary

The tools and techniques for the study of porcine T-cells lag behind what is currently attainable in human T-cells, so this thesis was initially focused on improvements in this field. This study established long-term culture of porcine T-cells, T-cell clone procurement and relevant T-cell assays. These techniques were then used to investigate cytotoxic T-cell responses to Influenza A virus (IAV) in pigs. IAV is highly mutative and novel strains can be generated following reassortment between different viral strains. IAV is endemic in the global pig population and in some circumstances the virus can pass between humans and pigs and other animals. Pigs can therefore, potentially be a source for the generation of new and possibly pandemic influenza strains. The risk this poses to global human health, together with the negative effects of IAV infection within pig herds, highlights the need to improve our knowledge of IAV in pigs.

This study identified four new MHC class I restricted IAV epitopes, derived from the viral nucleoprotein. Cytotoxic T-cells recognising these IAV epitopes were detected at high numbers *ex vivo* in samples from vaccinated pigs. The structures of these IAV epitopes in complex with their respective MHC class I molecules were resolved and revealed the primary anchor positions within the peptides. This enabled peptide binding motifs to be defined for two porcine MHC-I alleles. These peptide binding motifs can be utilised for efficient epitope prediction. This study also identified super-agonist ligands for two of the MHC-I restricted IAV epitopes.

Overall, this work has opened up the study of porcine T-cells to a level previously unattainable and has contributed to our knowledge of IAV in pigs. It has paved the way for further experiments investigating IAV in pigs, other porcine diseases and for using pigs as an animal model for human disease.

## Published work incorporated in this thesis

**Tungatt K**, Bianchi V, Crowther MD, Powell WE, Schauenburg AJ, Trimby A, Donia M, Miles JJ, Holland CJ, Cole DK, Godkin AJ, Peakman M, Straten PT, Svane IM, Sewell AK and Dolton G **(2015).** Antibody stabilization of peptide-MHC multimers reveals functional T cells bearing extremely low-affinity TCRs. *J Immunol.*, 194(1), 463-74.

Dolton G*, **Tungatt K***, Lloyd A, Bianchi V, Theaker SM, Trimby A, Holland CJ, Donia M, Godkin AJ, Cole DK, Straten PT, Peakman M, Svane IM and Sewell AK **(2015).** More tricks with tetramers: a practical guide to staining T cells with peptide-MHC multimers. *Immunology*, 146(10), 11-22. Review article. *These authors contributed equally.*

## Other papers published during my PhD

Dolton G, Lissina A, Skowera A, Ladell K, **Tungatt K**, Jones E, Kronenberg-Versteeg D, Akpovwa H, Pentier JM, Holland CJ, Godkin AJ, Cole DK, Neller MA, Miles JJ, Price DA, Peakman M and Sewell AK **(2014)**. Comparison of peptide-major histocompatibility complex tetramers and dextramers for the identification of antigen-specific T cells. *Clin Exp Immunol.*, 177(1), 47-63.

Pageon SV, Tabarin T, Yamamoto Y, Ma Y, Nicovich PR, Bridgeman JS, Cohnen A, Benzing C, Gao Y, Crowther MD, **Tungatt K**, Dolton G, Sewell AK, Price DA, Acuto O, Parton RG, Gooding JJ, Rossy J, Rossjohn J and Gaus K **(2016)**. Functional role of T-cell receptor nanoclusters in signal initiation and antigen discrimination.  Proc Natl Acad Sci USA, 113(37).

## Abbreviations

| | |
|---|---|
| Aa | Amino acid |
| AF647 | Alexa Fluor 647 |
| APC | Antigen presenting cell |
| APCy | Allophycocyanin |
| $\beta_2 m$ | B-2-microglobulin |
| BAL | Bronchoalveolar lavage |
| BSA | Bovine serum albumin |
| C | Celsius |
| CD (number) | Cluster of differentiation (number) |
| cDNA | Complementary deoxyribonucleic acid |
| CDR | Complementarity-determining regions |
| CFSE | Carboxyfluorescein succinimidyl ester |
| CTLs | Cytotoxic T lymphocytes |
| D | Diversity TCR gene fragment |
| DMSO | Dimethyl sulfoxide |
| DTT | Dithiothreitol |
| *E.coli* | *Escherichia coli* |
| EDTA | Ethylenediaminetetraacetic acid |
| ELISA | Enyzme Linked ImmunoSorbent Assay |
| ELISpot | Enzyme Linked ImmunoSpot |
| E:T | Effector to target ratio |
| FACS | Fluorescence activated cell sorting |
| FBS | Foetal bovine serum |
| FMO | Fluorescence minus one |
| FITC | Fluorescein isothiocyanate |
| FPLC | Fast Protein Liquid Chromatography |
| g | Gram |
| h | hour |
| HA | Haemagglutinin |
| HAI | Haemagglutination inhibition |
| HLA | Human leukocyte antigen |
| HLA-A2 | HLA A*0201 |
| HRP | Horse radish peroxidase |
| IFNγ | Interferon-γ |
| Ig | Immunoglobulin |
| IAV | Influenza A virus |
| IL | Interleukin |
| IU | International Unit |
| IPTG | Isopropyl β-D-thio-galactoside |
| J | Joining TCR gene fragment |
| kDa | Kilodalton |

| | |
|---|---|
| L | Litre |
| LB | Luria-Bertani |
| LN | Lymph Node |
| m | milli |
| M | molar |
| M1 | Matrix 1 protein |
| M2 | Matrix 2 protein |
| MACS™ | Magnetic-activated cell sorting |
| MFI | Mean fluorescence intensity |
| mg | Milligram |
| MHCI | Major histocompatibility complex class I |
| MHCII | Major histocompatibility complex class II |
| min | minute |
| NA | Neuraminidase |
| NEP | Nuclear export protein |
| ng | Nanogram |
| N-terminus | Amino-terminus |
| NP | nucleoprotein |
| NS1 | Non-structural protein 1 |
| OD | Optical density |
| PA | Polymerase acidic protein |
| PB | Pacific blue fluorochrome |
| PB1 | Polymerase basic protein 1 |
| PB2 | Polymerase basic protein 2 |
| PBG | Peptide binding groove |
| PBMC | Peripheral blood mononuclear cells |
| PBS | Phosphate buffered saline |
| PCR | Polymerase chain reaction |
| PDB | Protein data bank |
| PE | Phycoerythrin |
| PHA | Phytohaemagglutinin |
| PKI | Protein kinase inhibitor (dasatinib) |
| pMHC | peptide- major histocompatibility complex |
| PR8 | [A/PuertoRico/8/1934(H1N1)] IAV |
| pTα | pre-T-cell α chain |
| RACE | Rapid Amplification of cDNA Ends |
| RAG | Recombination activation genes |
| RBC | Red blood cell |
| rpm | Revolutions per minute |
| RPMI | Roswell Park Memorial Institute medium |
| RNA | Ribonucleic acid |
| RNP | Ribonucleoprotein complex |

| | |
|---|---|
| RT | Room temperature |
| RU | Response units |
| SAP | Shrimp Alkaline Phosphatase |
| SDS-PAGE | Sodium dodecyl sulphate – polyacrylamide gel electrophoresis |
| sec | seconds |
| *SMART*<sup>TM</sup> | Switching Mechanism At the 5' end of RNA Template |
| SLA | Swine Leukocyte Antigen |
| SP | Single positive thymocyte (CD4$^+$ or CD8$^+$) |
| Sp/Sw | H1N1 virus [A/Swine/Spain/SF11131/2007] |
| SwIV | Swine Influenza virus |
| TAP | Transporter associated with antigen presentation |
| TBLN | Tracheobronchial lymph nodes |
| TCID | Tissue Culture Infective Dose |
| TCR | T-cell receptor |
| TNFα | Tumour necrosis factor α |
| TRAJ | T-cell receptor α joining gene |
| TRAV | T-cell receptor α variable gene |
| TRBD | T-cell receptor β diversity gene |
| TRBJ | T-cell receptor β joining gene |
| TRBV | T-cell receptor β variable gene |
| vdW | Van der Waals |
| μ | Micro |
| V | Variable TCR gene fragment |
| V | Volts |
| x g | G force or relative centrifugal force |

# Contents

# Figures

# Tables

# 1 <u>Introduction</u>

## 1.1 Overview of the immune system

The immune system is a complex network of organs, cells and molecular processes that are responsible for protecting us against pathogens. The immune response is broadly divided into two arms, the innate and the adaptive immune responses. The former is the 'front-line' defence rapidly able to broadly combat pathogens and also contributes to the induction of the latter. The adaptive response involves a specific response directed to a particular pathogen usually resulting in the formation of immunological memory which can protect against re-infection. Innate immunity comprises many components including anatomical barriers to pathogens, i.e. skin and mucosal epithelia and innate immune cells which can recognise common features of pathogens, via pattern recognition receptors, initiating their destruction and the recruitment of further innate cells and responses. The complement system is a network of proteins that also plays an important role in innate immunity as it can opsonise pathogens, lyse cells and increase local immune responses. There are three complement pathways (alternative, lectin and classical) which are activated differently but all involve a sequential cascade of enzymatic reactions converging in the formation of the membrane attack complex enabling cell lysis (Sarma and Ward 2011). It is, however, important to note that innate and adaptive immunity are not mutually exclusive, as the divide between what constitutes each has become less defined as further cell subsets and responses have been discovered  (Lanier 2013). This study is focused on the adaptive immune response so innate immunity will not be discussed further here.

## 1.2 Adaptive immune system

The adaptive immune response is the 'second-line' of defence which can initially take days rather than hours to develop in the absence of existing immunological memory. It is orchestrated by two lymphocyte subsets, B-cells and T-cells, which recognise antigens, substances capable of inducing an immune response, by highly variable receptors on their cell surface. Upon successful antigen recognition, lymphocytes become activated from naïve to effector lymphocytes (Murphy & Weaver 2016).  B cells and T-cells represent two distinct lineages, first defined in 1965 following initial studies in the chicken; the former develop in the bone marrow and produce antibodies providing the humoral response and the latter develop in the thymus providing the cell mediated response (Cooper et al. 1965). B cells express a large repertoire of clonally diverse B cell receptors (BCR), a membrane bound antibody, generated by

Immunoglobulin (Ig) gene segment rearrangement. Upon recognition of their antigen in the secondary lymphoid tissue, B cells mature into long-lived antibody-producing plasma cells and memory B cells (Lebien and Tedder 2008). This study focused on T-cell responses and discussion will be limited to this lymphocyte subset herein.

## 1.3 T-cells

T-cells are broadly classified into two groups, αβ and γδ T-cells, based on the chain composition of the heterodimeric T-cell receptors (TCR) they express on their cell surface. Each individual T-cell will only express one clonal TCR, termed their clonotype, which can recognise antigens to initiate an immune response. Unlike BCRs, TCRs are only found in a membrane-bound form however both have similar features and modes of gene segment rearrangement. αβ T-cells are referred to as conventional T-cells and usually recognise antigen in the form of peptides presented by classical major histocompatibility (MHC) molecules. αβ T-cells comprise two major subsets, CD8+ (cytotoxic) and CD4+ (helper) T-cells, based on their co-receptor expression and their immune roles. CD8+ T-cells have cytotoxic capabilities and are able to kill infected cells via recognition of endogenous peptides in the context of MHC class I (MHC-I). In contrast CD4+ T-cells generally recognise peptides from exogenous antigens presented in the context of MHC class II (MHC-II). Conventional, CD4+ T-cells act to 'help' and regulate immune responses and are often viewed as the master orchestrators of immune responses. Less is known about γδ T-cells. γδ T-cells are classified as unconventional T-cells as they are not restricted by classical MHC molecules and are known to recognise antigens in different forms, including lipids and small-molecule metabolites. There are also unconventional αβ T-cell subsets including MR1-restricted mucosal associated invariant T-cells (MAIT) and natural killer T-cells (NKT cells). Unconventional T-cells typically provide a more rapid response, upon initial pathogen exposure, which is not donor restricted. They have traditionally been less well studied than their conventional counterparts, but knowledge of unconventional T-cells is rapidly expanding (Godfrey et al. 2015). This study focuses on conventional αβ T-cells (from herein referred to simply as T-cells) so other T-cell subsets shall not be discussed further.

### 1.3.1 T-cell development and generation of diversity

Common lymphocyte progenitors in the bone marrow differentiate to give rise to various immune cells, T-cell precursors will migrate to the thymus where they undergo a series of events to become mature T-cells. Mature T-cells then migrate from the thymus to populate the

peripheral lymphoid tissues. Unlike B cells, new T-cells are not continually produced throughout the life span of an individual and their development slows with age (Murphy & Weaver 2016). A highly diverse TCR repertoire is required to enable antigen recognition across the vast scope of pathogens and is generated through gene segment recombination events and the addition of nucleotides to give junctional diversity. The TCR α chain gene locus contains multiple variable (V) and joining (J) gene segments and the TCR β chain comprises V, diversity (D) and J gene segments. These undergo gene rearrangement, called V(D)J recombination, in conjunction with a constant (C) domain to give a functional TCR following splicing (Davis and Bjorkman 1988; Attaf, Legut, et al. 2015). The potential diversity in humans is $10^{18}$ different TCRs (Sewell 2012a) however the expressed diversity is estimated to be around 25 x $10^6$ αβ TCRs in any given individual (Arstila et al. 1999). Thymocytes then undergo a selection process whereby those cells which are able to recognise self peptide-MHC complexes (pMHC) are positively selected for survival and non-reactive cells are left to undergo cell death (von Boehmer et al. 1989). And thymocytes which strongly recognise self pMHC are removed by negative selection to prevent any auto-reactivity. This study focused in on cytotoxic, MHC-I-restricted T-cell responses to influenza A virus as such cells have been shown to offer broad protection against viral strains as discussed below. I will thus limit further discussions to CD8+ cytotoxic T-cells.

### 1.3.2 CD8+ (cytotoxic) T-cells

Cytotoxic T-cells express the co-receptor CD8 on their surface and are responsible for the effector immune function. CD8+ T-cells recognise MHC-I molecules, which are expressed by nearly all nucleated cells in the body. This enables cytotoxic T-cells to inspect the internal proteome of all the cells in the body for anomalies. Upon successful engagement between TCR and pMHC, a tyrosine phosphorylation cascade and a series of signalling events are initiated in association with the CD3 complex (expressed on all mature T-cells) leading to the activation of the T-cell (Andersen et al. 2006). This productive interaction leads to the formation of a specialised junction between the T-cell and the target cell, providing positional stability and precise killing, termed the immunological synapse (Dustin et al. 1998). Advanced microscopy techniques have elucidated immune synapse formation involving rapid actin depletion across the synapse followed by TCR clustering and cytotoxic granule clustering; the complete cycle takes approximately 30 min after which the T-cell can engage further target cells (Ritter *et al.*, 2015; reviewed in Dieckmann *et al.*, 2016). T-cells can initiate target cell apoptosis by three distinct routes; the precise release of perforin and granzymes into the target cell, the binding of

Fas ligand to Fas receptors on target cells and the release of cytokines such as IFNγ and TNFα (Andersen et al. 2006).

### 1.3.3   MHC-I structure

MHC-I molecules are highly polymorphic membrane glycoproteins with each individual possessing a set of different alleles. In humans, they are referred to as human leukocyte antigen (HLA) molecules and classical HLA-I are grouped into HLA-A, -B and -C. In swine, they are known as swine leukocyte antigen (SLA) molecules and classical SLA-I are grouped into SLA-1, -2 and -3.  As shown in **Figure 1.1**, MHC-I molecules consist of a heavy polypeptide chain, which spans the cell membrane, non-covalently associated with a light polypeptide chain, namely $\beta_2$-microglobulin ($\beta_2$m). The heavy chain consists of three domains α1, α2 and α3 the latter of which is proximal to the membrane along with $\beta_2$m. The α1 and α2 domains are distal to the cell membrane, are polymorphic and comprise the peptide binding groove (PBG) where peptides can be loaded and presented to T-cells (Bjorkman et al. 1987). The PBG in MHC-I molecules is not open ended as in MHC-II molecules so this restricts to some extent the length of peptides that can be bound. Although human and mouse MHC-I molecules can present peptides of 8-15 amino acids in length, MHC-I molecules show a preference for peptides that are 9 amino acids long (Falk et al. 1991; Schumacher et al. 1991; Trolle et al. 2016). Most (>70%) of CD8+ T-cell epitopes are 9 amino acids long with ~20% being 10 amino acids long (Ekeruche-Makinde et al. 2013).

### 1.3.4   Peptide-MHC Class I antigen processing and presentation

Classically, MHC-I molecules present peptides derived from proteins of intracellular origin following a series of processing steps (reviewed in Neefjes *et al.*, 2011). Initially the proteins are degraded to peptides either in the cytosol or nucleus by proteasomes (large multi-catalytic protease complexes) which defines the carboxyl termini of the peptides. Next, peptides 8-16 amino acids in length in the cytosol are translocated to the endoplasmic reticulum (ER) lumen by transporter associated with antigen presentation (TAP) where they can undergo further processing before loading onto MHC-I. The highly polymorphic ER-associated aminopeptidase (ERAP) trims the N-termini of peptides generating favourable peptides for MHC-I binding (Serwold et al. 2002). The peptides are then loaded onto partially folded MHC-I molecules which are stabilised by chaperone proteins until successful assembly of pMHC-I complexes. Stable pMHC-I complexes are transported via the Golgi apparatus for presentation at the cell surface.

Presentation of exogenous protein is typically associated with MHC-II molecules, however exogenous antigens are able to enter the MHC-I presentation pathway in some cell subsets; known as cross-presentation (reviewed in (Reimann and Kaufmann 1997; Heath and Carbone 2001)). Endocytosed proteins from other cells are diverted into the classical MHC-I presentation pathway enabling cytotoxic immune responses to viruses that may not infect APCs or impair them.

As shown in **Figure 1.1** certain peptide residues will sit within the MHC-I PBG, defined as the anchor residues, and others will be prominent above the groove likely involved in TCR engagement. Anchor residues were defined by Falk and colleagues as positions which were ''occupied by a fixed residue or by one of a few residues with closely related side-chains'' (Falk et al. 1991). Saper and colleagues analysed the structural environment of the PBG and noted six distinct sub-sites within the PBG to which they assigned the following nomenclature: pockets A, B, C, D, E and F (Saper et al. 1991). The conformation of the PBG pockets varies between different MHC alleles and determines which peptide residues can bind. The conformation of peptides within the PBG can vary, although primary anchor positions have commonly been identified at position 2 (P2) and the carboxy terminus (PC) in pMHC-I sitting within pockets B and F respectively (Matsumura et al. 1992). Also, typically where longer peptides have been identified this usually results in a larger 'bulging' of the peptide backbone (**Figure 1.1C**) (Rist et al. 2013). However there are many pMHC-I structures which display different conformations including observations where the N- (P1) or C- (PC) terminus of a peptide will extend out of the PBG rather than sitting within pockets A or F (Collins et al. 1994; Pymm et al. 2017). The variability observed in pMHC-I complexes makes structural studies essential for determining the primary anchor residues, which can be defined to predict which peptides will bind to a given MHC allele, as shall be discussed further in chapters 5 and 7.
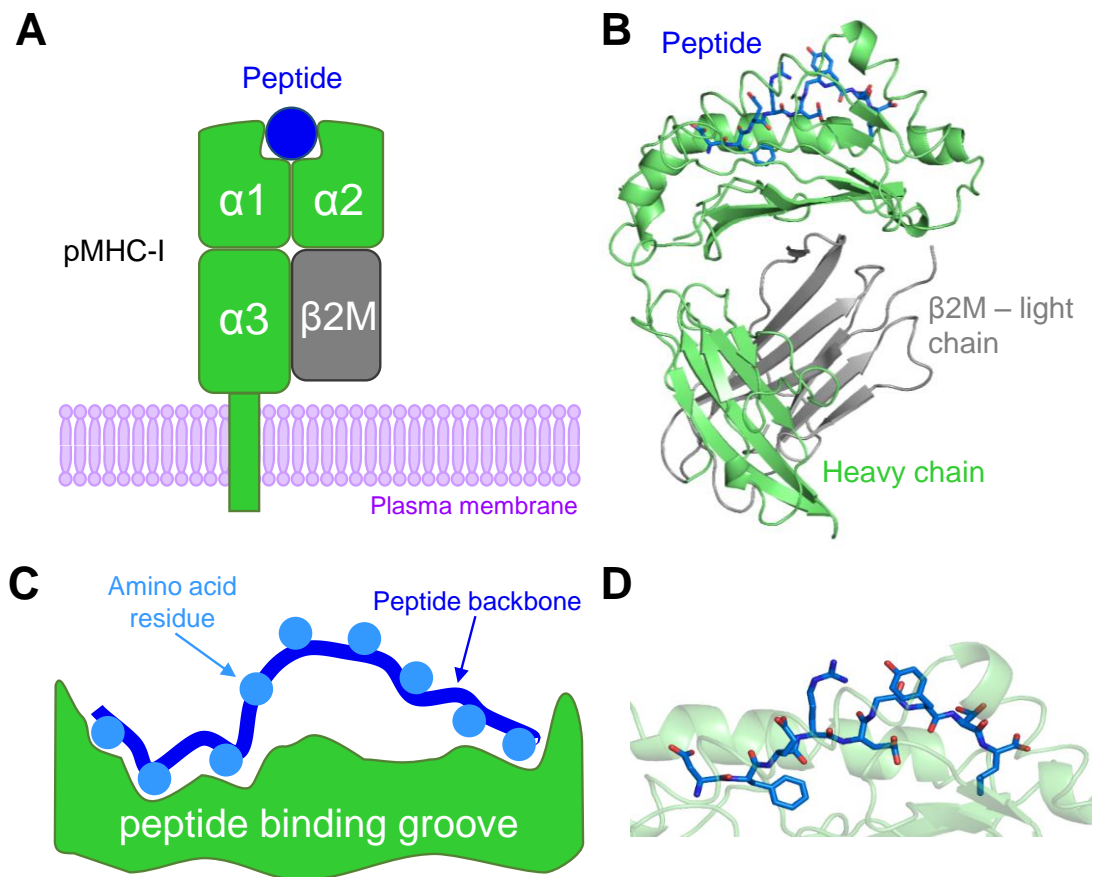
**Figure 1.1. Peptide-MHC class I structure.**
**A)** Schematic of Peptide-MHC-I (pMHC-I) at the cell surface. **B)** Structure of pMHC-I (PDB code: 5NQ0). **C)** Schematic of MHC-I binding groove with bound peptide. **D)** Structural depiction of (C) (PDB code: 5NQ0; Tungatt et al. *unpublished*).

## 1.3.5   The T-cell receptor

The αβ TCR is a heterodimer comprised of two disulphide-linked polypeptide chains, α- and β-chain, both consisting of a constant domain (cell membrane proximal) (Cα and Cβ) and a variable domain (distal to cell membrane) (Vα and Vβ) with a hypervariable region comprising the antigen binding site (Chothia et al. 1988) (**Figure 1.2**). This region consists of three hairpin loops in each TCR chain called complementarity-determining regions (CDR), CDR1-3 α and β, through which the TCR binds pMHC (Garboczi et al. 1996) (**Figure 1.2B**). The CDR3 loops display the greatest diversity generated by both gene segment recombination and junctional diversity (Attaf, Huseby, et al. 2015). The TCR needs to associate with the multimeric protein complex CD3 to enable its correct assembly and translocation to the T-cell surface (Kuhns et al. 2006). CD3 forms part of the TCR complex and signalling pathway and is commonly used as a marker for T-cell identification, however it is omitted from **Figure 1.2** for simplicity. The co-receptor CD8, in addition to its role in TCR signal transduction, also plays a key role in stabilising the TCR-

pMHC interaction particularly when the affinity of the interaction is weak (Wooldridge et al. 2005) (**Figure 1.2**). CD8 binds the pMHC at a non-polymorphic site distinct from the TCR docking platform and decreases the dissociation rate of the pMHC and TCR increasing the chance for successful T-cell signalling (Wooldridge et al. 2005).
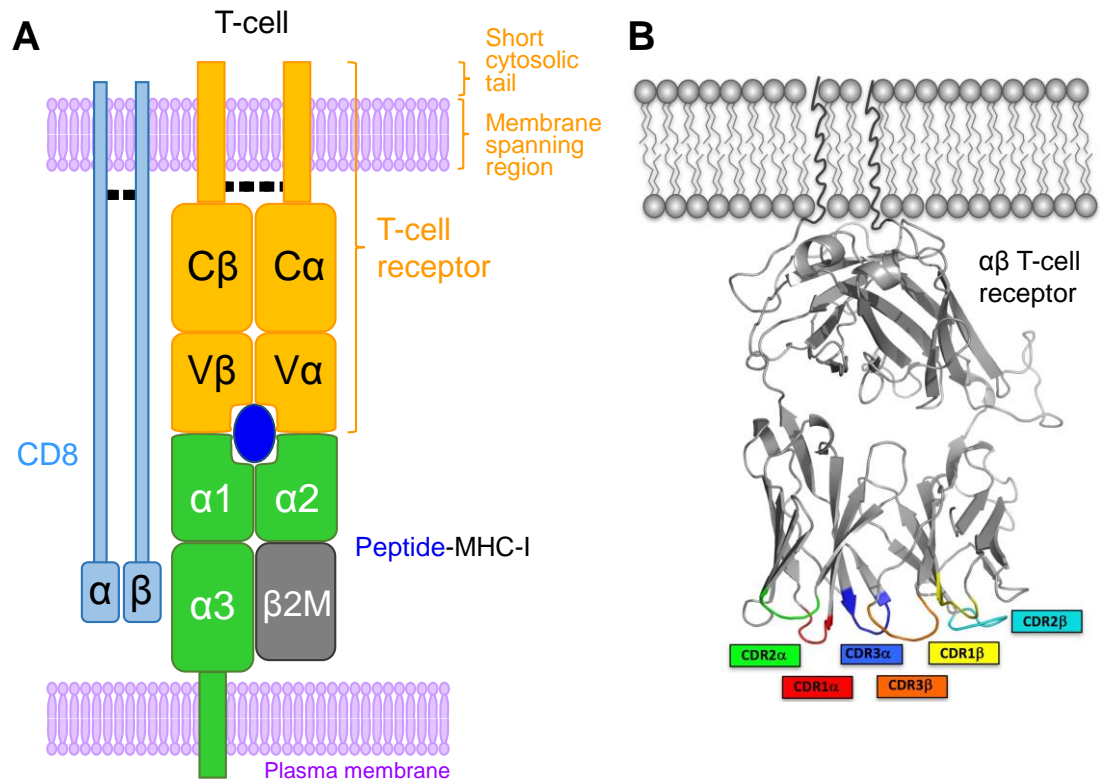


**Figure 1.2. T-cell receptor structure and its interaction with peptide-MHC-I class molecules.**
**A)** Schematic of T-cell receptor complexed with peptide-MHC-I at the cell surface including CD8 interaction. **B)** Structural depiction of T-cell receptor with CDR loops colour coded as displayed (Attaf, Legut, et al. 2015).

### 1.3.6   T-cell epitope identification

Immunoproteomics is a term that encompasses numerous methods that are concerned with the identification of antigenic peptides or proteins, the knowledge of which is important for our understanding and combating of diseases (Fulton and Twine 2013). MHC-I restricted T-cell epitopes can be identified by different approaches including peptide elution, *in silico* predictions and scanning peptide sequences for functional T-cell responses. Peptide-MHC-I complexes can be isolated from cells of interest and peptides eluted which can then be identified by mass spectrometry. Mass spectrometry allows the rapid identification of many peptides with no assumptions made about the peptide length (Fulton and Twine 2013). However, this approach can be cost and labour intensive, requires an antibody to the MHC molecule of interest for

isolation and large sample sizes. Bioinformatic approaches can also be utilised for T-cell epitope identification, with algorithms incorporating the peptide binding motifs of a given MHC allele to predict the peptide sequences that will bind and their affinities. Peptide prediction algorithms, such as 'NetPanMHC', are well established for humans, primate and mouse MHC alleles and provide an informed list of peptide epitopes for further validation which can reduce experimental costs and time (Nielsen et al. 2007). However this approach does make assumptions about the peptide length and can fail to identify all immunogenic peptides (Grant et al. 2013). A well-established non-assumptive approach is to synthesise overlapping peptides that span the protein of interest and that can be assessed for T-cell recognition by functional assays (Draenert et al. 2003). Peptides can initially be pooled together to decrease experimental load and any T-cell responses can then be subsequently narrowed down to individual peptides and truncated peptide sequences (Fiore-Gartland et al. 2016). This approach does not make assumptions about peptide length, MHC binding or immunodominance, however it should be noted that it can still fail to detect all possible responses (Draenert et al. 2003). T-cell epitopes produced by these methods can undergo further validation including functional assays and pMHC multimer staining and flow cytometry.

### 1.3.7   In vitro culture of T-cells

Cells can be isolated from the body, i.e. T-cells from blood, and cultured within the laboratory for further study. The ability to culture T-cells *in vitro* and generate T-cell clones has been implemental in our knowledge to date of T-cells across multiple subject matters. For instance, T-cell clones can be used to assess the function of antigen-specific T-cells, such as cytotoxicity, to define T-cell epitopes, to isolate monoclonal TCRs and to optimise cell based protocols. The division of somatic cells is subject to 'Hayflick's limit', which means that any given cell will undergo a finite number of cell divisions before reaching senescence (Hayflick and Moorhead 1961; Effrod and Pawelec 1997). The progression to cell senescence is relative to the continual degradation of telomeres, which are crucial to chromosomal integrity, that occurs with each cell division (Harley et al. 1990). This characteristic of cells can therefore limit the number of passages a given cell may be cultured for *in vitro* which in turn can limit experimental pursuits. Immortal cells can overcome the Hayflick's limit by the expression of telomerase which compensates for telomere degradation by mediating telomere elongation (Morin 1989; Harley et al. 1990).

Telomerase is expressed in T-cells *in vivo* following cellular activation, enabling T-cells and immune memory to be maintained long-term in an individual. T-cells can also express telomerase following *in vitro* stimulations, although this is not infinite, which may account for the ability to culture T-cells *in vitro* longer term than that which is achievable in other somatic cell types (Hodes et al. 2002). *In vitro* culture protocols for human T-cells are well established and will typically involve the use of T-cell mitogens, accessory cells or anti-costimulatory molecules antibodies (Raulf-Heimsoth 2008). In our laboratory, the approach that is most frequently used, combines the known T-cell mitogen phytohaemagglutinin (PHA), irradiated allogeneic peripheral blood mononuclear cells (PBMC) and stimulatory cytokines to stimulate T-cells to undergo cell expansion and maintain them in culture. The culture of mouse T-cell clones has been performed but with the generation of TCR transgenic models and the ability to fuse mouse T-cells with a cancer cell to form a T-cell hybridoma (Kruisbeek et al. 2001) it has circumvented the need for long-term *in vitro* culture of mouse T-cell clones. In addition to routine re-stimulations *in vitro*, there are many other conditions that need to be considered for successful T-cell culture. Cell culture medium conditions are designed to provide the essential nutrients required for cell culture, maintain the pH at physiological condition, to prevent any bacterial contamination and where required provide non-essential amino acids (Raulf-Heimsoth 2008). Cytokines are also needed to support T-cell division and survival in culture, in particular interleukin (IL)-2 (Smith 1988) and IL-15 (Lodolce et al. 2002; Li et al. 2005). Considering the breadth of components implemented for *in vitro* T-cell culture, there are many aspects that may affect optimal culture conditions as shall be discussed further in Chapter 3.

## 1.4 Influenza

Influenza A, B and C are negative-sense, single stranded RNA viruses belonging to the family Orthomyxoviridae. The three influenza types are genetically diverged encompassing varying pathogenicity and different host species range although all three are capable of infecting humans. Influenza A and B viruses can cause severe disease in humans. However, the former is the most diverse, the most significant threat and associated with pandemic infection (Kidd 2014). My work focussed on infection with Influenza A virus (IAV); a major cause of global human morbidity and mortality. IAV is a highly infectious and highly mutative intracellular pathogen and is known to infect a range of host species including humans, pigs and birds. IAV infection can cause a range of clinical features ranging from asymptomatic, to respiratory discomfort, to fever, to viral pneumonia caused by the virus itself or in conjunction with secondary infections and to sepsis. Severe cases of IAV infection can be mediated by both direct viral damage and an

uncontrolled and overwhelming host immune response (Dela Cruz and Wunderlink 2017). The World Health Organisation currently estimates that annual Influenza epidemics cause around 3 to 5 million cases of severe illness and around 250,000 to 500,000 deaths globally. Thus, human Influenza infection places a large burden on health care resources as well as generating significant indirect costs associated with loss of workplace productivity. Cost estimates range between >$29 to >$85 billion annually in the United States (Molinari et al. 2007; Mao et al. 2012). Vaccination strategies in humans to combat seasonal epidemics currently require annual inoculations to account for the mutative nature of the virus.

### 1.4.1 Influenza A virus characteristics

IAV is an enveloped virion with a genome consisting of eight distinct RNA segments that were initially identified to encode 10 viral proteins (**Figure 1.3A**); polymerase acidic protein (PA), polymerase basic proteins 1 and 2 (PB1 and PB2), hemagglutinin (HA), neuraminidase (NA), nucleoprotein (NP), matrix proteins 1 and 2 (M1 and M2), non-structural protein 1 (NS1) and NS2 since renamed nuclear export protein (NEP) (Palese and Schulman 1976; Ritchey et al. 1976; Allen et al. 1980; O'Neill et al. 1998). M1 is the most abundant protein per virion followed by NP, HA and then NA (Hutchinson et al. 2014). In recent years further viral proteins have been identified and begun to be characterised, with the viral genomic segments now thought to encode at least 18 proteins (reviewed in (Vasin et al. 2014)). Each gene segment is contained in a ribonucleoprotein complex (RNP) consisting of the RNA bound by multiple copies of NP and the addition of a viral polymerase (a trimer comprising PA, PB1 and PB2) (Zheng and Tao 2013). HA and NA are surface glycoproteins (**Figure 1.3**) involved in host cell attachment and entry and host cell exit. The subtypes of HA and NA are numbered and used to discriminate between different IAV strains and used in the standard international nomenclature for IAV. In this system each strain is named as follows: A/host of origin (if not human)/geographical origin/strain number/year of isolation (HA and NA subtype numbers) (WHO 1980). For example: A/Swine/England/1353/2009 (H1N1).

### 1.4.2 Influenza A virus infection cycle

IAV particles are highly infectious and new strains are able to spread rapidly within a population and even worldwide. The virus must first successfully enter the host and there are three main routes of IAV transmission. (i) Droplet transmission – infectious droplets expelled by an infected host can deposit in the upper respiratory tract. (ii) Aerosol transmission – inhalation of smaller particles, called 'droplet nuclei', capable of reaching the lower respiratory tract. (iii) Contact

transmission – by direct contact with virus-contaminated objects or infected individuals. The relative contribution of each transmission route on the spread of IAV is not yet clear (Killingley and Nguyen-Van-Tam 2013). IAV particles infect the epithelial cells of the respiratory tract wherein they can initiate production and assembly of more virions which can exit the cell and spread. HA binds to sialic acids on the host cell surface initiating endocytosis of the virion. Once internalised, the acidity of the endosome increases inducing conformational changes in certain viral proteins enabling viral RNPs to enter the cytoplasm of the infected cell before being trafficked to the nucleus. Once in the nucleus the RNPs dissociate allowing viral genome replication and viral protein expression. Newly assembled RNPs are then transported to the plasma membrane where new virions are assembled and then released from the cell by budding. The new virions are then able to infect further cells (Bouvier and Palese 2008; Hutchinson and Fodor 2013).

### 1.4.3   Antigenic shift and drift

Influenza A viruses can generate vast genetic diversity and evade the immune system by two main processes as shown in **Figure 1.3B**; (i) by altering the amino acid sequences of its surface glycoproteins, HA and NA, termed antigenic drift and/or (ii) by genetic reassortment whereby a strain may acquire a novel HA and/or NA gene segment, termed antigenic shift. In the former, the accumulation of point mutations in these proteins drives strain evolution and the resulting variants lead to annual epidemics. The latter is a consequence of the segmented viral genome which can undergo gene reassortment when a cell is infected by two or more IAV subtypes. The emergence of these antigenically distinct subtypes may have pandemic potential if entering an immunologically naïve population (Nicholson et al. 2003). Current vaccines induce antibody responses to these surface glycoproteins therefore they require annual updates as circulating strains mutate. These vaccines will likely be ineffective against the emergence of a novel pandemic strain. As IAV can infect multiple species, gene reassortment could occur in a host between diverse virus strains from different animal origins. Global human health is at risk from this zoonotic reservoir of novel influenza strains.
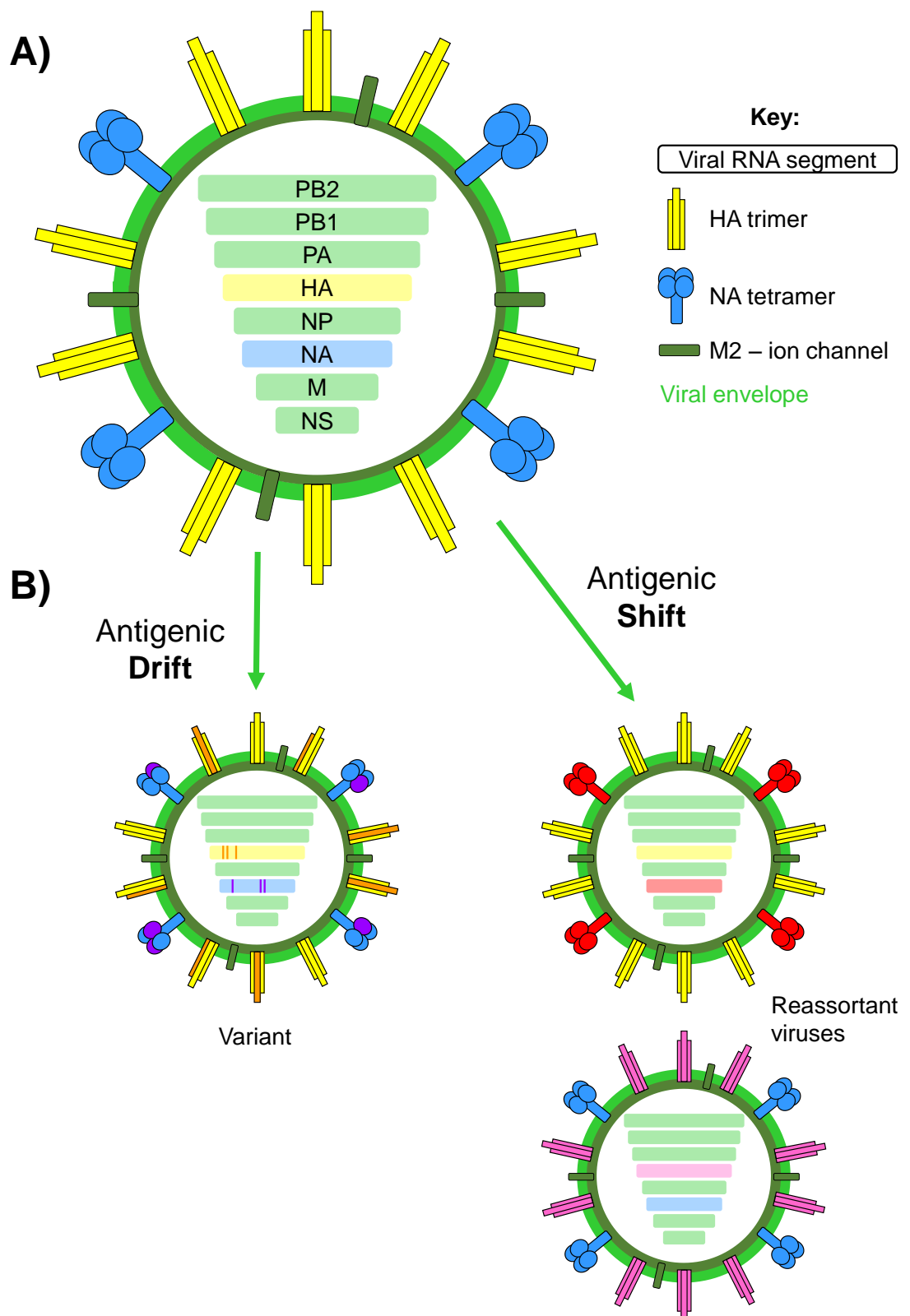
**Figure 1.3. Influenza A virion structure and antigenic variants.**
**A)** Schematic of Influenza A virus particle. Eight gene segments encode for ten main proteins: PB2, PB1, PA, HA, NP, NA, M1, M2, NS1 and NS2. **B)** Influenza A viruses can undergo antigenic drift (accumulating changes in their surface proteins) and antigenic shift (gene reassortment to give new HA or NA genes). This generates strain diversity and new subtypes. Figure adapted from (Lederberg 2001).

### 1.4.4 Influenza A virus vaccines

There are two types of human influenza vaccines currently licensed worldwide, inactivated vaccines typically administered intramuscularly and a live attenuated vaccine administered intranasally. Inactivated influenza virus vaccines induce neutralising antibodies against viral surface glycoproteins which can prevent influenza infection with matching or closely conserved strains (Cox et al. 2004; Baz et al. 2015). In addition to the induction of neutralising antibodies, live attenuated vaccines have also been shown to induce influenza-specific T-cell responses (Hoft et al. 2011). As shall be discussed in section 1.5, T-cell responses are important for cross-strain protection. Vaccines administered intranasally are also desirable as they elicit immune responses that better resemble natural influenza infection (Cox et al. 2004).

### 1.4.5 Zoonotic potential and Swine Influenza

There has been substantial research already undertaken to understand Influenza infection in humans including efforts to develop a universal vaccine that could encompass antigenic drift and shift to provide protection across viral strain variants. However, despite IAV being endemic in the global pig population and the risk of zoonosis, the virus has not been well-studied or monitored in pigs.

Pig farming represents a significant sector of the global livestock industry, with animal numbers rising annually from 856 million in 2000 to 985 million in 2014 worldwide (FAO 2014). There are three common subtypes of swine influenza virus (SwIV) circulating in the global pig population, H1N1, H3N2 (both of these lineages also circulate in humans) and H1N2, and inactivated virus vaccines are commercially available however they do not always prevent infection but can lead to milder symptom presentation (reviewed in (Rahn et al. 2015)). SwIV is not currently a notifiable disease in the UK and unlike in the US, vaccines are currently not widely used. Infection typically causes mild respiratory symptoms and fever similar to those observed in humans, but in other instances SwIV can be more severe contributing to reduced growth and reproductive rates. These symptoms are further exacerbated, and mortality risk increased, where secondary viral or bacterial co-infections occur (Chen et al. 2012). Subsequently, there can still be significant economic losses incurred in some SwIV cases, due to mortality, morbidity and the implementation of control measures. Effective vaccination strategies and biosecurity practices would help eliminate the financial burden of SwIV and concurrently improve animal welfare.

In addition to the circulating strains of SwIV, pigs can also be infected with both avian and human influenza. Host tropism is mainly determined by the binding preferences of HA proteins for particular sialic acid (SA) receptors and their distribution within the host. Human viruses preferentially bind to SA α2, 6-galactose linked receptors and avian viruses to SA α2, 3-glactose linked receptors (Rogers and D'Souza 1989). In humans, the former predominates, particularly in the upper respiratory tract whereas the latter can be found in the lower respiratory tract (Shinya et al. 2006). This underpins the ability of avian viruses to infect humans and replicate in the lower respiratory tract. Both SA receptors have also been found in the respiratory tract of swine (Ito et al. 1998) displaying similar distribution patterns to that found in humans (Nelli et al. 2010). This provides molecular evidence that pigs can be infected by swine, human and avian influenza viruses enabling them to play an important role in shaping influenza epidemiology. Simultaneous infection of pigs with different strains and subsequent antigenic shift could give rise to novel and potentially dangerous IAV strains to which the human population are immunologically naïve (Scholtissek et al. 1985). This phenomenon has resulted in pigs being referred to as ''mixing vessels'' (Scholtissek 1990)(reviewed in Ma et al. 2009). Thus, the generation of antigenic shift in IAV in pigs represents a substantial zoonotic threat to the human population and is a major and significant factor driving research in this area in addition to pig health and welfare.

There have been several recorded influenza pandemics in the last century with differing mortality rates. The recombination of influenza strains in pigs is believed to have produced the viruses responsible for the Asian H2N2 and Hong Kong H3N2 pandemics in 1957 and 1968 respectively (Ito et al. 1998). These outbreaks were estimated to have caused over 1 million and 1-3 million deaths worldwide respectively. The largest and most virulent pandemic on record is that of "Spanish" flu between 1918-1920 which was retrospectively identified to be a novel H1N1 subtype (Taubenberger et al. 1997). Historically pandemic surveillance would not have been that extensive so global mortality estimates vary but it is thought that "Spanish" flu was responsible for up to 50 million deaths worldwide (Johnson and Mueller 2002). A reoccurrence of a pandemic of this magnitude would be devastating, however, the health care available in 1918 along with limited containment approaches would likely have contributed to this substantial mortality rate. A more recent, less severe pandemic occurred in 2009 with a novel H1N1 strain referred to as pdmH1N1 that was estimated to have caused 284,000 deaths globally (Dawood et al. 2012). This novel strain was first detected in early 2009 in Mexico and the US and had rapidly spread to 74 countries by June, when a pandemic was declared, and continued to spread worldwide before the World Health Organisation declared the pandemic over in August

2010. PdmH1N1 was unrelated to the circulating human influenza viruses at the time and was derived from several circulating SwIV following a complex series of transmission and antigenic shift events, in part facilitated by the movement of pigs between Eurasia and North America (Smith et al. 2009).

In the majority of cases, pigs are infected with a single influenza subtype however multiple studies have demonstrated that pigs can be co-infected with two, or in rare cases more than two, different SwIV strains simultaneously (Kyriakis et al. 2013; Rose et al. 2013). Indeed, reassortment has been demonstrated following experimental co-infection of pigs with swine H3N2 and H1N1 viruses, however, the reassorted viruses were unable to transmit in this study (Ma et al. 2010). Natural reassortment events over the years have shaped the current genetics of circulating SwIV subtypes and novel strains continue to arise which given the correct genetics and conditions could establish themselves in the pig population. For example, in Germany novel reassortment H1N2 strains were isolated which were determined by sequencing to be the result of reassortment between circulating European H1N2 and H3N2 SwIV (Zell et al. 2008). Also in recent years, novel reassortment H1N2 SwIV were identified and became prevalent in Denmark. Sequence data confirmed that these novel strains was generated by reassortment of Danish avian-like H1N1 and swine H3N2 (Trebbien et al. 2013).

The transmission of Influenza viruses between the human and pig populations has been well documented globally. A recent study reviewed data from all published incidences of avian or swine influenza transmission to humans (Freidl et al. 2014). They found 1023 reports of avian influenza transmission to humans of which the majority of cases, 648, were associated with subtype H5. There were 396 reports of natural human infection with SwIV the majority of which were with SwIV H3N2. Where data was available, the majority of patients had been exposed to animals indicating a direct transmission route. The authors advised that the number of SwIV transmission to humans may be underestimated since the clinical presentation would be similar to that of human seasonal flu. Reverse zoonoses are also prevalent; between 2009-2011 one study identified almost 50 human to pig transmission events globally of pdmH1N1, along with over 20 transmissions of H1 and H3 viruses since 1990 globally (Nelson et al. 2012). Indeed reassortment viruses have been identified in swine containing gene components of human pdmH1N1 (Howard 2011). A study that analysed 290 SwIV genomes circulating between 2009-2013, isolated from 14 countries across Europe including the UK, found that 27% contained internal genes derived from pdmH1N1 lineage (Watson et al. 2015)

## 1.5   T-cells and Influenza

It is widely documented that T-cell responses, particularly CD8+ T-cells, are key to limiting the severity of disease following IAV infection (McMichael et al. 1983; Sridhar et al. 2013; La Gruta and Turner 2014; Wang et al. 2015), particularly when the antibody response is insufficient. Upon infection, CD8+ T-cells will be activated and migrate to the respiratory system where they can initiate apoptosis of virus-infected epithelial cells and thus limit viral spread. Cytotoxic T-cells can kill IAV-infected cells by releasing perforin and granzymes into the infected cells, by the Fas/Fas ligand apoptotic pathway (Topham et al. 1997) and by the secretion of other cytokines (Bot et al. 1998; Brincks et al. 2008).

### 1.5.1   Heterotypic immunity

The term 'heterotypic immunity' (also known as heterosubtypic) refers to the phenomenon where an individual previously infected by one influenza subtype, displays reduced or absent pathology following subsequent influenza infection with a different subtype in the absence of neutralising antibodies. This term was first used in 1965 by Shulman and Kilbourne, who demonstrated experimentally in mice the ability of previous infection with H1N1 to improve immunity to subsequent challenge with a H2N2 virus (Schulman and Kilbourne 1965). Although this form of protection does not prevent infection, it was found to reduce viral titres, viral pathology and mortality all in the absence of neutralising antibodies. Heterotypic immunity has been investigated by numerous studies since and a landmark natural experiment was made possible by the 2009 H1N1 pandemic. Sridhar and colleagues were able to monitor a group of individuals, that lacked pre-existing antibodies to pdmH1N1, throughout the pandemic waves of infection during 2009-2011 (Sridhar et al. 2013). Higher levels of pre-existing effector memory IAV-specific CD8+ T-cells in individuals was correlated with milder symptoms or asymptomatic presentation following natural pdmH1N1 infection and reduced viral shedding. Furthermore, pre-existing cytotoxic T-cells were shown to respond to epitopes from three conserved influenza proteins. Cytotoxic T-cells recognising epitopes derived from conserved internal Influenza proteins have been documented in humans both *ex vivo* and *in vitro* and are of substantial interest because of their ability to confer broad protection against influenza strains (Lee et al. 2008; Grant et al. 2013; Liu et al. 2013; Sridhar et al. 2013). Inducing T-cells that recognise conserved epitopes is therefore of high interest when it comes to developing universal Influenza vaccines.  I will discuss the sequence conservation of IAV proteins further in Chapter 4 on page 58.

## 1.6 T-cell immunology of swine Influenza

The study of immune responses in pig, both generally speaking and in the context of Influenza, lags behind that of humans and laboratory mice. This is likely due in part to the fact that historically immunological tools for pig research have been limited and only in the past decade has interest increased in understanding SwIV and monitoring SwIV epidemiology. This study has been facilitated by the increased availability of reagents in recent years (reviewed for αβ T-cells in (Gerner et al. 2015)) although further commercially available antibodies and reagents are still desirable to make T-cell research in pigs even more accessible.

### 1.6.1 Porcine T-cells overview

For the most part, comparisons have shown human and porcine T-cells to be similar with few noteworthy differences. In pigs, a range of different T-cells are known to express the CD8αα homodimer (Gerner et al. 2009) in particular CD4+ T-cells will express CD8αα upon activation and memory, whereas (CD4-) cytotoxic T-cells permanently express the CD8αβ heterodimer (Zuckermann and Husmann 1996; Yang and Parkhouse 1997). Also pigs are one of a number of species that have high circulating levels of γδ T-cells and in pigs a small subset of these also express CD8α. Traditionally cytotoxic T-cells have been distinguished in flow cytometry studies as CD3+, TCRγδ-, CD4- and CD8α$^{high}$ cells. However, an antibody to the CD8β chain is now commercially available and was particularly useful for this study as it enabled clear distinction of cytotoxic porcine T-cells, which express the CD8αβ heterodimer. To my knowledge there is no antibody available for the αβ TCR in pigs, this would be highly desirable for future research.

### 1.6.2 T-cells in Swine Influenza

Influenza infection in pigs induces neutralising IgA and IgG antibodies and an increase in lymphocytes in the lungs, including a large increase in cytotoxic T-cells and heterotypic immunity has also been demonstrated in pigs (Heinen et al. 2001). There are a limited number of studies investigating T-cell responses in SwIV in depth and few cytotoxic T-cell epitopes have been published that have also been confirmed experimentally. There has been some recent progress with a study in outbred pigs that used an *in silico* prediction algorithm to identify four putative SwIV epitopes presented by one of the most commonly occurring SLA-I in livestock; SLA-1*0401 (Pedersen et al. 2014). Pedersen and colleagues were able to confirm these epitopes (from HA, NP and PB2) by peptide-MHC multimer staining of blood samples from pigs each inoculated with a chemically inactivated SwIV strain given with adjuvant over four repeated immunisations. Recent studies by Talker and colleagues presented the most in-depth analysis of porcine T-cell

responses so far in pigs, experimentally infected with high doses of SwIV H1N2 intratracheally, looking at phenotypes and function both locally and systemically (Talker et al. 2015; Talker et al. 2016). In the peripheral blood mononuclear cells (PBMC), multifunctional T-cells were detected in response to virus; CD4+ T-cells produced IFN-γ, TNF-α and IL-2 and CD8β+ T-cells produced IFNγ and TNFα and stained positive for the degranulation marker CD107a (Talker et al. 2015). The latter were only detected in low frequencies *ex vivo* so samples were stimulated with virus *in vitro* to enable cytokine analysis of these multifunctional CD8β+ T-cells in 4 out of 6 animals. Proliferative and perforin+ cytotoxic (CD8β+) T-cells were detected directly *ex vivo* by flow cytometric analysis in the blood of 3 out of 6 animals after primary infection. The second study inoculated 31 pigs and analysed local responses in the lungs and tracheobronchial lymph nodes (TBLN) in addition to PBMC, and detected virus specific IFNγ+ CD8β+ T-cells in the lung at frequencies up to 30 times higher than that seen in PBMC and TBLN following infection (Talker et al. 2016). The authors also incubated lung and PBMC samples *in vitro* with heterologous SwIV strains which induced production of IFNγ and TNFα in CD8β+ T-cells.

## 1.7   Aims

Despite their role as important antigenic 'mixing vessels' with potential to generate highly dangerous viral strains, the immune response to IAV in pigs has not been as well studied or monitored. This deficiency has arisen, at least in part, due to a lack of research tools to study T-cell responses in pigs and the inability to culture porcine T-cells long term *in vitro*. At the outset of my thesis work nobody had been able to culture porcine T-cells beyond very short term lines (3 weeks). The initial focus of this project was therefore to establish porcine T-cell culture (chapter 3) so that I could study T-cell responses to SwIV. I then aimed to identify Influenza epitopes using Influenza-specific T-cell lines and clones (chapters 3 & 4). These epitopes were then used to produce soluble pMHC-I complexes for structural analyses (chapter 5) and pMHC tetramer staining of relevant samples *ex vivo* (chapter 6). Finally, I aimed to use the structural data and the T-cell clones to define MHC-I binding motifs to enable informed epitope predictions (chapter 7).

This study, aimed to increase our understanding of T-cell responses to Influenza in pigs in the context of vaccination and expand the immunological toolbox for swine studies bringing approaches up to the speed that is already routinely available for human and mouse studies. My study aimed to contribute directly to our influenza knowledge in pigs by application of our developed techniques on clinically relevant samples. It further aimed to inform future studies

including assessing vaccination routes, predicting T-cell influenza epitopes and monitoring correlates of protection. The techniques I developed could also be applied to studies of other economically important swine diseases. Furthermore, the pig makes a good model of human IAV infection (reviewed in (Rajao and Vincent 2015)) and both swine and human flu strains are known to replicate to similar levels on the upper and lower respiratory tract of pigs and exhibit similar patterns of viral shedding (Brown 2000). Pigs are also known to exhibit a comparable arrangement of viral attachment to that observed in humans (Van Poucke et al. 2010). Additionally pigs and humans share a high degree of anatomical and physiological similarities with studies of immune parameters showing 80% orthology between humans and pigs in those analysed compared to only 6% between humans and mice (Dawson 2011; Dawson et al. 2013). Some of the advantages to using pigs as models of human diseases are reviewed in (Meurens et al. 2012). A long-term aim of this work was to aid the establishment of pigs as the closest non-primate model to human for studies of infection, autoimmune disease, transplant tolerance and organ regeneration.

# 2   <u>Materials & Methods</u>

## 2.1   Animals, virus and Influenza vaccination

### 2.1.1   *Babraham and outbred pigs*

Experiments in this study were performed on the Babraham ('large white') inbred pig line, which all carry identical swine leukocyte antigen (SLA) genes. Pig experiments were conducted at the Pirbright Institute in accordance with the Pirbright Institute ethics committee and the U.K. Animal (Scientific Procedures) Act of 1986. All pig experiments described in this thesis were performed by my collaborators at the Pirbright Institute (Dr. Sophie Morgan, Dr. Hanneke Hemmink, Dr. Maria Montoya, Dr. Bryan Charleston and Dr. Elma Tchilian). Frozen samples or EDTA-treated blood from experimental pigs were sent to Cardiff University for this study. All Babraham pigs used in these experiments were confirmed Influenza A virus (IAV) free by screening for the absence of IAV infection by matrix (M) gene real time RT-PCR (Slomka et al. 2010), and antibody-free status was confirmed by haemagglutination inhibition (HAI) using 4 swine influenza virus (SwIV) antigens. Outbred pigs (pedigree and cross-breed) were also used to procure 'feeder' peripheral blood mononuclear cells (PBMC) with blood collected as a by-product (with assistance from either Prof. Mick Bailey or Dr. Emily Porter) from the University of Bristol, Veterinary School abattoir, adhering to EU regulated methods. PBMC were then isolated from blood samples at Cardiff University.

### 2.1.2   *Swine Influenza viruses*

The candidate vaccine, S-FLU, was provided by Prof. Alain Townsend, University of Oxford. The H5-S-FLU expressed the HA of the avian influenza virus A/Vietnam/1203/2004(H5) and N1 and internal genes from PR8 [IAV (A/PuertoRico/8/1934(H1N1))] (Morgan et al. 2016). H1 S-FLU, [S-eGFP/N1(Eng)].H1(Eng), expresses the HA and NA of the A/England/195/2009 [pandemic H1N1] (N1 GenBank accession no. GQ166659.1 and surface H1 HA GenBank accession no. ACR15621.1) and internal protein genes of PR8. Inactivated virus of the following H1N1 strain was also utilised; [A/Swine/Spain/SF11131/2007] (Sp/Sw); provided by the Pirbright Institute.

### 2.1.3   *Influenza vaccination and tissue harvest*

Two sows, pigs #625 and #650, were immunised simultaneously with $8 \times 10^7$ $TCID_{50}$ H5-S-FLU intranasally using a mucosal atomization device (MAD300, Wolfe Tory Medical) and with $2 \times 10^7$ $TCID_{50}$ inactivated H1N1 (Sw/Sp) with montanide adjuvant intramuscularly. The animals

received identical booster immunisation 25 days later. Pigs were euthanised (stunning with exsanguination) at day 38 (day 13 post boost) and peripheral blood, Bronchoalveolar Lavage (BAL) and Tracheobronchial lymph nodes (TBLN) were harvested. In short, BAL samples were obtained by washing the lung with 250 mL of phosphate buffered saline (PBS) from which 100 mL was harvested. The BAL fluid was centrifuged at 800 $x$ $g$ for 15 min to isolate any cells present. The cell pellet was washed in PBS, filtered through a 70 µm cell strainer and frozen. TBLN were dissected at post mortem and dissociated into single cell suspensions, which were filtered twice using a 70 µm cell strainer and washed in PBS before being frozen. PBMC were isolated from peripheral blood (see section 2.2.2) and frozen.

In a second experiment, five pigs were divided into two groups, pigs #1 and #2 were left unvaccinated and pigs #6, #7 and #8 received H1-S-FLU [S-eGFP/N1(Eng)].H1(Eng)] via aerosol administration (~ 2 x $10^7$ TCID$_{50}$ per dose) using a InnoSpire Deluxe Philips Respironics nebulizer fixed to a small-sized anaesthetic mask held over the animal's nose and mouth. Vaccinated pigs received an H1-S-FLU boost at day 28. All pigs were euthanised at day 57 (day 28 post boost) and PBMC and BAL were harvested as described above. Details of all pigs are shown in **Table 2.1.**

**Table 2.1. Weight and age of pigs used in experiments.**

| Pig# | Sex | Age at day 0 | Weight (kg) at day 0 |
|------|-----|--------------|----------------------|
| 625 | F | 2 years | 173.5 |
| 650 | F | 3 years | 192 |
| 1 | F | 91 days | 21.0 |
| 2 | M | 94 days | 30.5 |
| 6 | M | 91 days | 27.0 |
| 7 | F | 91 days | 29.5 |
| 8 | M | 91 days | 29.0 |

## 2.2 Porcine Tissue Culture, peptides and T-cells.

All cells were cultured in 37 °C, 5% $CO_2$ incubators unless otherwise stated.

### 2.2.1 Porcine Media and Buffers

| Media/Buffer | Composition |
|---|---|
| R0 medium | RPMI-1640 Medium, pH 7-7.4 (Life Technologies)<br>2 mM L-glutamine (Life Technologies)<br>100 U/mL Penicillin, 100 µg/mL Streptomycin ('Pen Strep', Life Technologies) |
| R5 medium | R0 medium supplemented with 5% Heat-inactivated foetal bovine serum (FBS) (Life Technologies) |
| R10 medium | R0 medium supplemented with 10% FBS |
| Pig R5 medium | R0 medium supplemented with 5% in-house pig serum |
| Pig T-cell expansion medium | R0 medium supplemented with:<br>10% in-house pig serum<br>10 mM HEPES buffer (Life Technologies)<br>0.5X MEM Amino Acids (Life Technologies)<br>1 mM Sodium Pyruvate (Life Technologies)<br>50 µM 2-Mercaptoethanol<br>12.5 - 25 ng/mL swine IL-15 (Kingfisher Biotech)<br>300 IU/mL human IL-2 (aldesleukin, brand name Proleukin, Promethus) |
| Pig T-cell priming medium | As above but with swine IL-15 removed and 20 IU/mL IL-2 |
| APC-1 medium | DMEM medium (Life Technologies)<br>2 mM L-glutamine<br>100 U/mL Penicillin Streptomycin<br>10% FBS<br>10 mM HEPES buffer<br>0.5X MEM Amino Acids<br>1 mM Sodium pyruvate |
| APC-2 medium | DMEM/F12 medium (1:1) (Life Technologies)<br>2 mM L-glutamine<br>100 U/mL Penicillin Streptomycin<br>10% FBS<br>15 mM HEPES buffer |
| PBS | PBS Dulbecco A tablets, pH 7.3 (-Ca) (-Mg) (Oxoid, U.K.)<br>Dissolved in double distilled $H_2O$ and sterilised by autoclaving as per the manufacturer's instructions |
| Freezing Buffer | 90% FBS<br>10% Dimethyl sulfoxide (DMSO) (Sigma) |
| FACS Buffer | PBS<br>2% FBS |
| Red Blood Cell (RBC) lysis buffer | 0.1 mM EDTA, pH8 (Sigma)<br>10 mM Potassium bicarbonate ($KHCO_3$) (Fisher Scientific)<br>155 mM Ammonium chloride ($NH_4Cl$) (Sigma)<br>*Adjust pH to 7.2-7.4 where required* |
| PBS-EDTA | 'D-PBS' (1x) (-Ca) (-Mg) (Life Technologies)<br>2 mM EDTA |
| MACS buffer | 'D-PBS' (1x) (-Ca) (-Mg) (Life Technologies)<br>0.5% Bovine serum albumin (BSA) purified by heat shock fractionation, pH 7 (Sigma)<br>2mM EDTA, pH 8 |

*All cell culture media were 0.22 µm filtered before use.*

### 2.2.2 PBMC Isolation

Ethylenediaminetetraacetic acid (EDTA)-treated Babraham pig blood was obtained by venepuncture or for 'feeder' pigs by exsanguination. PBMCs were isolated by density centrifugation over an equal volume of Lymphoprep (Axis Shields, Oslo, Norway). Blood was slowly layered onto the Lymphoprep before being centrifuged at 900 *x g* for 20 min without a brake (to prevent disruption of the lymphocyte layer upon deceleration). The mononuclear cell layer was then harvested using a pasteur pipette and transferred to a fresh tube and washed with R0 medium (centrifuged at 600 *x g* for 10 min). The cell pellet was then resuspended in 25 mL RBC lysis buffer and incubated at 37°C in a water bath for 10 min. Samples were then washed with R0 medium (centrifuged at 300 *x g* for 6 min; to remove platelets) before being resuspended in R10 medium for cell counting. PBMCs were either used immediately or cryopreserved for future use.

### 2.2.3 In-house pig serum isolation

In-house pig serum was obtained from blood collected as a by-product from an abattoir that was allowed to clot in 50 mL tubes. The blood was centrifuged at 900 *x g* for 20 min upon which the serum was carefully aspirated off and transferred to fresh tubes. This step was repeated as necessary to ensure maximum serum harvest. Serum was then heat-inactivated at 56°C for 1 h before being frozen for storage. Serum was 0.22 μm filtered before being added to any medium.

### 2.2.4 Cryopreservation and thawing of cells

Cells were thawed rapidly in a 37 °C water bath before being resuspended in pre-warmed R10 medium and centrifuged at 400 *x g* for 5 min. The supernatant was then removed before resuspending the cells in the required medium. Whenever PBMC were defrosted they were treated at this point with 10-50 mg/mL DNase-I (Roche, Burgess Hill, U.K.) at 37°C for at least 20 min. This ensured digestion and prevention of any negative effects of dead cell debris. Cells to be frozen were centrifuged at 400 *x g* for 5 min to remove any medium and were resuspended in freezing buffer then placed in 1 mL cyrovials and frozen using a controlled rate freezing device (either CoolCell, Biocision or "Mr Frosty", Nalgene) at -80 °C. Cells were moved within 48 h to liquid nitrogen for long term storage.

### 2.2.5 Cell counting

Cells were resuspended and typically 10 μL of sample was mixed in a 1:1 ratio with trypan blue solution (Sigma). This mixture was then loaded onto a counting slide and viable cell numbers were enumerated by trypan blue exclusion and put into the following equation: (number of cells counted in slide section) x (dilution factor) x $10^4$ x (mL of sample) = total cell number.

### 2.2.6 CD8β T-cell isolation

Cytotoxic T lymphocytes (CTLs) were isolated using MACS anti-PE Microbeads (Miltenyi Biotech) based on the manufacturer's protocol. Throughout this method the centrifuge was kept at 4 °C and antibody staining took place on ice. PBMC were defrosted as described in section 2.2.4 then distributed between sterile capped FACS tubes (Falcon, Corning) at 2-3 x $10^6$ cells per tube. Cells were then washed with 3 mL MACS buffer per tube (centrifuged at 300 $x$ $g$ for 10 min) and the supernatant removed. Next, 0.5 μL of mouse anti-pig CD8β (clone PG1G4A, Kingfisher Biotech) were added per tube and incubated for 20 min. The wash step was then repeated before adding 0.5 μL of goat anti-mouse PE-conjugated antibody (Ab) (Ig polyclonal; BD Biosciences) for 20 min. The cells were then combined into a 15 mL falcon tube and washed with 10-15 mL MACS buffer. The supernatant was aspirated and the cells were resuspended in 80 μL of MACS buffer and 20 μL of anti-PE Microbeads per 1 x $10^7$ PBMC. This mixture was then incubated in the refrigerator for 15 min. The cells were then washed, the supernatant aspirated and the cell pellet resuspended in 500 μL of MACS buffer. This suspension was then passed through a MACS MS column (where the maximum number of total cells was 2 x $10^8$) and washed appropriately to obtain the CD8β- flow through and the isolated CD8β+ cells. Pre and post-sort samples were taken where required to ascertain sorting efficiency using flow cytometric analysis.

### 2.2.7 Peptides

S-FLU expresses PR8 internal genes from which overlapping peptides were designed, by Dr. Garry Dolton, to span the entire protein sequences of the Matrix protein (M1) (GenBank accession no. NP_040979.2] and nucleoprotein (NP) (sequenced in-house by Prof. Alain Townsend's laboratory). Peptides of 18 amino acid (aa) in length each overlapping by 10 aa were obtained using a Peptide Library Design and Calculator Webtool (Sigma Aldrich). Peptide sequences were adjusted by deletion, or addition, of amino acids from neighbouring peptides to increase the likelihood of them solubilising in aqueous solution. In total 40 overlapping peptides were designed for M1 and 81 peptides for NP and split into pools for screening (**Tables 10.1 & 10.2**). Peptides were synthesised to >70% purity (GL Biochem Shanghai Ltd.)

and reconstituted in DMSO to 30 mM. Truncated peptides used to map minimal epitopes, alanine scan and anchor SLA substituted peptides were designed and synthesised to >40% purity (GLS Biochem Shanghai Ltd.) and reconstituted in DMSO to 20 mM. All peptides were soluble in DMSO and stored at -20°C or -80 °C as DMSO stocks (20 - 30 mM) and working concentrations of peptides were made in R0 medium. Peptides used for *in vitro* protein refolding were synthesised to >90% purity (Peptide Protein Research Ltd, U.K.).

### 2.2.8   *Generation of Influenza peptide-specific T-cell lines and clones*

Porcine PBMC samples were defrosted and separated into CD8β+ and CD8β- cell populations as described above. The CD8β+ cells were plated 50,000 cells per well in 50 µL of priming medium in 96 multiwell round bottom plates. The autologous CD8β- cells were resuspended in priming medium (50 µL per 200,000 cells) and incubated with either DMSO (control) or an influenza peptide pool (3 µM with respect to each individual peptide within a pool) at 37 °C for 1 h before irradiation at 3000-3100 rad. These cells were then plated at 50 µL per well on top of the CD8β+ cells. The CD8β+ cell lines were cultured for two weeks and fed with 100 µL priming medium twice a week. They were then tested for peptide responses using intracellular cytokine staining. Where the percentage of peptide responsive T-cells was relatively high the line could be used directly for T-cell cloning. T-cell clones were procured by limiting dilution whereby typically 0.5 cells were plated per well in a 96 multiwell round bottom plate for expansion. In some instances, 1 cell was distributed per well to account for the low viability of porcine T-cells in culture. Following expansion set up, cloning plates were fed on day 7 and day 14 with 50 µL expansion medium before being tested for peptide reactivity.

### 2.2.9   *Porcine T-cell clone expansion*

Porcine T-cell clones were routinely expanded typically every 2-3 weeks in 96 multiwell round bottom plates. For established T-cell clones, 1000 cells were plated per well with 200,000 irradiated feeder cells in a total of 100 µL of expansion medium with phytohaemagluttinin (PHA) (Remel, ThermoFisher Scientific) added at 1-4 µg/mL. Feeder cells were defrosted allogeneic PBMC from 3 'feeder' pigs mixed together in an equal ratio and irradiated at 3000-3100 rad. Feeder cells were washed in R0 medium after irradiation and re-counted. Expansions were fed at day 5 and day 10 with 100 µL of expansion medium. At least two weeks of culture were required before the T-cell clones were used for assays, further expansion or frozen for storage. T-cell clones were usually harvested and counted at day 14 and plated at $1x10^6$ cells per well in 48 multiwell plates. The clones were maintained in culture where required by feeding them every 4-5 days.

## 2.2.10 CFSE labelling of cells

CD8β+ T-cells or PBMC were washed twice with PBS before being resuspended in PBS; this volume was varied depending on the cell numbers that were used. CFSE dye (eBioscience) was added at a final concentration of 2 µM. Cells were protected from light and labelled at 37°C for 10 min. R10 medium was then added to stop the reaction and the cells were washed. Cells were then used as required and protected from light during cell culture.

## 2.2.11 Kidney cell line culture

The embryonic kidney cell line, ESK-4, expresses both SLA-1*14:02 and SLA-2*11:04 (formerly known as SLA-1*es11 and SLA-2*es22) molecules (Ho et al. 2009) as found in the Babraham pig line. ESK-4 cells were obtained from the 'European Collection of Authenticated Cell Cultures' and cultured in APC-1 medium. Babraham pig kidney cells were isolated by Dr. Liz Reid at the Pirbright Institute and cultured in APC-2 medium at Cardiff University. The culture medium was changed every 7 days or as required and cells were passaged upon reaching confluency. Adherent cells were detached from tissue culture flasks by firstly aspirating off any medium before gently rinsing the cells with calcium and magnesium chloride–free Dulbecco's PBS (Life Technologies). This was followed by incubation with either pre-warmed Dulbecco's PBS mixed with 0.05% Trypsin-EDTA (1X) (manufacturer formulated; 25300054; Life Technologies) or TrypLE™ Express (Life Technologies) at 37˚C, until the cells detached. The former was only used during routine culture and the latter used routinely or when cells were being harvested for use in assays. Gentle tapping was used to encourage cell detachment.

## 2.3 Porcine Flow Cytometry and Functional Assays

### 2.3.1 Compensations, acquisition and analysis

Anti-mouse Ig antibody compensation beads (BD Biosciences) were used to prepare individual compensations for each fluorochrome used in any experiment. However, when using CFSE labelling it was necessary to use the relevant cells instead for fluorochrome compensations. Unless otherwise stated all staining steps were performed in the dark. All data were acquired on a BD FACSCanto II flow cytometer using FACSDiva software (both BD Biosciences). Fluorescence-activated cell sorting (FACS) was performed on a BD FACSAria (BD Biosciences) operated by central biotechnology services (Cardiff University). All data analyses were performed using FlowJo version 10.0 (TreeStar Inc., U.S.). Typically, T-cell clones were gated on for single, viable CD8β+ lymphocytes then displayed as histograms of tetramer fluorescence

and PBMC samples were gated on single, viable CD14-CD3+CD4+CD8β+ lymphocytes and displayed in bivariate tetramer versus CD8β plots.

### 2.3.2  Antibodies

The following antibodies were used subject to each experiment:

| Host Species | Antibody | Clone | Supplier |
|---|---|---|---|
| Mouse | Purified anti-phycoerythrin (PE) | PE001 | Biolegend |
| Goat | Anti-mouse Ig (multiple absorption) PE | Polyclonal | BD Biosciences |
| Mouse | Anti-pig CD8β | PG164A | Kingfisher Biotech |
| Mouse | Anti-pig CD3ε PE-Cy7 | BB23-8E6-8C8 | BD Biosciences |
| Mouse | Anti-pig CD4 Alexa Fluor 647 (AF647) | 74-12-4 | BD Biosciences |
| Mouse | Anti-human* CD14 PB | TUK4 | Bio-Rad |
| Mouse | Anti-pig CD8β FITC | PPT23 | Bio-Rad |
| Mouse | Anti-human* TNFα PerCP | MAb11 | Biolegend |
| Mouse | Anti-pig MHCI | 74-11-10 | Kingfisher Biotech |
| Mouse | Anti-pig MHCII | MSA3 | Kingfisher Biotech |
| Mouse | Anti-pig CD4 | MIL17 | # |
| Mouse | Anti-pig CD8α | MIL12 | # |
| Mouse | Anti-pig TCR-γδ | PPT16 | # |
| Mouse | Anti-pig CD3ε | PPT3 | # |

*These antibodies have been shown to be cross reactive to pigs.*
*# These mouse monoclonal antibodies (Yang et al. 1996; Yang et al. 2005; Gerner et al. 2015) were kindly provided as supernatants by Prof. Mick Bailey; University of Bristol.*

### 2.3.3  Surface marker staining of porcine T-cell clones

T-cell clones were placed in 5 mL FACS tubes (Elkay Laboratory Products Ltd., U.K.) and washed in PBS (700 $x$ $g$ for 3 min) and stained in approximately 50 μL of residual PBS with 1 μL LIVE/DEAD Violet stain (Life Technologies) (diluted 1:40 in PBS) at room temperature for 5 min, before incubation on ice for 20 min with either of the following antibodies; 0.8 μL anti-pig CD4, 3 μL anti-pig CD8α, 5 μL anti-pig TCR-γδ, 1 μL anti-pig CD3ε (all supernatants), 0.5 μL anti-pig CD8β, 0.5 μL anti-pig MHCI or 0.5 μL anti-pig MHCII. Cells were then washed with FACS buffer and all labelled with 2 mg/mL (0.1 mg/sample) anti-mouse Ig-PE on ice for 20 min. The wash step was then repeated and the cells resuspended in FACS buffer for analysis.

### 2.3.4 Intracellular cytokine staining (ICS) and TAPI-0 assays

T-cell lines were washed in R0 medium prior to activation. Cells were incubated in a 96 round bottom plate together with 1 µL/mL brefeldin A (GolgiPlug; BD Biosciences), 0.7 µL/mL monensin (GolgiStop; BD Biosciences) and 2 µM peptide(s). The cells were incubated at 37°C for 5 h before being washed with PBS three times (700 $x g$ for 3 min). Porcine T-cells were then stained with 1 µL LIVE/DEAD Violet stain (Life Technologies) (diluted 1:40 in PBS) at room temperature for 5 min, and then with 10 µg/mL (0.5 µg/sample) anti-pig CD8β on ice for 20 min. The wash step was repeated with FACS buffer followed by the addition of 1 µg/mL (0.05 µg/sample) anti-mouse Ig-PE on ice for 20 min. The PBS wash step was repeated and cells were fixed and permeabilised with 100 µL BD Cytofix/Cytoperm solution (BD Biosciences) on ice for 20 min. All wash steps were performed from this point on with 10% BD PermWash buffer (BD Biosciences). Following another wash step, the cells were incubated with 2.4 µg/mL (0.12 µg/sample) anti-human TNFα PerCP per well on ice for 20 min before a further wash and resuspended in PBS for acquisition. For TAPI-0 assays cells were co-incubated with peptide, 10 µM TAPI-0 (Calbiochem) and 1 µL anti-TNFα at the start of the experiment in 100 µL of medium per well. Cells then received the relevant surface antibodies and could either be used for analysis or for FACS, as this method does not kill the cells unlike ICS.

### 2.3.5 Peptide-SLA multimer assembly

Soluble biotinylated pSLA were assembled into tetramers by the successive addition of streptavidin-R-PE conjugate (Life Technologies) over five separate 20 min steps. A molar streptavidin:pMHC ratio of 1:5 was used requiring 0.015 mM of pMHC to 0.003 mM of streptavidin-R-PE conjugate. This required 6.25 µL PE conjugate (1 mg/mL) per 5 µg pMHC monomer (1.25 µL added per step). Following assembly, tetramers were made to a final concentration of 0.1 µg/µL (with respect to the pMHC component) with PBS. Tetramers were stored in the dark at 4 °C and used within 3 days of assembly and protease inhibitors (set 1; Merck, London, U.K.) were added to the final solutions. Multimers were always spun for 1 min before each use to remove any aggregates.

### 2.3.6 'Boost' antibodies

Following multimer staining cells were washed in FACS buffer and labelled with 10 µg/mL (0.5 µg/sample) unconjugated anti-PE Ab (termed 1° Ab) on ice for 20 min. Cells were then washed twice in FACS buffer and labelled with 2 µg/mL (0.1 µg/sample) anti-mouse Ig-PE (termed 2°

Ab) on ice for 20 min. The conjugated fluorochrome here corresponds to that used in the pMHC multimer. Each Ab was spun for 1 min before use to remove any aggregates.

### 2.3.7 Tetramer staining of porcine T-cell clones

T-cell clones were stained in 5 mL FACS tubes either with or without incubation with 50 nM protein kinase inhibitor (PKI) (Dasatinib, Axon Medchem) at 37°C for 30 min. PKI treatment was followed directly by 0.3 μg (with respect to the pMHC component) of tetramer on ice for 30 min before a PBS wash. Next they received, in approximately 50 μL of residual PBS, 1 μL LIVE/DEAD Violet stain (Life Technologies) (diluted 1:40 in PBS) at room temperature for 5 min, before incubation on ice for 20 min with 1.5 μL anti-pig CD8β-FITC. Cells were then washed and resuspended in FACS buffer for analysis.

### 2.3.8 Ex vivo tetramer staining of porcine PBMC, BAL and TBLN samples.

PBMC, BAL or TBLN samples were stained in 5 mL FACS tubes; for PBMC no more than $2 \times 10^6$ cells were allocated per tube. Cells were incubated with 50 nM PKI at 37°C for 30 min followed directly by 0.3 μg tetramer on ice, both for 30 min. PKI was stored in 1 mM one-use aliquots at -20°C and dilutions were made up fresh for each experiment. Next, cells were washed and received 10 mg/mL anti-PE on ice for 20 min. Cells were then washed with PBS and stained in approximately 50 μL of residual PBS with 2 μL LIVE/DEAD Violet stain (1:40 dilution) at room temperature for 5 min followed by surface antibodies (fluorochrome conjugated) on ice for 20 min; 1.5 μL anti-pig CD3ε PE-Cy7, 3 μL anti-pig CD4 AF647, 2 μL anti-human CD14 PB and 1.5 μL anti-pig CD8β FITC. Cells were washed and resuspended in PBS for data acquisition. Where required cells were fixed at this stage with 2% paraformaldehyde (PFA) on ice for 20 min. Tetramer positive cells could also be isolated at this point using FACS.

### 2.3.9 Enzyme Linked Immunosorbent Assay (ELISA)

Porcine T-cell clones were harvested and washed in R0 medium before incubation for 6 h in pig R5 medium. During this incubation in pig R5 medium, the cells are exposed to reduced serum and no cytokines in the culture medium which limits the spontaneous release of cytokines and chemokines during the activation assay. Cells were then washed in R0 medium prior to activation. Cells were incubated at 37°C overnight in pig R5 medium with either peptide(s) ($10^{-4}$ to $10^{-12}$ M), medium alone or 10 μg/mL PHA (positive control). All conditions were typically performed in duplicate. The following day cells were pelleted by centrifugation and 50 μL of culture supernatant was harvested per well and diluted with 70 μL R0 medium (dilution factor

= 2.4) either for immediate use or frozen storage. ELISA half-well flat bottom microplates (Corning Costar) were coated with 50 μL (1.5 μg/mL) anti-swine MIP-1β polyclonal Ab (Kingfisher Biotech) and incubated at room temperature overnight. ELISA plates were washed between each step using an automated microplate washer with wash buffer (0.05% Tween 20-PBS). ELISA plates were blocked with reagent diluent (1% BSA-PBS) for at least 1 h before incubation for at least 75 min with 50 μL supernatant or protein standards; swine MIP-1β recombinant protein (Kingfisher Biotech) titrated from 2000 to 31.25 pg/mL in reagent diluent. Next, plates were incubated with 50 μL (0.4 μg/mL) biotinylated anti-swine MIP-1β polyclonal Ab (Kingfisher Biotech) for at least 75 min, followed by HRP-conjugated streptavidin, substrate solution (reagents A and B mixed 1:1) and stop solution as per the manufacturer's instructions (DuoSet, R&D systems). The $OD_{450nm}$ of the wells was read using a Bio-Rad iMark microplate reader with correction set to 570 nm. The protein standards were used to generate a linear regression line equation enabling the calculation of MIP-1β released in each sample.

### 2.3.10 IFNγ Enzyme Linked ImmunoSpot (ELISpot) assay

ELISpot plates (MultiScreen$_{HTS}$ IP filter sterile (MSIPS4510) PVDF plates, Merck Millipore) were coated with 50 μL mouse anti-pig IFNγ Ab (clone P2G10, BD Biosciences), diluted to 5 μg/mL in PBS, per well and incubated at 37 °C for 4 h wrapped in cling film. Plates were washed 5 times with 250 μL PBS per well and blocked for at least 1 h at RT with 100 μL R10 medium per well. PBMC and BAL samples were defrosted as previously described and plated in R5 medium at ~300,000 and 150,000 cells per well respectively. Peptide was added to give a final concentration of $10^{-5}$ M per well. H1-S-FLU was used at 3.5 x $10^6$ TCID$_{50}$, UV inactivated Sw/Sp was used at ~1.8 x $10^6$ TCID$_{50}$/mL alongside the MDCK supernatant control and live MDCK cell-grown A/Sw/Eng/1353/09 used at titre 6 x $10^7$ pfu/mL. Where possible all conditions were performed in duplicate and every well was made up to a final volume of 100 μL pig R5 medium. The plates were incubated at 37 °C for 16-18 h, washed 3 times with 150 μL PBS and incubated with 100 μL sterile $H_2O$ per well at RT for 10 min before two further washes. Plates were incubated with 50 μL biotinylated mouse anti-pig IFNγ Ab (clone P2C11, BD Biosciences), diluted to 1 μg/mL in PBS, per well at RT for 2 h. The plates were protected from light during this and proceeding incubation steps. Plates were then washed 5 times with PBS before incubation with 50 μL (1:1000) Streptavidin-Alkaline phosphatase (BioRad) per well at RT for 2 h before being washed a further 5 times with PBS. Plates were then developed according to the manufacturer's instructions (AP conjugate substrate kit, BioRad). Briefly, 25X AP colour development buffer was combined with AP-conjugate substrate reagents A and B in sterile $H_2O$ and 50 μL added per well. Plates were protected from light and left to develop until spots were

clearly visible (10-15 min) upon which the reaction was stopped by washing plates with tap water. Plates were left to air dry in the dark before an Immunospot analyser (Cellular Technology Limited, US.) was used to count the number of spots per well and the frequency of responding cells displayed graphically as spot forming cells (SFCs), per initial cell number.

### 2.3.11  Chromium ($^{51}$Cr) release cytotoxicity assay

Some parts of this assay were performed by Dr. Garry Dolton at Cardiff University, to meet radiation training requirements. ESK-4 cells were used here as target cells, washed twice in PBS then aspirated to give a dry pellet which was labelled with 30 μCi $^{51}$Cr (PerkinElmer, U.S.) per 1 x 10$^6$ cells at 37°C for 1 h. The target cells were then washed and resuspended in R10 medium and were pulsed either with peptide, ranging from 1 x 10$^{-5}$ to 10$^{-11}$ M, or without peptide at 37°C for 1 h. This h also allowed time for leaching of any excess $^{51}$Cr to occur. Target cells were then washed and plated at 2000 cells per well with 10,000 T-cells (effector cells) (incubated overnight in pig R5 medium) in a final volume of 150 μL of R10 medium. This gave an effector to target (E:T) ratio of 5:1. Conditions were all performed in triplicate and controls were also plated to account for spontaneous release (target cells alone) and maximum release (target cells in medium containing 2% Triton X). The cells were then incubated at 37°C for 4 h and overnight, at both points the plates were centrifuged at 300 *x g* for 5 min before 15 μL of supernatant was harvested from each well. The supernatants were transferred to 96-well polyethylene terephthalate plates (Perkin Elmer) containing 150 μL of Optiphase supermix scintillation cocktail (Perkin Elmer) per well. The plates were sealed and placed into a 1450-Microbeta counter (Perkin Elmer) for data collection. The % of target specific cell lysis = [(experimental – spontaneous $^{51}$Cr release)/(maximum release – spontaneous release) x 100]. Any $^{51}$Cr waste was disposed of per local standard operating procedures.

### 2.3.12  Combinatorial peptide library (CPL) screens

T-cell clones were harvested and washed in R0 medium before incubation in pig R5 medium for 6 h. Cells were then washed in R0 medium prior to assay use. Babraham pig kidney cells were used to act as an APC, following detachment 60,000 cells were plated for each condition. These cells were then incubated at 37°C for 2 h with a nonamer positional-scanning combinatorial peptide library (PS-CPL) screen in positional scanning format (Pepscan). This format sequentially fixes each peptide residue in turn for each L-amino acid, whilst the other positions are degenerate covering every amino acid combination. Cysteine is not included in the degenerate distribution to avoid disulphide bond formation and thus, peptide aggregation. The nonamer PS-CPL is divided into 180 different peptide mixes. Following APC incubation,

30,000 T-cells were added to each well and plates were then left at 37°C overnight. Responses to peptide mixes were identified by MIP-1β release detected by ELISA. Data were then input into a novel webtool (developed by Dr. Barbara Szomolay), PI-CPL, accessible at http://wsbc.warwick.ac.uk/wsbcToolsWebpage. The output ranked the different peptide sequences in order of the likelihood that they would be recognised by the cognate T-cell clone (Szomolay et al. 2016) and enabled optimal peptide sequences to be identified.

## 2.4   Generation of pMHCI complexes

### 2.4.1   *Protein sequences for Babraham pig MHCI molecules and porcine $\beta_2$m*

The following proteins (sequences provided by the Pirbright Institute) were synthesised with 5' EcoR1 and 3' BamH1 restriction sites and cloned into vector pUC57-Amp (Genewiz LLC, U.S.).

SLA-1*14:02 (formerly known as SLA-1*es11) **(**without/**with biotinylation site)**:

```
MGPHSLSYFSTAVSRPDRGDSRFIAVGYVDDTQFVRFDSDAPNPRMEPRAPWIQQEGQEYWDR
NTRNVMGSAQINRVNLKTLRGYYNQSEAGSHTLQWMYGCYLGPDGLLLRGYDQFAYDGADYLA
LNEDLRSWTAADMAAQISKRKWEAADAAEHWRSYLQGTCVESLRRYLQMGKDTLQRAEPPKTH
VTRHPSSDLGVTLRCWALGFHPKEISLTWQREGQDQSQDMELVETRPSGDGTFQKWAALVVPP
GEEQSYTCHVQHEGLQEPLTLRWDPGLNDIFEAQKIEWHE
```

SLA-2*11:04 (formerly known as SLA-2*es22) **(**without/**with biotinylation site)**:

```
MGPHSLSYFYTAVSRPDRGEPRFIAVGYVDDTQFVRFDSDAPNPRMEPRAPWIQQEGQDYWDR
ETQIQRDNAQTFRVNLRTALGYYNQSEAGSHTFQSMYGCYLGPDGLLLRGYSQYGYDSADYIA
LNEDLRSWTAADTAAQITKRKWEAADEAEQWRSYLQGLCVEGLRRYLEMGKDTLQRAEPPKTH
VTRHPSSDLGVTLRCWALGFYPKEISLTWQREGQDQSQDMELVETRPSGDGTFQKWAALVVPP
GEEQSYTCHVQHEGLQEPLTLRWDPGLNDIFEAQKIEWHE
```

Porcine $\beta_2$m:

```
MVARPPKVQVYSRHPAENGKPNYLNCYVSGFHPPQIEIDLLKNGEKMNAEQSDLSFSKDWSFY
LLVHTEFTPNAVDQYSCRVKHVTLDKPKIVKWDRDH
```

## 2.4.2 Reagents and Buffers used in these techniques

| Buffer | Composition |
|---|---|
| Agarose Gel | 1% agarose (Life Technologies) dissolved in double distilled $H_2O$<br>2.5 µL/50 mL of Midori Green Advanced DNA stain (Nippon Genetics Europe) added upon cooling |
| Biomix A | 0.5 M Bicine Buffer pH 8.3, 100 µL Biomix B (Avidity LLC, U.S.) |
| Biomix B | 100 mM ATP, 100 mM MgOAc, 500 µM Biotin (Avidity LLC) |
| BirA enzyme | biotin ligase (provided at 1mg/mL by Avidity LLC) |
| Carbenicillin | Always used at 50 µg/mL |
| Crystal buffer # | 10 mM TRIS pH 8.1<br>10 mM NaCl |
| Guanidine buffer | 6M guanidine<br>50 mM TRIS pH 8.1<br>100 mM NaCl<br>2 mM EDTA |
| Ion exchange buffer A # | 10 mM TRIS pH 8.1 (0.45 µm filtered) |
| Ion exchange buffer B # | As above but with 1 M NaCl |
| LB medium | 10 g/L tryptone (Fisher Scientific)<br>5 g/L yeast extract (Fisher Scientific)<br>5 g/L NaCl |
| LB agar medium | As above but with 15 g/L bacteriological agar (Oxoid) |
| Lysis buffer | 10 mM TRIS pH 8.1<br>10 mM MgCl$_2$<br>150 mM NaCl<br>10% glycerol (Sigma) |
| Refold Buffer # | 50 mM TRIS pH 8.1<br>2 mM EDTA pH 8<br>400 mM L-arginine<br>0.74 g/L cysteamine and 0.83 g/L cystamine added last |
| Non-reducing loading buffer | 125 mM TRIS pH 6.8<br>4% SDS<br>20% glycerol<br>20 µg/mL bromophenol blue |
| Reducing loading buffer | As above but with 10% DTT |
| Resuspension buffer | 50 mM TRIS pH 8.1<br>100 mM NaCl<br>10 mM EDTA |
| S.O.C medium (provided by Invitrogen ready-made) | 2% tryptone<br>0.5% yeast extract<br>10 mM NaCl<br>2.5 mM KCl<br>10 mM MgCl$_2$<br>10 mM MgSO$_4$<br>20 mM glucose |
| Triton wash buffer | 0.5% Triton X-100 (Fisher Scientific)<br>50 mM TRIS pH 8.1<br>100 mM NaCl<br>10 mM EDTA |
| TYP medium | 16 g/L tryptone<br>16 g/L yeast extract<br>3.3 g/L potassium phosphate dibasic (Acros organics)<br>5 g/L NaCl |

*# 0.45 µm filtered before use.*

### 2.4.3  Digestion of Babraham pig SLAI molecules and porcine $\beta_2$m inserts and pGMT7

Any water used throughout this protocol was nuclease-free. The Genewiz inserts were diluted with water to the concentration recommended by the manufacturer for each insert. Firstly, to digest the insert the following mix was incubated at 37°C for 2 h; 2000 ng insert, 0.5 μL BamH1, 0.5 μL EcoR1, 1 μL EcoR1 10x buffer and water to make a total volume of 10 μL. The whole digested samples were then separated by gel electrophoresis (70 V for 30 min) on a 1% agarose gel sat in Tris-acetate-EDTA buffer. A molecular weight marker was also ran in one well for size identification (HyperLadder I, Bioline). The DNA bands were then visualised with a transilluminator, the smaller of the two bands was excised as this was the insert. The DNA was purified using the Wizard SV Gel kit as per the manufacturer's instructions (Promega). Briefly, the gel slice was dissolved, washed and passed through an SV minicolumn into 30 μL water. The DNA concentration was then measured on a Nanodrop. pGMT7 was digested in a similar manner but starting with 1000 ng insert and before electrophoresis the digest was treated with Shrimp Alkaline Phosphatase (SAP) to prevent re-annealing. The pGMT7 digest was incubated at 37°C for 15 min with SAP and 10x SAP buffer followed by 2 min at 65°C. Appropriate controls were used for all digestions.

### 2.4.4  Ligation of digested SLAI and porcine $\beta_2$m inserts with pGMT7

The ratio of digested insert to pGMT7 vector was calculated using the following equation: [(amount of pGMT7 in ng X size of the insert in base pairs)/size of pGMT7 in base pairs] X 3 = amount of insert required ng. The resulting amounts of insert and vector were then combined with 2 μL T4 ligase buffer, 2 μL T4 ligase (New England BioLabs) and made up to 20 μL with water. This ligation mixture was left at room temperature for 2 h (or overnight). The ligation product was then isolated by gel electrophoresis as described above.

### 2.4.5  Sodium Dodecyl Sulphate-Polyacrylamide Gel Electrophoresis (SDS-PAGE)

The protein sample was combined with loading buffer in a 5:1 ratio and incubated at 90°C for <5 min then centrifuged briefly to collect condensation. The samples were loaded into pre-cast 10% Bis/Tris gel (NuPAGE, Invitrogen) immersed in 1x running buffer (NuPAGE, Invitrogen) along with a pre-stained protein ladder for reference (BLUeye, 10-245 kDa, Geneflow Ltd.). The gel was electrophoresed at 200 V for 20 min. Protein bands were visualised by staining the gel with 25 mL 'Quick Coomassie Stain' (Generon) followed by de-staining in water.

### 2.4.6 Transformation into E. coli and purification of plasmid DNA

2 µL of ligation mix was transformed into 20 µL of One Shot® (TOP10): *E. coli* (Invitrogen) competent cells being placed on ice for 5 min, 42°C for 2 min and a further 5 min on ice. Next, 200 µL of LB medium was added for 1 h incubation at 37°C 220 rpm in an orbital shaker (Sanyo, U.K.; MIR-222U) before the transformation mixture was plated on LB agar plates containing 50 µg/mL carbenicillin and left to grow overnight at 37°C. An empty pGMT7 vector was used as a control. The following day a selection of colonies were harvested and each placed into 12 mL LB medium containing carbenicillin and left overnight at 37°C 220 rpm (Sanyo; MIR-222U). Plasmid DNA was then isolated using the 'Zyppy plasmid miniprep kit' (Zymo Research) as per the manufacturer's instructions. The purified plasmid DNA was measured and then sent for sequencing, using T7 primers, by either CBS or Eurofins Genomics. Sequences were checked against the original insert to ensure the process had been successful, those that worked were then used to produce soluble protein in *E. coli.*

### 2.4.7 Production of soluble SLAI and $\beta_2$m in E.coli

SLAI and porcine $\beta_2$m plasmids were transformed into Rosetta$^{TM}$ 2(DE3) pLysS: *E. coli* (Novagen) competent cells as described above and cultured on LB agar plates containing carbenicillin overnight. Colonies were then placed into starter cultures, 1-3 colonies into 30 mL TYP medium with carbenicillin, and incubated at 37°C 220 rpm (Sanyo; MIR-222U) until the optical density (OD$_{600nm}$) reached 0.5. The starter cultures were transferred to 1 L of TYP medium supplemented with carbenicillin and incubated as before until OD$_{600nm}$ reached 0.5. Next, 0.5 mM isopropyl β-D-thio-galactoside (IPTG) (Fisher Scientific) was added to induce vector expression (in the form of inclusion bodies) and the cultures were left at 37°C 220 rpm (Sanyo; MIR-222U) for a further 3 h. Samples were taken before and after IPTG addition and between the proceeding steps to ascertain quality of protein expression by SDS-PAGE. Cells were harvested following centrifugation at 3450 *x g* for 20 min and resuspended in 40 mL of lysis buffer and sonicated (MS73 probe; Bandelin) at 60% power at 2 sec intervals for 20 min. The lysed cells were then incubated with 0.2 mg/mL DNase (Sigma) for at least 1 h at 37 °C 220 rpm (Sanyo; MIR-222U). The lysate was washed in 100 mL triton wash buffer with centrifugation at 15,180 *x g* for 20 min. The supernatant was discarded and the wash step repeated (the cell pellet was homogenised into the wash buffer). The final pellet was resuspended with homogenisation in 12 mL guanidine buffer and stored at -20 °C. The concentration was measured using a spectrophotometer (typically 5-25 mg/mL).

### 2.4.8    Refolding of peptide-SLAI complexes

The following were combined at 37°C for 15 min for a 1 L refold; 30 mg MHCI inclusion bodies and 30 mg $\beta_2$m inclusion bodies in guanidine buffer (see section 2.4.7), 4 mg peptide (>90% purity) and 10 mM DTT. This mixture was then added into the 1 L refold buffer, which was prepared in advance with the cysteamine/cystamine pair added at the final moment, and left stirring at 4°C overnight. The refold mixture was then transferred to dialysis tubing and placed in 10 mM TRIS pH 8.1 at 4°C (20 L per 1 L refold) and transferred to fresh 10 mM TRIS pH 8.1 the next day. The refold mixture was left to dialyse until the conductivity reached <2 mS/cm upon which it was removed from the tubing and filtered through a 0.45 μm (Fisher Scientific) filter before purification.

### 2.4.9    Purification of peptide-SLAI using Fast Protein Liquid Chromatography (FPLC)

Purifcation steps were carried out on an AKTA FPLC machine using the Unicorn software (GE Healthcare, UK). All buffers were 0.45 μm filitered before use. The refold mixture was initially loaded onto an anion exchange column (POROS 50HQ, Life Technologies) which had been washed in buffer B and equilibrated into buffer A at 20 mL/min flow rate (pressure limited to 5 MPa). The sample was eluted from the column into FPLC tubes (Greiner Bio-One) and then centrifuged in 4 mL Vivaspin concentrator tube (Sartorius) to < 1 mL. Samples were taken before concentration and analysed on SDS-PAGE to ascertain the presence of pMHC complexes before proceeding. Protein that was to be used for multimer staining was biotinylated at this point. The 1 mL sample was then loaded onto a Superdex HR 200-size-exclusion column (Amersham Pharmacia) equilibrated into the required buffer (PBS or crystal buffer) at 0.5 mL/min (pressure limited to 1.5 MPa). Again, the samples were eluted into FPLC tubes, tested with SDS-PAGE and concentrated then measured by spectrophotometry. The final protein concentration was calculated accounting for the extinction co-efficient of each protein combination (these were obtained using the ProtParam webtool accessible at http://web.expasy.org/protparam/). Biotinylated pMHC was aliquoted into one-use aliquots and stored at -80°C and pMHC for crystallography was used straight away.

### 2.4.10  Biotinylation of peptide-SLAI complexes

Peptide-MHC complexes that were made for use in multimer staining required biotinylation to enable streptavidin mediated multimerisation. Following anion exchange, the protein was concentrated down to 700 μL. The following reagents were added and left overnight at room temperature; 100 μL Biomix A, 100 μL Biomix B, 100 μL biotin and 2 μL BirA enzyme (3 mg/mL)

(all from Avidity LLC). The mix was then washed thoroughly in PBS, to remove excess biotin, and concentrated to 1 mL for further purification.

## 2.5 Crystallisation, diffraction data collection, structure solution and model refinement of Babraham pig SLA-I molecules

Peptide-MHCI (with either human or porcine $\beta_2$m) were concentrated down to around 10 mg/mL in crystal buffer. Crystallisation screens were set up using a Gryphon crystallography robot (Art Robbins Instruments, U.S.) via the sitting drop technique in 96-well Intelli-plates (Art Robbins Instruments). In summary, 60 µL of each screen condition was dispensed into the reservoirs, then a 1:1 ratio screen: protein volume was dispensed into the small well (0.2 µL of each). Protein crystals were grown by vapour diffusion at 18°C and visualised using RockImager and RockMaker software (Formalatrix, U.S.). The following crystallisation screens, consisting of 96 different buffer compositions, were set up for each protein; JBScreen Basic HTS (Jena Bioscience), PACT premier HT-96 (Molecular Dimensions) and TOPS (developed in-house at Cardiff; (Bulek, Madura, et al. 2012)).

Crystals were harvested by either Dr. Pierre Rizkallah or Dr. Dave Cole and placed into liquid nitrogen and transported to the Diamond Light Source, Oxfordshire, U.K., for X-ray diffraction data collection. Beamlines I02, I03, I04 and I04-1 were used for data collection. Data collection was performed by either Dr. Pierre Rizkallah or Dr. Dave Cole. All data analyses and structure resolution was performed by Dr. Pierre Rizkallah. Reflection intensities were estimated with XDS (Kabsch 2010) as implemented in the XIA2 package (Winter 2010) and the data were scaled, reduced and analysed with AIMLESS and TRUNCATE in the CCP4 package (CCP4 1994; Winn et al. 2011). All structures were solved by molecular replacement with PHASER (McCoy et al. 2007) using 3QQ3 as a starting model (Zhang et al. 2011). Sequences were adjusted with COOT (Emsley and Cowtan 2004) and the models refined with REFMAC5 (Murshudov et al. 1997). Graphical representations were prepared in PYMOL (The PyMOL Molecular Graphics System, Version 1.8 Schrödinger, LLC.). The five X-ray structures solved in this thesis were deposited into the Protein Data Bank (http://www.rcsb.org/pdb/). The models SLA-1-EFEDLTFLA-p$\beta_2$m, SLA-1-DFEREGYSL-p$\beta_2$m, SLA-2-IAYERMCNI-p$\beta_2$m, SLA-1-EFEDLTFLA-h$\beta_2$m and SLA-1-DFEREGYSL-h$\beta_2$m were assigned accession codes 5NPZ, 5NQ0, 5NQ2, 5NQ3 and 5NQ1 respectively.

## 2.6 TCR sequencing of porcine T-cell clones

All sequencing methods were performed by Dr. Meriem Attaf, Cardiff University.

### 2.6.1 Total RNA extraction

T-cell clones were washed in PBS, aspirated and resuspended in 200 µL of Trizol and frozen at -80°C. RNA was then extracted using phase separation with all centrifugation steps performed at 4°C. Briefly, 40 µL chloroform was added per sample and centrifuged at 12,000 *x g* for 5 min upon which the aqueous (upper) phase was harvested for incubation with 100% propan-2-ol, followed by centrifugation for 10 min. The resulting pellet was then washed in 70% ethanol and once dried resuspended in RNAse-free water at 55°C for 15 min.

### 2.6.2 SMARTer™ RACE cDNA amplification

cDNA was generated using the SMARTer™ (Switching Mechanism at 5' end of RNA Transcript) RACE (Rapid Amplification of cDNA Ends) kit (Clontech) as per the manufacturer's instructions. Extracted RNA was incubated with 1 µL 5' RACE CDS Primer (in a total volume of 10 µL) at 72°C and 42°C for 3 and 2 min respectively. Each sample then received a mastermix, containing 4 µl 5X First Strand buffer, 0.5 µl DTT (100 mM), 1 µl dNTP (20 mM), 0.5 µL RNAse Inhibitor (20 U) and 2 µL SMARTScribe RT (100), and 1 µL SMARTer II oligo A primer. Samples were then incubated at 42°C and 70°C for 90 and 10 min respectively. cDNA samples were stored at -20°C.

### 2.6.3 PCR amplification

In the first PCR, cDNA was amplified for the entire variable and part of the constant regions for TCRα or TCRβ. The following PCR 'master mix' was used: 2 µL of cDNA sample, 10 µL Phusion® 5x Green buffer, 0.5 µL 100 mM DMSO, 1 µL 20mM dNTPs, 5 µL 10X Universal Primer A (forward primer), 1 µL TRAC or TRBC primer (reverse primer), 0.25 µL Phusion® HF DNA polymerase and 30.25 µL $H_2O$ to give a final volume of 50 µL. The following reverse primers were used for TRAC and TRBC respectively; 5'-GCAGGTTAAACCCAACCATTTTCAGG-3' and 5'-GAGACCCTCAGGCGGCTGCTC-3'. Samples were incubated at 94°C for 5 min for initial denaturation followed by 30 cycles of 94°C for 30 sec, 60°C (TCRα) or 65°C (TCRβ) for 30 sec and 72°C for 90 sec, and finally incubated at 72°C 10 min for final extension. A second PCR was then performed using 2 µL sample from the first PCR with the same incubations and 'master mix' as above but with the following nested primers for TRAC and TRBC respectively; 5'-CTGCCGGAAGGTGCTTTGACATTC-3' and 5'-TGTGGCCAGGCACACCAGTGTG-3'. Samples were

then electrophoresed on a 1% agarose gel in Tris-acetate EDTA (TAE) buffer and correctly sized DNA bands extracted and purified using the Wizard SV Gel kit (Promega) as per the manufacturer's protocol.

### 2.6.4    Molecular cloning, bacterial transformation and colony PCR

PCR products were cloned into a PCR-Blunt II-TOPO® vector using the Zero Blunt® TOPO® PCR cloning kit (Life Technologies) according to the manufacturer's instructions. The following reaction was incubated at RT for 5 min then placed on ice; 4 µL PCR product, 1µL salt solution and 1µL vector. Next, 2 µL of the TOPO® cloning reaction was transformed into 20 µL of One Shot® (TOP10): E. coli (Invitrogen) competent cells; placed on ice for 30 min, 42°C for 30 sec and a further 2 min on ice. Then 250 µL of S.O.C medium (Invitrogen) was added for 1 h incubation at 37°C 220 rpm (Sanyo; MIR-222U) before the transformation mixture was plated on LB agar plates containing 50 µg/mL carbenicillin and left to grow overnight at 37°C. Individual colonies only contain one *tr* sequence. Individual colonies were screened by colony PCR using the following mix (primers at 10 µM stock); 1 µL M13 forward primer (5'-TTTTCCCAGTCACGAC-3'), 1 µL M13 reverse primer (5'-CAGGAAACAGCTATGAC-3') and 23 µL DreamTaq® Green master mix. This reaction underwent thermocycling as follows: 94°C for 10 min for initial denaturation followed by 27 cycles of 94°C for 30 sec, 57°C for 30 sec and 72°C for 90 sec, and finally incubated at 72°C for 10 min. Samples were electrophoresed on a 1% agarose gel and positive bands were extracted, purified and sent to Eurofins Genomics for sequencing.

### 2.6.5    Analysis of sequenced TCR cDNA

Sequences were visualised using ApE software (M. Wayne Davis) and compared between clones to determine sisterhood for future experiments. Sequence data is displayed in chapter 3, **Table 3.1**. At the time of writing this thesis the pig TCR loci had not been fully sequenced and annotated, therefore no database currently existed for defining the TCRα and β gene segment usage in these clones.

## 2.7 Human Studies

### 2.7.1 Human cell culture media and buffers

In addition to those already described in section 2.2.1 the following media was used in human
T-cell culture:

| Media | Composition |
|---|---|
| **Human T-cell expansion medium** | R10 medium supplemented with:<br>10 mM HEPES buffer<br>0.5X MEM Amino Acids<br>1 mM Sodium pyruvate<br>25 ng/mL Human IL-15 (PeproTech)<br>20 IU or 200 IU/mL IL-2 |

### 2.7.2 Human PBMC, T-cell clones and cell lines

Human fresh blood samples were obtained by venepuncture from volunteers (heparinized) or
buffy coats (EDTA treated) from the Welsh Blood Service in accordance with the appropriate
ethical approval and informed consent. The latter were also utilised as 'feeder' cells for human
T-cell expansion. PBMC were isolated as described in section 2.2.2. T-cell clones and Tumour
Infiltrating Lymphocytes (TILs) were cultured in human T-cell expansion medium. T-cell clones
were expanded in T25 culture flasks (Greiner) in 15 mL medium as follows; 0.5-1 x $10^6$ T-cell
clone, 15 x $10^6$ irradiated 'feeder' PBMC (combined from 3 donors) and 1 µg/mL PHA. The CD8+
T-cell clones listed below were used along with tumour infiltrating lymphocytes (TILs) that
were derived from a successful immune response to melanoma (Ellebaek et al. 2012). Spiked
samples were created by mixing clonal T-cells (1 x $10^4$) with defrosted PBMC (1 x $10^6$). The
spiked PBMCs were minimally HLA matched for the restricting HLA of the spiking clone (HLA
HLA-A*0201).

| Clone Name | MHC restriction | Epitope Target | Epitope Sequence | Residues | Reference |
|---|---|---|---|---|---|
| **ILA-1** | HLA-A*0201 | Human telomerase-derived peptide (hTERT) | ILAKFLHWL<br>ILAKFLHEL (8E)<br>ILALFLHWL (4L)<br>ILAKYLHWL (5Y)<br>ILGKFLHWL (3G) | 540-548 | (Purbhoo et al. 2007) |
| **1E6 & 3F2** | HLA-A*0201 | Preproinsulin (PPI) | ALWGPDPAAA | 15-24 | (Skowera et al. 2008; Bulek, Cole, et al. 2012) |
| **VB6G4.24** | HLA-A*0201 | Melan A | ELAGIGLTV (heteroclitic residue underlined) | 26-35 | (Tungatt et al. 2015) |

### 2.7.3   pHLA multimer assembly

Tetramers were assembled as described in section 2.3.5. Dextramers (Immudex Limited, Copenhagen, Denmark) consist of a dextran polymer backbone with covalently linked streptavidin molecules and fluorochromes. Dextramer-PE conjugates on average each contain 3 fluorochromes and 6 streptavidin molecules (Dolton et al. 2014). For each batch of dextramer backbone the manufacturer calculates the number of streptavidin molecules per dextran molecule. This information was required to assemble the final dextramers; monomeric pMHC was added at a molar ratio of 3:1 with respect to the streptavidin component. Dextramers were then left at room temperature for 30 min protected from light.  Following assembly, dextramers were diluted, stored and used as described for tetramers, except instead of PBS they received dextramer buffer (0.05 M Tris-HCL, 15 mM NaN3, 1% BSA, pH 7.2).

### 2.7.4   Peptide-HLA Tetramer staining

In addition to those already described in section 2.3.2, the following antibodies were used:

| Host Species | Antibody | Clone | Supplier |
| --- | --- | --- | --- |
| Mouse | Anti-human CD3ε PerCP | BW264/56 | Miltenyi Biotech |
| Mouse | Anti-human CD8α PE | BW135/80 | Miltenyi Biotech |
| Mouse | Anti-human CD8α APCy | BW135/80 | Miltenyi Biotech |
| Mouse | Anti-human CD8α PE-Vio770 | BW135/80 | Miltenyi Biotech |
| Mouse | Anti-human CD8α APC-Vio770 | BW135/80 | Miltenyi Biotech |
| Mouse | Anti-human IFNγ APCy | 45-15 | Miltenyi Biotech |
| Mouse | Anti-human CD19 PB | HIB19 | Biolegend |
| Mouse | Anti-human CD14 PB | M5E2 | Biolegend |
| Mouse | Anti-HLA-A2 APCy | BB7.2 | eBioscience |

Tetramer (0.3 or 0.5 µg per stain) or dextramer (0.3 µg) staining was performed as described in sections 2.3.7 and 2.3.8 with or without PKI treatment, anti-PE Ab and anti-mouse Ig-PE. Typically, $0.5\text{-}1 \times 10^5$ of a T-cell clone and $1\text{-}3 \times 10^6$ TILs, PBMCs, T-cell line, or spiked samples, were stained in 5 mL FACS tubes. The following surface marker antibodies were used; anti-human CD3, CD8, CD19 and CD14. Typically, PBMC samples were gated on for size, single cells, viable CD19-CD14-CD3+ lymphocytes and displayed in bivariate CD8 versus tetramer/dextramer plots. T-cell clones were typically gated on for size, single cells, viable CD8+ lymphocytes then displayed as histograms of tetramer fluorescence.

### 2.7.5 Intracellular Cytokine Staining

Tumour infiltrating lymphocytes (TILs) were incubated in R5 medium for 24 h prior to activation. Subsequently, cells were incubated at 37˚C for 4 h, with and without autologous tumour cells, at a 1:1 ratio, in 2 mL R5 medium (24 well culture plate with a total cell density of 3-6 x $10^6$/mL) (cells were moved to FACS tubes prior to staining) containing GolgiStop and GolgiPlug reagents as described previously, section 2.3.4. However, these cells underwent tetramer staining prior to cell surface marker staining (anti-human CD3 and CD8) and received 0.75 μL anti-human IFNγ per sample.

### 2.7.6 Tetramer decay assays

The CD8+ T-cell clone, 3F2, (5 x $10^5$) was pre-treated with PKI then stained with cognate tetramer with and without both anti-PE (1° Ab) and anti-mouse Ig-PE (2° Ab). Cells were washed with FACS buffer, supernatant aspirated, and incubated with 10 μg anti-HLA-A2 Ab or diluted in 3 mL buffer and incubated at room temperature in the dark. PKI was present throughout some of the decay assays. Cells were sampled at various time points, washed with excess FACS buffer, and fixed with 4% PFA.

### 2.7.7 Production of biotinylated pHLA monomers

HLA-A2 and human $β_2$m plasmids had already been previously generated in the lab and were ready for inclusion bodies production and protein refolding performed as described in sections 2.4.7, 2.4.8, 2.4.9 and 2.4.10.

## 2.8 Figures and Data Analysis

Data analysis and figures were produced using GraphPad Prism 5 (GraphPad Software Inc., La Jolla, U.S.) or Microsoft Office™ Excel.

# 3  Optimisation of Porcine T-cell culture and cloning

## 3.1  Background

There are no published studies using porcine T-cell clones and, as far as I am aware, porcine T-cells had never been cultured *in vitro* for longer than 3 weeks when I initiated my studies. I aimed to study porcine T-cell responses to Influenza A virus (IAV).  Ideally, this required development of long-term culture techniques for porcine T-cells as is available for the more established human and murine models of infection. This study was run in collaboration with the Pirbright Institute (Dr. Sophie Morgan, Dr. Hanneke Hemmink, Dr. Maria Montoya, Dr. Bryan Charleston and Dr. Elma Tchilian) and the School of Veterinary Sciences, Bristol University (Dr. Emily Porter and Prof. Mick Bailey). The former provided access to the Babraham large white, inbred pig line that is 85% identical by genome wide SNP analysis. This pig was selected as the model to be used throughout this study. Babraham pigs all express identical MHC-I and MHC-II alleles which is an invaluable trait for immunological studies as it allows adoptive transfer of immune cells between individuals and enables the use of smaller numbers of animals per group than required for most studies using outbred pigs. Furthermore, use of the Babraham pig line meant I could quickly determine MHC-I restriction of any influenza epitopes identified and that I could expect similar T-cell responses in all animals. A previous study immunised Babraham pigs with human pdmH1N1 vaccines which induced high levels of antibody and, following *in vitro* stimulation of PBMC samples, induced proliferation of CD8β and CD4 T-cells and IFNγ production (Lefevre et al. 2012).

For initial optimisation experiments performed in this chapter, I was provided with PBMC and spleen cells from Babraham pigs that had been inoculated with inactivated SwIV [A/Swine/Spain/SF11131/2007 (H1N1)] (Sw/Sp) with montanide adjuvant (Seppic, Air Liquide Healthcare, France). Two doses were administered intramuscularly 28 days apart. Previous unpublished data had shown PBMC from these inoculated pigs responded to overlapping peptides (by IFNγ ELISpot) derived from the influenza NP of a human IAV strain [A/Panama/2007/1999 (H3N2)]. These peptides are referred to as "pool 2 peptides" and consist of 26 peptides (numbered 27–52) ranging from 15 to 20 amino acids in length and each overlapping by 10 amino acids. This peptide pool was provided by the Pirbright Institute. The use of overlapping peptides in conserved epitope identification shall be discussed further in chapter 4.

## 3.2 Hypotheses

- The expertise on human T-cell culture within my laboratory group can be applied to develop successful long-term culture of porcine T-cells for the first time.

- Medium conditions and T-cell expansion protocols can be enhanced for optimal porcine T-cell culture.

- Culturing porcine T-cells at the body temperature of pigs and not that of humans will be optimal for porcine T-cell culture.

- Porcine T-cell culture techniques can be applied to procure influenza-specific T-cell lines and clones.

## 3.3 Results

### 3.3.1 Human T-cell culture translation to porcine T-cell culture

My first attempt at culturing porcine T-cells was with PBMC samples cultured with PHA in 12 different media conditions. The cell culture medium used in human T-cell culture in our lab contains several components including 10% serum (FBS), IL-2, IL-15. I decided to test three different serums (FBS, commercial porcine serum and in-house porcine serum), and two concentrations of each IL-2 (20 IU or 200 IU) and swine IL-15 (25 or 50 ng/mL). This gave 12 different culture media compositions which were tested along with two different concentrations of PHA (0.5 or 1 μg/mL). Most human T-cell clone expansions in our lab are performed with 1 μg/mL PHA. 500 PBMC with 100,000 feeders and PHA were seeded in 30x 96-round-bottom plates per condition and monitored for proliferation. This experiment was duplicated for PBMC from two different Babraham pigs. Initial optimisation experiments were assessed by eye in terms of the number of wells containing live cells and rating the extent to which any cell population filled the microscope field of vision. After two weeks of culture it was clear by eye that FBS and commercial porcine serum were not conducive to cell survival or proliferation. Consequently, I only used in-house product, produced from blood collected at the Bristol Veterinary School abattoir, for further experiments. There may now be other good commercial sources of porcine serum available that could be tested for porcine T-cell culture as this would certainly make things easier in the future. In these initial experiments, there were no substantial differences noted between 0.5 or 1 μg/mL PHA and the higher concentrations of IL-2 and IL-15 looked preferable but required further clarification. Overall expansion of PBMC was mediocre.

My next step was to isolate CD8β T-cells and test expansion conditions on this cell subset independently, as cytotoxic T-cells were the focus of this study and I also wished to see if they would survive in culture better than whole PBMC samples. CD8β cells were isolated from PBMC using magnetic cell sorting with CD8β Ab, PE-conjugated secondary Ab and anti-PE beads. CD8β T-cells were cultured as above with 3 different concentrations of PHA (1, 2 or 4μg/mL), either 20IU or 200IU of IL-2, and either 25 or 100 ng/mL IL-15. Following two weeks of culture, those cells in the lower (20IU) IL-2 were dying but any difference between IL-15 concentrations was unclear. In this expansion 1 μg/mL PHA was optimal so this concentration was used going forward.

## 3.3.2   T-cell culture temperature optimisation

Pigs have higher body temperatures than that of humans (37°C) with healthy Babraham pig temperatures averaging at 38.6 ± 0.2°C (Lefevre et al. 2012). Therefore, I wished to examine whether varying the standard incubator temperature used in human T-cell culture (37°C) would improve proliferation rates in porcine T-cells. PBMC from an unvaccinated Babraham pig were labelled with the cell proliferation dye carboxyfluorescein succinimidyl ester (CFSE) and cultured in the presence of 1μg/mL PHA at 37°C and 38.5°C in expansion medium containing 300IU IL-2 and 50 ng/mL IL-15. CFSE passively diffuses into cells where its acetate groups are cleaved by intracellular esterases enabling it to covalently couple by its succinimidyl group with intracellular amines. This process forms fluorescent conjugates that are retained within the cell which are divided equally between progeny following cell division allowing detection of successive cell divisions (Lyons and Parish 1994). Samples were taken for comparison at three different time points and stained with CD3 Ab and analysed by flow cytometry (**Figure 3.1**). The percentage of CD3+ proliferating lymphocytes showed no substantial difference between the two temperatures at each time point; at day 13 84.4% and 83.7% of cells were proliferating at 37 °C and 38.5 °C respectively. The proliferation profiles at each temperature were also similar across the three time points (**Figure 3.1B**). Further comparisons quantifying clone procurement and growth between the two temperatures did not suggest substantial differences (data not shown) and I concluded that there was no advantage in using 38.5 °C; all subsequent experiments were conducted at 37 °C.
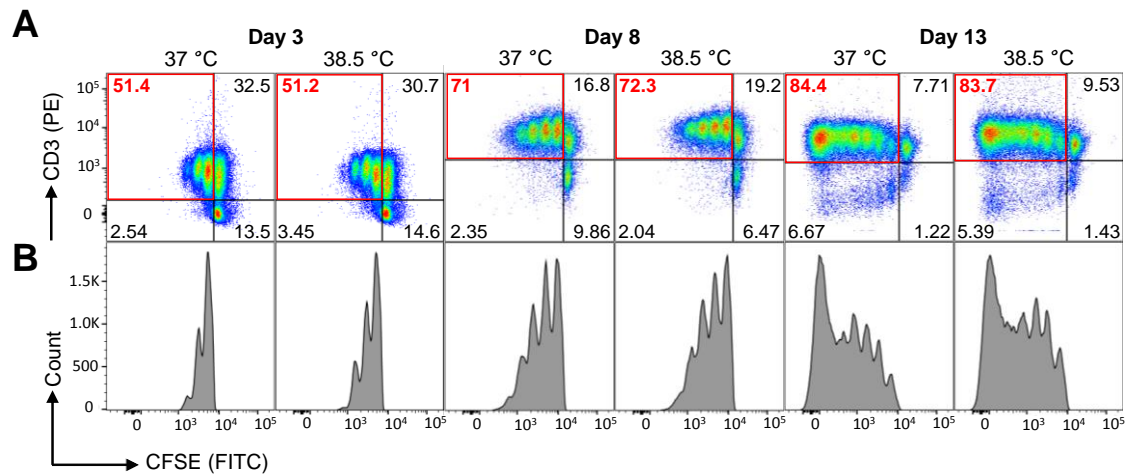
**Figure 3.1. PHA induced proliferation of porcine CD3+ cells was similar at 37°C and 38.5°C.**
**A)** CFSE-labelled PBMC from an unvaccinated Babraham pig was cultured with PHA, IL-2 and IL-15 in 48-well plates. PBMC were stained for CD3 (unconjugated CD3 Ab with PE-conjugated secondary Ab) at three different time points (day 3, 8 and 13). Cells were gated on for size and viability and are displayed as a pseudocolour dot plot. The percentage of cells found in each quadrat is displayed inset. Red boxes highlight CD3+ dividing cells. **B)** Histograms displaying the CFSE staining from the CD3+ dividing cell population.

### 3.3.3    Influenza-specific line and clone generation – preliminary studies

Following the extensive optimisation discussed above, I then wished to test these culture conditions on relevant samples from pigs inoculated with inactivated SwIV [A/Swine/Spain/SF11131/2007 (H1N1)] (Sw/Sp) with montanide adjuvant to see whether I could culture influenza-specific T-cells. CD8β T-cells were separated from other PBMC with the latter then used as autologous 'feeder' cells that were pulsed with peptides or DMSO (control) prior to irradiation. The use of this protocol is well established in my laboratory for use with human PBMC samples.

Initial experiments isolated CD8β T-cells from PBMC from pig#563. A peptide pool 2 specific line was established and visualised by CFSE proliferation (**Figure 3.2A**). 86.5% of viable cells were CFSE-low compared to the control of 21.5%. The line was analysed for IFNγ responses, by ELISpot, using the individual peptides from pool 2 and peptide 40 was identified as a promising candidate (**Figure 3.2B**). I next tried to grow monoclonal T-cells from the T-cell line that reacted to peptide pool 2 using medium containing 10% in-house porcine serum, 300 IU IL-2 and 50 ng/mL IL-15. Peptide pool 2-specific clones were procured successfully and shown to respond to peptide 40 from this pool (limited cell numbers prevented testing all the individual peptides).

Following unsuccessful attempts to detect IFNγ response by ELISA, I then decided to measure macrophage inflammatory protein (MIP)-1β as previous studies have found that it provides an extremely sensitive readout for human CD8+ T-cells (Price et al. 1998). Clones KT32.563 and KT47.563 both released copious MIP-1β in response to Pool 2 (1802.4 ± 25.9 and 1129 ± 123.4 pg/ml respectively) and to peptide 40 (1308.8 ± 105.1 and 836.5 ± 7.6 pg/ml respectively) (**Figure 3.2C**). Consequently, I concluded that MIP-1β was also a good readout for porcine cytotoxic T-cells and made use of this sensitive assay going forward. KT32.563 and KT47.563 both stained positively for CD8β and negatively for CD4 and TCRγδ confirming their cytotoxic T-cell like phenotype (**Figure 3.2D)**. To the best of my knowledge these are the first porcine Influenza-specific T-cell clones ever successfully grown in culture. These results provided confidence that my project aims might be possible.

Interestingly, I also procured a further clone, KT10.557, from these experiments that released large amounts of MIP-1β (2448.5 pg/ml) in response to peptide pool 2 (**Figure 3.3A**). The response to the peptide pool was narrowed down to peptide 43 which induced very high MIP-1β release (4858.2 pg/ml) (**Figure 3.3B and C**). Unexpectedly, T-cell clone KT10.557 was negative for CD8β and found to be a CD4+ antigen experienced (CD8α+) helper T-cell (**Figure 3.3D**). The cloning of this first ever porcine helper T-cell confirmed that my initial selection of only CD8β+ cells was not watertight. I next investigated the response of KT10.557 to truncated versions of peptide 43 by MIP-1β ELISA (**Figure 3.3E**). Peptides were titrated to reveal the optimal peptide length. The best responses were observed to the index peptide, peptide 43 which is 20 amino acids in length, and the carboxyl terminus (C)-2 peptide truncation which induced 3129.5 and 3004.7 pg/ml MIP-1β release respectively at $10^{-7}$ M peptide. When shorter peptides were tested than those displayed in **Figure 3.3E**, no MIP-1β response was detected at any peptide concentration. The strongest response measured for clone KT10.557 was to the 20aa peptide.
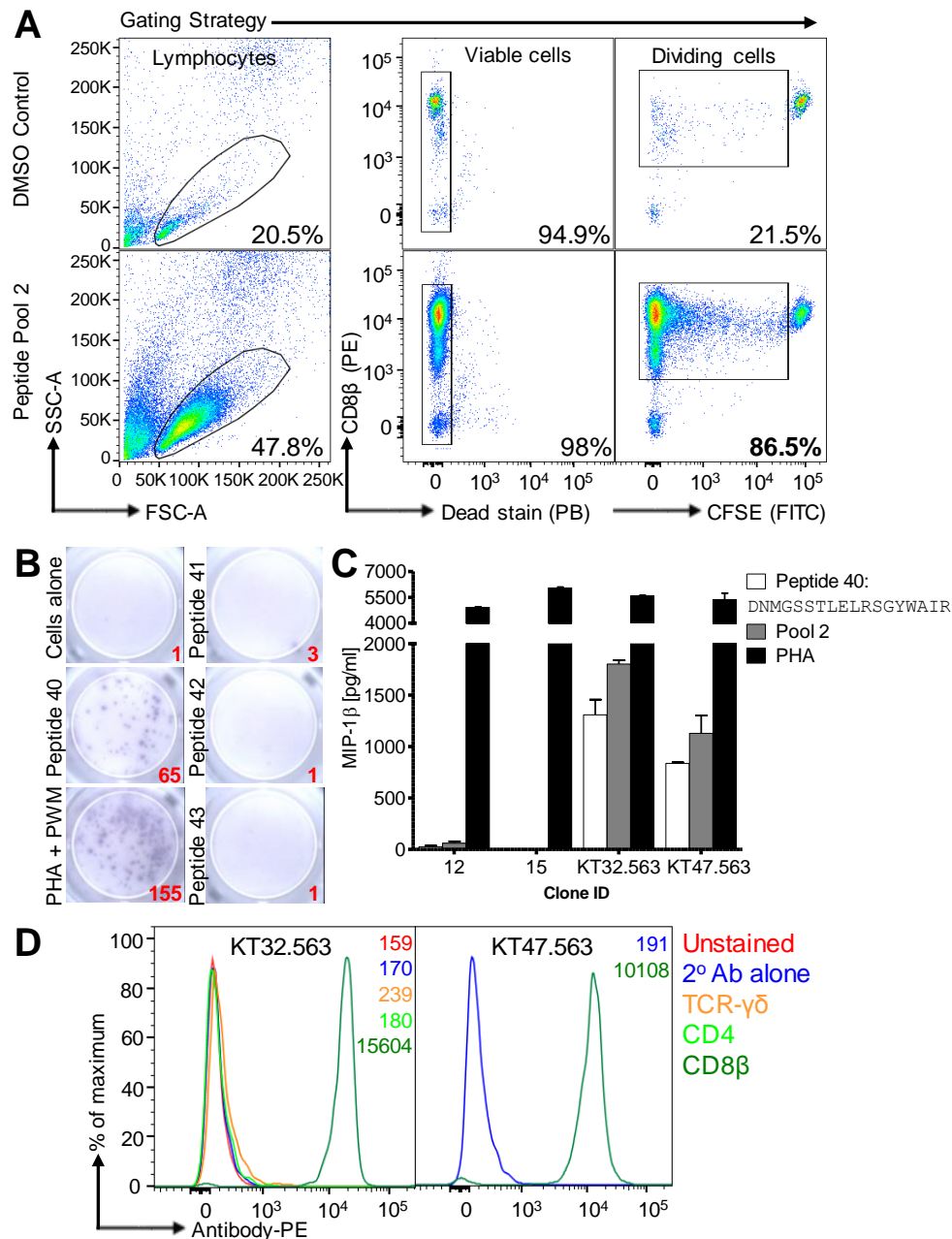
**Figure 3.2. Influenza-specific cytotoxic T-cell clones procured from pig#563 inoculated with inactivated H1N1 (Sw/Sp) virus.**
**A)** CD8β cells were cultured with Pool 2 peptides (26 overlapping peptides derived from the nucleoprotein from a human IAV H3N2 strain) and 20IU IL-2 and analysed after two weeks. As displayed cells were gated on for size and viability. The % of cells in each gate is shown inset. **B)** The T-cell line generated in (A) was incubated with the individual constituent peptides of peptide pool 2 and IFNγ release detected by ELISpot. ~ 15,000 T-cells were plated per well along with 50,000 irrelevant PBMC from an unvaccinated Babraham pig, except for the positive control where T-cells were incubated alone with 30 µg/mL PHA and 20 µg/mL Pokeweed mitogen (PWM). **C)** T-cell clones were procured and analysed by ELISA for MIP-1β release following exposure to peptide pool 2 (5 µg/mL of each peptide), an individual peptide (50 µg/mL) from this pool (peptide 40: DNMGSSTLELRSGYWAIRTR) and PHA (10 µg/mL) as a positive control. Conditions were performed in duplicate and data are displayed as mean + SD, with all final values minus the background response (cells alone). Clones 12 and 15 are displayed to demonstrate healthy but unreactive clones. **D)** Clones KT32.563 and KT47.563 were stained for cell surface markers (unconjugated in combination with PE-conjugated secondary Ab) and analysed by flow cytometry to confirm their cytotoxic phenotype. Mean fluorescence intensities are displayed inset.

48
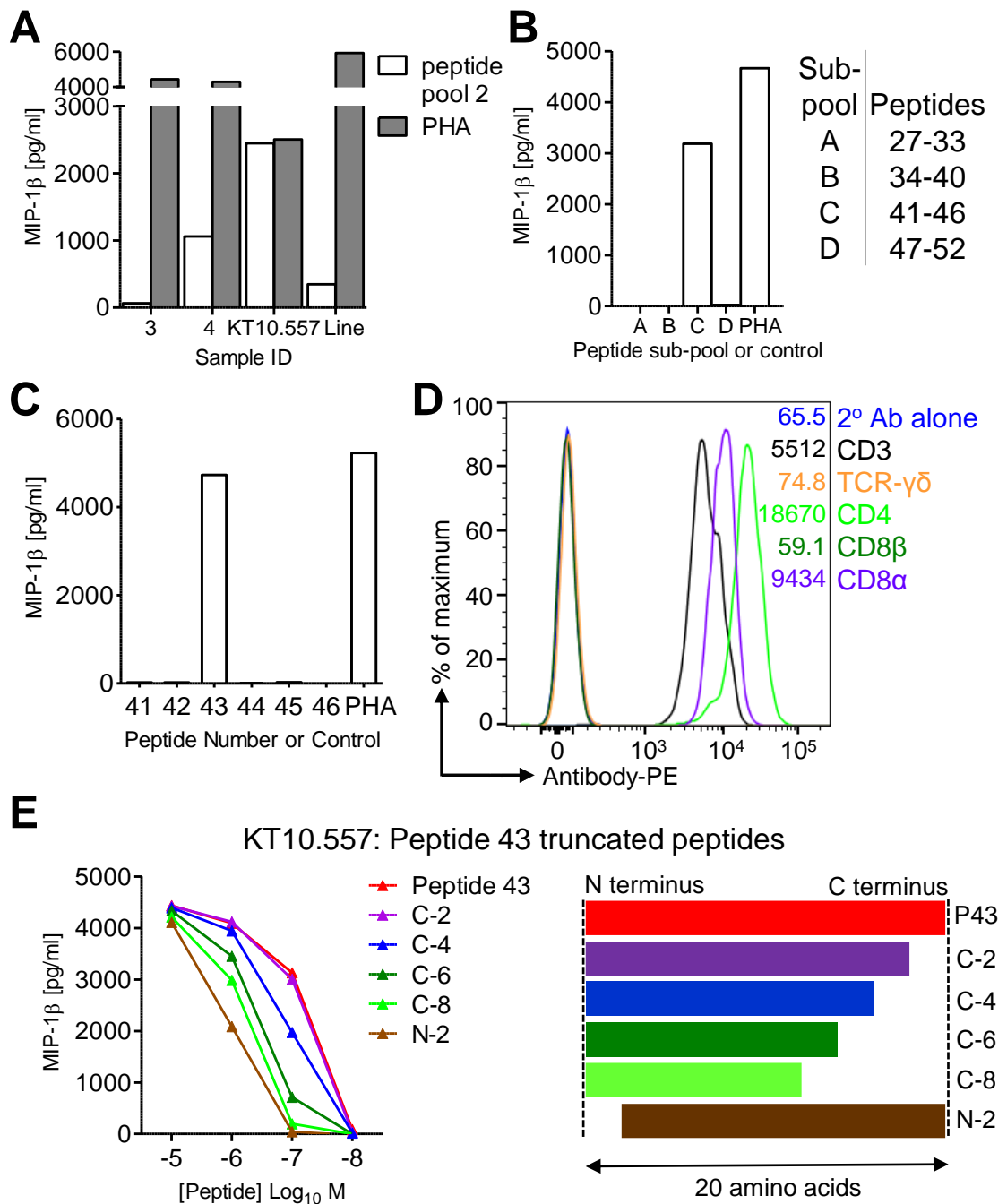
**Figure 3.3. Influenza-specific helper T-cell clone procured from pig#557 inoculated with inactivated H1N1 virus.**
**A)** T-cells were cultured with Pool 2 peptides (26 peptides each overlapping by 10 amino acids derived from the nucleoprotein from a human IAV H3N2 strain) and low 20IU IL-2. T-cell clones were then procured from this line and analysed, along with the line itself, by ELISA for MIP-1β release following exposure to peptide pool 2. All ELISA data are displayed as means minus the background response (cells alone) with PHA used as a positive control. **B & C)** Clone KT10.557 was analysed to ascertain which peptide it was responding to; MIP-1β ELISA data are shown for sub-pools and then individual constituent peptides. **D)** KT10.557 was stained for cell surface markers and analysed by flow cytometry. Mean fluorescence intensities are displayed inset. **E)** MIP-1β release by KT10.557 incubated with indicated concentrations of peptide 43 (NQQRASAGQISVQPTFSVQR) and truncated peptide derivatives. The truncated peptides design is displayed with C (carboxy terminus) and N (N terminus) indicating which peptide terminus the amino acids have been removed from. MIP-1β was not released in response to shorter peptides (data not shown).

### 3.3.4  Optimisation of T-cell cloning

The expansion rate of the T-cell clones was not as high or consistent as required or that can be achieved with human T-cell clones. I therefore undertook further optimisation experiments. Initial expansions were performed using 1000 cells of a T-cell clone with 100,000 'feeder' cells per well. This seems to work well and attempts to seed more clone per well or to expand in cell culture flasks produced lower expansion rates. Basic optimisations calculating overall fold expansion rates demonstrated that using less than 100,000 feeders per culture well decreased expansions rates, from 31 to 18.3x, and less than 1000 T-cells could be seeded per well if required (**Figure 3.4A)**. The concentration of IL-15 was also further optimised and following two consecutive clonal expansions it was clear that lower concentrations were preferable, with 12.5 and 25 ng/mL inducing 38.8x and 30.6x fold expansion respectively in the $2^{nd}$ expansion compared to 3.6x with 50 ng/mL IL-15 (**Figure 3.4B**). From this point on, lower concentrations of IL-15 were adopted for all T-cell clone expansions.

I also wished to reaffirm PHA as the choice of mitogen and to ensure that it was being used at an optimal concentration. A T-cell clone was expanded in different concentrations of either PHA or Pokeweed mitogen. Expansion rates after two weeks of culture showed that PHA was the superior mitogen inducing at best 57.5x fold expansion, whereas Pokeweed mitogen induced at best 15x fold expansion (**Figure 3.5A**). The best PHA concentrations, 1, 2 and 4 µg/mL were taken forward through to a second expansion and cultured in the usual 96 round-bottom well plates as well as 24-well plates and T25 culture flasks (**Figure 3.5B**). The former again facilitated the best T-cell clone expansion rates (37x versus 30x and 12x) and during this passage PHA used at 4 µg/mL induced greater fold T-cell clone expansion (37x) than when used at 2 or 1 µg/mL (23x and 1x respectively). This T-cell clone was then passaged again with different starting cell numbers, 500-16,000, in 96U well plates (**Figure 3.5C**). The best expansion rates were observed with 500, 1000 or 2000 T-cell clone seeded per well (69x, 41.5x and 23.7x respectively at 2µg/mL PHA). In this case 1000 or 2000 seeded cells would induce the highest total cell yield per well. A recent expansion I performed also showed a similar pattern where the starting clone number displayed the following hierarchy in expansion rates 1000>500>2000 (18.5x, 17.1x and 13x respectively). The fold expansion is similar for 500 or 1000 cells/well in this comparison and accounting for total cell yield this data would suggest 2000 cells/well would be optimal.
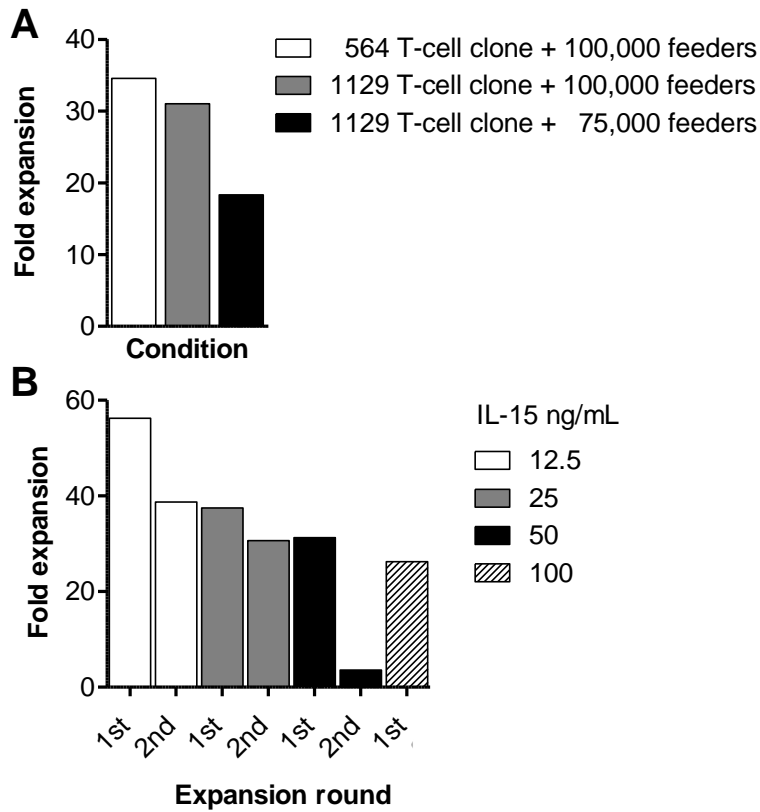
**Figure 3.4. Optimisation of cell numbers and IL-15 concentration in T-cell clone expansions.**
T-cell clones were expanded with 1 μg/mL PHA in expansion medium containing 300IU IL-2, 50 ng/mL IL-15 (in panel A) and 10% pig serum. Following two weeks of culture T-cell clones were counted and total fold expansion calculated. **A)** The same T-cell clone was expanded in three different clone and feeder cell ratios in 180-360 wells each. **B)** The same T-cell clone was expanded at 1000 cells per well plus 100,000 feeder cells over two consecutive expansions. Each condition was performed across 16 wells for the 1st expansion and 32 wells for the 2nd. 100 ng/mL IL-15 was not carried forward for the second expansion.
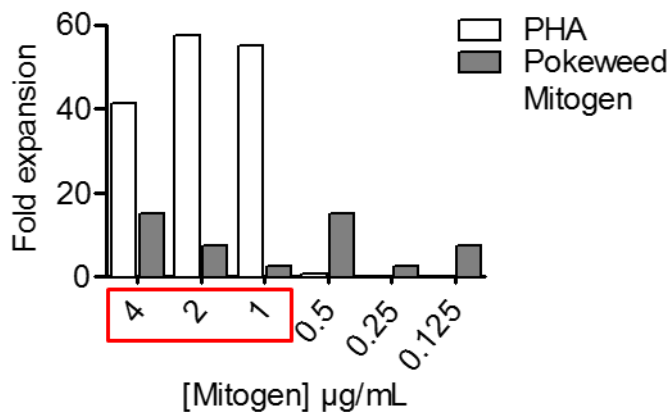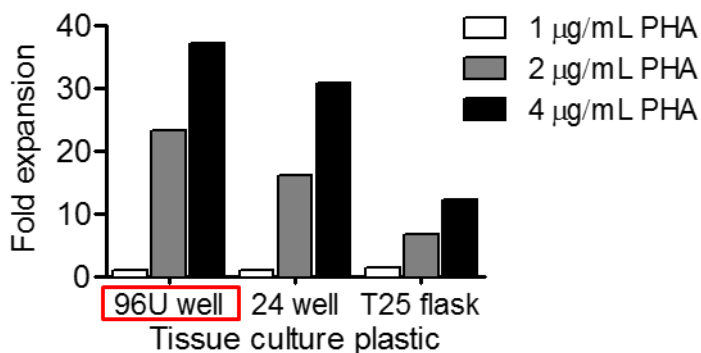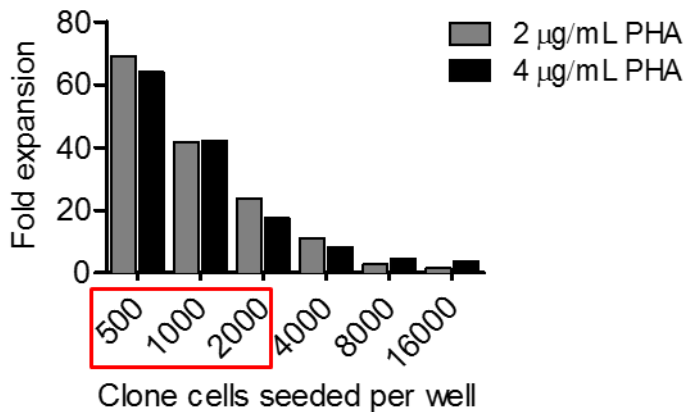
**Figure 3.5. Optimisation of mitogens, tissue culture plastic ware and seeding density on T-cell clone expansions.**

Different culture conditions were tested on a cytotoxic T-cell clone over three consecutive passages. The best conditions in each are highlighted in red. **A)** Each condition comprised eight 96U wells, with 1000 cells of T-cell clone, 100,000 irradiated 'feeder' PBMCs from three pigs and either PHA or pokeweed mitogen at the indicated concentrations. Cells were observed every 2-3 days under a light microscope to observe healthy T-cells. Expanding T-cells were evident with 1 and 2 μg/mL PHA from day 5-6 onwards, whereas those that grew with 4 μg/mL of PHA and pokeweed mitogen did not appear until day 8-10 onwards. At day 13 each condition was counted and the fold expansion is shown. **B)** T-cells that were expanded using conditions determined in (A) with either 1, 2 or 4 μg/mL of PHA were re-expanded with the PHA concentration used in (A), but expansions were performed across 96U well plates, 24 well plates and T25 flasks. **C)** T-cells that were expanded as in (B) with either 2 or 4 μg/mL of PHA were re-expanded but seeded from 500-16000 cells per 96U well as displayed (8 wells per condition).

### 3.3.5 T-cell clones and epitopes used in study

Numerous cytotoxic T-cell clones were procured during this study and shall be discussed further in proceeding chapters. Each clone was assigned a clone name, the second part of which corresponds to the number ID of the pig the clone was derived from. E.g. KT47.563 was procured from pig#563 samples. Preliminary TCR sequencing was performed by Dr. Meriem Attaf on T-cell clones to determine clonality and 'sisterhood' which helped direct which clones to use in further experiments. The TCR CDR3 sequences are displayed in **Table 3.1** for each clone. As discussed already in chapter 2, in-depth analysis of TCR clonotypes was not pursued as at the time of this study no database was established to easily assign TCR chains in swine, like that already available for human and mouse.

**Table 3.1. Cytotoxic T-cell clones procured during this study grouped by their SLA-I restricted epitope and preliminary TCR sequencing data.**

| Epitope Sequence | SLA-I restriction | Clone Name | CDR3α | CDR3β |
|---|---|---|---|---|
| not defined | unknown | KT32.563 | | |
| | | KT47.563 | | |
| EFEDLTFLA | SLA-1*14:02 | KTS.650 | CAVRGGYQKLVF | – |
| | | KLT.650 | CALSRKMNTGYQKLVF | – |
| | | KTe.650 | CALSRKMNTGYQKLVF | – |
| | | KTe2.650 | CALSRKMNTGYQKLVF | – |
| DFEREGYSL | SLA-1*14:02 | KT3.650 | CVLGGVWQFTF | – |
| | | KT4.650 | CVLGGVWQFTF | – |
| | | KT7.650 | CVLGGVWQFTF | – |
| | | KT12.650 | CVLGGVWQFTF | – |
| | | KT31.650 | CVLGGVWQFTF | – |
| | | KT37.650 | CVLGGVWQFTF | – |
| IAYERMCNI | SLA-2*11:04 | Sue.625 | CAMSVGSYAQSLT | CASSPGTGLIWNDLHF |
| | | Bab.625 | CALGGGNNRFTF | – |
| | | Ham.625 | – | CASSHTPTDNYGYTF |
| NGKWMRELI | SLA-2*11:04 | KT22.625 | CTLSEGDSGSRQLVF | – |
| | | KT13.650 | CALQGSGDKLTF | – |
| | | KT14.650 | CALQGSGDKLTF | – |
| | | KT16.650 | CALQGSGDKLTF | – |
| | | KTP.650 | CALQGSGDKLTF | – |
| | | KT36.650 | CAVNIGSFKYIF | – |

*"Sister" TCR clones are colour grouped. -: no sequencing data available*

## 3.4 Discussion

The initial focus of this study was to establish long-term culture of porcine T-cells lines and clones and methods for procuring and measuring cytotoxic T-cell clone responses. I demonstrated that proliferation was not enhanced by increasing incubator temperature from 37°C (human cell culture) to the average swine body temperature of 38.5°C. As such, all T-cell culture in this study was performed at 37°C because logistically this was preferable in accordance with the temperature we use for growing human and murine cells. I also adapted human T-cell expansion protocols to establish successful porcine T-cell line culture and clone procurement by testing different media conditions and mitogen concentrations to formulate an optimal culture medium. These conditions were successfully used to expand monoclonal populations of IAV-specific porcine T-cell clones for the first time. Preliminary experiments isolated cytotoxic T-cells, from pigs inoculated with inactivated Sw/Sp H1N1, capable of recognising a peptide pool (derived from NP). Flow cytometry was used to define the key surface phenotype of these cytotoxic T-cell clones (CD8β+, CD4- and TCRγδ-). The individual peptide from NP recognised by the clones KT32.563 and KT47.563 was identified as peptide 40; DNMGSSTLELRSGYWAIRTR NP$_{372-391}$. Unexpectedly I also cultured a CD4 T-cell clone, KT10.557, that recognises peptide 43; NQQRASAGQISVQPTFSVQR NP$_{397-416}$. Peptide truncations were designed and tested indicating that this CD4 T-cell clone preferentially recognises the longer peptides. This result is consistent with this clone being an MHC-II restricted CD4+ helper T-cell. As my primary aim was to examine cytotoxic T-cells, I did not undertake further studies with this clone. It remains backed up in liquid nitrogen storage in Cardiff in the hopes that it might be useful for future studies.

T-cell clones were regularly expanded throughout this study and maintained in culture using the methodology described above for months at a time. Small optimisation comparisons were run where possible, I demonstrated that using less than 100,000 feeder cells per expansion well decreased the fold expansion by around 40%. Although less T-cell could be seeded per well and a high expansion rate still achieved, the relative yield was still higher seeding ~1000 cells per well. The expansion rate when seeding half the number of cells would need to be double or more for this set up to give the highest overall cell yield. The majority of expansions were therefore carried out with 1000 clone and 100,000 feeders/well. For human T-cell culture our laboratory routinely uses IL-15 as it is known to enhance T-cell survival in our hands. I established that decreased IL-15 concentration in expansion medium dramatically increased fold expansion of porcine T-cells, this could be due to higher concentrations being detrimental or perhaps the high IL-2 concentration compensates for less IL-15. I continued to use IL-15 at low concentrations

to aid cell survival however future work could test whether any IL-15 is required for long-term, repeated expansions of porcine T-cell clones. Initial observations suggested that 1 µg/mL of PHA per expansion was optimal however a later experiment suggested 2 and particularly 4 µg/mL is superior. These concentrations are all rather similar and batch variations in the product activity probably explain the inconsistency. Overall, I opted to use 2 µg/mL PHA going forward. However, the concentration of PHA is not a ''one size fits all'' across porcine T-cell clones and it is best to regularly reassess this particularly if working with clones that grow poorly. T-cell expansion rates were highest when culturing the T-cell clones in 96U well plates, although further optimisation of 24 well plates could be explored. Porcine T-cell clones seeded at lower densities (500-2000 cells/well) gave the highest fold expansion rates and further increase in cell numbers was detrimental to total cell yield. Further optimisation could assess the use of more feeder cells per well. I witnessed varying growth rates across different porcine T-cell clones, this is also seen in human T-cell clones where some will have very high fold expansions and others will always yield low cell numbers.

The preliminary work discussed in this chapter was important for establishing successful experimental protocols for clone procurement and characterisation. However, these samples and data were superseded by more abundant and clinically relevant vaccinated pigs as shall be discussed in chapter 4. Although the protocols developed in this thesis were successful in generating the large T-cell clone expansions required for complex experiments, further optimisation would be desirable in future. As I still observed variation in growth within and across individual T-cell clone expansions, it is likely that further improvements to the protocol are possible, although as discussed below some variables are hard to control.

Our laboratory has extensive experience of growing clonal T-cells (Bulek, Cole, et al. 2012; Ekeruche-Makinde et al. 2012; Wooldridge et al. 2012; Ekeruche-Makinde et al. 2013; Dolton et al. 2014; Tungatt et al. 2015; Theaker et al. 2016; Tan et al. 2017) and its senior members have noted that successful culture of T-cells can depend on many factors. Testing serum (either human or bovine) is imperative, as batch-to-batch variations can prove problematic for successful cell culture. We witness greater variations between human serum donors and as such purchase large volumes of batch-tested bovine serum to aid uninterrupted human T-cell culture. Furthermore, the correct reconstitution, storage and handling of mitogens, cytokines and media additives are also of importance. Unknown variables, in particular, differences in the individual feeder cells can lead to success or failure during T-cell clone expansion phases. For human T-cell

expansion we use fresh PBMCs (less than 48 h post venipuncture) and adhere to good laboratory protocols by efficiently processing blood and keeping them on ice until used, as we find this leads to superior T-cell culture (personal communication, Dr. Garry Dolton). These T-cell clone techniques have been applied within our laboratory across different human T-cell subsets (αβ T-cells: CD8, CD4, CD4+/CD8+ and CD4-/CD8-. Also, γδ T-cells and MAITs), from different activations states (naïve and antigen experienced) from various sources, such as peripheral blood, ascites, synovia, TILs, adults, pediatric samples and patients with active disease such as HIV or type I diabetes (personal communication, Dr. Garry Dolton). Although T-cells are biologically capable of maintaining memory populations that can exist for years within the body it is harder to recapitulate this *in vitro* culture and is therefore a careful balance between finding a middle ground between neglect and overstimulation, both of which can lead to cell death. In light of this, the ability to grow human T-cell clones and maintain them correctly in order to conduct research requires training and skill, with the microscope being an important component in assessing when T-cells need to be re-stimulated.

Overall, I applied knowledge I gained through culturing T-cell clones from type I diabetes patients and advice from Professor Andrew Sewell and Dr. Garry Dolton to translate knowledge gained from culturing human T-cell clones to growing porcine clones. Overall, given some basic ingredients and approaches I think it would be possible to culture T-cells from other vertebrate species such as chickens, by applying what has been learnt from the culture of human and porcine T-cell clones. The study of T-cells from chickens and other poultry could be invaluable considering the virulence of bird influenza strains and the risks they pose for humans. In summary, the successful optimisations described in this chapter formed the cornerstone of my PhD work and enabled me to go on and perform a thorough initial characterisation of porcine T-cell responses to IAV.

# 4 <u>Identification of Influenza T-cell epitopes in pigs</u>

## 4.1 Background

Following on from the cell culture protocols established in chapter 3 for porcine T-cell culture, this chapter focuses on the identification of MHC-I IAV epitopes through procurement of IAV-specific cytotoxic T-cell lines and clones. This work used cryogenically stored PBMC, BAL and TBLN samples from a different cohort of vaccinated Babraham pigs than that used in the previous chapter. The PBMC samples used in chapter 3 were from pigs inoculated with inactivated H1N1 Sw/Sp virus whereas the samples in this chapter are from pigs vaccinated with both the inactivated Sw/Sp and S-FLU. S-FLU is a universal IAV vaccine candidate (Powell et al. 2012) which is currently being validated across different animal models and viral challenges, therefore making the study of these samples clinically relevant for vaccination studies. TBLN are the main draining lymph nodes of the lung and along with BAL samples allow investigation of local cellular immune responses.

S-FLU is a non-pathogenic pseudotyped Influenza virus, which has its HA-signal sequence suppressed therefore preventing the virus from replicating within the host (Powell et al. 2012). This suppression was achieved by replacing the start codon to prevent translation of the signal sequence. Two further mutations were made to safe guard in the event of the start codon returning. A single base was deleted within the signal sequence to create a frameshift (meaning the sequence would be translated out of frame) and the HA cleavage site was inactivated. The lack of a viable HA viral RNA means reassortment cannot occur with seasonal IAV strains (a source of antigenic shift), which is a risk associated with the use of live attenuated IAV vaccines. S-FLU virus expresses the internal proteins from the PR8 strain [IAV (A/PuertoRico/8/1934(H1N1))] and can be coated with a chosen HA, using a transfected complementing cell line, to enable initial host cell entry. The conserved internal proteins are expressed and can be processed and presented by the infected cells to T-cells without any risk of productive infection.

S-FLU has shown protective efficacy (in the absence of or low levels of neutralising antibodies) following homologous and heterologous viral challenge in both mice and ferrets and prevented airborne transmission in the latter (Powell et al. 2012; Baz et al. 2015). A notable induction of T-cell responses was observed in the lungs of S-FLU vaccinated mice detected *ex vivo* by responses

to a conserved NP epitope by IFNγ ELISpot or pMHC multimer staining. The vaccine candidate S-FLU has also been evaluated in outbred pigs, where immunisation reduced viral load upon homologous challenge in the absence of neutralising antibodies (consistent with the previous studies in mice and ferrets) (Morgan et al. 2016). This protection was correlated with strong local immune responses detected in the BAL following challenge. S-FLU administered by aerosol, targeting the lower respiratory tract, afforded the most effective protection and induced high numbers of IFNγ producing cytotoxic and helper T-cells in the lung. Further experiments are required to determine if these cells mediate the protection observed and to investigate if S-FLU can protect against heterologous challenge in pigs.

For this study two sows, pigs #625 and #650, were immunised with two doses of S-FLU intranasally and with inactivated SwIV Sw/Sp H1N1 with montanide adjuvant intramuscularly. The second dose (boost) of each was administered at day 25 and PBMC, BAL and TBLN were harvested at day 38 (day 13 post boost). I wished to identify conserved epitopes because, as previously discussed, they are important for conferring heterotypic immunity against influenza strains and have already been well documented in human IAV studies. Heiny and colleagues performed a comprehensive analysis of human and avian IAV protein sequences in the public database and found that viral proteins PB1, PB2, PA, NP and M1 were the most conserved historically, with many conserved regions evident across subtypes and host-origin (Heiny et al. 2007). Similar findings have been reported by other studies (ElHefnawi et al. 2011; DiPiazza et al. 2016). NP and M1 are major targets of cytotoxic T-cell responses in humans (Gotch et al. 1987) and have been widely investigated across numerous studies. The H1N1 M1$_{58-66}$ [GILGFVFTL] cytotoxic T-cell epitope has been well characterised in humans and is the immunodominant epitope found in HLA-A2 individuals (Gotch et al. 1987; Morrison et al. 1992). NP has long been identified as a key immunogenic protein in inducing cross-reactive cytotoxic T-cell responses (Townsend and Skehel 1984; Yewdell et al. 1985). Wu and colleagues screened PBMC from 8 healthy HLA-A2+ donors for CD8+ T-cell responses to 11 influenza proteins, and found NP (5 out of 8) and M1 (3 out of 8) to be immunodominant (Wu et al. 2011). This approach was extended in a further study using HLA-A2-negative donors that again demonstrated NP as the immunodominant protein (Grant et al. 2013). NP induced the highest CD8+ T-cell responses in 6 out of 7 donors. M1 and NP are highly abundant in Influenza virions; consistent with previous studies Hutchinson and colleagues detected by mass spectrometry NP at a mean abundance of 0.31 (relative to M1 protein – the most abundant) in Influenza A/WSN/33 virions (Hutchinson et al. 2014). These features and prior studies in humans and mice made NP and M1 prominent targets for epitope identification in my studies.

## 4.2 Hypotheses

This section of the study applied the ability to culture porcine T-cells long term (as developed in chapter 3) to identify cytotoxic T-cell responses to IAV vaccination in Babraham pigs, specifically identifying the epitopes (viral derived peptides) recognised by these T-cells in the context of pMHC-I complexes. I was interested in identifying responses to overlapping peptides from conserved Influenza proteins NP and M1. The hypotheses were as follows:

- Peptide specific cytotoxic T-cell lines can be obtained from PBMC isolated from pigs (#625 and #650) simultaneously immunised with inactivated virus and the vaccine candidate S-FLU.

- T-cell clones can be procured from these influenza-specific T-cell lines.

- Minimal epitopes (the shortest peptide inducing the highest response sensitivity) can be defined by identifying the individual peptide response followed by testing truncated versions.

- Influenza-specific CD8β T-cell clones will display cytotoxic activity when exposed to peptide.

## 4.3 Results

### 4.3.1 IAV-specific T-cell line procurement from pigs #625 and #650.

I initially set out to define T-cell epitopes from IAV NP and M1 in two pigs, #625 and #650, which had been vaccinated with H5-S-Flu and inactivated H1N1 Sw/Sp virus. To identify T-cell epitopes in this study, overlapping peptides were designed, by Dr. Garry Dolton, spanning the whole protein sequences of NP and M1 from S-FLU (**Table 10.1 & 10.2**). The peptides in this study were designed to be 18 amino acids in length, to facilitate identification of MHC-I as well as MHC-II epitopes in other studies, and overlapping by 12 residues to ensure no potential epitopes were missed. Responses were screened for using the NP and M1 overlapping peptides divided across 4 (A-D) and 2 (E-F) pools respectively. Peptide-specific cytotoxic T-cell lines were procured as discussed in chapter 3. During those preliminary experiments CFSE dye was used to detect proliferation in response to peptides, however the DMSO gave a high background of proliferating cells, e.g. in **Figure 3.2** 21.5% and 86.5% of cells proliferated in response to DMSO and the peptide pool respectively. To enable clearer distinction and quantification of genuine peptide responses I instead measured TNFα by ICS for testing the T-cell lines. Samples from T-cell lines were taken and incubated with the relevant peptide(s) or control for 5 h before cells then received the relevant surface antibodies and were analysed. This approach gave minimal

background when the T-cell lines were incubated with DMSO alone. Additionally, this experiment could also be run in the presence of TAPI-0 and TNFα Ab from the incubation step. The use of TAPI-0 (TNFα converting enzyme protease inhibitor) prevents the release of TNFα from the cell membrane allowing direct detection of TNFα producing cells by flow cytometry (Haney et al. 2011). This method does not kill cells, unlike ICS, so it allows isolation of viable, peptide-responsive T-cell populations by flow cytometry.

Cytotoxic T-cells were isolated from both pigs #625 and #650 PBMC and lines set up with all the NP and M1 peptide pools. Peptide-specific cytotoxic T-cell lines, as determined by ICS of TNFα production, were grown to NP peptide pools A, B and C for pig#625 (**Figure 4.1**) and peptide pools A and C for pig#650 (**Figure 4.2**). The other peptide pools (NP: D, M1: E and F) did not elicit responses during these experiments (data not shown). Once a response to a peptide pool had been identified the T-cell line was re-tested with the peptide pool and the individual peptides of that pool. This allowed identification of the individual peptides eliciting the cytotoxic T-cell response. This analysis was performed on the first batch of T-cell lines and the data are displayed in the appendix (**Figure 10.1**). A second batch of T-cell lines were established in larger numbers and the flow cytometry data is displayed in **Figures 4.1 and 4.2** and summarised in **Figure 4.3** for ease of interpretation. Substantial TNFα production was detected in response to peptide pools A (51.8% and 12.9% respectively in pig#625 and #650) and C (27.8% and 23.7% respectively in pig#625 and #650).  The response to peptide pool B in pig#625 was of lower magnitude (3.9%). Responses to peptide pools A and C, were mapped to overlapping peptides NP16 and NP17 and peptides NP42, NP43, NP48 and NP49 respectively, in both pigs (**Figure 4.3**). The high level of response in these T-cell lines to peptide pools A and C enabled direct T-cell clone procurement by limiting dilution.

For the peptide pool B specific T-cell line procured from pig#625, the response was identified as overlapping peptides NP36 and NP37. These peptides were then used to generate a new line (**Figure 4.1C**) from which T-cell clones were procured following isolation of TNFα+ cells by flow cytometry to account for their low abundance here (3.96 and 3.18% respectively for peptides NP36 and NP37). The following cytotoxic T-cell clones were procured from these samples (see **Table 3.1**): KT4.650 and KT7.650 recognising peptides NP48/49, KTS.650 and KLT.650 recognising peptides NP42/43, KT22.625 and KT13.650 recognising peptides NP16/17 and clones Sue.625 and Bab.625 recognising peptides NP36/37. The numbers 625 or 650 denote

which pig the T-cell clone was isolated from. These T-cell clones along with T-cell lines were then used to determine the minimal epitope that was recognised (**Figures 4.4 – 4.7**).
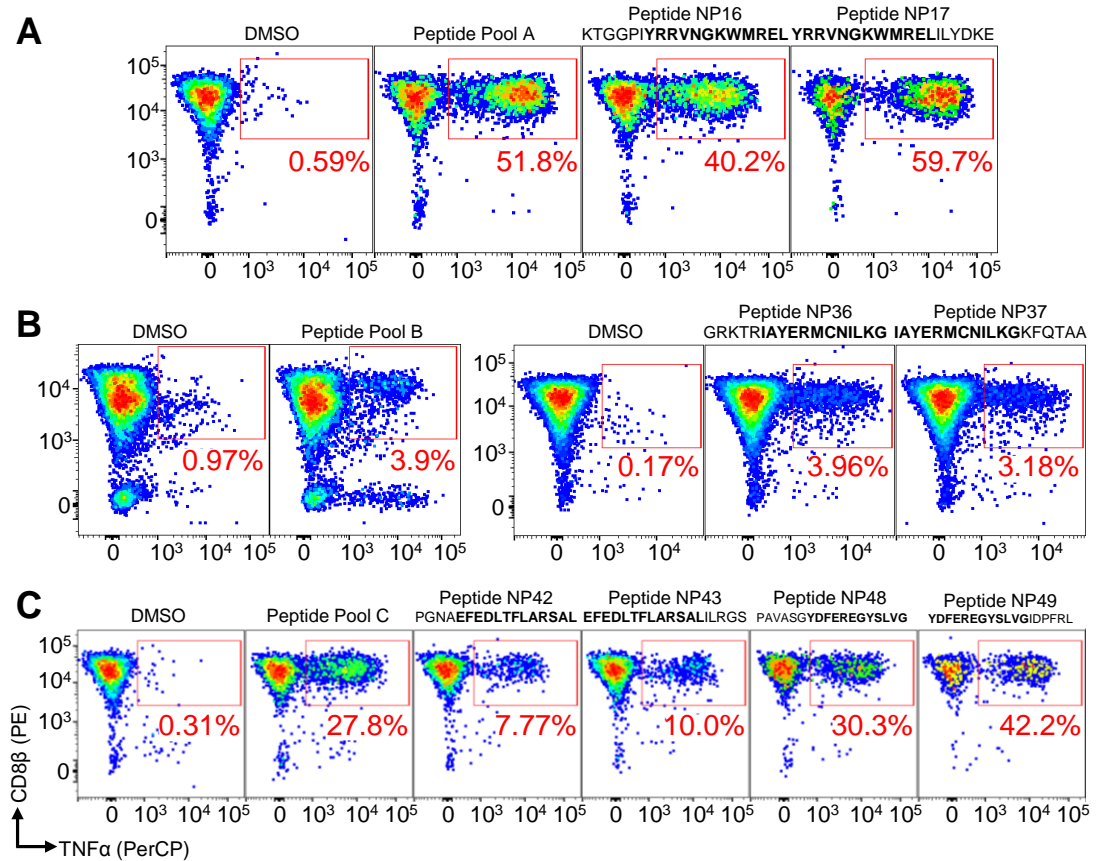


**Figure 4.1. Influenza-specific CD8β T-cell line procurement from Pig#625.**
Flow cytometry data of Influenza-specific T-cell lines from Pig#625 raised against NP peptide pools **A**, **B** and **C**. All CD8β sorted T-cell lines displayed were raised for two weeks against their respective peptide pool except the second line in (B) which was raised against peptides NP36 and NP37 alone. T-cell lines were incubated with DMSO or 2 μM peptide pool/peptide for 5 h then stained for CD8β and intracellular TNFα. Cells were gated on for size and viability and the percentage of TNFα+ cells is displayed in red.

**A**

DMSO — Peptide Pool A — Peptide NP16 KTGGPI**YRRVNGKWMREL** — Peptide NP17 **YRRVNGKWMREL**ILYDKE

2.24%    12.9%    14.5%    18.3%

**B**

CD8β (PE)

DMSO — Peptide Pool C — Peptide NP42 PGNA**EFEDLTFLARSAL** — Peptide NP43 **EFEDLTFLARSAL**ILRGS — Peptide NP48 PAVASG**YDFEREGYSLVG** — Peptide NP49 **YDFEREGYSLVG**IDPFRL

0.29%    23.7%    10.0%    13.2%    22.7%    23.9%

TNFα (PerCP)
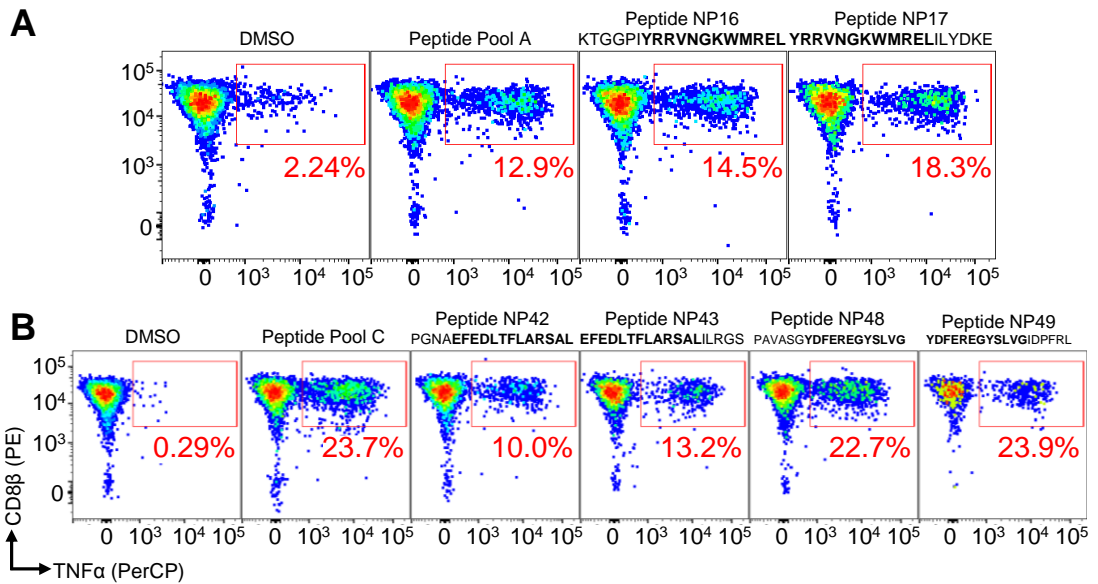
**Figure 4.2. Influenza-specific CD8β T-cell line procurement from Pig#650.**
Flow cytometry data of Influenza-specific T-cell lines from Pig#650 raised against NP peptide pools **A** and **C**. All CD8β sorted T-cell lines displayed were raised for two weeks against their respective peptide pool. T-cell lines were incubated with DMSO or 2 µM peptide pool/peptide for 5 h then stained for CD8β and intracellular TNFα. Cells were gated on for size and viability and the percentage of TNFα+ cells is displayed in red.
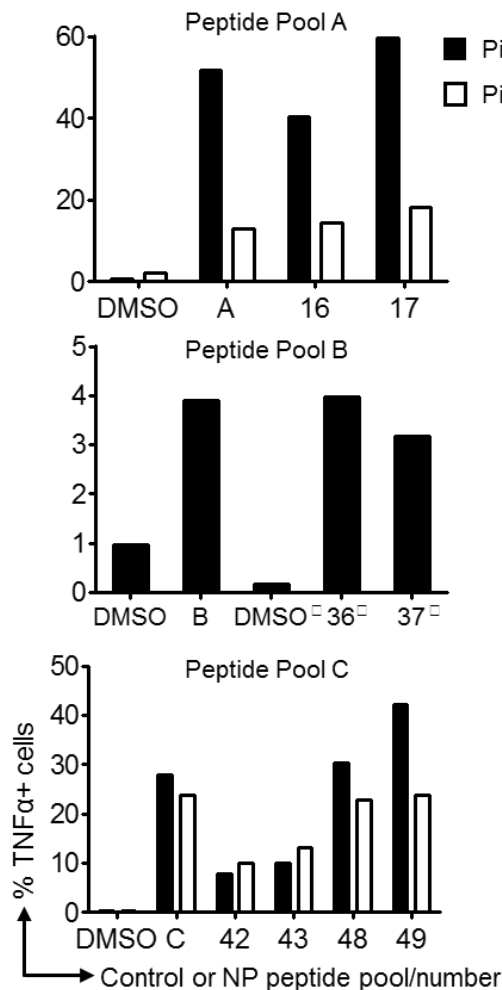


**Figure 4.3. Influenza-specific CD8β T-cell line procurement.**
Summarised flow cytometry data of Influenza-specific cytotoxic T-cell lines from pigs #625 and #650 raised against NP peptide pools **A**, **B** and **C**. All CD8β sorted T-cell lines displayed were raised for two weeks against their respective peptide pool except the second line in B (☐) which was raised against peptides NP36 and NP37 alone. T-cell lines were incubated with DMSO or 2 µM peptide pool/peptide for 5 h then stained for CD8β and intracellular TNFα. Cells were gated on for size and viability and the percentage of TNFα+ cells is plotted on the *y* axes.

62

*4.3.2   Epitope optimisation on T-cell lines*

Human and mouse MHC-I molecules can present peptides between 8-14 amino acids in length; the closed-ended peptide binding groove prevents longer peptide conformations. The majority (>70%) of cytotoxic T-cell epitopes are 9 amino acids long and ~20% are 10 amino acids long (Ekeruche-Makinde et al. 2013). Similarly, the limited studies of SLA-I in pigs to date have identified responses to peptides of 9 or 10 amino acids in length (Zhang et al. 2011; Pedersen et al. 2013; Pedersen et al. 2014; Fan et al. 2016; Gutiérrez et al. 2016; Baratelli et al. 2017). Therefore, we truncated the overlapping peptides identified in **Figure 4.3** down to a minimal length of 8 amino acids to establish the minimal epitopes that were being recognised by the cytotoxic T-cells. The overlapping regions of the peptides were truncated one amino acid at a time from both the N and carboxyl (C) termini (**Tables 10.3-10.6**). I generated a new batch of T-cell lines, as above, to peptide pools A and C in pigs#625 and #650. The relevant T-cell lines were then incubated with their respective peptide truncations, the full-length peptides and their overlapping region and TNFα release quantified.

The overlapping region between peptides 48 and 49 [YDFEREGYSLVG] elicited stronger TNFα responses than the full-length peptides and truncations of -2 or -3 amino acids from the N- or C-terminus respectively were not tolerated well (**Figure 4.4**). These data were consistent across both pigs#625 and #650 and three peptides [N-1: DFEREGYSLVG, N-1 C-2: DFEREGYSL and C-2: YDFEREGYSL] elicited the strongest responses. In pig#625 these three peptides induced 28.5%, 28.6% and 30.3 % CD8β+ TNFα+ cells (accounting for background). Similar responses of 34.8%, 34% and 32.6% were induced in pig#650 (**Figure 4.4A)**. Neither of these three peptide truncations [DFEREGYSLVG, DFEREGYSL and YDFEREGYSL] were substantially better than each other so further experiments were required to identify which was the minimal epitope. The overlapping region between peptides NP42 and NP43 [EFEDLTFLARSAL] induced 6.8% and 12.3% CD8β+ TNFα+ cells in pigs#625 and #650 respectively however a single truncation from the N-terminus reduced these responses to 0.78% and 2.79% respectively, close to the background level of activation (**Figure 4.5**). Truncations from the C-terminus were well tolerated and the C-4 truncation [EFEDLTFLA] induced the highest TNFα responses, 8.75% and 19.9% in pig#625 and #650 cytotoxic T-cell lines respectively. The minimal epitope was less clear when testing truncations of the 12 amino acid overlapping region between peptides NP16 and NP17 [YRRVNGKWMREL] (**Figure 4.6**). Truncations from the N-terminus were well tolerated and did not improve responses much above that seen with the overlap. In pig#625 the percentage of CD8β+ TNFα+ cells induced by the overlap and these N-terminus truncations ranged only from

26 - 27.6%. Truncations from the C-terminus negated the TNFα response (**Figure 4.6A**). Peptide truncations of peptides NP36 and NP37 were not tested on T-cell lines. The use of T-cell lines to define minimal epitopes was not conclusive in this study, although it did begin to establish which amino acid residues were essential for SLA-I presentation to cytotoxic T-cells.
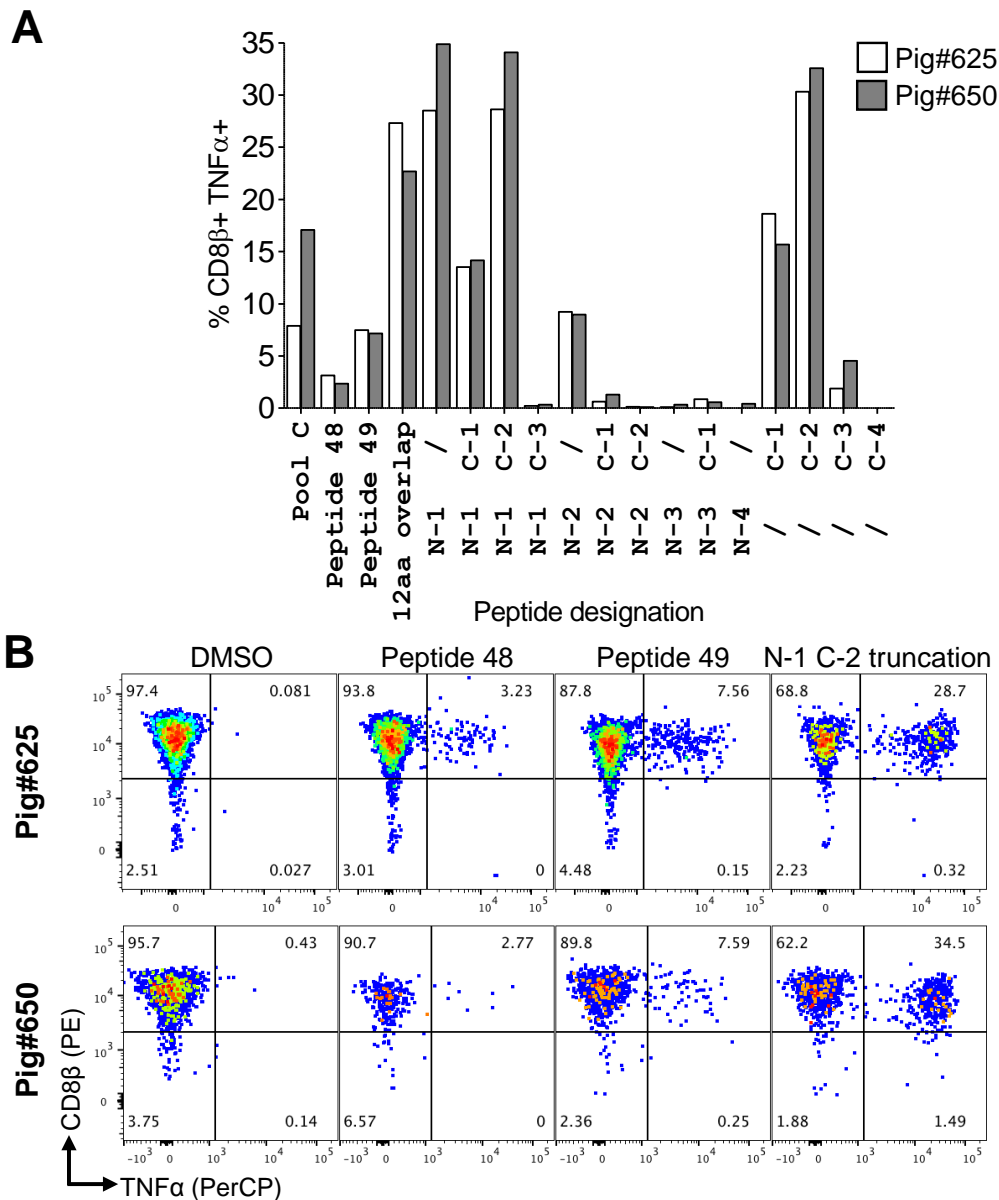


**Figure 4.4. Minimal epitope identification from peptides 48 and 49 using Influenza-specific T-cell lines.**
Flow cytometry data of Influenza-specific CD8β sorted T-cell lines from pigs#625 and #650 raised for two weeks against NP peptide pool C. The overlapping region [YDFEREGYSLVG] between peptides 48 and 49 identified in figure 4.3 was truncated one amino acid at a time from both the amino- (N) and carboxyl- (C) termini down to 8 amino acids long. T-cell lines were incubated with DMSO or 5 µM peptide pool/peptide for 5 h then stained for CD8β and intracellular TNFα. **A)** Percentage of CD8β+ TNFα+ cells detected for each peptide. Data are displayed minus DMSO background. **B)** Representative flow cytometry data from each pig. Cells were gated on size and viability and the percentage of each cell population is displayed inset.
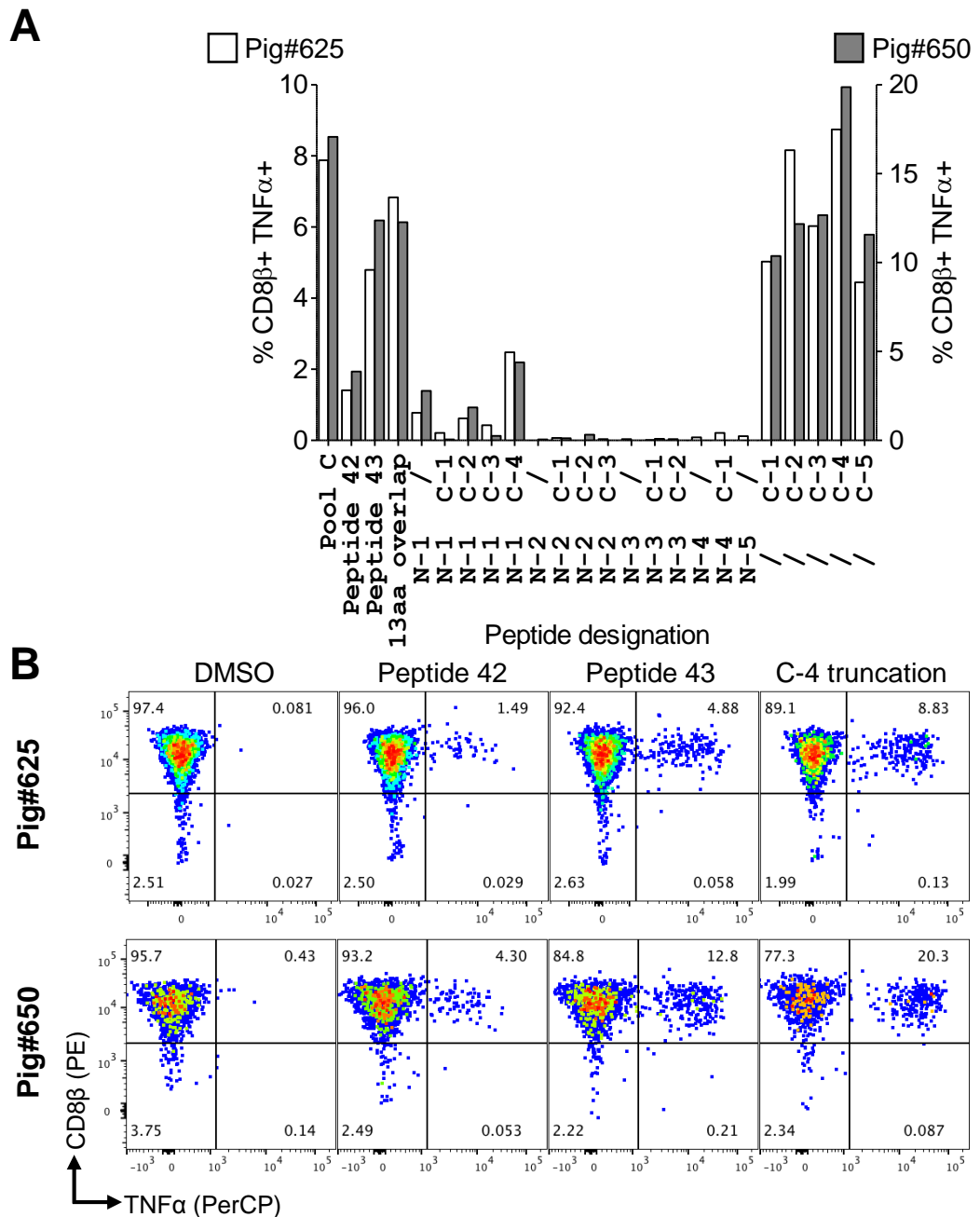
**Figure 4.5. Minimal epitope identification from peptides 42 and 43 using Influenza-specific T-cell lines.**

Flow cytometry data of Influenza-specific CD8β sorted T-cell lines from pigs#625 and #650 raised for two weeks against NP peptide pool **C**. The overlapping region [EFEDLTFLARSAL] between peptides 42 and 43 identified in figure 4.3 was truncated one amino acid at a time from both the amino- (N) and carboxyl- (C) termini down to 8 amino acids long. T-cell lines were incubated with DMSO or 5 µM peptide pool/peptide for 5 h then stained for CD8β and intracellular TNFα. **A)** Percentage of CD8β+ TNFα+ cells detected for each peptide. Data are displayed minus DMSO background. **B)** Representative flow cytometry data from each pig. Cells were gated on for size and viability and the percentage of each cell population is displayed inset.
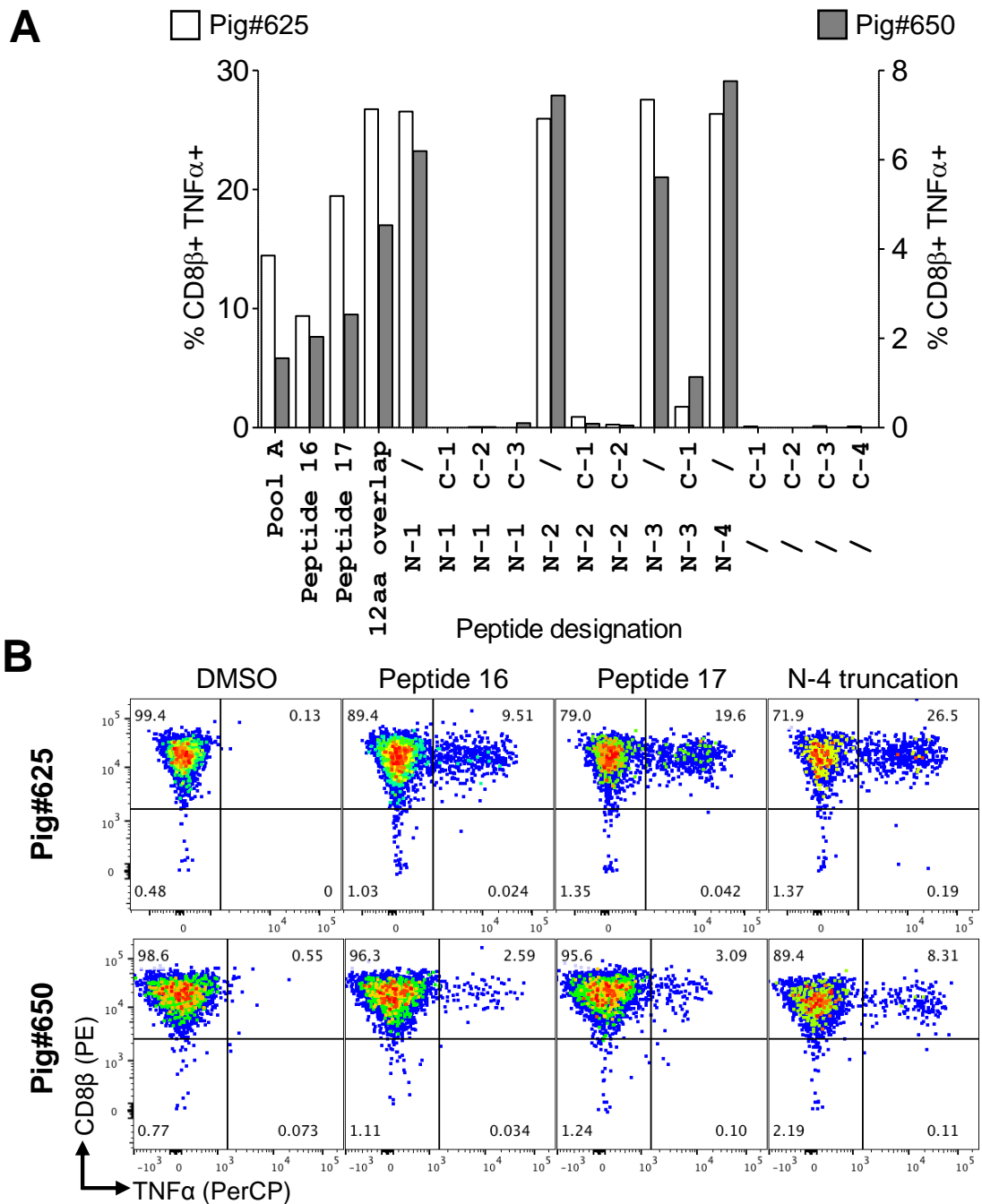
**Figure 4.6. Minimal epitope identification from peptides 16 and 17 using Influenza-specific T-cell lines.**
Flow cytometry data of Influenza-specific CD8β sorted T-cell lines from pigs#625 and #650 raised for two weeks against NP peptide pool A. The overlapping region [YRRVNGKWMREL] between peptides 16 and 17 identified in figure 4.3 was truncated one amino acid at a time from both the amino- (N) and carboxyl- (C) termini down to 8 amino acids long. T-cell lines were incubated with DMSO or 5 µM peptide pool/peptide for 5 h then stained for CD8β and intracellular TNFα. **A)** Percentage of CD8β+ TNFα+ cells detected for each peptide. Data are displayed minus DMSO background. **B)** Representative flow cytometry data from each pig. Cells were gated on size and viability and the percentage of each cell population is displayed inset.

### 4.3.3 Epitope optimisation on T-cell clones

Experiments using T-cell lines were superseded by minimal epitope definition using T-cell clones which I was able to expand to sufficient cell numbers required for these types of assays. Titration of truncated peptides in T-cell assays with 4 different clones identified the most sensitive responses (**Figure 4.7**). Cytotoxic T-cell clones KT7.650, KTS.650, Sue.625 and KT22.625 responded with highest sensitivity to the 9 amino acid long sequences `DFEREGYSL`, `EFEDLTFLA`, `IAYERMCNI` and `NGKWMRELI`. Other clones specific for these peptides gave similar results (data not shown). The identification of the minimal epitope `EFEDLTFLA` is consistent with the T-cell line data discussed above. As before, this peptide truncation induced higher responses than the other peptides (7.4 ng/mL of MIP-1β at $10^{-6}$ M peptide). The use of clone KT7.650 for testing the truncations of peptides NP48 and NP49 enabled clearer distinction between the preferred three sequences from the T-cell line data [N-1 C-2: `DFEREGYSL`, N-1: `DFEREGYSLVG` and C-2: `YDFEREGYSL`]. The minimal epitope `DFEREGYSL` induced 9.94 ng/mL MIP-1β at $10^{-7}$ M peptide, nearly double that seen with the latter two truncations (4.59 and 5.12 ng/mL) (**Figure 4.7**).

The minimal epitope `IAYERMCNI` induced by far the strongest MIP-1β responses with clone Sue.625 at both $10^{-5}$ and $10^{-6}$ M peptide. The identification of the minimal epitope in peptides NP16 and NP17 was not as straightforward, from the T-cell line data it was already clear that the C-terminus of the overlapping region was essential. Initial experiments on clone KT22.625 found that peptide NP17 afforded higher sensitivity over both NP16 and all of the truncations (data not shown). Therefore a second batch of peptide truncations was designed, extending the C-terminus into peptide NP17 (**Table 10.5**) and these truncations were tested on T-cell clone KT22.625 (**Figure 4.7**). This enabled clear detection of the minimal epitope as the highest sensitivity was observed to peptide `NGKWMRELI` which was the only peptide that induced MIP-1β release at $10^{-8}$ M peptide.
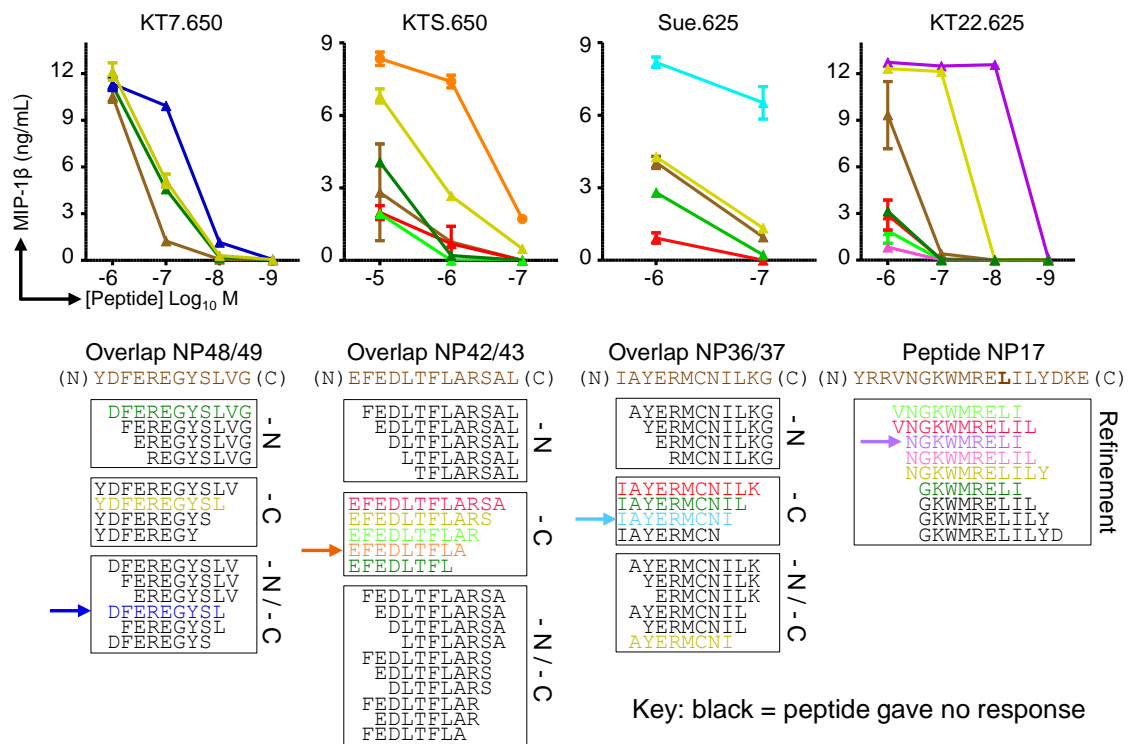
**Figure 4.7. Minimal epitope identification using Influenza-specific T-cell clones.**
T-cell clones were procured from Influenza-specific T-cells lines. The overlapping regions identified in figure 1 were truncated one amino acid at a time from both the N and C terminus down to 8 amino acids long. T-cell clones KT7.650, KTS.650, Sue.625 and KT22.625 responded to the following overlapping peptide regions respectively; YDFEREGYSLVG, EFEDLTFLARSAL, IAYERMCNILKG and YRRVNGKWMREL. T-cell clones were incubated overnight with titrations of each peptide truncation and MIP-1β release was measured by ELISA. All conditions were performed in triplicate and data are displayed as mean ± SEM. Peptide truncations that did not elicit a response at the concentrations displayed are shaded black. Peptide sequences are displayed colour coded for each graph. For clone KT22.625, initial experiments demonstrated that any substitution from the C terminus of the overlapping sequence [YRRVNGKWMREL] was not tolerated. Also, the full-length peptide NP17 was preferred to any N terminus substitution. Therefore, the C terminus was also extended to ascertain the minimal epitope here (refinement).

## 4.3.4 Additional IAV-specific T-cell responses

During the procurement of IAV specific T-cell lines using overlapping peptide pools spanning the NP and M1 proteins, two further peptide responses were identified in addition to those discussed above. These were not taken forward for in depth studies and will be discussed briefly here. Responses to M1 peptide pools were not clearly detected in pig#625 and #650 PBMC samples and no novel epitopes were defined for this protein, whereas I have defined 4 novel epitopes for NP. However, a cytotoxic T-cell line to M1 peptide pool E was procured on one occasion. During initial testing, this line produced 4.3% CD8β+ TNFα+ cells in response to the peptide pool E (**Figure 4.8A**). This line was re-stimulated with the peptide pool in order to increase the peptide responsive population and remove the need for cell sorting for clone procurement. This was unsuccessful and the peptide responsive population decreased with

these further re-stimulations. The remaining T-cell line was used to test individual peptides and the response was mapped to peptides M88 and M89 which share the overlapping sequence `MEWLKTRPILSP` (**Figure 4.8B**). However, it should be noted that the percentage of CD8β+ TNFα+ cells in response to peptide was very low by this point, with 1.15%, 0.9% and 1.08% for the peptide pool and peptides M88 and M89 respectively. This data ideally needed repeating to confirm the immunogenic region however a second attempt at procuring a cytotoxic T-cell line from pig#625 using peptides M88 and M89 produced no detectable response.
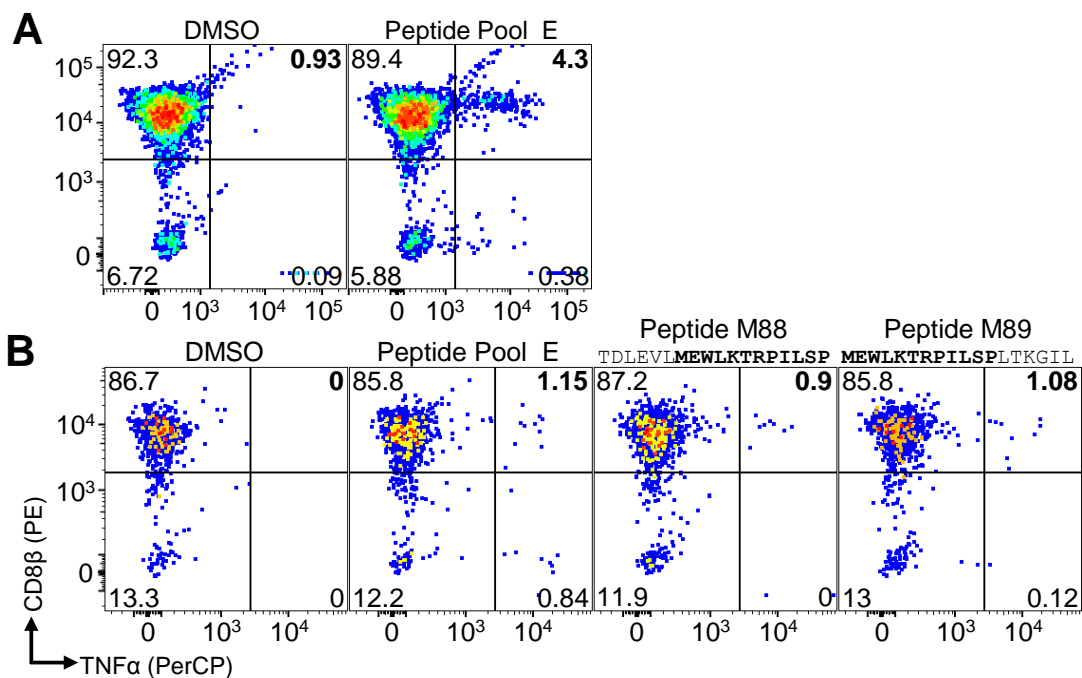


**Figure 4.8. Influenza M1-specific cytotoxic T-cell line procurement from Pig#625.**
Flow cytometry data of an Influenza-specific T-cell line from Pig#625 raised against M1 peptide pool E. T-cell lines were incubated with DMSO or 2 µM peptide pool/peptide for 5 h then stained for CD8β and intracellular TNFα. Cells were gated on for size and viability and the percentage of CD8β+ TNFα+ is displayed in bold. **A)** Detection of responses to peptide pool E. **B)** Identification of individual peptide responses. This line recognises overlapping peptides 88 and 89; `TDLEVL`**`MEWLKTRPILSP`** and **`MEWLKTRPILSP`**`LTKGIL`.

BAL samples from pig#625 were also used in attempts to procure influenza-specific T-cell lines but these were not initially sorted into CD8β+ cells as performed with PBMC samples. These experiments produced a T-cell line specific for peptide pool D with the strongest response seen in the CD8β- cell population at 10.8% CD8β- TNFα+ cells compared to 2.55% background in the DMSO control (**Figure 4.9A**). Following a round of expansion and a further re-stimulation of this T-cell line, the CD8β- TNFα+ response was mapped to CD4+ T-cells with 9% CD4+ TNFα+ T-cells detected in response to peptide pool D compared to 0.32% in the DMSO control (**Figure 4.9B**).

This CD4+ response was mapped to individual overlapping peptides NP68 and NP69; sequences AGQISIQ**PTFSVQRNLPFDR** and **PTFSVQRNLPFDR**TTVM; and peptides NP76 and NP77; sequences ARPEDV**SFQGRGVFELSD** and **SFQGRGVFELSD**EKAASP.
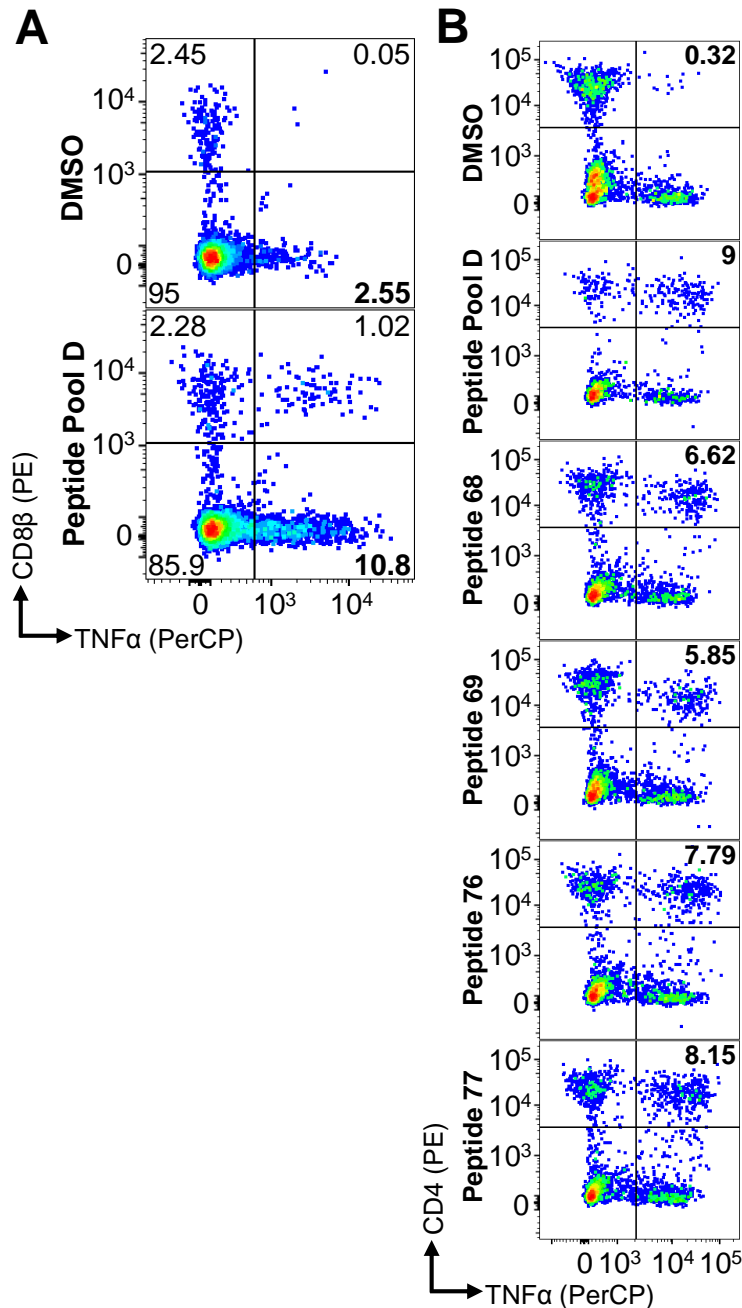


**Figure 4.9. Influenza NP-specific helper (CD4) T-cell line procurement from Pig#625 BAL samples.**
Flow cytometry data of an Influenza-specific T-cell line from Pig#625 BAL raised against NP peptide pool D. T-cell lines were incubated with DMSO or 2 μM peptide pool/peptide for 5 h then stained for CD8β (A) or CD4 (B) and intracellular TNFα. Cells were gated on size and viability and the percentage of CD8β- TNFα+ (A) or CD4+ TNFα+ (B) is displayed in bold. **A)** Detection of responses to peptide pool D in BAL line. **B)** Identification of individual peptide responses. The CD4+ fraction of this line recognises overlapping peptides 68 and 69; AGQISIQ**PTFSVQRNLPFDR** and **PTFSVQRNLPFDR**TTVM, and overlapping peptides 76 and 77; ARPEDV**SFQGRGVFELSD** and **SFQGRGVFELSD**EKAASP.

70

## 4.3.5   *Porcine CD8β+ T-cells are cytotoxic*

The main aims of this study were focused on conserved IAV epitope identification and detection in clinically relevant samples and defining the interaction between these peptides and the Babraham pig SLA-I molecules. Therefore, I did not pursue extensive phenotypic or functional assays with the cytotoxic T-cell clones isolated during this study. I felt that it was important to establish the cytotoxic nature of these T-cell clones so a killing assay was performed with T-cell clones KT13.650 and KT22.625. The commercially available ESK-4 cell line was labelled with $^{51}$Cr, incubated with the newly identified epitope NP$_{101-109}$ NGKWMRELI and acted as target cells in this assay at an E:T ratio of 5:1. The porcine kidney derived ESK-4 cell line has previously been shown to express the two Babraham pig SLA-I molecules (Ho et al. 2009). CD8β T-cell clone KT13.650 killed 26% and 62.5% of the target cells after 4 h and overnight, respectively, at $10^{-5}$ M peptide (**Figure 4.10**). Target cell killing was reduced but still prevalent at the lower peptide concentration of $10^{-9}$ M, where 12% and 49.5% of target cells were killed following 4 h or overnight incubation respectively. T-cell clone KT22.625 also killed target cells; 23.5% at $10^{-6}$ M peptide.
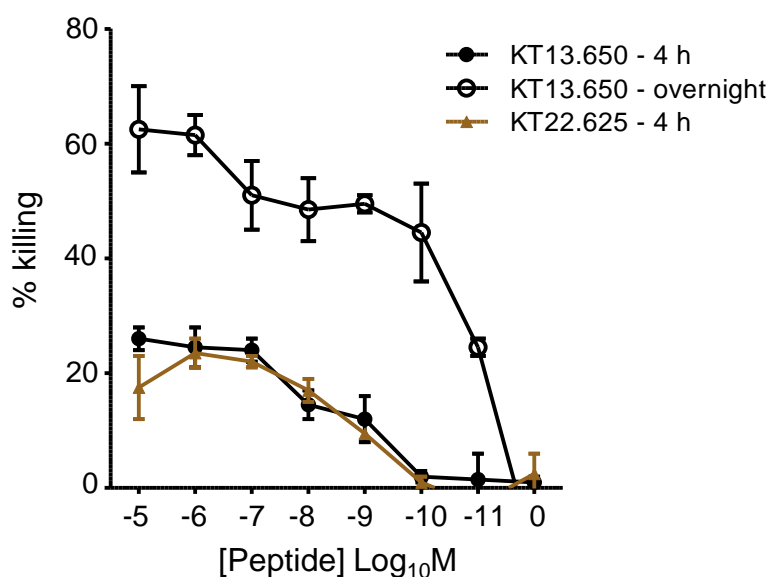


**Figure 4.10. Cytotoxic response of T-cell clones KT13.650 and KT22.625.**
ESK-4 cells were used as $^{51}$Cr labelled target cells incubated with or without peptide; NP$_{101-109}$ NGKWMRELI. T-cell clones KT13.650 and KT22.625 (effector cells) were plated with target cells at an E:T ratio of 5:1. Supernatant was harvested after 4 h and overnight (KT13.650 only) and $^{51}$Cr release recorded. The % killing of target cells = [(experimental – spontaneous $^{51}$Cr release)/(maximum release – spontaneous release) x 100]. All conditions were performed in triplicate and data are displayed as mean ± SEM.

## 4.4 Discussion

This chapter focused on the screening of two Babraham pigs, #625 and #650, vaccinated with H5-S-FLU and inactivated H1N1 Sp/Sw virus for cytotoxic T-cell responses to the conserved viral proteins NP and M1, using a non-assumptive approach of overlapping peptides spanning the whole protein sequences. The cytotoxic T-cell responses detected in this chapter were dominated by the NP. PBMC samples from pigs #625 and #650 were used to generate IAV-specific cytotoxic T-cell lines against three pooled sets (A, B and C) of NP peptides. Individual overlapping peptides and truncated versions of these sequences were used to define four new optimal IAV epitopes in the Babraham pig; NP$_{290\text{-}298}$ DFEREGYSL, NP$_{252\text{-}260}$ EFEDLTFLA, NP$_{217\text{-}225}$ IAYERMCNI and NP$_{101\text{-}109}$ NGKWMRELI. The testing of truncated peptides on T-cell lines did not conclusively define the minimal epitope in every case although it indicated which residues were required for successful T-cell engagement and identified the minimal epitope EFEDLTFLA. The procurement of porcine T-cell clones was instrumental to defining the minimal epitopes recognised for the other immunogenic regions. During the identification of the minimal epitope in peptides NP16 and NP17 it became apparent that the overlapping region between the two was not the optimal sequence but rather that additional residues in NP17 were required. This result highlights that it should not always be presumed that the minimal epitope is located within the overlapping sequence.

I searched the immune epitope database (www.iedb.org) and the immune epitope search tool provided by the Influenza research database (available at www.fludb.org) for these four epitopes and found only IAYERMCNI produced a direct match which has been identified as an MHC-I epitope in mice (Thomas et al. 2007). If the search criteria are reduced to 90% or 80% sequence match then all of the four regions of NP identified in this study appear in the immune epitope database (varying across MHC-I and MHC-II responses in humans and mice). This suggests the possibility of cross-species epitopes and identifies these regions of NP as immunogenic across different IAV strains and T-cell responses.

I failed to find robust cytotoxic T-cell responses to M1 during these studies. Although a cytotoxic T-cell line grown from pig#625 did show low reactivity to M1 peptide pool E. This response was mapped to overlapping peptides M88 and M89 [TDLEVL**MEWLKTRPILSP** and **MEWLKTRPILSP**LTKGIL] but as a second attempt failed to procure this T-cell line again, no T-cell clones were procured meaning I was unable to define a minimal epitope. This M1 peptide response was not pursued further due to time constraints of this project. Additionally, a CD4 T-cell response was identified in the vaccinated pig samples whilst I was searching for cytotoxic

responses in the BAL of pig#625 to NP peptide pool D. The BAL sample sizes were limited so these cells were not subjected to CD8β sorting enabling detection of responses across T-cell subsets. The CD4 response was mapped to two NP regions; peptides NP68 and NP69 [AGQISIQ**PTFSVQRNLPFDR** and **PTFSVQRNLPFDR**TTVM] and peptides NP76 and NP77 [ARPEDV**SFQGRGVFELSD** and **SFQGRGVFELSD**EKAASP]. The former peptides are in the same region of NP identified in preliminary studies in chapter 3 where a CD4 T-cell clone, procured from a pig inoculated with inactivated H1N1 Sw/Sp, was shown to recognise the peptide NQQRASAGQISVQPTFSVQR. Further investigation of these responses was not pursued in this study as my focus was on CD8β cytotoxic T-cell responses, due to their documented importance in heterotypic immunity.

The overlapping peptides, spanning NP and M1, used in this study were synthesised to >70% purity and the truncated peptides used for minimal epitope determination were synthesised to >40% purity. Despite the lower purity, it was still possible to clearly distinguish between T-cell responses to the different peptide truncations. The peptides were all reconstituted based on their peptide composition to improve accuracy. This approach is more economically viable that using higher purity peptides, however it is important to consider that it may lead to the identification of false positives as has been documented by other laboratories previously (Reid et al. 2014). This concern was addressed by self-validation in this study, as following minimal epitope identification pure peptides were used to confirm the response in subsequent T-cell activation assays and pMHC *in vitro* refolding and pMHC multimer detection of the corresponding T-cell clones.

A previous approach in outbred pigs identified four putative SLA-I SwIV epitopes using an *in silico* prediction algorithm (Pedersen et al. 2014). The use of overlapping peptides in my study made no assumptions about SLA binding or immunodominance. Indeed IAV studies in humans have identified immunodominant epitopes in NP utilising overlapping peptides that were not flagged by the existing prediction algorithms (Wu et al. 2011; Grant et al. 2013). A similar approach using a proteome-wide pentadecamer peptide library has previously been used in outbred pigs to successfully identify CD8β and CD4 T-cell epitopes in porcine reproductive and respiratory syndrome virus (PRRSV) following experimental infection (Mokhtar et al. 2016). To my knowledge, no published study has yet utilised this approach to identify IAV cytotoxic T-cell epitopes in pigs. Although the use of overlapping peptides was successful for T-cell epitope identification during my studies, there are alternative approaches that could have been pursued as previously discussed in section 1.3.6. For example, cell lines expressing the Babraham pig SLA

alleles could have been transduced with a protein of interest, i.e. NP, or infected with virus. Peptide-SLA complexes could then have been isolated and the peptides eluted for identification by mass spectrometry.

Finally, in this chapter I preliminary assessed the cytotoxicity of the porcine T-cell clones isolated in this study. For this, I used T-cell clones KT13.650 and KT22.625 which both recognise the NP epitope `NGKWMRELI`. Cytotoxic T-cell clones KT13.650 and KT22.625 displayed effective cytotoxicity and were able to kill peptide-pulsed target cells that express the Babraham pig SLA-I molecules. This suggests that these cytotoxic T-cells would be capable of directly killing IAV infected cells *in vivo*; the clinical relevance of which could be a subject for future investigations. Extensive phenotypic and functional studies of the cytotoxic T-cell responses I identified were not part of the overall aims of this current study so were not pursued further. However, the tools developed in this thesis will facilitate future studies of this kind.

The main aim of this chapter was to define minimal epitopes from conserved IAV proteins, NP and M1, from which 4 novel epitopes in swine were defined from the immunodominant NP. The identification of these epitopes facilitated progression of the study, as discussed in proceeding chapters, to quantify these cytotoxic T-cell responses in clinically relevant samples *ex vivo* and to perform structural analyses on the Babraham pig SLA-I molecules using IAV derived peptides.

# 5 Using Babraham pig peptide-SLA-I structures to define the primary MHC anchor residues

## 5.1 Background

Peptide, MHC-I heavy chain (extracellular domain) and $\beta_2$m (light chain) can be refolded *in vitro* to produce soluble pMHC-I complexes for use in a range of experiments. pMHC-I complexes can be used in crystallisation screens to produce crystallised protein for analysis by X-ray diffraction. Diffraction data can be used to produce 3D structures of the proteins and their interactions. The Research Collaboratory for Structural Bioinformatics (RCSB) consortium operate a freely available online protein data bank (PDB) (available at http://www.rcsb.org/pdb) in which protein structures can be deposited. To date, just two pSLA-I structures have been deposited in the PDB (Zhang et al. 2011; Fan et al. 2016), PDB entries 3QQ3 and 5H94, compared to several hundred pHLA structures.

As previously discussed, MHC-I molecules have a closed peptide binding groove (PBG) limiting the length of peptides that they can bind. The PBG consists of six distinct sub-sites which are referred to as pockets A, B, C, D, E and F (Saper et al. 1991). Pockets A and F are "closed off" resulting in a restriction in MHC-I-restricted peptide length, unlike that seen within the open-ended MHC-II PBG. The MHC-I pockets are suited to binding different side-chains from the peptide residues and can determine which residues, and therefore which peptides, are tolerated by the protein product of any one MHC-I allele. Within a MHC-I bound peptide there will be residues called anchor positions that will be, as defined by Falk and colleagues, ''occupied by a fixed residue or by one of a few residues with closely related side-chains" (Falk et al. 1991). These residues sit within the PBG pockets and anchor the peptide to the MHC-I molecule. The binding motif of each anchor position is therefore determined by the pocket and what residues it can accommodate. These anchor motifs vary across different MHC-I alleles enabling each MHC-I protein to bind and present a different subset of peptides. A typical MHC-I binding motif may be written like so: [xLxxxxxxL/V]; where x signifies any amino acid and the capital letters define the residues that can be tolerated at primary MHC anchor positions using amino acid single letter code. Though not always the case, the primary anchor residues in MHC-I molecules are commonly found at position (P) 2 and P9 (or PC; carboxyl terminus) accommodated in pockets B and F respectively (Matsumura et al. 1992). Knowledge of the pocket composition of any given MHC-I and its peptide binding motif allows predictions to be made of which peptide

sequences it can bind. In turn, this knowledge can be used to predict CD8+ T-cell epitopes. I therefore set out to visualise the interaction between the four IAV epitopes identified in chapter 4 and their respective SLA-I molecules to enable determination of which residues act as anchors between the peptide and the SLA-I molecule.

## 5.2 Hypotheses

I aimed to determine the structures of the newly identified IAV epitopes in this study in complex with the Babraham pig SLA-I molecules to enable definition of the key peptide residues that interact with the SLA-I so that I could subsequently define the SLA-I binding motifs (chapter 7). I also wished to produce soluble pSLA-I for pMHC multimer studies (chapter 6). Specifically, my hypotheses were:

- The SLA-I restriction of each of the 4 NP epitopes, identified in chapter 4, can be determined by *in vitro* refolding with the Babraham pig SLA-I molecules.
- Peptide-SLA complexes can be refolded *in vitro*, both unbiotinylated for crystal generation and biotinylated for construction of pSLA tetramers.
- Structures can be resolved for the 4 NP epitopes in complex with their SLA-I.
- Human $\beta_2$m will be interchangeable with porcine $\beta_2$m for *in vitro* refolding and structural analyses of pSLA-I.

## 5.3 Results

The inbred nature of the Babraham pig line means that all animals express identical MHC-I and MHC-II alleles. SLA-I typing, performed by the Pirbright Institute identified two SLA-I alleles in these animals; SLA-1*14:02 or SLA-2*11:04. The structures of these SLA-I molecules had not been resolved. To determine which of the two Babraham pig SLA-I molecules presented the four IAV epitopes I refolded them with $\beta_2$m and the extracellular domain of either SLA-1*14:02 or SLA-2*11:04. Each SLA-I heavy chain produced a good refolded pSLA-I protein product with two of the four peptides, so I could be confident that `DFEREGYSL` and `EFEDLTFLA` are restricted by SLA-1*14:02 while `IAYERMCNI` and `NGKWMRELI` are restricted by SLA-2*11:04.

### 5.3.1 Manufacture of peptide-SLA-I (example)

An example of the process used to produce pSLA-I complexes in this study is displayed in **Figures 5.1-5.3**. Peptide-MHC complexes can be refolded *in vitro* using extracellular heavy chain and $\beta_2$m expressed separately in *E. coli* as insoluble inclusion bodies (Parker et al. 1992). Only peptides capable of stably binding to the MHC-I molecule will lead to successful assembly of pMHC complexes *in vitro* by slow dilution of denaturing conditions using dialysis. Peptide-MHC complexes produced in this way are very stable and can be placed at 4 °C for short term storage or frozen in the long term. Initially the soluble protein must be produced in high enough quantities to facilitate *in vitro* refolding. Insoluble inclusion bodies produced in *E. coli* were isolated and washed by centrifugation and then dissolved in guanidine to denature them (Garboczi et al. 1992). Samples can be taken at difference stages throughout refolding and purification and monitored for composition by SDS-PAGE. Samples taken before and after IPTG-induced expression of the protein chains and after washing are displayed in **Figure 5.1**. Clear protein bands can be seen for both SLA-1 and SLA-2 heavy chains (~35 kDa) increasing in intensity following purification.

After protein expression and inclusion body clean up, SLA-I heavy chain was refolded with $\beta_2$m and peptide by removal of the guanidine denaturant by dialysis. Refolded protein was purified by anion exchange (**Figure 5.2A**). Fractions containing individual peaks consisting of SLA and $\beta_2$m by SDS-PAGE were combined (**Figure 5.2B**). At this stage pSLA-I molecules produced for pMHC multimer staining were labelled with biotin overnight. A gel filtration step was then used to further purify the pSLA complex by size and to remove any excess biotin from the biotinylated proteins (**Figure 5.3**). The fractions of refolded protein were combined and concentrated for storage. As seen in the anion exchange example in **Figure 5.2A**, some refolded proteins will be separated into two separate peaks. When two peaks are observed in anion exchange, the peaks are kept separate for subsequent purification steps but typically both will produce similar gel filtration results, as in **Figure 5.3**, (they could be combined at this stage) and usually both will be functional for use in pMHC multimer staining or crystallography studies. Anion exchange separates the refolded protein based on charge and perhaps the multiple peaks could be due to the accessibility of surface charge possibly affected by protein aggregation.
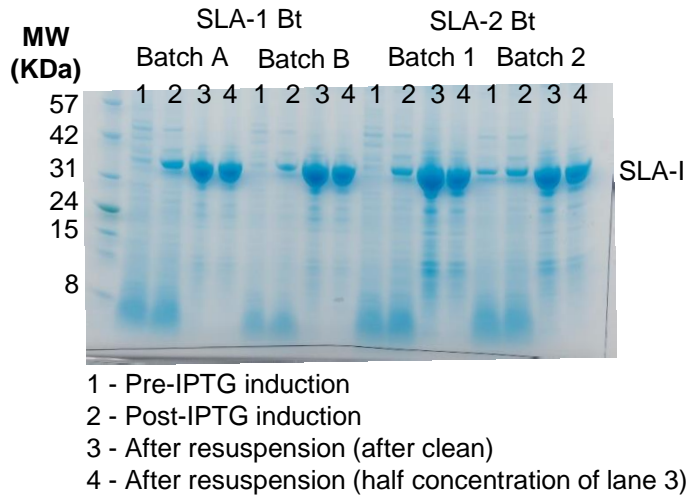
**Figure 5.1. Representative data from inclusion body preparations of SLA-I heavy chains.**
Coomasie stained SDS-PAGE on a pre-cast 10% Bis/Tris gel under reducing conditions of samples taken at different points during production of SLA-I protein chains. Samples from both Babraham pig SLA-I molecules and different inclusion body batches are displayed. Bands of SLA-I heavy chain (~35 kDa) are seen.

1 - Pre-IPTG induction
2 - Post-IPTG induction
3 - After resuspension (after clean)
4 - After resuspension (half concentration of lane 3)
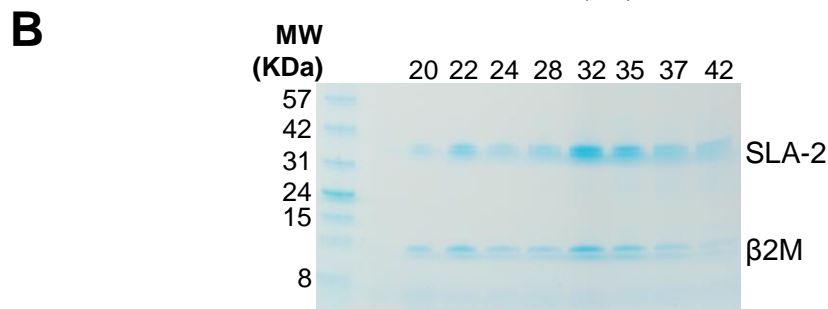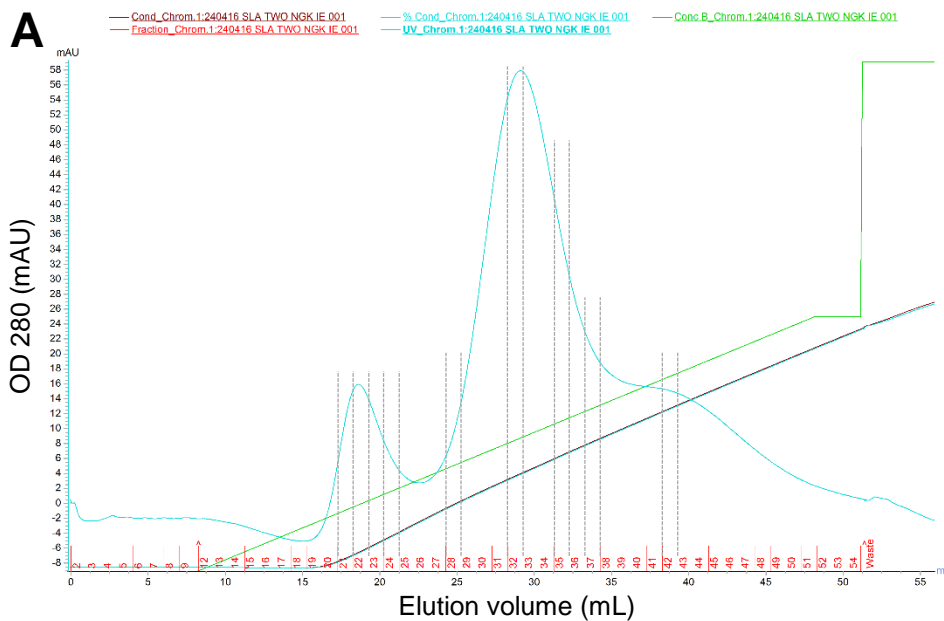


**Figure 5.2. Representative data from anion exchange purification of in vitro refolded peptide-SLA-I.**
**A)** Anion exchange chromatograph of a 250 mL refold of SLA-2*11:04 and peptide NGKWMRELI run through a 8 mL POROS 50HQ column eluted with a salt gradient (0-500 mM NaCl in 10 mM Tris pH 8.1). 54 fractions were collected as shown (labelled in red). Fractions used for sampling in (B) are indicated by dotted lines. **B)** Evaluation of protein quality of sample fractions using Coomassie stained SDS-PAGE on a pre-cast 10% Bis/Tris gel under reducing conditions. Lane 1: molecular weight ladder; Lane 2: blank; Lane 3-10: fractions as labelled. Bands of SLA-2 heavy (α) chain (~35 kDa) and $β_2m$ (~10 kDa) are seen.

**Figure 5.3. Representative data from gel filtration purification of in vitro refolded peptide-SLA-I.**
**A)** Gel filtration chromatographs of pooled peaks 1 and 2 (from the anion exchange of a 250 mL refold of SLA-2*11:04 and peptide `NGKWMRELI`) run through a Superdex S200 column eluted with PBS into 33 fractions (labelled in red). These proteins were biotin-tagged before this purification step. Fractions used for sampling in (B) are indicated by dotted lines. **B)** Evaluation of protein quality of sample fractions using Coomassie stained SDS-PAGE on a pre-cast 10% Bis/Tris gel under reducing conditions. Lane 1: molecular weight ladder; Lane 2-10: fractions as labelled. Bands of SLA-2 heavy (α) chain (~35 kDa) and $\beta_2$m (~10 kDa) are seen.

Soluble, unbiotiylated pSLA-I proteins were set up in crystal trials as described in the materials and methods (see section 2.5). The length of time for crystal formation varied greatly and took between 2 hours to >4 weeks to form. Crystals were harvested and taken to the Diamond Light Source (Oxfordshire, U.K.) for X-ray diffraction and data collection by either Dr. Pierre Rizkallah or Dr. David Cole. Crystals and good diffraction data were obtained for SLA-1*14:02-DFEREGYSL, SLA-1*14:02-EFEDLTFLA and SLA-2*11:04-IAYERMCNI. I was unable to generate good data for SLA-2*11:04-NGKWMRELI. Data reduction and refinement statistics for the three pSLA-I structures were collated by Dr. Pierre Rizkallah and are shown in **Table 5.1**. Each structure is now discussed in turn. The images I have assembled into **Figures 5.4-5.7** were designed in PyMOL by Dr. Pierre Rizkallah and Dr. David Cole.

**Table 5.1. Data reduction and refinement statistics.**

| Date collection/ reduction statistics | DFEREGYSL Porcine $\beta_2$m | EFEDLTFLA Porcine $\beta_2$m | IAYERMCNI Porcine $\beta_2$m | DFEREGYSL Human $\beta_2$m | EFEDLTFLA Human $\beta_2$m |
|---|---|---|---|---|---|
| Wavelength (Å) | 0.9795 | 0.92819 | 0.92819 | 0.9795 | 0.9795 |
| Beamline | DLS I04 | DLS I04-1 | DLS I04-1 | DLS I02 | DLS I04 |
| Space Group | P 1 | P 1 2₁ 1 | C 1 2 1 | P 1 | P1 |
| a (Å) | 41.616 | 42.034 | 93.478 | 59.39 | 59.30 |
| b (Å) | 46.340 | 128.29 | 80.843 | 60.29 | 59.70 |
| c (Å) | 66.735 | 46.794 | 61.964 | 65.64 | 66.44 |
| a (°) | 104.36 | 90.0 | 90.0 | 81.24 | 81.48 |
| b (°) | 101.21 | 101.89 | 119.66 | 67.59 | 67.62 |
| g (°) | 102.20 | 90.0 | 90.0 | 67.94 | 68.60 |
| Resolution Range (Å) | 1.1 – 39.28 | 1.429 - 42.77 | 1.541 - 57.31 | 2.14 – 55.88 | 1.57 - 61.44 |
| Highest Resolution Shell | 1.1 – 1.13 | 1.429-1.47 | 1.541 – 1.62 | 2.14 – 2.20 | 1.57 – 1.61 |
| Total measurements | 323,722 (19,334) | 325,172 (20,495) | 219,987 (32,873) | 79,873 (5,623) | 202,004 (14,602) |
| Unique Reflections | 170,825 (11,419) | 89,178 (6,585) | 57,504 (8,350) | 41,686 (3,024) | 105,240 (7,578) |
| I/s | 6.0 (1.1) | 10.7 (1.4) | 12.7 (2.2) | 3.4 (1.7) | 5.7 (1.3) |
| Completeness | 92.3 (83.1) | 99.9 (99.7) | 97.6 (97.2) | 96.9 (96.0) | 96.0 (93.3) |
| Redundancy | 1.9 (1.7) | | | | |
| CC$_{1/2}$ | 0.998 (0.596) | 0.998 (0.568) | 0.998 (0.778) | 0.979 (0.522) | 0.991 (0.514) |
| Rmeas (%) | 8.6 (178.9) | 6.9 (107.0) | 6.7 (76.4) | 12.8(66.9) | 6.0 (66.5) |
| B(iso) from Wilson (Å²) | 10.6 | 12.0 | 19.3 | 18.9 | 23.1 |
| **Refinement Statistics** | | | | | |
| Non-H atoms | 4,033 | 3,862 | 3,701 | 6,747 | 7,239 |
| R-factor (%) | 19.1 | 18.6 | 19.1 | 22.0 | 21.6 |
| R-free (%) | 21.2 | 21.4 | 25.1 | 28.3 | 26.1 |
| B-factor from refinement | 17.3 | 19.0 | 22.8 | 28.0 | 27.4 |
| rmsd bond lengths (Å) | 0.0196 | 0.0189 | 0.0187 | 0.0181 | 0.0188 |
| rmsd bond angles (°) | 2.111 | 1.801 | 1.951 | 1.931 | 1.937 |
| ESU Max. Likelihood (Å) | 0.036 | 0.058 | 0.093 | 0.265 | 0.119 |

Figures in brackets refer to the highest resolution shell

### 5.3.2 SLA-1*14:02 NP$_{290-298}$ DFEREGYSL structure

The structure of SLA-1*14:02 in complex with IAV epitope `DFEREGYSL` and porcine β$_2$m was resolved by Dr. Pierre Rizkallah to 1.1 Å and is displayed in **Figure 5.4.** The structure fits the expected pSLA-I format and within the peptide sequence, different residues sit within or above the PBG (**Figure 5.4A**). Closer inspection shows that the amino acids at P2 (Phe) and P9 (Leu) in `DFEREGYSL` sit deep within the SLA-1*14:02 PBG in pockets B and F respectively and were thus determined to be the primary anchor residues for this SLA-I (**Figure 5.4C&D**). Residue Arg4 sits prominently above the PBG ready for TCR engagement.
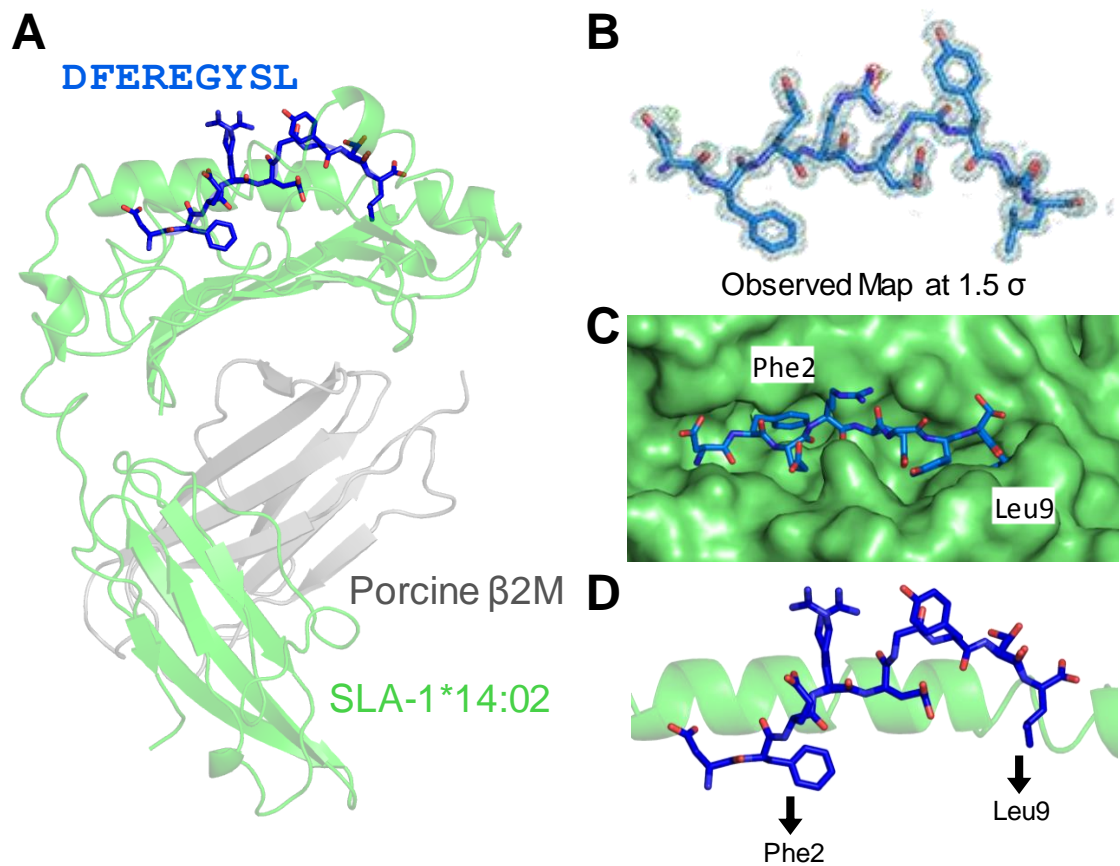


**Figure 5.4. Structural overview of SLA-1*14:02 binding peptide (NP290-298) DFEREGYSL.**
**A)** A schematic representation of NP$_{290-298}$ (peptide represented by blue sticks) bound by SLA-1*14:02 (green) (α1, α2 and α3 domains) refolded with porcine β$_2$m (grey). **B)** Final observed density map at 1.5 σ following refinement (displayed in grey surrounding the peptide). Positive and negative difference density is shown in green and red, respectively. **C&D)** Position of the NP$_{290-298}$ peptide within the SLA-1*14:02 binding groove. Phe2 and Leu9 sit deep within the B and F pockets of the binding groove anchoring the peptide.

### 5.3.3    SLA-1*14:02 NP$_{252-260}$ EFEDLTFLA structure

The structure of SLA-1*14:02 in complex with IAV epitope `EFEDLTFLA` and porcine β₂m was resolved by Dr. Pierre Rizkallah to 1.4 Å and is displayed in **Figure 5.5.** The amino acids at P2 (Phe) and P9 (Ala) in `EFEDLTFLA` sit within the SLA-1*14:02 PBG in pockets B and F respectively (**Figure 5.5C&D**), as seen in the SLA-1*14:02 `DFEREGYSL` structure, and thus reiterates these residues as the primary anchors for this SLA-I. Residues Asp4 and Leu5 in `EFEDLTFLA` sit prominently above the PBG.
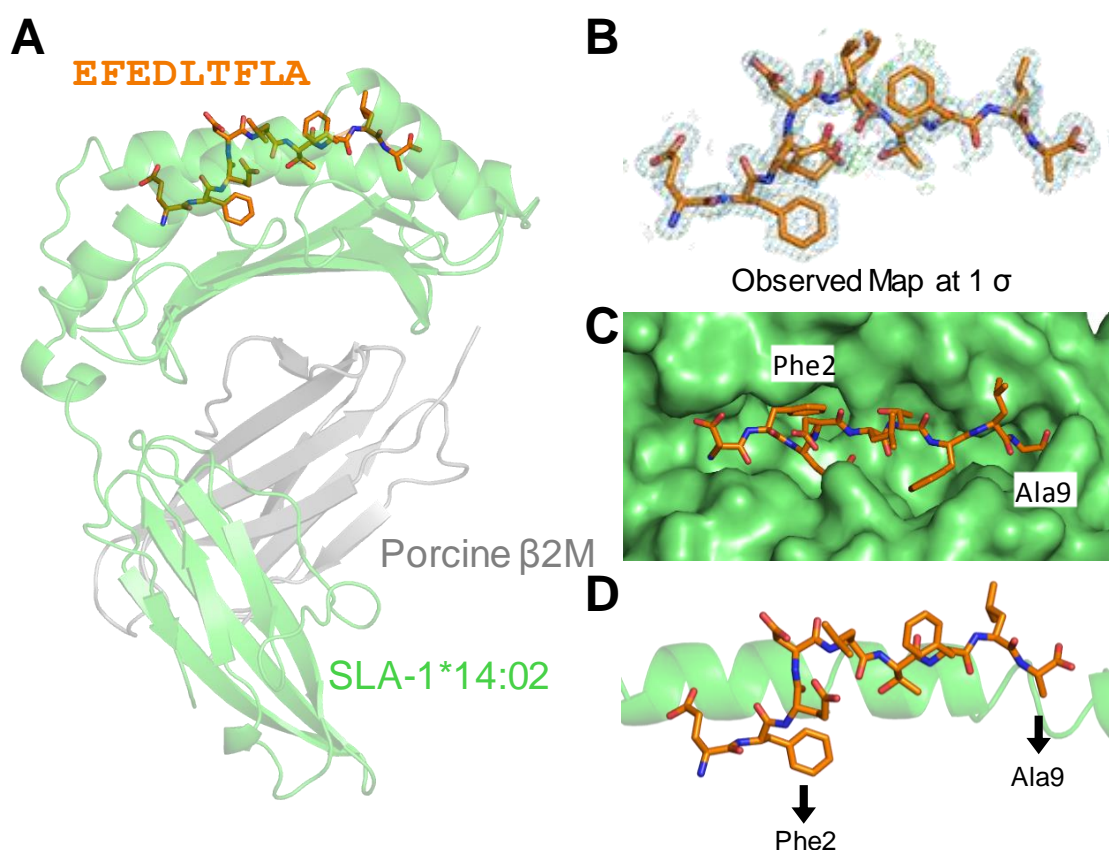


**Figure 5.5. Structural overview of SLA-1*14:02 binding peptide (NP252-260) EFEDLTFLA.**
**A)** A schematic representation of NP$_{252-260}$ (peptide represented by orange sticks) bound by SLA-1*14:02 (green) (α1, α2 and α3 domains) refolded with porcine β₂m (grey). **B)** Final observed density map at 1 σ following refinement (displayed in grey surrounding the peptide). Positive and negative difference density is shown in green and red, respectively. **C&D)** Position of the NP$_{252-260}$ peptide within the SLA-1*14:02 binding groove. Phe2 and Ala9 sit within the B and F pockets of the binding groove anchoring the peptide. Double conformers have been omitted from each image except in panel B.

### 5.3.4    SLA-2*11:04 NP$_{217-225}$ IAYERMCNI structure

The structure of SLA-2*11:04 in complex with IAV epitope `IAYERMCNI` and porcine β₂m was resolved by Dr. Pierre Rizkallah to 1.5 Å and is displayed in **Figure 5.6.** The amino acids at P2 (Ala) and P9 (Ile) in `IAYERMCNI` sit within the SLA-2*11:04 PBG in pockets B and F respectively (**Figure 5.6**) and were thus determined as the primary anchor residues for this SLA-I. The amino acids at P3 (Tyr) and P5 (Met) also sit within the PBG but to a lesser extent, **Figure 5.6C&D**, and are likely acting as secondary anchor residues. Residues Arg5 and Asn8 in `IAYERMCNI` sit prominently above the PBG.
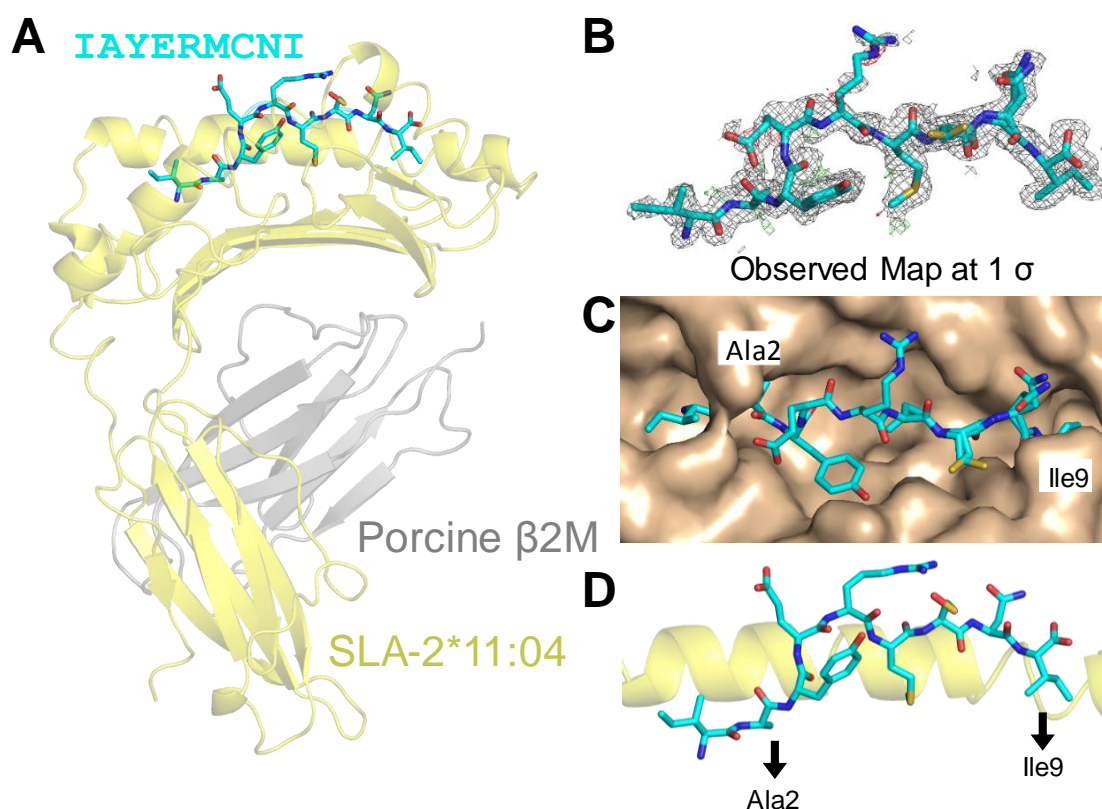


**Figure 5.6. Structural overview of SLA-2*11:04 binding peptide (NP217-225) IAYERMCNI. A)** A schematic representation of NP$_{217-225}$ (peptide represented by cyan sticks) bound by SLA-2*11:04 (gold) (α1, α2 and α3 domains), refolded with porcine β₂m (grey). **B)** Final observed density map at 1 σ following refinement (displayed in grey surrounding the peptide). Positive and negative difference density is shown in green and red, respectively. **C&D)** Position of the NP$_{217-225}$ peptide within the SLA-2*11:04 binding groove. Ala2 and Ile9 sit within the B and F pockets of the binding groove anchoring the peptide

### 5.3.5    Use of porcine versus human β₂m

The structures of SLA-1*14:02 with peptides `DFEREGYSL` and `EFEDLTFLA` were also solved using human β₂m to determine compatibility. These complexes successfully refolded *in vitro* with human β₂m and produced crystals and diffraction data. The resolved structures are

compared to those produced with porcine $\beta_2$m in **Figure 5.7.** Comparisons between the overall pSLA-I structures show no substantial difference between the structures using either $\beta_2$m, with low Root-means-square deviations (RMSD) of 0.675 Å and 0.934 Å **(Figure 5.7A&C)**. RMSD can be used to quantify the similarity between equivalent atoms in two structures. It is reliably used to compare different conformations of the same protein. In the case of identical protein structures the RMSD would be 0, increasing as identity decreases between the two structures (Carugo and Pongor 2001). The different species of $\beta_2$m in each structure were also compared in isolation from the rest of the complex and again low RMSD of 0.604 Å and 0.609 Å were determined (**Figures 5.7B&D**).

SLA-1*14:02- DFEREGYSL– porcine β2M
SLA-1*14:02- DFEREGYSL– human β2M

SLA-1*14:02- EFEDLTFLA– porcine β2M
SLA-1*14:02- EFEDLTFLA– human β2M

**A**

RMS = 0.675 Å

**C**

RMS = 0.934 Å

**B**

porcine β2M
human β2M

RMS = 0.604 Å

**D**

porcine β2M
human β2M

RMS = 0.609 Å
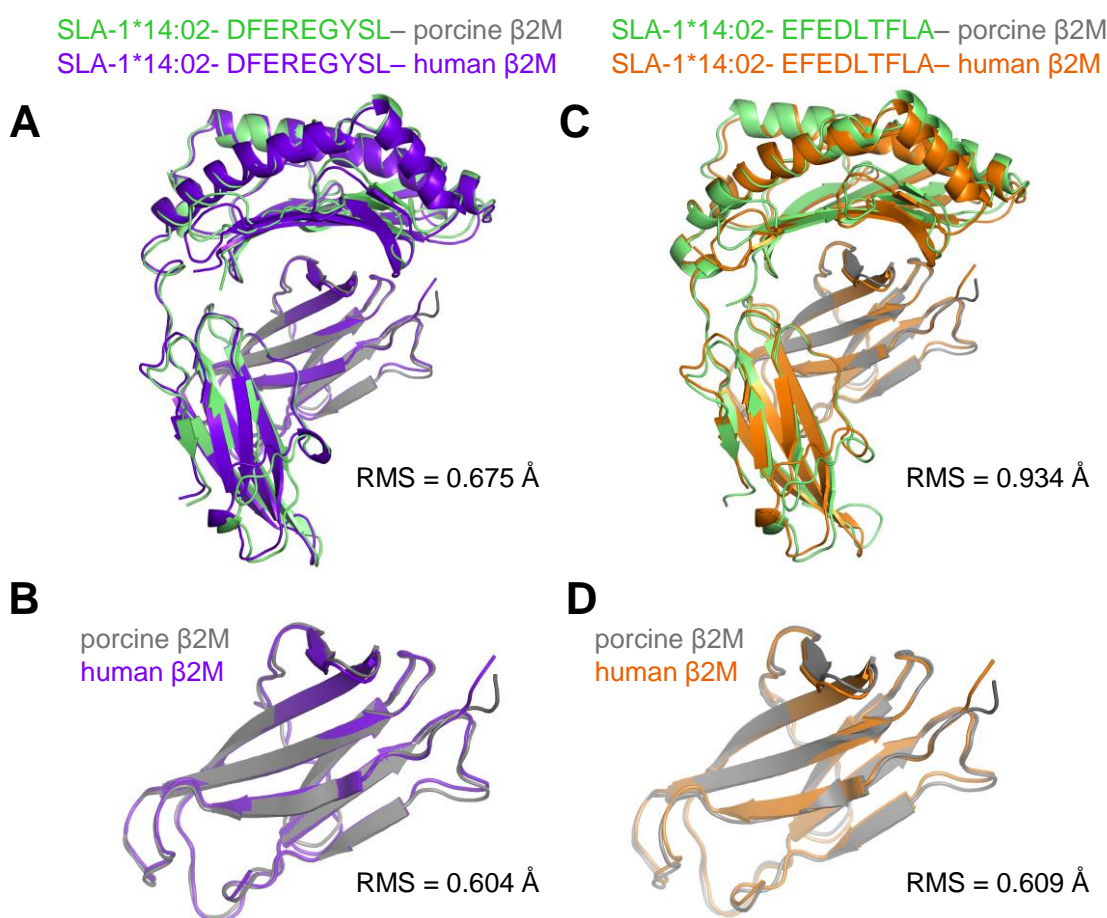
**Figure 5.7. Comparison of SLA-1*14:02, with peptide DFEREGYSL and EFEDLTFLA, using either porcine or human β2m.**
The overall structure of SLA-1*14:02 binding peptide NP$_{290-298}$ `DFEREGYSL` refolded with either porcine β2m (green and grey) or human β2m (purple). **B)** Porcine and human β2m from (A) compared only. **C)** The overall structure of SLA-1*14:02 binding peptide NP$_{252-260}$ `EFEDLTFLA` refolded with either porcine β2m (green and grey) or human β2m (orange). **D)** Porcine and human β2m from (C) compared only. Root-means-square (RMS) deviations are displayed for each comparison.

## 5.4 Discussion

In this chapter, the four IAV epitopes that were identified in chapter 4 were refolded with the Babraham pig SLA-I molecules; SLA-1*14:02 and SLA-2*11:04 (which are 89% identical by protein sequence). This determined the SLA-I restrictions for these peptides; `DFEREGYSL` and `EFEDLTFLA` bound to SLA-1*14:02 while `IAYERMCNI` and `NGKWMRELI` bound to SLA-2*11:04. Soluble pMHC-I complexes were then produced for all epitopes for use in pMHC multimer staining (chapter 6) and for the structural analyses presented in this chapter.

High-resolution structures were generated for three of the four IAV epitopes, SLA-1*14:02-DFEREGYSL, SLA-1*14:02-EFEDLTFLA and SLA-2*11:04-IAYERMCNI. This is the first deposition of an SLA-2 protein in the PDB. These structures allowed identification of the primary anchors for both Babraham pig SLA-I molecules. The primary anchor positions in both SLA-1*14:02 and SLA-2*11:04 are at P2 and P9 (C-terminus) in the peptide sequences. This matches a common primary anchor pattern across human MHC-I molecules with the residues sitting within pockets B and F respectively (Sidney et al. 2008). It is also consistent with previously published pSLA-I structures where P2 and the C-terminus can be seen sitting within the PBG in pockets B and F and acting as primary anchors for SLA-1*0401 (Zhang et al. 2011) and SLA-3*hs0202 (Fan et al. 2016). Identification of the primary anchor residues for the Babraham pig SLA-I molecules was necessary for determining their allelic peptide binding motifs in chapter 7.

Human and porcine $\beta_2$m are 75% identical by protein sequence and a previous study demonstrated that both could support complex formation with either HLA-I and SLA-I (Pedersen et al. 2011). This was observed again in a further study that noted no difference between the use of human or porcine $\beta_2$m in supporting complex formation with an SLA-2 allele (Pedersen et al. 2013). Studies that have utilised pMHC-I thus far for pMHC multimer staining have all used human $\beta_2$m in these formulations, using "one-pot, mix-and-read peptide-MHC tetramers" (Leisner et al. 2008; Patch et al. 2011; Pedersen et al. 2014; Pedersen et al. 2016). Both porcine and human $\beta_2$m were utilised throughout this study for pMHC multimer production. The existing SLA-I structures deposited in the PDB both comprise only porcine $\beta_2$m (Zhang et al. 2011; Fan et al. 2016). This study describes the first structures deposited of SLA-I molecules complexed with human $\beta_2$m. The substitution of porcine $\beta_2$m for human $\beta_2$m made no substantial difference to the overall peptide-SLA-1*14:02 structures presented in this chapter. The efficiency of refold yields were not compared across the two different $\beta_2$m species within this project. Human $\beta_2$m is usually used when refolding murine pMHC-I for use in pMHC multimer staining. Substitution

of murine $\beta_2$m for the human molecule in murine pMHC-I improves binding to murine CD8 (Purbhoo et al. 2001) and can result in better performing pMHC tetramers. Further investigations could be performed in the future to determine if similar effects can be observed in porcine pMHC multimer staining and if human $\beta_2$m affords any other advantages in terms of protein yields.

# 6 Optimisation of pMHC tetramer staining for characterisation of IAV responses in pigs

## 6.1 Background

Antigen-specific T-cells can be detected using a combination of fluorochrome-conjugated multimeric pMHC and flow cytometry. The multiple binding sites of peptide-MHC multimers allow them to bind to T-cells with a far greater half-life than the equivalent individual monomers due to the avidity effect , thereby enabling cell staining (Wooldridge et al. 2009). Since their first description in 1996, pMHC multimers have been utilised in many thousands of studies for detection of antigen-specific T-cells (Altman et al. 1996; Burrows et al. 2000). The most popular approach for multimeric pMHC labelling has been the use of biotinylated pMHC bound to fluorochrome-conjugated streptavidin molecules to generate pMHC tetramers. This physical detection technology does not require cellular activation so it can be used directly *ex vivo* without being influenced by the activation status, or effector capability, of target antigen-specific T-cell populations. pMHC multimers are compatible with T-cell phenotyping and can be incorporated into large polychromatic, or heavy metal labelled, antibody panels to generate phenotypic information in addition to defining antigen specificity.

Observations by my laboratory have noted that standard pMHC tetramer staining protocols can fail to detect fully functional T-cells, indicating a disparity between the binding affinity threshold required for T-cell activation and pMHC tetramer engagement (Laugel, van den Berg, et al. 2007). This means that in some cases antigen-specific T-cells have been severely under detected resulting in an underestimation of the T-cell response or, at worse, a failure to identify a specific clinically-relevant response altogether. This prompted my laboratory to pursue improvements in this technology and led to a number of highly cited studies that describe improvements to the sensitivity of pMHC multimer staining (Wooldridge et al. 2009; Dolton et al. 2015).

The failure of pMHC tetramers to detect antigen-specific T-cells is most prominent when the TCRs display low affinity for their cognate pMHC. This is typically the case in T-cell responses to 'self' antigens, such as anti-tumour and autoimmune responses, which can bear TCRs with substantially lower binding affinities than viral responses (Cole et al. 2007; Aleksic et al. 2012; Bridgeman et al. 2012). Furthermore, TCR-pMHC-II binding is also substantially weaker than that seen with pMHC-I (Cole et al. 2007; Bridgeman et al. 2012). In addition, the CD4 co-receptor does not aid stabilisation of TCR-MHC-II interactions (Crawford et al. 1998). The weaker binding

of MHC-II-restricted TCRs combines with the lack of co-receptor help to mean that CD4+ T-cells are generally more difficult to stain with pMHC tetramers than CD8+ T-cells. In contrast to CD4, the CD8 co-receptor, which binds to MHC-I, improves the on rate and dwell time of TCR-pMHC-I interactions thereby impacting the binding of pMHC-I tetramers (Daniels and Jameson 2000; Wooldridge et al. 2005; Laugel, van den Berg, et al. 2007). Anti-CD8 antibodies have also been described as having either positive or negative effects on the capture rate of pMHC-I tetramers depending on the individual antibody clone (Clement et al. 2011). The inclusion of a particular clone of anti-CD8 antibody during staining enhanced the staining intensity of pMHC tetramers across interaction affinities and improved detection of low affinity T-cells (Clement et al. 2011). Our research group have also shown improvements in pMHC tetramer staining when carried out in the presence of a reversible protein kinase inhibitor (PKI) (Lissina et al. 2009). The main PKI we use is Dasatinib as its effects are reversible allowing cells to be cultured after staining and sorting (Lissina et al. 2009). The use of PKI prevents TCR internalisation facilitating increased capture of pMHC multimers by cell surface TCRs and increases fluorescence intensity and the number of T-cells detected with many pMHC multimers. The addition of PKI during pMHC multimer staining provides an important, simple and inexpensive improvement to the technique and is now routinely used in our laboratory for detection of CD4 T-cells and anti-tumour and autoimmune CD8 T-cells. The use of higher-order pMHC dextramers, which include more fluorescent molecules (ultra-bright) and pMHC monomers per multimer, also improves fluorescence staining intensity and the detection of T-cells bearing low affinity TCRs compared to pMHC tetramers (Dolton et al. 2014). All of the above techniques can be used in combination providing synergistic improvement in T-cell staining (Wooldridge et al. 2009; Dolton et al. 2015).

Despite the protocol improvements to pMHC multimer staining of T-cells discussed above, at the start of this study there were still antigen-specific T-cell clones within our laboratory that could not be stained effectively with their cognate antigen in multimeric form - even as a dextramer. To address this problem, I investigated whether the use of anti-fluorochrome and secondary-conjugated Abs could improve pMHC multimer staining. This work was completed during my PhD and published (Tungatt et al. 2015) (see Appendix). I shall present some of these studies within this chapter to demonstrate that this method represents a further advancement for pMHC multimer staining of T-cells. I then applied these optimised staining protocols to detect IAV-specific porcine cytotoxic T-cells.

## 6.2 Hypotheses

This chapter is broadly divided into two sections; the optimisation of pMHC multimer staining protocols (tested with human T-cells where the technology is well established) and their application for detecting clinically relevant porcine T-cells. The hypotheses were as follows:

- The addition of anti-fluorochrome in combination with secondary-conjugated Abs will enhance the detection of antigen-specific human T-cells with pMHC multimers, by increasing the total number of fluorochrome molecules per labelled T-cell.
- The optimal detection of T-cells by pMHC multimer staining requires appropriate techniques throughout the protocol.
- Soluble peptide-SLA-I molecules (produced in chapter 5) assembled into pSLA tetramers will stain IAV-specific porcine T-cell clones.
- Optimised pMHC multimer staining protocols developed in human T-cells will also be optimal on porcine T-cells.
- Peptide-SLA tetramers can be used to assess the magnitude of IAV-specific cytotoxic T-cell responses in pigs *ex vivo*.
- Peptide-SLA tetramers can be used to assess the magnitude of IAV-specific cytotoxic T-cell responses in BAL *ex vivo* from Babraham pigs vaccinated with S-FLU alone.

## 6.3 Results

### 6.3.1 Optimisation of pMHC multimer staining with anti-fluorochrome antibodies

A new approach was applied to pMHC multimer staining to see if further improvements in human T-cell detection would allow the detection of antigen-specific clones we had in the laboratory that we were unable stain with cognate pMHC multimer. Two additional steps were added to our optimal protocol; a mouse anti-fluorochrome antibody to the corresponding fluorochrome on the pMHC multimer (1˚), followed by a goat anti-mouse Ig secondary antibody conjugated to this fluorochrome (2˚). A number of tests and controls were used in each experiment to ensure the specificity of any improvements afforded. T-cells were stained with pMHC multimer alone, with or without (+/-) the 1˚ Ab and +/- the 2˚ Ab (**Figure 6.1**). I aimed to directly compare the 'test' conditions (1 and 2 of **Figure 6.1**), alongside the controls to ensure any background staining was accounted for in analysis. The optimisation concept was that for each T-cell binding pMHC multimer, more fluorochromes would be added per T-cell hopefully improving its detection in flow cytometry.
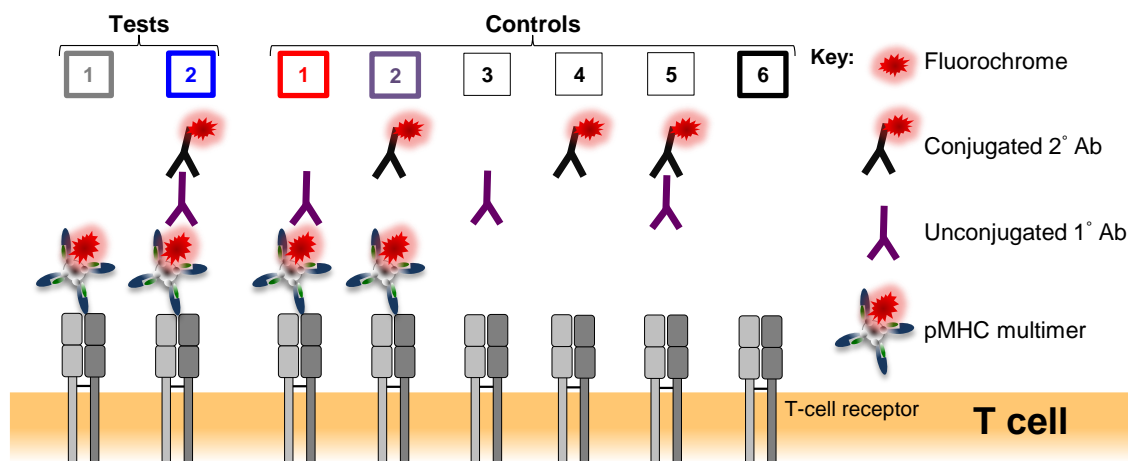
**Figure 6.1. Schematic representation of the test and control conditions used in this study.**
Alongside a standard pMHC multimer (tetramer or dextramer) staining protocol (test 1), the binding of a mouse anti-fluorochrome unconjugated 1° Ab to the pMHC multimer associated fluorochrome followed by a goat anti-mouse conjugated 2° Ab (test 2) was tested to see whether the fluorescence intensity of pMHC multimer staining could be improved. A number of controls were performed: control 1: pMHC multimer with 1° Ab; control 2: pMHC multimer with 2° Ab; control 3: 1° Ab alone; control 4: 2° Ab alone; control 5: 1° and 2° Abs in combination; and control 6: unstained. The colour coding for tests 1 + 2 and controls 1 + 2 + 6 is used throughout the figures of this optimisation.

To examine the use of 1° and 2° Abs, initial tests were performed with the ILA1 human CD8+ T-cell clone, which recognises the HLA-A2 restricted ILAKFLHWL epitope from $hTERT_{540-548}$ (Purbhoo et al. 2007). This T-cell clone is a good model system for optimisation experiments for two key reasons. Firstly, this hTERT peptide is not naturally presented on tumour cells removing any complications from a natural ligand when staining. Secondly, this T-cell clone recognises several altered peptide ligands (APLs), including 8E, 4L, 5Y and 3G that bind to the ILA1 TCR with differing affinities from $K_D$ ~3 μM to $K_D$ ~2 mM by surface plasmon resonance but bind to the HLA-A2 equally (Laugel, van den Berg, et al. 2007; Laugel, Price, et al. 2007). The unprecedented range of agonist ligands in the ILA1 system, that differ in affinity by almost 1000-fold, allows variation in TCR-pMHC affinity while other variables such as surface densities of TCR, CD8 and pMHC antigen remain constant. The 4L ligand ($K_D$ ~117 μM) is representative of a weakly binding TCR ligand such as those typically associated with autoimmunity. This ligand was therefore utilised in initial experiments. When used on its own, the 4L pMHC tetramer barely stained the ILA1 T-cell clone (mean fluorescence intensity (MFI): 203), addition of 1° and 2° Abs alone enhanced MFI by ~20-fold and by >6-fold in the presence of PKI (**Figure 6.1A**). The use of 1° and 2° Abs could therefore improve pMHC tetramer staining in the absence of PKI but also be used in combination with PKI synergistically. Crucially, and unexpectedly, these data revealed that the

use of 1° Ab alone could enhance tetramer staining in the absence of any additional fluorochromes when compared to tetramer alone (control 1 versus test 1 in **Figure 6.1**). The use of 1° Ab alone increased MFI >10-fold and almost 4-fold in the absence and presence of PKI respectively (**Figure 6.2A**). The realisation that the 1° Ab alone could have substantial effects on pMHC multimer staining ensured that the use of 1° Ab alone was also assessed in all proceeding experiments.

ILA1 cells were spiked into HLA-A2+ PBMC and stained with pMHC tetramers made with the index peptide and four APLs: 8E, 5Y, 4L and 3G ± PKI and ± 1°Ab (**Figure 6.2B**). The 3G ligand ($K_D$ = 2.9 µM) recovered T-cells in all conditions and was used to define 100% recovery. The use of 1°Ab or PKI alone were sufficient to obtain 100% recovery using 4L or wildtype tetramers, compared to 6% and 71% respectively with tetramer alone. However, for the 4L ligand it is important to note that the use of PKI and 1° Ab together substantially increased the MFI of recovered ILA1 cells. Complete recovery of the ILA1 clone at lower TCR affinities with 8E and 5Y ligands required the use of both 1° Ab and PKI in combination. This level of detection was not observed using 8E and 5Y tetramers alone where 0% and 0.1% recovery was seen respectively. The full recovery of ILA1 T-cells using the low affinity 8E tetramers was remarkable, as previous optimisations in the laboratory using PKI in combination with pMHC dextramers only afforded minimal detection of ILA1 cells when directly staining the clone and when the clone was spiked into PBMC samples (Dolton et al. 2014). I concluded that simple addition of 1° Ab to existing protocols extended the limit of TCR affinities detectable by pMHC multimer staining.

Improvements to pMHC tetramer staining were also seen with 1° Ab ± 2° Ab on an autoimmune CD8 T-cell clone (grown from a type 1 diabetes patient and known to poorly bind tetramer) and an MHC-II restricted CD4 influenza-specific T-cell clone, whether using PE or APCy fluorochromes (Tungatt et al. 2015). The use of higher amounts of pMHC tetramer (up to 2.4 µg/test) did not enhance staining of an anti-tumour CD8 T-cell clone and 1° Ab ± 2° Ab was still required for detection. Furthermore, as little as 0.003 µg of pMHC tetramer per test (with respect to pMHC content) could be used in combination with 1° Ab ± 2° Ab to successfully detect viral T-cells in PBMC. The use of 1° and 2° Abs also dramatically improved detection of anti-tumour CD8 T-cell responses directly *ex vivo* in tumour infiltrating lymphocytes (TILs). My optimised protocol could also be used in combination with pMHC dextramers and PKI to further enhance staining of T-cells bearing low affinity TCRs (Tungatt et al. 2015).
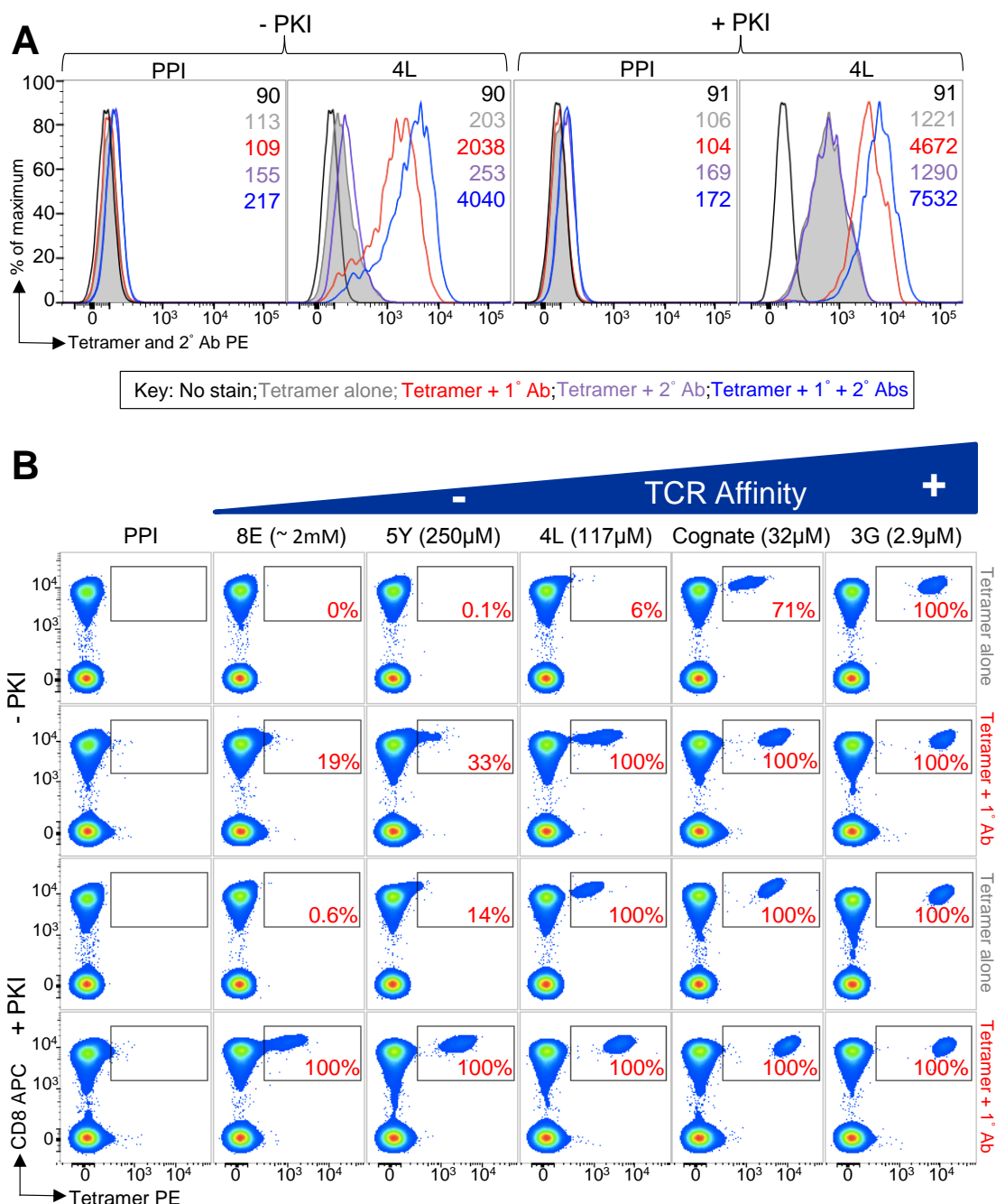
**Figure 6.2. Enhanced pMHC tetramer staining of T-cells using an anti-fluorochrome unconjugated Ab (1°).**
**A)** ILA1 hTERT-specific CD8+ T-cells ± 50 nM PKI were stained with HLA-A2 PE-conjugated tetramers, assembled with the 4L peptide ($K_D$ = 117 μM) or irrelevant (HLA-A2–ALWGPDPAAA, PPI) tetramers. Cells were stained with tetramers alone or with an anti-PE unconjugated 1° Ab, a 2° PE-conjugated Ab, or 1° + 2° Abs together. The mean fluorescent intensity is shown for each histogram. **B)** In a separate experiment, the ILA1 CD8+ clone was spiked in to PBMCs from an HLA-A2+ donor (used from frozen), treated ± PKI, and stained with PE-conjugated tetramers folded with cognate and APL agonists of the ILA1 clone ($K_D$ shown in parentheses) or irrelevant epitope (as in A). Tetramers were used alone or in combination with anti-PE 1° Ab. 2° Ab was not used in this experiment to highlight the unexpected effect of 1° anti-fluorochrome Ab. The percentage recovery of gated cells is displayed in the inset and was determined relative to the proportion of cells that stained with the 3G variant (considered 100%) after subtracting any background seen with the PPI tetramer. Cells were gated on viable CD3+ CD14- CD19- cells.

TCR/CD3 complexes downregulate from the T-cell surface upon antigen engagement (Valitutti et al.), the resulting low TCR density makes successful pMHC multimer staining more difficult (Dolton et al. 2014). I therefore wished to assess whether the use of anti-flurochrome 1° Ab and fluorochrome-conjugated 2° Ab could enhance pMHC multimer staining of recently activated T-cells. TILs from a metastatic melanoma patient were exposed to autologous tumour for 4 h and IFNγ response was detected by ICS alongside pMHC tetramer staining with a Melan-A peptide (**Figure 6.3**). The number of tetramer+ cells detected in TILs not exposed to tumour with 1° Ab and 2° Ab was defined as 100% recovery. In TILs exposed to tumour only 29%, 62% and 80% tetramer+ cells could be recovered using tetramer alone, + 1° Ab alone or with 2° Ab respectively. Similar effects were also observed on an autoimmune T-cell clone following antigen exposure. The use of the 1° and 2° Abs substantially improved detection and MFI of recently activated T-cells.
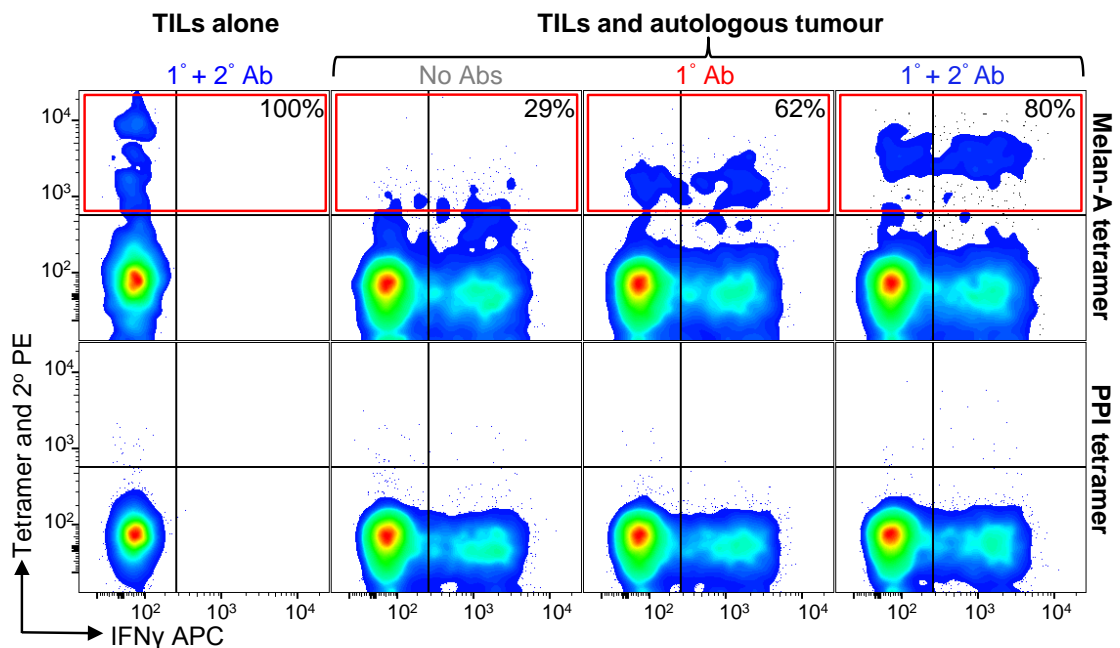


**Figure 6.3. Activated T-cells could be detected when tetramers were used with anti-fluorochrome and secondary Abs.**
TILs from a HLA-A2+ metastatic melanoma patient were incubated with brefeldin A and monensin ± autologous tumour. Cells were stained with cognate HLA-A2–ELAGIGILTV (Melan A) or HLA-A2–ALWGPDPAAA (PPI) PE-conjugated tetramers (Tet) alone or further labelled with an anti-PE unconjugated 1° Ab ± PE conjugated 2° Ab. Cells were also stained intracellularly for IFNγ. Tetramer+ cells (red box) from the TILs with autologous tumour are expressed as a percentage (inset, top panel) of tetramer+ cells (Tet + 1° + 2° Abs) from the TILs alone after subtracting the number of gated cells seen with the PPI tetramer (bottom panel).

Finally, I wished to investigate the mechanism behind the dramatic enhancements observed in MFI and detection of pMHC multimer positive cells by inclusion of an unconjugated anti-fluorochrome Ab. It was theorised that the 1° Ab was somehow stabilising the pMHC interaction or enhancing the emission of detectable fluorescence directly. It was shown that the enhancement occurred with all fluorochromes tested (PE, APCy and FITC) and also with different Ab clones making it unlikely that the increase in MFI was due to an effect on flurochrome detection. Instead, it seemed more likely that the 1° Ab was functioning by stabilising the pMHC multimer at the T-cell surface. To formally test this hypothesis, I stained an autoimmune CD8+ T-cell clone with tetramer ± PKI ± 1° Ab ± 2° Ab and fixed samples with PFA after staining or after taking the samples through incubation and wash steps to stimulate a normal tetramer staining protocol (**Figure 6.4A**). The MFI of cells stained with tetramer alone was almost halved at the end of the protocol indicating the loss of bound pMHC tetramers but staining was entirely maintained by addition of 1° Ab. A similar pattern was seen when cells were diluted following staining and MFI measured at subsequent time points. In the absence of 1° Ab nearly half of the staining was lost in just 30 min (**Figure 6.4B**). A similar experiment measuring the off-rate of pMHC tetramer was performed in the presence of anti-HLA-A2 Ab to prevent re-binding of pMHC to TCR and exaggerate the effect of tetramer dissociation (**Figures 6.4C&D**). This experiment again showed substantial loss (almost 90%) of tetramer staining in the absence of 1° Ab after 5 min. The use of 2° Ab in combination with 1° Ab afforded no additional improvements to stability in this set of experiments. It is likely that the anti-fluorochrome antibody exerts a cross-linking effect on the pMHC multimers decreasing the off-rate.

The protocol improvements discussed here were further consolidated in a review article I co-authored on pMHC multimer staining (Dolton et al. 2015) (see Appendix). The protocol we now use routinely for pMHC multimer studies is displayed in **Figure 6.5**. In addition to protocol optimisations, i.e. PKI and anti-fluorochrome Ab, it is also important to establish effective exclusion of dead cells and correct storage and use of reagents amongst other considerations. We find that PE is the best fluorochrome for use in pMHC multimer staining when compared to Brilliant-violet-421, APCy and FITC. My extensive pMHC staining optimisation work was all performed on human T-cells as the systems were in place in the laboratory for these types of experiments. Our previous experiments have shown that this optimisation works for CD8+ and CD4+ T-cells and for both human and murine T-cells.  I therefore made use of these optimised pMHC multimer protocols for the efficient detection of IAV-specific T-cells in samples from vaccinated Babraham pigs.

**Key: No stain; Cognate or Irrelevant tetramer alone; Cognate or Irrelevant tetramer + 1° Ab; Cognate or Irrelevant tetramer + 1° + 2° Abs.**
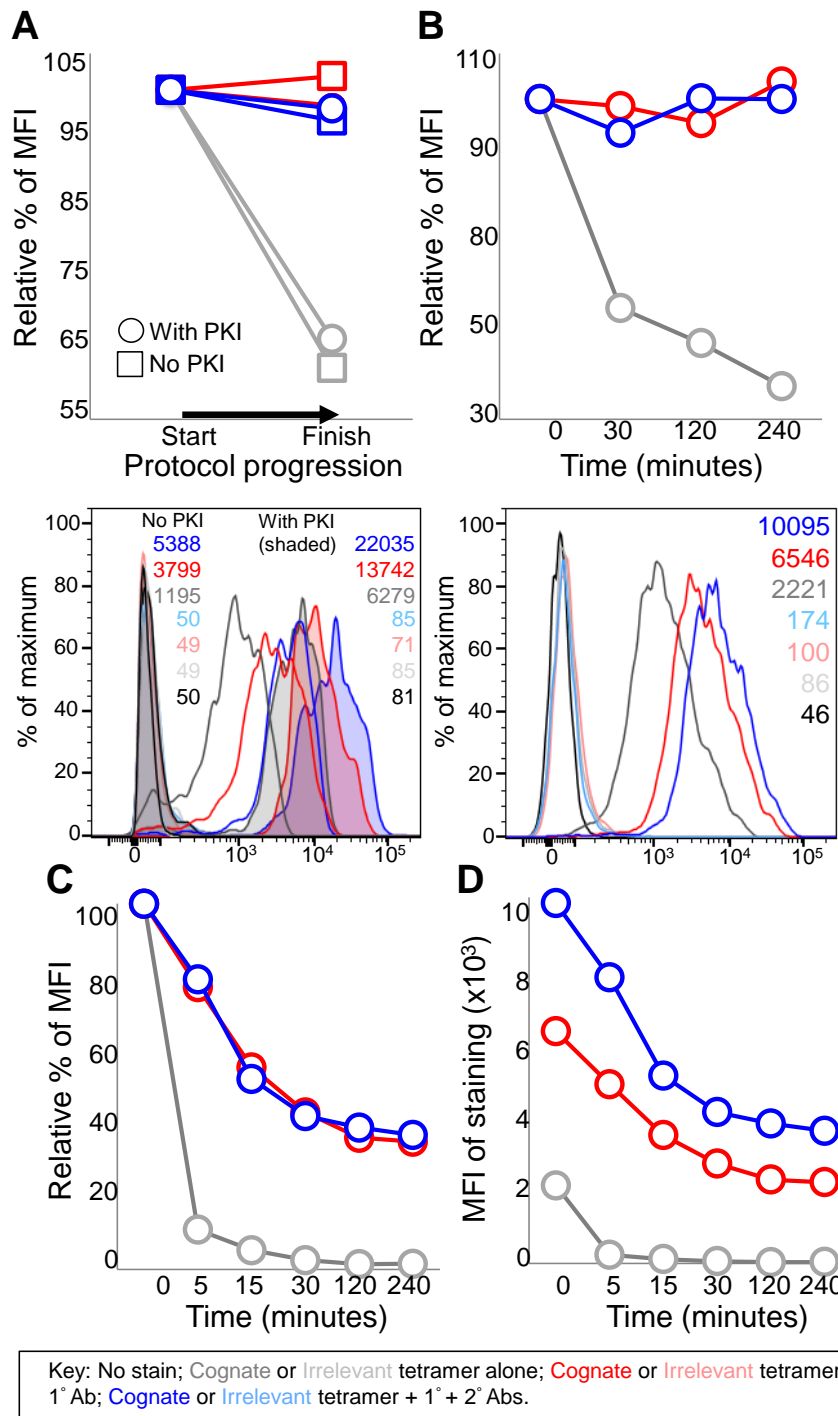
**Figure 6.4. Stabilisation with an anti-fluorochrome Ab preserves tetramer staining at the surface of T-cells.**
**A)** The CD8+ T-cell clone 3F2 was treated PKI, or left untreated, and stained with cognate HLA-A2–ALWGPDPAAA (from preproinsulin) PE-conjugated tetramers or irrelevant HLA-A2–NLVPMVTAV (from CMV) tetramers. Cells were stained with tetramer alone (grey) or tetramer with anti-PE unconjugated 1° Ab (red) ± a PE-conjugated secondary 2° Ab (blue). Once stained with tetramer ± 1° Ab ± 2° Ab (Start), the cells were taken through three incubations (20 min on ice) and associated wash steps (two times) before being analysed (Finish). The histogram shows the staining at the start of the assay. **B)** Clone 3F2 was treated with PKI and stained as in (A), then diluted in an excess volume of buffer (3 ml), and incubated at RT for the times shown. The histogram shows the staining at the start of the assay. **C and D)** From the same experiment in (B), cells were incubated at RT with an anti–HLA-A2 Ab (BB7.2) in 0.1 ml of buffer and samples taken at the times shown. Graphs display the percentage of tetramer staining relative to the start of the experiment for each condition (A–C) or the MFI (D). PKI was present throughout the assay for (B)–(D).

**Protocol flow**                    **Considerations**

Prepare PBMC sample from fresh or frozen material

Treat defrosted samples with DNase to remove cell clumps. Filter if necessary.

*Wash with staining buffer (2% FBS in PBS)*

Treat with 50 nM PKI at 37°C for 30 minutes

Store PKI in working aliquots at -20°C and make a fresh dilution weekly.

*No wash*

Tetramer* or dextramer* staining for 30 minutes on ice

*Wash with staining buffer*

Label with 1° Ab for 20 minutes on ice

*Wash 2X with staining buffer*

Label with 2° Ab for 20 minutes on ice

Remove aggregated reagent before use by spinning at full speed for 1 minute in microfuge. Avoid aggregates when pipetting.

*Wash with staining buffer then PBS*

Add viability stain for 5 minutes at room temperature

Follow manufacturer's instructions and optimise for your system/material

*No wash*

Stain for cell surface markers for 20 minutes on ice

Optimise the amounts needed for your system/material

*Wash with staining buffer*

Flow cytometry, magnetic based sorting or fixing (2% PFA)

* We assemble our pMHC multimers 24h in advance of an experiment. We store them in the dark and only for short periods (1-2 weeks).

**Figure 6.5. Protocol for staining PBMC with pMHC multimers.**
Staining is performed in 5 ml 'FACS' tubes. Our default protocol flow is shown by red arrows/text and involves using tetramer, PKI and 1° Ab. PKI is sometimes used without other tricks. Dextramers and/or 2° Ab are used when T-cells are particularly challenging to stain. The same protocol can be used for T-cell clones and lines.

*6.3.2   Porcine T-cell clone pMHC tetramer staining.*

The refolded pMHC-I monomers produced in chapter 5 were assembled into tetramers to confirm their ability to stain their respective T-cell clones. It was important to establish successful tetramer staining before proceeding to use these monomers to test optimised protocols for staining *ex vivo* porcine samples. Irrelevant tetramers (SLA-1*14:02 AFAAAAAAL, SLA-2*11:04 AGAAAAAAI and SLA-2*11:04 GAGGGGGGI) were also assembled and used as appropriate controls throughout these porcine studies. Influenza-specific CD8β T-cell clones were clearly detectable by pMHC tetramer staining (**Figure 6.6**). Importantly, this staining served to confirm both the peptide recognised and the restricting SLA-I molecule.
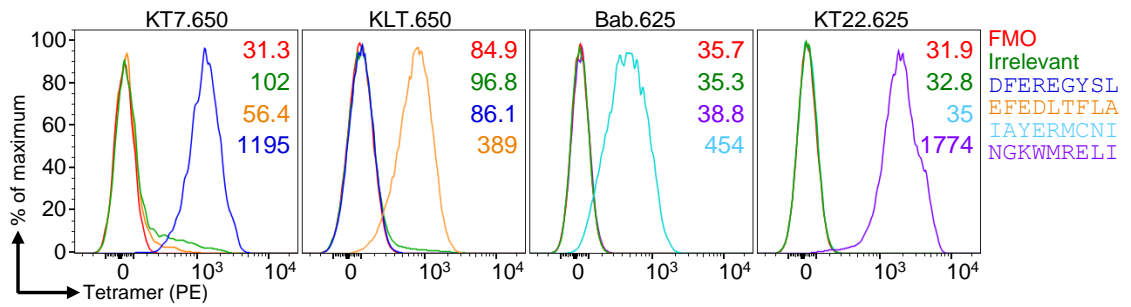
**Figure 6.6. Minimal epitope identification and pMHC tetramer staining of Influenza-specific porcine T-cell clones.**

Minimal epitopes defined in chapter 4 were used to produce pMHC tetramers and stain their cognate T-cell clones. Cells were gated for size and viability; mean fluorescent intensities (of Tetramer-PE) are displayed inset. T-cell clones KT7.650, KTS.650, Sue.625 and KT22.625 recognise the following epitopes; `DFEREGYSL`, `EFEDLTFLA` (both restricted by SLA-1*14:02) and `IAYERMCNI` and `NGKWMRELI` (both restricted by SLA-2*11:04). The following irrelevant tetramers were used: SLA-1*14:02 `AFAAAAAAL` and SLA-2*11:04 `AGAAAAAAI`.
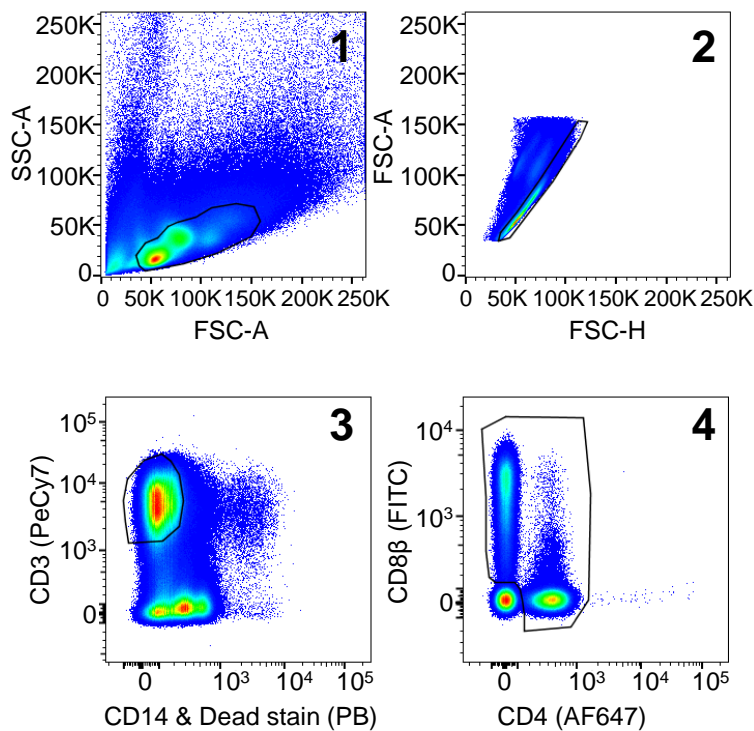


**Figure 6.7. Gating strategy for pMHC tetramer staining of PBMC, BAL and TBLN samples.**

A representative sample is displayed. Cells were gated on size, singlets, viability, CD14-, CD3+, CD4+ and CD8β+. Data were then displayed as CD8β expression versus pMHC tetramer staining.

### 6.3.3  Gating strategy for PBMC, BAL and TBLN samples

Before proceeding to staining *ex vivo* porcine samples, a gating strategy was established to provide optimal staining (**Figure 6.7**) and display data in a similar format to that used in human T-cell studies. One key difference was that γδ T-cells, which are found in substantially higher numbers in pigs than in humans, were excluded from the final display to improve staining clarity. Gamma Delta T-cells were not excluded directly as there was no conjugated γδ-TCR Ab readily available for use in pigs, therefore samples were gated on for both CD8β+ and CD4+. As extrathymic γδ T-cells are negative for CD8β and CD4 with some subsets expressing just the CD8α chain (Gerner et al. 2009).

### 6.3.4  Comparison of optimised and traditional pMHC tetramer protocols in pig PBMC

Initial testing on porcine PBMC samples was performed to establish whether the optimised pMHC multimer staining protocols discussed earlier in this chapter were effective for detecting porcine T-cells. Although the biggest improvements to pMHC multimer staining were detected for T-cells bearing lower affinity TCRs, not usually associated with viral responses, it was still important to establish whether use of optimised methods was beneficial in pigs. Optimisation was deemed particularly relevant as the pig samples in this study were isolated relatively recently after vaccination/boosting (day 13 post boost) and recently activated T-cells, as already discussed, are likely to have less TCR on their cell surface for capturing pMHC multimers. The addition of PKI and anti-fluorochrome Ab (optimised) improved the detection of porcine T-cells with pSLA-I tetramers compared to tetramer alone (**Figure 6.8**) for all four IAV epitopes in this study in PBMC samples from pigs #625 and #650. The largest increase in staining was in pig#625 PBMC with SLA-2 `IAYERMCNI` tetramers detecting 0.046% and 0.18% of tetramer+ CD8β+ cells in the non-optimised and optimised protocol respectively. Overall enhancements varied across pigs and epitopes with the increase in tetramer+ cells ranging from ~1.2- to ~3.9-fold. These optimised conditions were therefore utilised for all subsequent tetramer staining. Further comparisons between staining protocols in different tissues was not pursued due to sample availability and the fact that use of PKI and anti-fluorochrome Ab was inexpensive and simple to apply in all subsequent experiments.
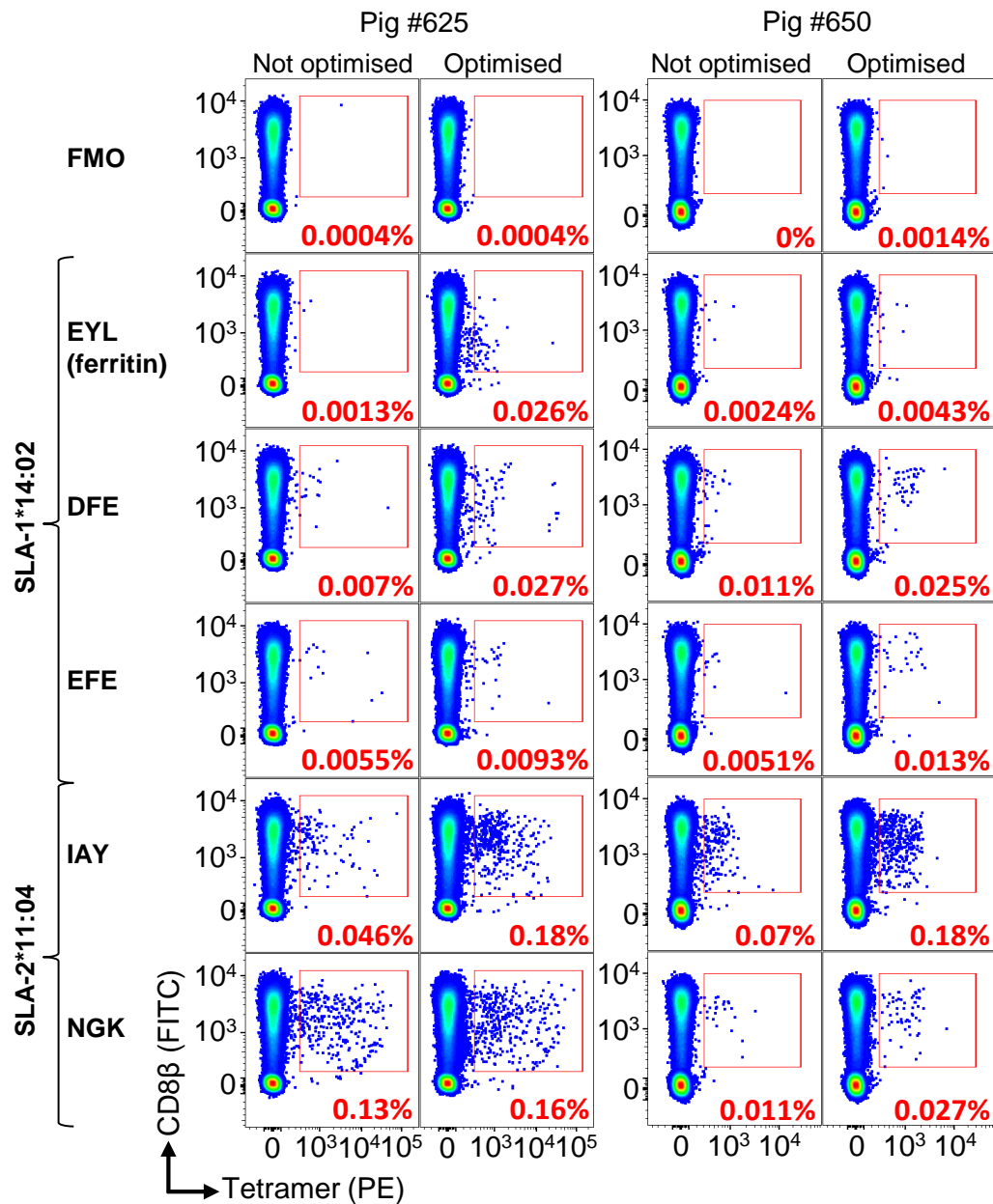
**Figure 6.8. Comparison between pMHC Tetramer staining protocols with and without optimisation on pigs #625 and #650 PBMC.**
pMHC tetramer staining was performed on pigs #625 and #650 PBMC samples either with or without optimisation – the addition of protein kinase inhibitor (dasatinib) and anti-fluorochrome (anti-PE) antibody. The following tetramers were used: DFEREGYSL, EFEDLTFLA, IAYERMCNI and NGKWMRELI. A self eluted peptide derived from ferritin (EYLFDKHTL) was also tested. The percentage of tetramer+ cells of CD8β+ cells is displayed in red.

### 6.3.5 Staining of ex vivo pig PBMC, BAL and TBLN samples with IAV-specific pMHC tetramers

I next wished to detect and quantify T-cells specific for the IAV epitopes identified in chapter 4 across different tissues from vaccinated pigs. Cryopreserved PBMC, BAL and TBLN samples (day 13 post boost) from pigs #625 and #650 were defrosted and stained with pSLA-I tetramers for the IAV epitopes, DFEREGYSL, EFEDLTFLA, IAYERMCNI and NGKWMRELI along with

appropriate irrelevant tetramer for each SLA-I molecule. Antigen-specific CD8β T-cells were detectable in both pigs across all samples (**Figures 6.9 and 6.10**). In pig#625, SLA-1*14:02 restricted DFEREGYSL and EFEDLTFLA responses accounted for 0.023% and 0.014% in PBMC, 0.091% and 0.37% in BAL and 0.052% and 0.047% in TBLN of cytotoxic T-cells, respectively (**Figure 6.9**). Similar responses were seen in pig#650 but with a higher detection of DFEREGYSL in BAL comprising 0.92% of cytotoxic T-cells (**Figure 6.10**). Responses to SLA-2*11:04 restricted epitopes IAYERMCNI and NGKWMRELI were notably higher in magnitude in both pigs, and particularly large local responses were detected in BAL. In pig#625 T-cells specific for the NGKWMRELI epitope accounted for 0.047%, 3.02% and 0.086% of cytotoxic T-cells in PBMC, BAL and TBLN respectively (**Figure 6.9**). Similar NGKWMRELI responses were detected in pig#650 with a higher percentage, 5.5%, present in BAL (**Figure 6.10**). The peptide IAYERMCNI was the immunodominant epitope across the three tissue samples and both pigs, except for in BAL from pig#650 but where IAYERMCNI still accounted for 4.63% of cytotoxic T-cells. IAYERMCNI responses comprised 0.1% and 0.13% in PBMC and 0.36% and 0.22% in TBLN, in pigs #625 and #650 respectively, of cytotoxic T-cells. The strongest response was detected in the BAL of pig#625 where 13% of the total cytotoxic T-cell population stained with SLA-2*11:04-IAYERMCNI tetramer (**Figure 6.9**).

### 6.3.6 *Peptide-MHC tetramer staining of BAL samples from S-FLU vaccinated pigs*

It was important that responses in comparable unvaccinated pigs were also examined. This required analyses of samples from a different vaccination experiment where unvaccinated control animals were available. In this experiment two pigs (#1 and #2) were left unvaccinated and three pigs received H1-S-FLU alone (#6, #7 and #8). This also meant I could determine which IAV T-cell responses were induced solely by S-FLU vaccination (not in combination with inactivated virus). BAL samples taken upon culling at day 57 were stained with pSLA-I tetramers to detect IAV-specific responses (**Figure 6.11**). Both unvaccinated pigs showed no substantial responses above background to the four IAV epitopes (data from pig #1 is shown). A small response was observed to EFEDLTFLA through SLA1*14:02 across the vaccinated pigs (0.078 – 0.17% of cytotoxic T-cells). In contrast, huge CD8β[+] tetramer[+] populations were seen in the BAL of the S-FLU vaccinated animals for the other three epitopes. The responses to DFEREGYSL, NGKWMRELI and IAYERMCNI ranged from 4.07-6.48%, 8.27-11.9% and 9.28-24.8% of total cytotoxic T-cells in BAL, respectively. In vaccinated pig #7 almost 40% of all CD8β T-cells in the BAL responded to just these three NP epitopes.
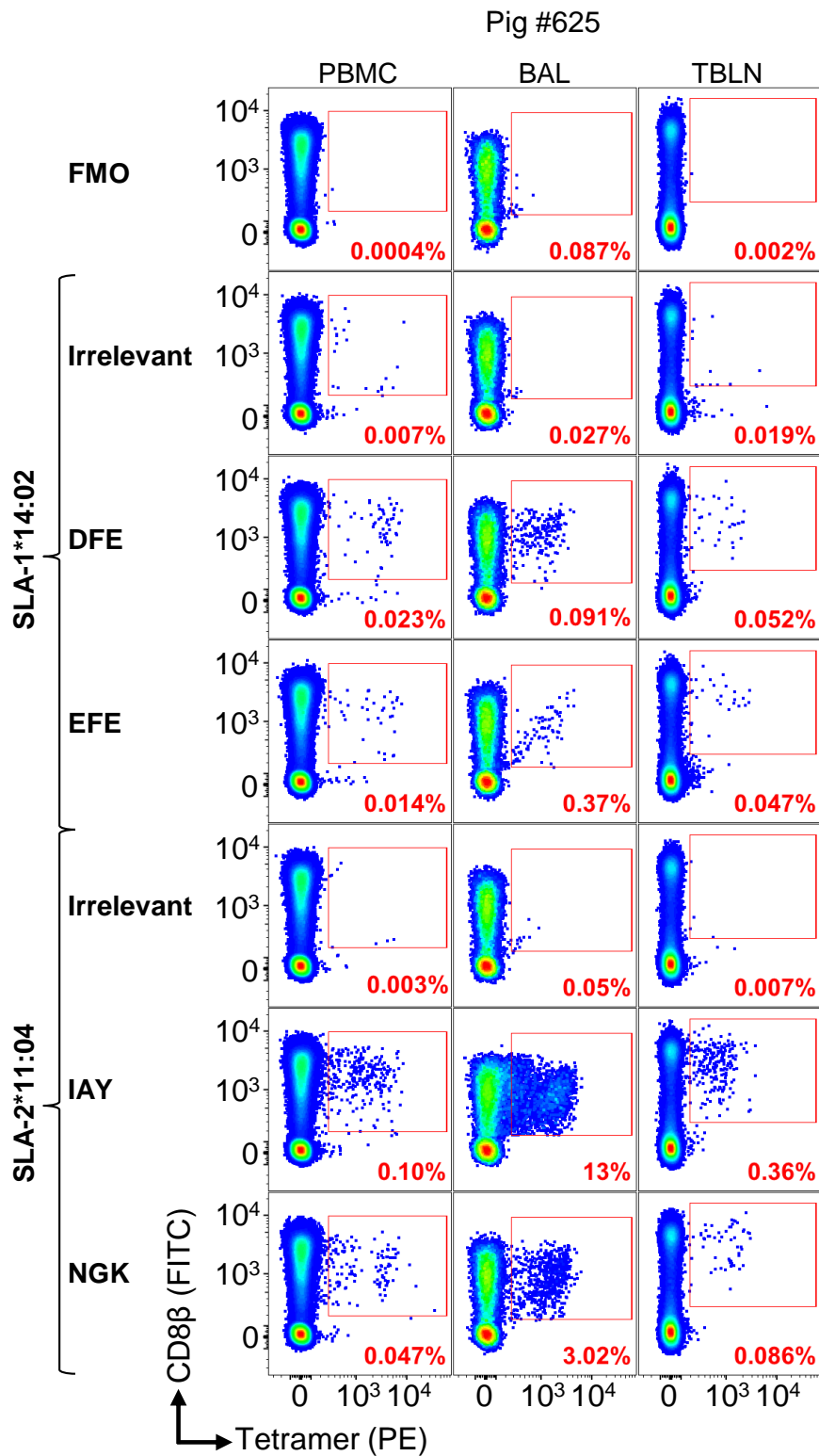
**Figure 6.9. Peptide-MHC Tetramer staining of PBMC, BAL and TBLN samples from inoculated Babraham Pig#625.**
Pig#625 received S-FLU intranasally and inactivated H1N1 virus [A/Swine/Spain/SF11131/2007] with montanide adjuvant intramuscularly, followed by a boost at day 25. Pigs were culled at day 38 (day 13 post boost) and PBMC, BAL and TBLN samples were harvested and frozen. Tetramer staining was performed on defrosted samples and the percentage of tetramer+ cells of CD8β+ (cytotoxic) cells is displayed in red. Tetramer staining of each pig and sample type were performed on different days. Irrelevant tetramers here refer to SLA-1 AFAAAAAAL, SLA-2 AGAAAAAAI (Pig #625) and SLA-2 GAGGGGGGI (Pig #650). Cells were gated on for size, viability, CD14-, CD3+, CD8β+ and CD4+.
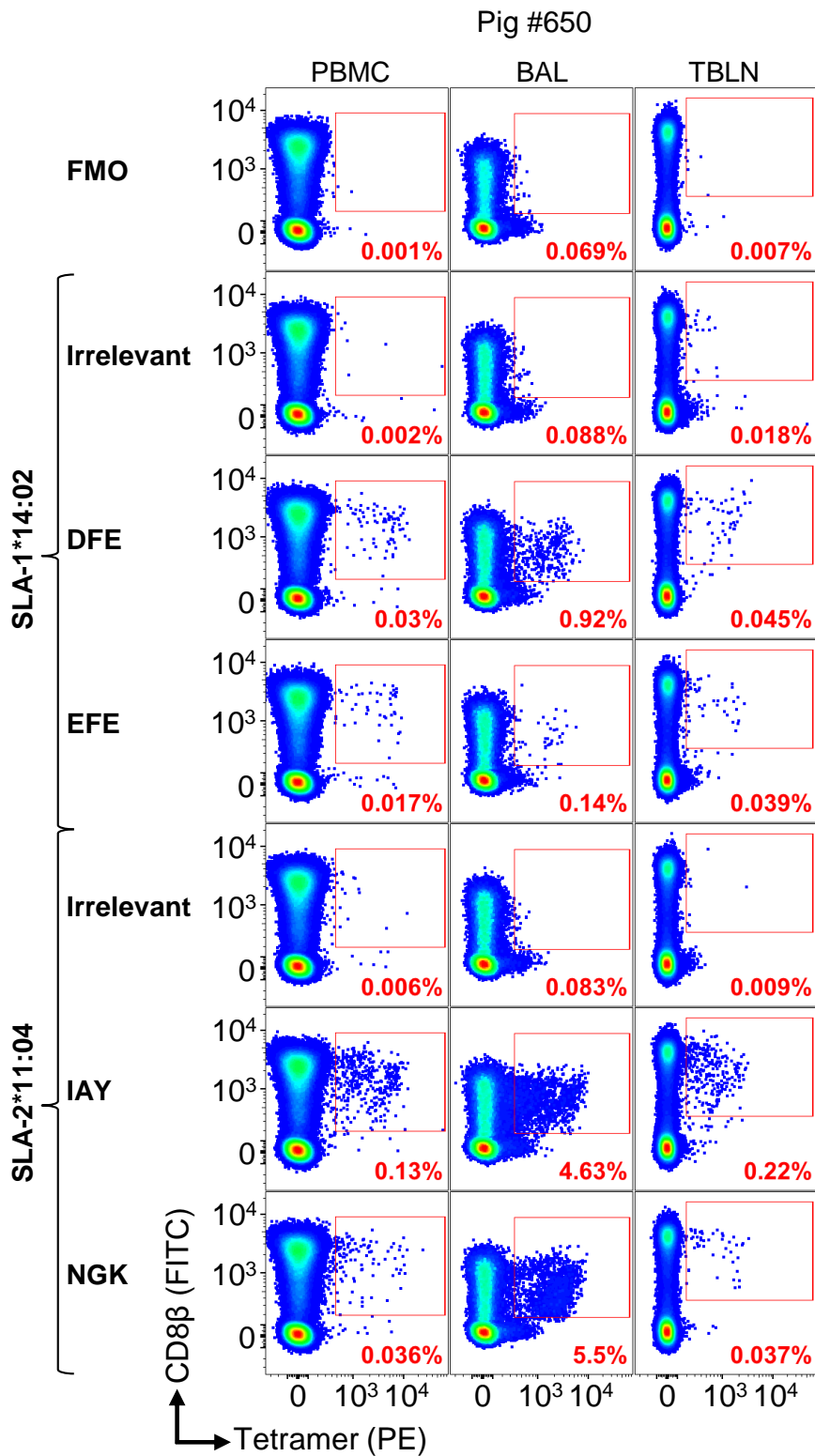
**Figure 6.10. Peptide-MHC Tetramer staining of PBMC, BAL and TBLN samples from inoculated Babraham Pig#650.**
Pig#650 received S-FLU intranasally and inactivated H1N1 virus [A/Swine/Spain/SF11131/2007] with montanide adjuvant intramuscularly, followed by a boost at day 25. Pigs were culled at day 38 (day 13 post boost) and PBMC, BAL and TBLN samples were harvested and frozen. Tetramer staining was performed on defrosted samples and the percentage of tetramer+ cells of CD8β+ (cytotoxic) cells is displayed in red. Tetramer staining of each pig and sample type were performed on different days. Irrelevant tetramers here refer to SLA-1 AFAAAAAL, SLA-2 AGAAAAAI (Pig #625) and SLA-2 GAGGGGGI (Pig #650). Cells were gated on for size, viability, CD14-, CD3+, CD8β+ and CD4+.

103

**Figure 6.11. Peptide-MHC Tetramer staining of BAL samples from Babraham pigs vaccinated with S-FLU.**
Babraham pigs were either left unvaccinated (Pigs #1 and 2) or received S-FLU [S-eGFP/N1(Eng)].H1(Eng)] via aerosol administration (Pigs #6, 7 and 8). Vaccinated animals received S-FLU twice with a boost at day 28. Animals were culled and BAL harvested at day 57. Tetramer staining was performed on defrosted BAL samples and the percentage of tetramer+ cells of CD8β+ (cytotoxic) cells is displayed in red. Both Pigs#1 and 2 exhibited similar tetramer staining so only Pig#1 is displayed here. Tetramer staining of Pig#8 was performed on a different day to the others. Irrelevant tetramers here refer to SLA-1 AFAAAAAAL and SLA-2 GAGGGGGGI. Cells were gated on for size, viability, CD14-, CD3+, CD8β+ and CD4+.

## 6.4 Discussion

### 6.4.1 Peptide-MHC multimer staining optimisation

The first focus of this chapter was on continuing work in our laboratory to improve pMHC multimer detection of antigen-specific T-cells. The threshold for pMHC multimer binding can be higher than that required for T-cell activation (Laugel et al., 2007). Improvements are particularly desirable where monomeric TCR-pMHC affinity is low preventing successful pMHC multimer binding. Weak T-cell interactions typically include those observed with anti-tumour and autoimmune responses and CD4/pMHC-II complexes (Cole et al., 2007; Aleksic et al., 2012). Enhancing detection of these T-cells will be beneficial across numerous, clinically relevant studies. Therefore, I conducted a comprehensive comparative study between the use of pMHC multimers alone and with existing improvements of PKI (Lissina et al., 2009) and dextramers (Dolton et al., 2014) and their use in combination with mouse anti-fluorochrome antibody (1° Ab) and goat anti-mouse Ig secondary antibody conjugated to the relevant fluorochrome (2° Ab). The concept being that the addition of more fluorochrome to each pMHC multimer labelled T-cell would enhance overall detection levels by flow cytometry. This study was published (Tungatt et al., 2015) (see Appendix) and has been summarised in this chapter. This part of my work also allowed me to learn the techniques of refolding pMHC and staining T-cells with pMHC multimers in the established human system before attempting to apply these techniques to pigs.

Along with the expected improvement in pMHC multimer staining when 1° Ab and 2° Ab were used in combination, I also observed an unanticipated improvement in staining when using just the 1° Ab alone. The low affinity ligand 4L barely stains the ILA1 T-cell clone as a tetramer but staining in the presence of 1° Ab ± PKI the MFI was substantially improved. The ILA1 T-cell clone was also spiked into HLA-A2+ PBMC to demonstrate this optimisation across different TCR-pMHC affinities in polyclonal T-cell populations. The recovery of ILA1 T-cells from HLA-A2+ PBMC with lower affinity ligands was substantially higher in the presence of 1° Ab alone and further enhanced with the addition of PKI. Our previous studies had been unable to detect the ILA1 clone with multimers of the 8E ligand so this result demonstrates the ability of 1° Ab and PKI in combination to extend the range of TCR affinities amenable to detection. For the higher affinity ligands, the 1° Ab is somewhat redundant for increasing the percentage of tetramer+ cells detected but it substantially improved MFI. The increases in MFI observed across comparisons in this study allowed clearer distinction of antigen-specific T-cells which can facilitate clearer analysis and clearer cell sorting by flow cytometry.

The use of 1° Ab and 2° Ab was tested across multiple systems and shown to be universally effective, including when tested on autoimmune and anti-tumour T-cell clones, pMHC-II restricted T-cell clones and clinically relevant TIL samples. This method can facilitate the detection of previously undetectable anti-tumour T-cells in TILs and could identify cell populations bearing different TCRs. Indeed an ongoing project within our laboratory has demonstrated that standard pMHC multimer staining fails to detect many fully functional T-cell clonotypes from clinically relevant samples. Surprisingly, this failure in detection can be considerable even with viral antigens suggesting that most previous studies using pMHC may have considerably underestimated the size of antigen-specific T-cell populations (Rius et al. unpublished). The use of 1° Ab and 2° Ab was compatible with use of PKI and pMHC dextramers; allowing researchers to adjust their combination of techniques to obtain optimal staining in their samples. I also showed that enhancements were independent of the amount of pMHC tetramer used, as even high amounts of tetramer failed to detect an anti-tumour T-cell clone that could be effectively stained in the presence of anti-fluorochrome antibody. Furthermore the use of 1° Ab ± 2° Ab enabled considerably less pMHC reagent to be used representing a considerable cost benefit (Tungatt et al., 2015). The detection of recently activated T-cells was also markedly improved by the addition of 1° Ab ± 2° Ab. The improved detection of recently activated T-cells is likely to be of benefit during *ex vivo* examination of autoimmune or cancer-specific T-cells where there is a high likelihood that such T-cells may have recently encountered cognate antigen.

The improvements afforded by the use of the 1° and 2° Abs were observed across all fluorochromes (PE, APCy and FITC) and different Ab clones tested. Experiments investigating the off-rate of pMHC tetramers indicated that the 1° Ab facilitates cross-linking of pMHC multimer on the T-cell surface substantially reducing the dissociation rate. This stabilisation effect may prove even more crucial when using more complex and lengthy staining protocols, such as ICS, during which there is ample opportunity for pMHC multimer dissociation from the T-cell surface. Overall, these data show that the use of anti-fluorochrome 1° Ab as well as 2° Ab offer considerable improvements over the current pMHC multimer tetramer technology particularly when investigating T-cells raised against low affinity TCR interactions. Although the inclusion of both Abs gave the best results, our laboratory now routinely uses just the 1° Ab in combination with PKI in pMHC tetramer staining. This removes the risk of increased background staining that can occur when using fluorochrome-conjugated 2° Abs. In addition, the use of only the 1° Ab provides the vast majority of the enhancement at very little cost (~GBP £0.16 per stain). It remains to be seen whether the optimised techniques discussed here used in combination are

capable of staining all antigen-specific T-cells within a sample, but the major improvements they afford, their low cost and ease of application suggest that these improvements should be applied routinely.

### 6.4.2   Peptide-MHC tetramer staining of porcine IAV-specific T-cells

The use of pMHC multimers, most frequently in the form of tetramers, for detecting antigen-specific T-cells has become commonplace in human and mouse studies since their initial description over 20 years ago (Altman et al. 1996). However, pMHC multimer staining in pigs has lagged far behind that in human and mouse due to a lack of relevant epitopes and soluble pSLA reagents. Since the first description of pSLA tetramers in 2011 (Patch et al. 2011) there have only been three further studies utilising these tools for detecting FMDV or Influenza-specific cytotoxic T-cells in PBMC samples only (Pedersen et al. 2014; Pedersen et al. 2016; Baratelli et al. 2017). Previous studies have not had the luxury of having T-cell lines and clones with which to optimise T-cell staining protocols.

The porcine T-cell clones procured in chapter 4 were stained with pMHC tetramer. This confirmed the ability of the pSLA-I tetramers to successfully stain their respective T-cell clones before advancing to *ex vivo* samples. New batches of pMHC complexes refolded within our laboratory are regularly tested in this way before widespread use in experiments. Irrelevant tetramers, using preferred residues at P2 and P9 with the remaining residues lacking side chains, were also designed for this study and confirmed not to stain in an unspecific manner. Previous studies using pSLA tetramers in pigs have utilised less stringent gating strategies than those described in this thesis. I aimed to apply the best strategies, reviewed in (Dolton et al. 2015), including effective exclusion of dead cells and CD14+ monocytes and neutrophils. Future panels could also look to include a marker to exclude B-cells, such as CD19 which is used when staining human T-cells. The antibody panel can also easily be extended to include further antibodies for phenotyping or effector functions. I used the CD8β Ab to distinguish porcine cytotoxic T-cells more clearly than the assessment of CD8α$^{high}$ CD4- populations which has traditionally been used in porcine studies. Our pSLA-I tetramers and stringent gating strategy provided clear and clean staining across samples with limited background and without unspecific binding to CD4+ T-cell populations.

Initial experiments on PBMC samples from pigs#625 and #650 confirmed that the optimised staining techniques developed in humans T-cells were applicable in porcine samples too. The

addition of PKI and anti-fluorochrome Ab increased the percentage of antigen specific T-cells detected in pigs without altering background staining. Consequently, the application of these simple protocol additions are recommended for porcine pSLA multimer studies to enable clearer staining and better T-cell detection. Enhancing T-cell detection with pSLA multimers was particularly relevant in my studies as samples were taken at day 13 post antigen boosting when T-cells were likely to be relatively activated and express low levels of surface T-cell receptor making then more difficult to detect by conventional staining techniques. Both PKI and 1° Ab were used in all subsequent pSLA-I tetramer staining in this study.

A comprehensive *ex vivo* pSLA-I tetramer stain was performed on PBMC, BAL and TBLN samples from pigs #625 and #650. This cohort of pigs, utilised for IAV epitope identification in chapter 4, were inoculated with both S-FLU and inactivated H1N1 Sw/Sp virus. All four of the NP epitopes (`DFEREGYSL`, `EFEDLTFLA`, `IAYERMCNI` and `NGKWMRELI`) could be detected in the PBMC, BAL and TBLN of pigs #625 and #650 providing clear validation of their presence following vaccination by H5-S-FLU and inactivated H1N1. T-cells specific for SLA-2*11:04 restricted epitopes `IAYERMCNI` and `NGKWMRELI` were more prevalent than those seen for the SLA-1*14:02-restricted epitopes `DFEREGYSL` and `EFEDLTFLA`. This suggests that IAV responses through SLA-2*11:04 are immunodominant in the Babraham pig line. As expected, the highest pSLA tetramer staining was seen in the BAL samples. This is in line with a previous study that infected outbred pigs intratracheally with H1N2 SwIV and detected virus specific IFN-γ+ CD8β+ T-cells in the lung (by ICS following *in vitro* restimulation of freshly isolated cells with H1N1 SwIV) in frequencies up to 30 times higher than that seen in PBMC and TBLN following infection (Talker et al. 2016). In pig#625, T-cells specific for `IAYERMCNI` accounted for 13% of cytotoxic T-cells in the BAL. In total around 16.5% and 11.2% of all cytotoxic T-cells in the BAL of pigs #625 and #650, respectively, respond to these four IAV epitopes. This high magnitude of local response was also replicated in the BAL from pigs vaccinated with S-FLU alone by aerosol. In this second cohort, a staggering percentage, ranging from 21.8 to almost 40%, of all CD8β T-cells in the BAL were specific for just these four IAV epitopes. This second cohort of pigs was particularly useful as it demonstrated that large T-cell responses to three of the four NP epitopes identified, `DFEREGYSL`, `IAYERMCNI` and `NGKWMRELI`, were induced by vaccination with S-FLU alone and were not already present in two unvaccinated pigs. Responses of this level in the BAL are highly likely to play a role in any protection mediated by this vaccine.

The use of pSLA-I multimers will allow the enumeration, phenotyping and isolation of T-cell responses to influenza and other diseases. Further viral challenge studies will be required to further investigate the T-cells capable of responding to the IAV epitopes identified in this study. Both phenotypical and functional analyses will need to be performed and it remains to be determined if these responses offer any correlates of protection following S-FLU vaccination. These technologies could be implemented to measure T-cell responses to different vaccination strategies and track their presence over the long-term in the Babraham pig model. The pSLA tetramer staining protocol described in this chapter could be utilised to provide robust detection of porcine antigen-specific T-cells in future studies.

# 7  Defining SLA-I Anchor motifs for epitope prediction and the generation of super-agonist peptides for defined epitopes

## 7.1  Background

As discussed in chapter 5, in any given peptide-MHC complex there are certain peptide residues that will sit within the peptide binding groove (PBG) and act as primary anchors for adhering the peptide to the MHC molecule. Different MHC alleles will have different PBG pocket compositions and this determines which peptides can be accommodated. Indeed, the huge polymorphism in the HLA is focussed around the PBG primary anchor positions and allows different HLA to present different peptides. (Hughes et al. 1990; Parham and Ohta 1996; Sette and Sidney 1998). The different amino acids that can be tolerated at each anchor residue are used to formulate the peptide binding motif for a particular MHC molecule. Peptide binding motifs can then be used to scan known proteins or sequences for peptides matching an MHC binding motif. Determination of the Babraham pig SLA-I binding motifs will facilitate further IAV CD8β T-cell epitope prediction across different viral proteins and strains.

## 7.2  Hypotheses

The primary anchor positions in both SLA-1*14:02 and SLA-2*11:04 were determined as P2 and P9 (C-terminus) (Chapter 5) in the peptide. I wished to determine which amino acid residues could be tolerated at these anchor positions and formulate the peptide binding motif for each Babraham pig SLA-I molecule. The binding motifs could then be tested for T-cell epitope identification across different influenza viral proteins. In the second half of this chapter, work was commenced to generate super-agonists of the IAV epitopes defined in this study (chapter 4). The concept behind these experiments shall be discussed in the relevant results section. The chapter hypotheses are listed below:

Part 1:

- Only certain amino acid residues will be tolerated at the anchor positions by a certain Babraham pig SLA-I molecule allowing the definition of peptide binding motifs.
- Peptide binding motifs can predict clinically relevant epitopes across different influenza viral proteins.

Part 2:

- Nonamer combinatorial peptide library (CPL) screens on IAV porcine CD8β T-cell clones will identify super-agonist peptides.

- Super-agonist peptides will induce greater responses in SwIV porcine CD8β T-cell clones than the corresponding index peptide sequences.

## 7.3 Results

### 7.3.1 Determination of peptide binding motifs for Babraham pig SLA-I molecules

The primary anchor residues for both Babraham pig SLA-I molecules are at P2 and P9 (C-terminus) within the peptide. To determine the peptide binding motif for each SLA-I, I examined which of the 20 proteogenic amino acids could be tolerated in these anchor positions by amino acid substitution in all four new SwIV epitopes described in chapter 4. Relevant porcine CD8β T-cell clones were incubated with these peptide mutations and the wildtype 'index' peptides overnight and MIP-1β release was measured (**Figure 7.1**). For SLA-1*14:02, clone KT4.650 saw the index amino acid at P2 in DFEREGYSL, Phe2, strongest with 3.61 ng/mL MIP-1β released however it also tolerated Ala, Met and Tyr at P2 with the latter being the second preference (**Figure 7.1A**). This clone also preferred the index amino acid at P9, Leu2, but also tolerated Phe and Met well and Ile and Val to a lesser extent at P9 (**Figure 7.1B**). CD8β T-cell clone KLT.650 gave a stronger response to Trp than to its index anchor 2, Phe (**Figure 7.1A**) inducing 1.07 and 0.611 ng/mL MIP-1β release respectively. Phe, Ile, Leu and Met were tolerated at P9 by this clone and preferred to the index amino acid, Ala (**Figure 7.1B**). These data for SLA-1*14:02 were collated to give a proposed binding motif as displayed in **Figure 7.1C**; [xF/Y/W/M/AxxxxxxL/F/M/I/A/V].
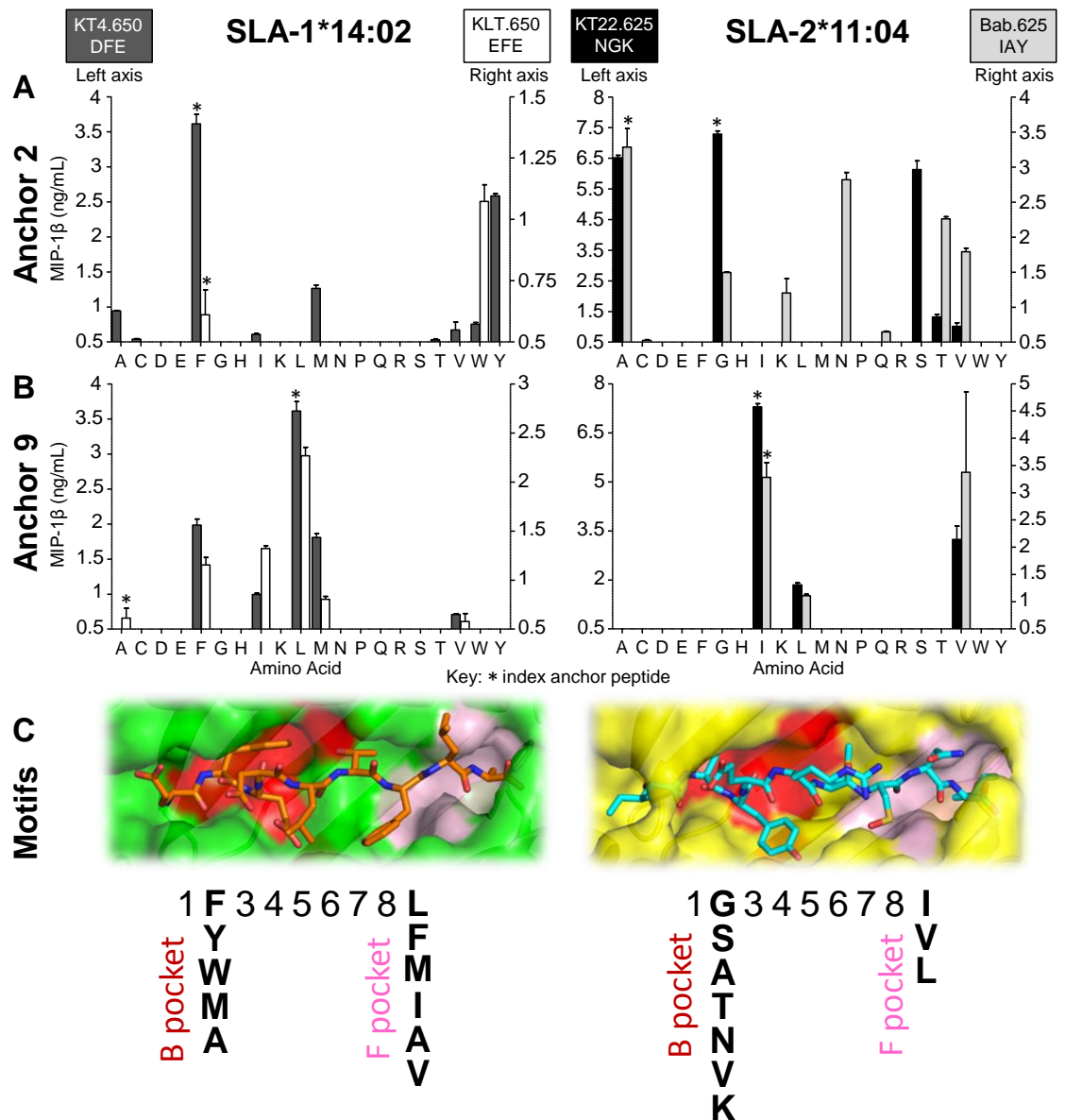
**Figure 7.1. Peptide-MHC anchor residue preference and proposed binding motifs for SLA-1*14:02 and SLA-2*11:04.**

Influenza-specific cytotoxic T-cells clones were incubated overnight with their index peptide and altered peptides covering all possible amino acids at anchor 2 **(A)** and anchor 9 **(B)** for both SLA-1 and SLA-2 restricted epitopes. T-cell clones were incubated with different titrations of the peptides and data at $10^{-7}$ M and $10^{-8}$ M are displayed for SLA-1 and SLA-2 respectively. All conditions were performed in duplicate and MIP-1β release was detected by ELISA and is displayed as mean + SEM. Results below 0.5 ng/mL have been omitted for clarity. T-cell clones KT4.650, KLT.650, KT22.625 and Bab.625 respond to the following index peptides respectively; DFEREGYSL, EFEDLTFLA, NGKWMRELI and IAYERMCNI. * denotes the index amino acid for each clone. **(C)** Binding pocket composition and proposed binding motif for SLA-1*14:02 and SLA-2*11:04 determined from the data in panels A&B. SLA-1*14:02 (green) with EFEDLTFLA (orange sticks) and SLA-2*11:04 (yellow) with IAYERMCNI (cyan sticks). Double conformers have been removed for visual clarity. B pocket is shown in red and the F pocket in pink.

For SLA-2*11:04, T-cell clones KT22.625 and Bab.625 displayed a preference for their index amino acid at P2 but other residues were also tolerated well (**Figure 7.1A**). The index residue at P2, Gly, for clone KT22.625 induced 7.29 ng/mL MIP-1β. Two other residues, Ala and Ser, also induced strong responses releasing 6.52 and 6.13 ng/mL MIP-1β respectively. Thr and Val at P2 were tolerated but to a much lesser degree. In contrast, Bab.625 tolerated strongly residues Thr and Val and was also able to tolerate Asn at P2 unlike clone KT22.625. The residue tolerance at the P9 anchor was more limited for the SLA-2*11:04-restricted clones. Both clones saw peptides with their P9 index residue, Ile, strongly but additionally responded to peptides with Val and Leu in this position (**Figure 7.1B**). The SLA-2*11:04 data were collated to give a proposed binding motif of [xG/S/A/T/N/V/KxxxxxxI/V/L] as displayed in **Figure 7.1C**. Application of pocket assignment as used in human MHC molecules (Matsumura et al. 1992) showed that for both SLA molecules P2 and P9 of the peptide sit within B and F pockets respectively (**Figure 7.1C**). Pockets B and F in SLA-1*14:02 are large and deep whereas the pockets are shallower in SLA-2*11:04.

### 7.3.2  Using SLA-I binding motifs for IAV epitope prediction

The binding motifs for the Babraham pig SLA-I molecules can be used to scan any protein sequence for 9 amino acid length peptides that contain the anchor residue preferences. I therefore wished to preliminary test whether these SLA-I binding motifs determined above could predict other IAV epitopes. The conserved Influenza protein PB2 was scanned with the SLA-2*11:04 motif using 'Motif Scan' available at www.hiv.lanl.gov. This generated 81 predicted epitopes for PB2 (**Table 10.7**). These peptides were initially incubated with vaccinated pig#650 PBMC samples *ex vivo* and IFNγ release was measured by ELISpot alongside the validated SLA-2*11:04 restricted epitope, IAYERMCNI, as a positive control (**Figure 7.2**). As expected, the percentage of IAV-specific T-cells in PBMC was low (as seen in pMHC tetramer staining in chapter 6) and background noise in the assays was high. Even the immunodominant IAYERMCNI peptide only gave ~20 spots per 300,000 PBMC in IFNγ ELISPOT with background being >5 spots.

The higher level of detection of IAV-specific T-cells by pMHC tetramer staining in BAL (chapter 6) meant that screening with such samples would have been preferable. Unfortunately, BAL samples were limited and this prevented all the PB2 predicted peptides from being screened using BAL. Therefore, I selected six peptides that gave 10 or more spots in PBMC screening (**Figure 7.2**); sequences RNGPMTNTV, GGEVKNDDV, QNPTEEQAV, VVVSIDRFL, NKATKRLTV and GTAGVESAV; to screen in the remaining pig#650 BAL samples. This identified peptide NKATKRLTV as a genuine epitope (**Figure 7.3**) with around 10 IFNγ SFCs per 150,000 BAL cells.

The peptide IAYERMCNI was again used a positive control and produced nearly 60 IFNγ SFCs per 150,000 BAL cells. Both PBMC and BAL samples responded, as expected, to the H1-S-FLU and the inactivated H1N1 Sw/Sp virus but also released IFNγ when incubated with another H1N1 strain; A/Sw/Eng/1353/09 virus. Ideally the new PB2 epitope, NKATKRLTV, needs further verification including pMHC tetramer staining. The NKATKRLTV peptide was refolded to produce pSLA-I tetramers but in an initial experiment I was unable to detect tetramer+ cells within BAL or PBMC samples from pigs#650. Project time restraints prevented producing new batches of pSLA-I monomer and pursuing this further. A recent experiment by a collaborator, Emily Porter, in Bristol has infected a new cohort of Babraham pigs intranasally with H1N1 [A/sw/Eng/1353/09]. The plan is to collect a large amount of BAL from these pigs. These samples will be used for testing the epitope predictions made herein. In addition, these pigs will allow screening of what T-cell responses Babraham pigs make to infection with IAV.
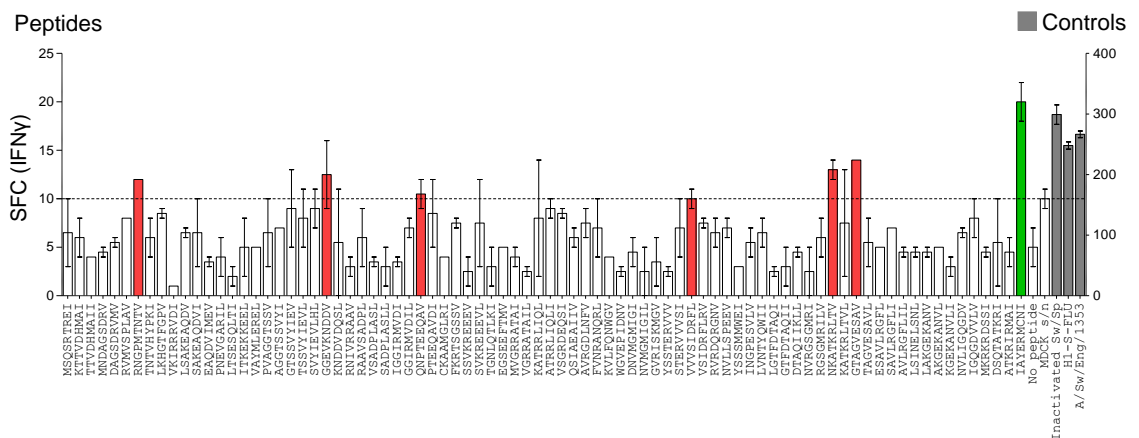


**Figure 7.2. Responses to epitope predictions in Pig#650 PBMC.**
Approximately 300,000 PBMC from Pig#650 were incubated per well for 16-18 h with $10^{-5}$M peptide or with relevant controls. All conditions were performed in duplicate and spot forming cells (SFC) by IFNγ release were detected by ELISpot and are displayed as mean ± SEM. The following epitopes (displayed in red) were selected for further testing: RNGPMTNTV, GGEVKNDDV, QNPTEEQAV, VVVSIDRFL, NKATKRLTV and GTAGVESAV. The previously validated epitope, IAYERMCNI (displayed in green) was used a positive control. Viral positive controls are shown in grey and on the right y axis.

Newly identified epitope:
NKATKRLTV
Viral protein: PB2
SLA-I Restriction: SLA-2*11:04
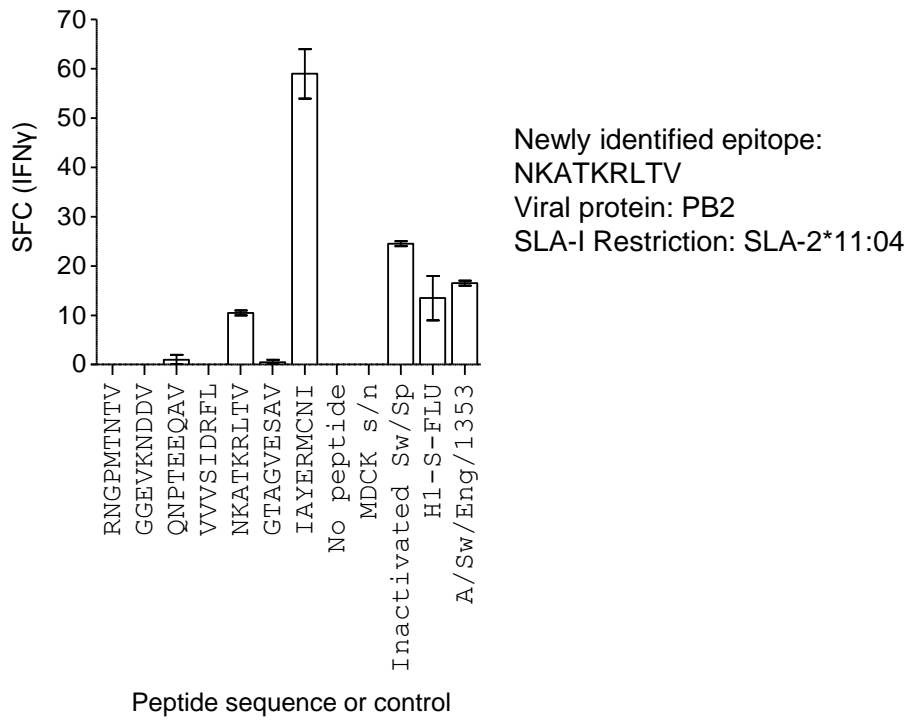
**Figure 7.3. Responses to PB2 epitope predictions in BAL from Pig#650.**
150,000 BAL cells from Pig#650 were incubated per well for 16-18 h with $10^{-5}$M peptide or with relevant controls. All conditions were performed in duplicate and spot forming cells (SFC) by IFNγ release were detected by ELISpot and are displayed as mean ± SEM. Previously validated epitope IAYERMCNI was used as a positive control.

### 7.3.3 Determining essential residues in IAV epitopes by alanine substitutions

To begin to investigate what peptide residues in the defined IAV epitopes may be essential for TCR interactions as well as MHC binding, each residue was substituted for Alanine one at a time. These experiments were performed with the following IAV epitopes, DFEREGYSL, EFEDLTFLA and NGKWMRELI, and their respective T-cell clones were used to detect sensitivity to each peptide substitution (**Figure 7.4**). T-cell clones KT13.650 and KT22.625 recognise the SLA-2*11:04 restricted peptide NGKWMRELI and despite expressing different TCRs both displayed similar responses to the alanine substituted peptides (**Figure 7.4A**). Alanine substitutions at P3, P4, P6, P8 and P9 were not tolerated by either clone. Alanine being tolerated at P2 but not P9 fits with the SLA-2*11:04 binding motif determined in **Figure 7.1**.

CD8β T-cell clone KT7.650 recognises the SLA-1*14:02 restricted peptide DFEREGYSL and did not tolerate alanine substitutions at P4, P5, P7 and P9 and displayed highest sensitivity to the index peptide (**Figure 7.4B**). The pSLA-I structure of this epitope resolved in chapter 5 showed Arg at P4 sitting prominently above the PBG suggesting it may be involved in TCR engagement

therefore mutation of this residue to alanine could prevent interaction with cognate TCRs. The SLA-1*14:02 binding motif tolerates alanine at both P2 and P9, however at P9 alanine may not be the preferred residue across all epitopes, as clone KT7.650 did not tolerate the P9 alanine substitution (**Figure 7.4B**) as also shown by its sister clone (same TCR clonotype) KT4.650 in **Figure 7.1B**.

CD8β T-cell clone KLT.650 recognises the SLA-1*14:02 restricted peptide `EFEDLTFLA` and did not tolerate alanine substitutions at any peptide residue except at P2 (**Figure 7.4C**). The pSLA-I structure of this epitope resolved in chapter 5 showed Asp at P4 and Leu at P5 sit prominently above the PBG suggesting they may be involved in TCR engagement therefore their mutation to alanine could prevent interaction with cognate TCRs.

## 7.3.4 Generation of super-agonist peptides – background

The adaptive immune response must be capable of recognising all possible foreign pathogens and therefore T-cells must be able to recognise a plethora of peptide-MHC complexes. For this breadth of immune coverage to be possible within an individual's T-cell pool, TCRs must be cross-reactive and capable of recognising numerous different peptides (Mason 1998; Sewell 2012b). Indeed, our research group has previously shown that individual T-cell clones can recognise vast numbers of different peptides in the context of a single MHC molecule (Wooldridge et al. 2012). A single TCR, isolated from a type 1 diabetes patient that recognises a preproinsulin-derived peptide in the context of HLA-A2, is capable of recognising > 1 million different decamer peptides (Wooldridge et al. 2012). The inherent cross-reactivity of TCRs make it unlikely that the cognate natural ligand will be optimal, and opens the possibility that more potent ligands could be identified (Sewell 2012b). Improvements to immunogenicity using optimised peptide ligands, also referred to as super-agonist peptides, are of particular interest for peptide-based vaccines.
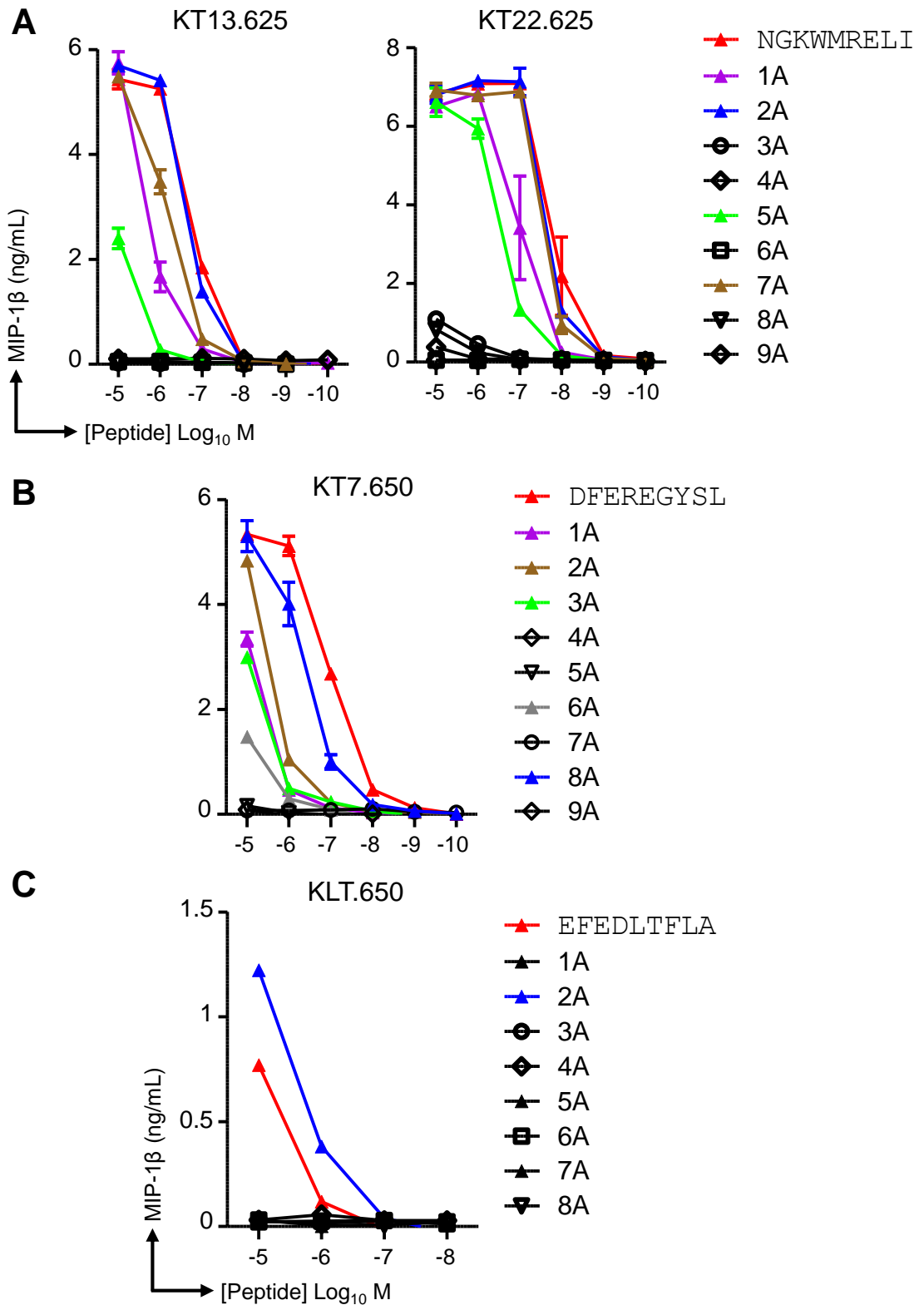
**Figure 7.4. Responses of porcine cytotoxic T-cell clones to alanine substituted IAV epitopes.**
CD8β+ T-cell clones (as labelled) were incubated with their respective index peptide, **(A)** NGKWMRELI, **(B)** DFEREGYSL, **(C)** EFEDLTFLA and single residue alanine substitutions for 16-18 h. MIP-1β release was detected by ELISA. Data were performed in duplicate and are displayed as mean ± SEM minus background (T-cells alone). T-cell clones KT13.650, KT22.625, KT7.650 and KLT.650 were plated at ~9000, ~24,000, ~7000 and ~5600 per 96U well respectively. Peptide sequences are colour coded and displayed inset. Sequences in black induced low or no response.

A super-agonist can be formed from the cognate natural peptide, also referred to as the index peptide, by substituting certain amino acid residues within the peptide sequence to improve T-cell sensitivity. These substituted peptides are also known as altered peptide ligands (APLs) (Sloan-Lancaster and Allen 1995; Kersh and Allen 1996). Positional-scanning combinatorial peptide libraries (PS-CPL) provide one technique for identifying APLs for individual T-cell clones and quantifying residue preference. PS-CPLs contain a number of peptide mixes each with a fixed amino acid at one peptide residue with the remaining residues comprising any of the proteogenic amino acids (excluding cysteine). PS-CPLs have been used in several studies that have identified more potent immunogenic peptides using this technique (Pentier et al. 2013). Previous studies by our group that have demonstrated improvements in TCR/pMHC binding affinity and functional improvements in anti-tumour and autoimmune T-cell responses using APLs identified by PS-CPL (Ekeruche-Makinde et al. 2012; Wooldridge et al. 2012; Ekeruche-Makinde et al. 2013). It is important to ensure the correct peptide length is used for a particular TCR to ensure optimal agonists are identified by PS-CPL as MHC-I TCRs are known to show a peptide length preference (Ekeruche-Makinde et al. 2013). The optimisation of T-cell epitopes is not just limited to self-derived peptides, where typically one would presume there is the greatest room for improvement, but has also been demonstrated for viral epitopes (Pentier et al. 2013). La Rosa and colleagues demonstrated that APLs, identified using a nonamer PS-CPL, derived from an immunodominant human cytomegalovirus epitope, were 1,000 to 10,000-fold more active than the index peptide (Rosa et al. 2001). At the end of this study I wished to preliminary investigate whether optimised ligands could be identified in this manner for porcine IAV T-cell responses and if they could induce greater T-cell sensitivity.

### 7.3.5 Increasing peptide sensitivity by inclusion of antigen presenting cells

In my laboratory, it has been found that when using PS-CPLs to scan T-cell clones it is preferable to use them in conjunction with an APC to increase T-cell responses and enable MIP-1β detection by ELISA. There was no porcine APC line available that expressed the Babraham pig SLA-I molecules therefore I needed to identify a "surrogate APC". The commercially available porcine kidney cell line, ESK-4, expresses both Babraham pig SLA-I molecules (Ho et al. 2009). The inclusion of ESK-4 cells with two different CD8β T-cell clones increased sensitivity to their respective index peptides, inducing high MIP-1β release at $10^{-9}$ M peptide that was not seen in the absence of ESK-4 cells (**Figure 7.5A and B**). This indicated ESK-4 cells could be used in Babraham pig T-cell assays to increase SLA-I responses. Unfortunately, I was unable to culture ESK-4 cells to the quantities required for PS-CPL scans. I therefore tested a Babraham pig kidney

cell 'line' which had been isolated by collaborators at the Pirbright Institute. Babraham pig kidney cells markedly improved T-cell sensitivity when incubated with T-cell clone KT7.650 and its index peptide (**Figure 7.5C**). In the presence of Babraham pig kidney cells, clone KT7.650 released 7.29 to 9.66 ng/mL MIP-1β at $10^{-9}$ M peptide, whereas in the absence of Babraham pig kidney cells only 0.48 ng/mL MIP-1β was detected at $10^{-9}$ M peptide (**Figure 7.5C**). The Babraham pig kidney cells were not immortalised but continued to grow in sufficient numbers to enable their use as an 'APC' in the PS-CPL scans performed in this study.
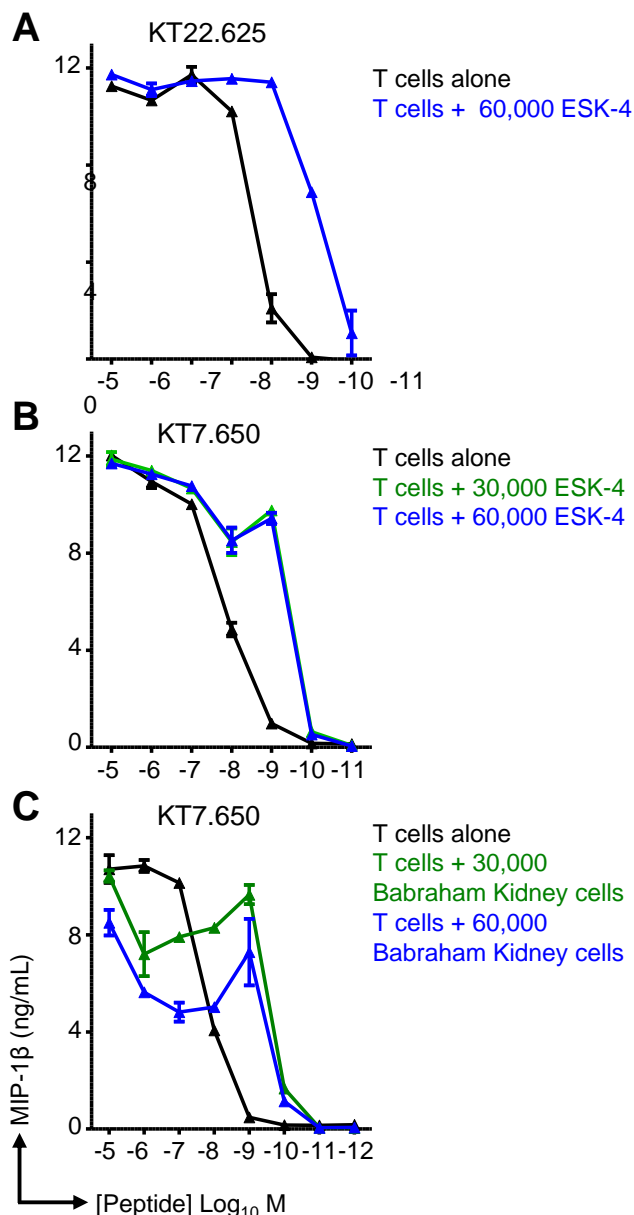


**Figure 7.5. Porcine T-cell clones tested for readout sensitivity with or without "APC".** CD8β+ T-cell clones (as labelled) were incubated with their index peptide for 16-18 h with or without ESK-4 cells **(A & B)** or Babraham pig kidney cells **(C)**. MIP-1β release was detected by ELISA. Data were performed in duplicate and are displayed as mean ± SEM (minus the corresponding background level). In all experiments the number of "APC" used per well is displayed together with either 30,000 **(A & B)** or 22,200 **(C)** T-cells per well.

## 7.3.6 Identification of super-agonists for IAV SLA-2*11:04 restricted epitope NGKWMRELI

The CD8β porcine T-cell clone KT22.625, that recognises the IAV derived peptide NGKWMRELI, was scanned using a nonamer PS-CPL (**Figure 7.6**). The residues at P3, P4, P6, and P9 in the index peptide sequence were optimal and induced the highest MIP-1β release in the peptide mixtures fixed at these positions. Different residues at the other positions along the peptide, P1, P2, P5, P7 and P8, afforded improved responses compared to the index peptide sequence. For example, when Trp was the fixed residue at P5, clone KT22.625 released 9.42 ng/mL MIP-1β compared to only 2.33 ng/mL MIP-1β with the index residue (Met). At P8, when either Ile or Val were fixed the peptide mixture induced substantially more MIP-1β, by ~20 to 28-fold, than the index residue at P8 (Leu) (**Figure 7.6**).
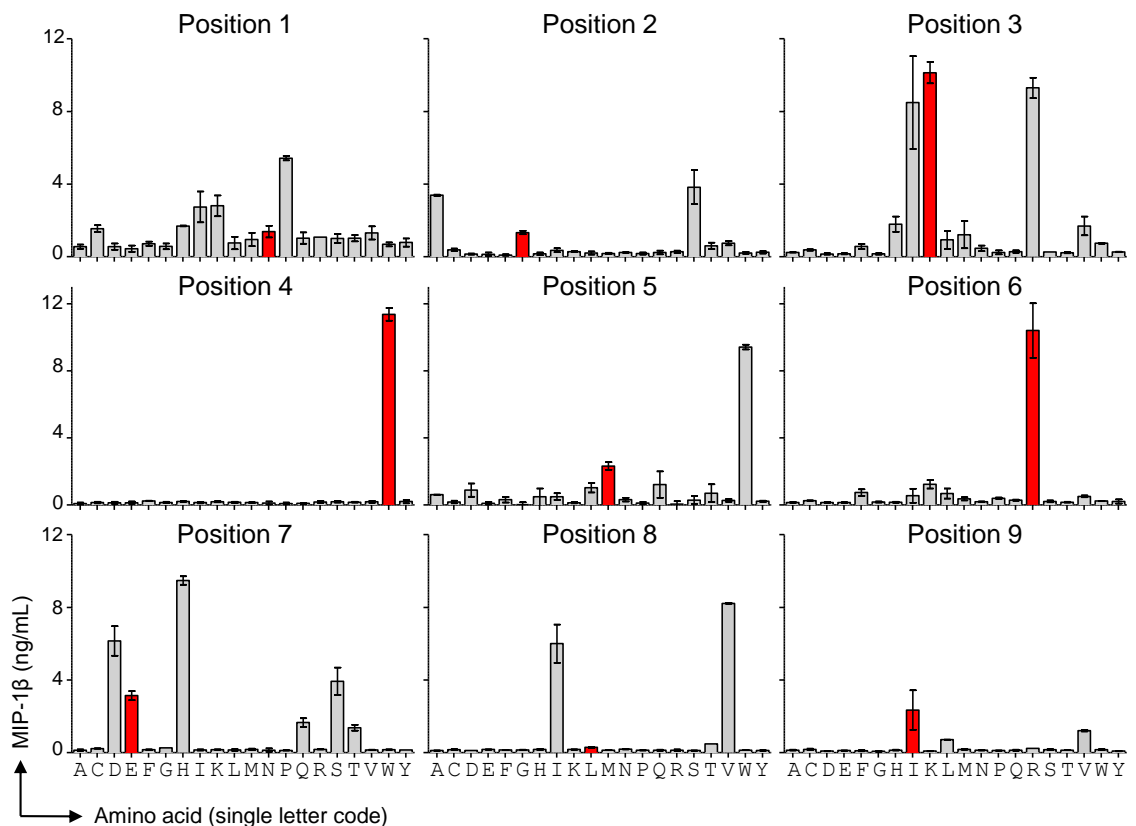


**Figure 7.6. Combinatorial Peptide Library screen of Influenza cytotoxic porcine T-cell clone KT22.625.**
Nonamer CPL screen of CD8β+ T-cell clone KT22.625 using Babraham pig kidney cells as antigen presenting cells and MIP-1β ELISA to detect activation. The index peptide amino acid sequence [NGKWMRELI] is represented as a red bar for each position. Data were performed in duplicate and are displayed as mean ± SD.

The PS-CPL data were input into a novel webtool, PI-CPL (Szomolay et al. 2016), that ranks different peptide sequences in order of the likelihood that they would be recognised by the cognate T-cell clone based on raw PS-CPL data. The top ten sequences from this list were tested for recognition by KT22.625 (**Figure 7.7**). The majority of these APLs induced were not recognised by the T-cell clone and induced little MIP-1β and the rest of the APLs (**PSI**W**W**R**HV**I, **PAI**W**W**R**HV**I and **PS**KW**W**R**DV**I) did not increase sensitivity over that observed with the index peptide (NGKWMRELI). Therefore, I took the index peptide sequence and substituted a single residue at a time with the amino acid(s) preferred at each residue position in the PS-CPL (**Figure 7.6**) and also combined these for double and triple substitution APLs. These APLs, listed in **Figure 7.8**, were tested for recognition by the cognate T-cell clone KT22.625. Single residue substitutions were tolerated well at P1, P7 and P8. But the substitution of Met, for Trp at P5 decreased MIP-1β release nearly 4-fold at $10^{-6}$ M peptide compared to the index sequence, and induced negligible MIP-1β at lower peptide concentrations. The double and triple substitution APLs incorporating Trp at P5 also displayed substantially less MIP-1β release than the index peptide. The three APLs that induced the highest sensitivity were sequences NGKWMRE**V**I, NGKWMRE**I**I and NGKWMR**DV**I which improved MIP-1β release by >4, ~3.5 and ~2.8-fold respectively at $10^{-9}$ M peptide compared to the index peptide (**Figure 7.8**).
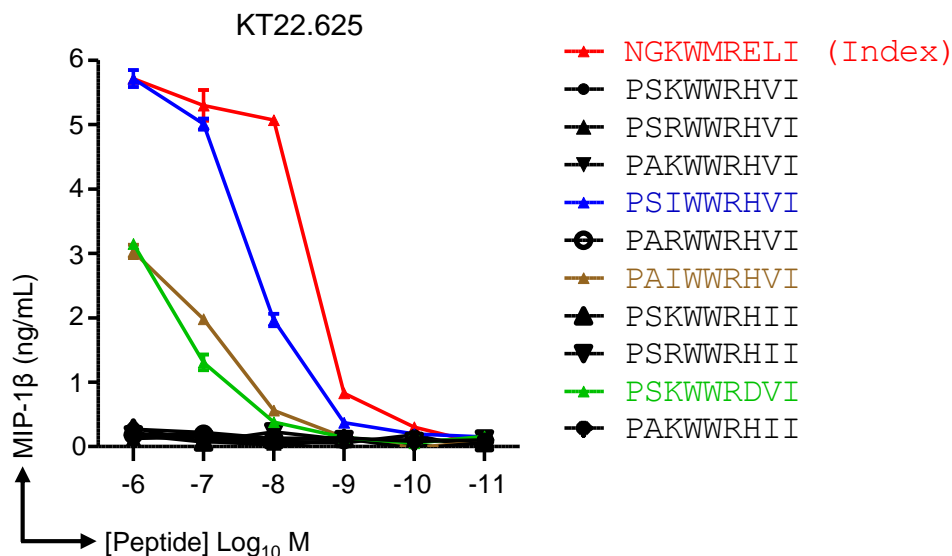


**Figure 7.7. Response of porcine T-cell clone KT22.625 to altered peptide ligands (APL).** CD8β+ T-cell clone KT22.625 was incubated with titrations of its index peptide and APLs for 16-18 h. MIP-1β release was detected by ELISA. Data were performed in duplicate and are displayed as mean ± SEM minus background (T-cells alone). Peptide sequences are colour coded and displayed inset. Sequences in black induced low sensitivity.

KT22.625

NGKWMRELI (Index)
Single residue substitutions
PGKWMRELI
NGKWWRELI
NGKWMRHLI
NGKWMRDLI
NGKWMREVI
NGKWMREII
Double residue substitutions
NGKWWRHLI
NGKWWRDLI
NGKWWREVI
NGKWWREII
NGKWMRHVI
NGKWMRHII
NGKWMRDVI
NGKWMRDII
Triple residue substitutions
NGKWWRHVI
NGKWWRHII
NGKWWRDVI
NGKWWRDII

**Figure 7.8. Response of porcine T-cell clone KT22.625 to altered peptide ligands (APL)**
CD8β+ T-cell clone KT22.625 was incubated with titrations of its index peptide and APLs for 16-18 h. MIP-1β release was detected by ELISA. Data were performed in duplicate and are displayed as mean ± SEM minus background (T-cells alone). Peptide sequences are colour coded and displayed inset. Sequences in black induced low sensitivity.

### 7.3.7 Identification of super-agonists for IAV SLA-1*14:02 restricted epitope EFEDLTFLA

The CD8β porcine T-cell clone KTe.650, that recognises the IAV derived peptide EFEDLTFLA, was scanned using a nonamer PS-CPL (**Figure 7.9**). The MIP-1β responses exhibited by KTe.650, and its sister clone KLT.650, have been substantially lower than that observed with other T-cells clones such as KT22.625 which recognises the epitope NGKWMRELI. The index residue was optimal at residues P1, P4 and P6 but at the other residue positions there were more optimal amino acids. For example, when Arg was fixed at P7, clone KTe.650 released 0.42 ng/mL MIP-1β compared to just 0.19 ng/mL MIP-1β with the index residue (Phe) (**Figure 7.9**). The strongest responses, although not by a large margin, at P2 and P9 were seen when Trp and Leu were fixed respectively, which fit within the SLA-1*14:02 binding motif in **Figure 7.1**. The index residue, Asn, at P4 induced substantially higher MIP-1β response than any other residue fixed at this position. The pSLA-I structure resolved in chapter 5 showed that the Asn at P4 sits prominently

above the SLA-1*14:02 binding groove indicating its likely involvement in TCR engagement which may explain why changes at this residue are not tolerated. The PS-CPL data from T-cell clone KTe.650 supports the earlier experiments, anchor and alanine scans, performed on its sister clone KLT.650 where alanine is not tolerated well at any residues other than P9.
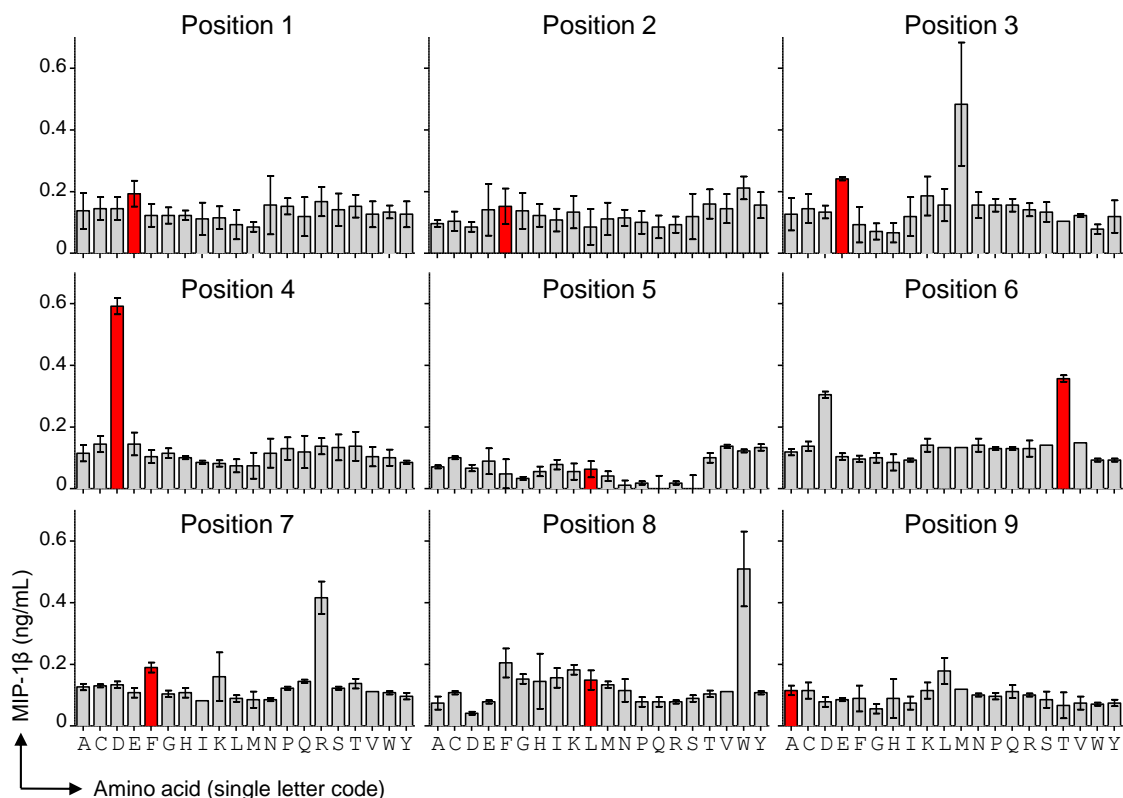


**Figure 7.9. Combinatorial Peptide Library screen of Influenza cytotoxic porcine T-cell clone KTe.650.**
Nonamer CPL screen of CD8β+ T-cell clone KTe.650 using Babraham pig kidney cells as antigen presenting cells and MIP-1β ELISA to detect activation. The index peptide amino acid sequence [EFEDLTFLA] is represented as a red bar for each position. Data were performed in duplicate and are displayed as mean ± SD.

The PS-CPL data from clone KTe.650 were input into the PI-CPL webtool (Szomolay et al. 2016) and the ten highest ranked sequences were tested for T-cell clone sensitivity along with single, double and triple substitution APLs (**Figure 7.10**). All of the highest ranked APLs assembled by the webtool induced considerably less response than the index peptide and induced no response at $10^{-7}$ M peptide and are therefore omitted from the graph in **Figure 7.10**. Furthermore, all APLs that displayed no or negligible MIP-1β release compared to the index peptide at $10^{-7}$ M peptide are also omitted from the graph. From the single substitution APLs, incorporating Met at P3, or Arg at P7, or Trp at P8, all substantially reduced the sensitivity below that seen with the index peptide (**Figure 7.10**). All of the ten highest ranked APLs generated by the webtool contained all three of these substitutions which likely accounts for their reduced sensitivity. A number of APLs

induced higher MIP-1β responses than that observed with the index peptide the best two of which were single substitution EFEDLTFL**L** and double substitution E**W**EDLTFL**A.** Both of these APLs induced ~7.3-fold more MIP-1β release at $10^{-8}$ M peptide than the index sequence and still induced T-cell responses at $10^{-9}$ M peptide (**Figure 7.10**).



Figure legend (peptide sequences, colour coded):

EFEDLTFLA (index)
Single residue substitutions
EWEDLTFLA
EFMDLTFLA
EFEDVTFLA
EFEDYTFLA
EFEDLTRLA
EFEDLTFWA
EFEDLTFLL
Double residue substitutions
EWMDLTFLA
EWEDVTFLA
EWEDYTFLA
EWEDLTRLA
EWEDLTFWA
EWEDLTFLL
EFMDVTFLA
EFMDYTFLA
EFMDLTRLA
EFMDLTFWA
EFMDLTFLL
EFEDVTRLA
EFEDVTFWA
EFEDVTFLL
EFEDYTRLA
EFEDYTFWA
EFEDYTFLL
EFEDLTRWA
EFEDLTRLL
EFEDLTFWL
Triple residue substitutions
EFMDLTRLW

**Figure 7.10. Response of porcine T-cell clone Kte.650 to altered peptide ligands (APL).** CD8β+ T-cell clone KTe.650 was incubated with titrations of its index peptide and APLs for 16-18 h. MIP-1β release was detected by ELISA. Data were performed in duplicate and are displayed as mean ± SEM minus background (T-cells alone). Peptide sequences are colour coded and displayed inset. Sequences in black induced low sensitivity and are omitted from the graph. Specifically, any APL displaying no response or less than half that of the index peptide at $10^{-7}$ M peptide are omitted from the graph.

## 7.4 Discussion

The identification of the primary anchor residues, P2 and P9 (PC), of the Babraham pig SLA-I molecules in chapter 5, enabled the establishment of MHC binding motifs here that were used in conjunction with a webtool to successfully predict a subdominant IAV T-cell epitope. Amino acid substitution at the anchor positions in all four defined IAV epitopes was used to establish which amino acids could be tolerated in these positions and build a peptide binding motif for each SLA-I allele. Other studies defining porcine SLA-I binding motifs have not had porcine T-cell clones for this purpose. The motif for SLA-1*14:02, [xF/Y/W/M/AxxxxxxL/F/M/I/A/V], conforms to that determined in preliminary studies using elution of self-peptides (*Immune function in healthy and African Swine Fever virus (ASFV) infected pigs. DEFRA final project report: SE 1509.* 2003) which produced a more stringent motif of [x-Y/F/A-xxxxxx-L/I]. A different motif, [xG/S/A/T/N/V/KxxxxxxI/V/L] was identified for SLA-2*11:04. The preferences for these residues became apparent when looking at the pockets of the SLA binding groove. P2 is accommodated by the B pocket which is large and deep in SLA-1*1402 allowing it to tolerate large aromatic residues whereas in SLA-2*11:04 the pocket is shallower. The F pocket accommodates the C-terminus (P9), again in SLA-1*1402 it is larger and can tolerate larger residues (F and M) whereas in SLA-2*11:04 it is shallower but with limited tolerance.

The peptide binding motifs were defined here in the context of T-cell recognition, and they enabled successful epitope prediction and determined a motif for SLA-1*1402 that fitted with previous mass spectrometry data. However, using such a T-cell informed technique could have disadvantages as a particular anchor mutation may alter the peptide landscape and prevent recognition by that specific TCR, but the peptide sequence itself could in fact be capable of binding to the MHC molecule. There are other MHC focused assays that could be pursued. A simple and well-established method in humans (T2 cells) and mice (RMA-S cells) utilises TAP-deficient cell lines which express structurally unstable MHC-I complexes only transiently at their cell surface (Cerundolo et al. 1990; Schumacher et al. 1990; Hoppes et al. 2010). The addition of exogenous peptides which are capable of binding t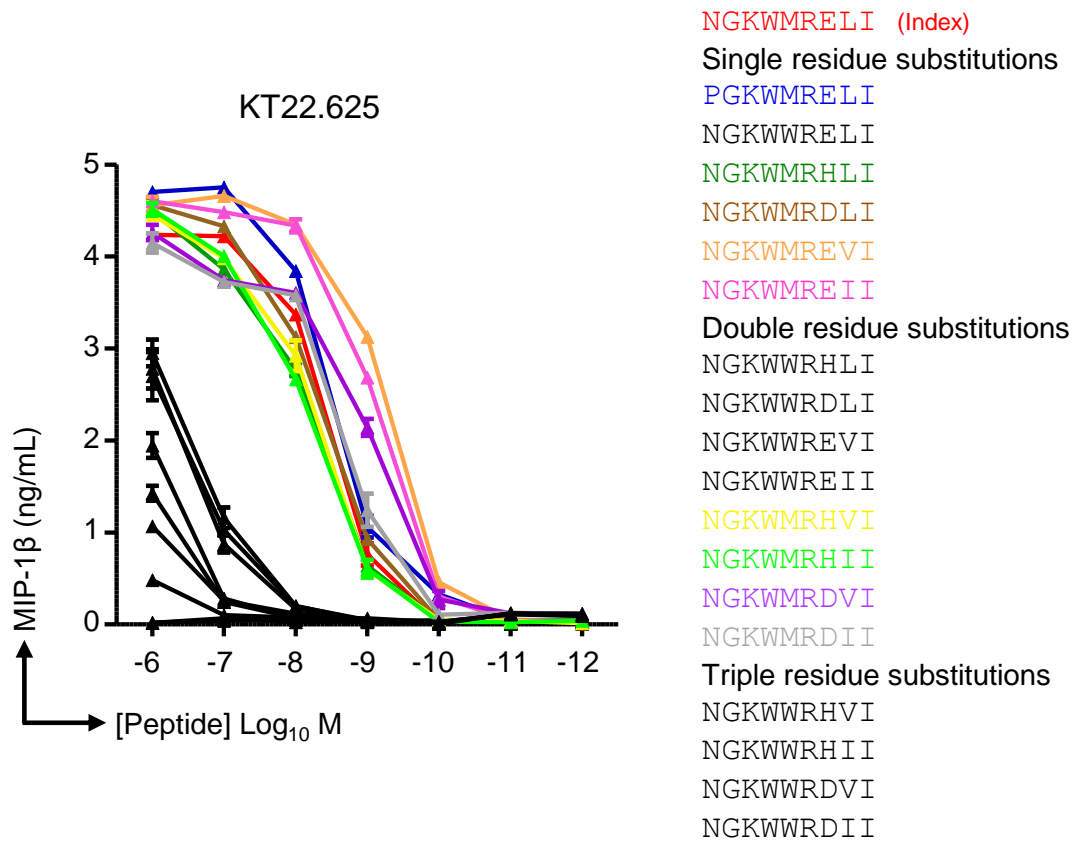he MHC-I allele of interest will stabilise pMHC complexes at the cell surface enabling their detection by flow cytometry (Hoppes et al. 2010). This technology could be adapted for SLA alleles and used to determine which anchor residues are can bind a specific SLA allele. Circular dichroism could also be used to measure pMHC complex stability across a range of anchor mutated peptides (Morgan et al. 1997). The anchor mutated peptides could also be refolded *in vitro* with their respective SLA allele and compatibility determined by successful complex formation. A broader approach could also be

undertaken using *in vitro* PS-CPL scanning to determine residue tolerance as previously undertaken by Pedersen and colleagues for SLA-1*0401 and SLA-2*0401 (Pedersen et al. 2011; Pedersen et al. 2013). Briefly, the level of *in vitro* refolding between SLA-I molecules and the different PS-CPL peptides was quantified by ELISA (measuring the concentration of p-SLA-I complexes) and predicted peptides were then validated by *in vitro* refolding (Pedersen et al. 2011; Pedersen et al. 2013). This technique does however require SLA allele-specific antibodies for pSLA complex detection which are not readily available in swine. Pedersen and colleagues circumvented this requirement by refolding the SLA-I heavy chain with human $\beta_2$m which enabled an anti-human $\beta_2$m antibody to be used for detection (Pedersen et al. 2011; Pedersen et al. 2013). Future work could pursue performing similar assays on the Babraham pig SLA alleles to obtain more comprehensive peptide binding motifs.

I next used the SLA-I binding motifs to identify further SwIV epitopes via *in silico* prediction as a proof of concept. Predicted peptides from the PB2 protein were tested *ex vivo* on PBMC and BAL samples from pig#650 (vaccinated with S-FLU and inactivated H1N1 Sw/Sp) and a new IAV epitope (NKATKRLTV) restricted to SLA-2*11:04 was identified. The lysine residue at P2 in NKATKRLTV was identified as a lower preference in the proposed SLA-2*11:04 binding motif so the discovery of this epitope adds confidence to the motifs produced in this study. An initial attempt to refold this PB2 epitope with SLA-2*11:04 and detect antigen-specific T-cells in the BAL was unsuccessful and time restraints for this study prevented further work. To further validate this epitope in future, this experiment could be repeated. Ideally a T-cell clone known to recognise NKATKRLTV would be derived to validate any new batches of pSLA-I monomer for effective tetramer staining. Limited samples meant that I was restricted to testing only a small number of putative epitopes. Though this preliminary work forms a good basis from which to extend this approach to other influenza proteins and both Babraham pig SLA-I molecules. It will also be important to use a refined motif that allows for selection of decamer peptides as extrapolation from human systems suggests that up to 20% of MHC-I epitopes might be of longer length. Overall, the successful prediction of the four NP epitopes and a further epitope from the PB2 protein indicates that the binding motifs generated here will be useful for identifying other disease epitopes.

The use of alanine substitutions in the IAV epitope sequences enabled preliminary conclusions to be formed about those residues that are essential for the successful engagement between these pSLA-I and their cognate TCR. To extrapolate these results fully on a biochemical level

structures resolved of the pSLA-I in complex with the TCR would be required. The T-cell clones KT13.650 and KT22.625 did not tolerate alanine substitutions at P3, P4, P6, P8 and P9 in the epitope `NGKWMRELI`. This tied up nicely with the PS-CPL derived super-agonists for this epitope which maintained the index residues at these positions, except for P8 where Val or Ile were optimal. Alanine substitutions in the `EFEDLTFLA` epitope were overall not well tolerated by a cognate TCR which matched up with the PS-CPL derived super-agonists which contained no alanine residues except for the index alanine at P9.

It is well established that TCRs can be cross-reactive to numerous peptides and therefore there is the potential to improve upon any cognate peptide and improve immunogenicity (Sewell 2012b). Super-agonists can be identified by PS-CPL which provides an unbiased and quantitative readout of residue preferences within a peptide sequence (Pentier et al. 2013). A major advantage with PS-CPL is that once in-house, one library can be used on any T-cell clone recognising any peptide, providing the library conforms to the peptide length preference of the particular TCR (Ekeruche-Makinde et al. 2013). In this thesis, I have used PS-CPL for the first time on porcine T-cell clones and was able to identify IAV super-agonists for two NP epitopes; SLA-2*11:04 restricted `NGKWMRELI` and SLA-1*14:02 restricted `EFEDLTFLA`. Both sets of PS-CPL data for T-cells clones KT22.625 and KTe.650 demonstrated the need to test several APLs to identify those with improved sensitivity over that exhibited by the index peptide. Indeed, the highest ranking APLs generated from the PS-CPL data sets were not found to be super-agonists and even had substantially reduced sensitivity compared to the index peptide. This highlights that although certain residues may be clear preferences within the PS-CPL data this does not mean that it will be the 'best' residue when amalgamated into the index peptide sequence.

In this chapter, I successfully generated peptide super agonist ligands for TCRs specific for two NP epitopes. This is the first time such an approach has been undertaken with porcine T-cells. These super-agonists will require further testing to verify if they in-fact induce stronger immune responses in clinically relevant samples. Initially, cytotoxic T-cell lines primed against the index peptide and the super-agonists could be procured and measured for the highest T-cell response. Other experiments could include comparing the TCR repertoires primed by the index peptides and the super-agonists, as if the repertoire was altered it may impact on clinical relevance. Nevertheless, the promising preliminary data in this study represents an exciting avenue for future research in this field and the pig would be a good animal model in which to test any super-agonists.

# 8 <u>General Discussion</u>

## 8.1 Summary of Work

The overall focus of my thesis was to bring the tools and techniques for the study of porcine T-cells up to the same level of that currently attainable with human T-cells and to apply this technology to investigate cytotoxic T-cell responses to IAV in pigs. The porcine studies in this thesis were undertaken in collaboration with the Pirbright Institute and the School of Veterinary Sciences, Bristol University. All porcine samples were obtained from the Babraham inbred pig line which is 85% identical by genome-wide SNP analysis and in which all pigs express identical MHC-I and MHC-II alleles. My laboratory have extensive knowledge in human T-cell culture which was applied, in chapter 3, to establish successful and long-term porcine T-cell culture including T-cell clone procurement. In chapter 3, different cell culture media compositions, T-cell mitogens and expansion protocols were assessed to establish an optimal protocol for long-term culture of porcine T-cells. This included the procurement and expansion of monoclonal populations of porcine T-cell clones. The PBMC samples utilised in chapter 3 were from Babraham pigs inoculated with inactivated IAV enabling IAV-specific T-cell clones to be procured. The region of the NP these IAV-specific T-cells recognise was also identified. To my knowledge, this is the first description of long-term porcine T-cell culture and T-cell clone procurement. The establishment of porcine T-cell culture in chapter 3 was essential to the progression of this project towards identifying and exploring IAV MHC-I restricted epitopes in clinically relevant porcine samples.

In chapter 4, IAV-specific T-cell clones were procured from two pigs vaccinated with a non-pathogenic virus, universal vaccine candidate S-FLU (Powell et al. 2012), and inactivated H1N1 SwIV. Epitope identification focused on the conserved influenza viral proteins NP and M1, and four MHC-I epitopes were identified within the NP in regions also previously identified as immunogenic in humans and mice. The use of overlapping peptides for IAV epitope identification made no assumptions about MHC-I binding or immunodominance and allowed complete scanning of the NP and M1 protein sequences. The four new NP epitopes identified in chapter 4 were refolded *in vitro* with SLA-I and $\beta_2$m. Each peptide produced refolded product with one of the two Babraham pig SLA-I molecules, strongly suggesting the SLA-I restriction of each epitope. Subsequent experiments with pSLA-I tetramer staining and the solving of 3 of the 4 pSLA-I complex structures confirmed these predictions.

The structures of both Babraham pig SLA-I molecules, SLA-1*14:02 and SLA-2*11:04, in complex with IAV derived peptides were resolved in chapter 5 and revealed the primary anchor positions to be at P2 and P9 (PC) within the peptides. This facilitated work in chapter 7 that defined the peptide binding motifs of both Babraham pig SLA-I molecules which were used to predict SLA-I restricted IAV epitopes. The epitope predictions preliminary identified a peptide derived from viral protein PB2 which when incubated with PBMC and BAL from a vaccinated pig induced production of IFNγ.

In chapter 6, I contributed to the long history of work within my laboratory to improve the detection of antigen-specific human T-cells by pMHC multimer staining (Whelan et al. 1999; Choi et al. 2003; Scriba et al. 2005; Wooldridge et al. 2006; Laugel, van den Berg, et al. 2007; Lissina et al. 2009; Wooldridge et al. 2009; Clement et al. 2011; Dolton et al. 2014). I demonstrated that the inclusion of anti-fluorochrome antibodies in pMHC multimer staining protocols greatly enhanced staining of antigen-specific human T-cells by stabilising the pMHC multimers bound to the T-cell (Tungatt et al. 2015). I applied the optimised pMHC multimer staining techniques for the detection of IAV-specific porcine T-cells. I was able to detect and compare the magnitude of IAV-specific T-cells, which recognise the four NP epitopes identified in chapter 4, across PBMC, TBLN and BAL isolated from vaccinated pigs. Few studies have utilised pMHC tetramer staining in pigs to date (Pedersen et al. 2014; Pedersen et al. 2016; Baratelli et al. 2017) and the data in chapter 6 represent the first description of pMHC tetramer staining across different porcine tissue samples and utilising optimised staining techniques. Tissue resident porcine IAV-specific cytotoxic T-cells were detected in high numbers in BAL. Large cytotoxic T-cell responses to the four NP epitopes were also detected in BAL from pigs vaccinated with S-FLU alone but were not detected in the equivalent unvaccinated pigs.

Additionally, the ability to culture large numbers of porcine T-cell clones enabled me to identify super-agonist peptides in chapter 7 for two IAV-specific T-cell clones using PS-CPL screens. IAV super-agonists were determined for two NP epitopes, SLA-2*11:04 restricted `NGKWMRELI` and SLA-1*14:02 restricted `EFEDLTFLA`, and shown to induce higher MIP-1β production when incubated with their cognate T-cell clones than compared to the index peptides. This is the first description of using PS-CPL on porcine T-cell clones. The testing of altered peptide ligands in chapter 7 reiterated the need to test numerous sequences to identify super-agonist peptide ligands that were more potent than the index peptides.

## 8.2   Implications of findings

### 8.2.1   *The long-term culture of porcine T-cells*

The establishment of protocols for long-term culturing of porcine T-cells as described above unlocks numerous possibilities in the field of porcine T-cell immunology. Antigen-specific porcine T-cells could be isolated and characterised from a variety of different swine diseases across different pig models and outbred breeds. For example, similar studies could be commenced on other economically important swine diseases, including Foot and Mouth Disease and African Swine Fever. My work was highly dependent on the culture of porcine T-cell lines and the establishment of T-cell clones for IAV epitope identification and clarifying the ability of pSLA-I tetramers to stain their cognate TCR. T-cell clones also enable super-agonist peptides to be identified by PS-CPL.

### 8.2.2   *Enhanced detection of antigen-specific T-cells by pMHC multimers*

The inclusion of anti-fluorochrome antibody to enhance pMHC multimer staining of antigen-specific T-cells (Tungatt et al. 2015) has been successfully implemented across multiple human T-cell studies by my colleagues and afforded improvements in the detection of porcine T-cells within this study. At the time of writing, my publication on this work (Tungatt et al. 2015) has already been cited over 15 times and it is very satisfying to see that other groups have already utilised this enhancement technology during pMHC multimer staining. The inclusion of anti-fluorochrome antibody is a simple, inexpensive addition to improve pMHC multimer staining protocols and is highly recommended particularly when detecting T-cells bearing low-affinity TCRs or where TCR density is expected to be low e.g. in recently or chronically activated T-cells. The review I co-authored on pMHC multimer staining highlighted the best techniques for optimal staining and noted several considerations when commencing pMHC multimer studies (Dolton et al. 2015). This practical guide together with the improvements afforded by anti-fluorochrome antibodies and other improvements previously published by my laboratory can all act synergistically to improve pMHC multimer staining of antigen-specific T-cells and enable the staining of previously undetectable, fully functional T-cells. Subsequent work in this area by my colleague, Cristina Rius, has revealed that standard pMHC tetramer staining fails to detect many fully functional T-cell clones and substantially underestimates the size of antigen-specific T-cells populations. Surprisingly, this is often even true with human pMHC tetramers for commonly used epitopes from the CMV and EBV herpes viruses (Rius et al. unpublished). Consequently, it begins to look as if the many thousands of studies that have previously used pMHC tetramer

staining may have underestimated the size of antigen-specific T-cell populations. My work in this thesis demonstrates that optimised pMHC multimer staining protocols can, and should, be applied across the breadth of T-cell studies and across different species.

### 8.2.3   Peptide-MHC multimer staining of antigen-specific porcine T-cells

The ability to detect porcine antigen-specific T-cells with pMHC tetramers enables enumeration, isolation, phenotyping and characterisation of disease relevant T-cells. The detection of the four IAV epitopes detected in this study following S-FLU vaccination could be used as a marker when assessing the use of this universal vaccine candidate in pigs. The magnitude of T-cell responses across different vaccination strategies could be assessed by pMHC tetramer staining. For example, pMHC tetramer staining could be used as a measure for assessing different vaccination routes and doses, as was the focus of a recent study that infected a commercial pig breed with SwIV (Hemmink et al. 2016). There is the potential to use pMHC tetramers to establish correlates of protection in vaccine studies.

### 8.2.4   SLA-I peptide binding motifs and epitope prediction

Different MHC alleles display different peptide binding motifs which can be used to predict which peptides can be accommodated within the PBG (Sette and Sidney 1998). The primary anchor residues are the key predictors of pMHC stability and typically only a handful of closely-related residues are tolerated in these positions (Falk et al. 1991). Knowledge of the peptide binding motif can be used to predict epitopes for a known MHC-I allele from any protein of interest. The binding motifs defined in this thesis for the two Babraham pig SLA-I alleles can be used for epitope prediction in this pig model for all IAV proteins as well as prove useful for other disease studies. Informed epitope predictions can be tested directly *ex vivo* and could provide a quicker and simpler route to epitope identification than the use of overlapping peptides and T-cell line procurement, although the latter approach is still useful when a non-assumptive approach is desirable. The use of peptide matrices allows large numbers of epitope predictions to be tested simultaneously.  The SLA-I binding motifs I have identified will be very useful for the simple establishment of minimal epitopes after a response to an overlapping peptide has been identified and should largely negate the need for extensive peptide optimisation via peptide truncation as I had to undertake here in the absence of any such motifs.

### 8.2.5   Understanding Influenza A virus

It is well established that cytotoxic T-cells are an integral part of the immune response to IAV infection and can limit disease severity (McMichael et al. 1983; Sridhar et al. 2013; La Gruta and Turner 2014; Wang et al. 2015). The highly mutative nature of IAV means a universal vaccine is highly desirable that can induce heterotypic immunity (Schulman and Kilbourne 1965) and protect across different IAV strains in the absence of neutralising antibodies. Cytotoxic T-cells are a key cell subset in conferring heterotypic immunity (Lee et al. 2008; Grant et al. 2013; Liu et al. 2013; Sridhar et al. 2013). Therefore, it is important we understand what viral components are inducing cross-protective cytotoxic T-cells following IAV infection or vaccination so that this knowledge can be incorporated into universal vaccine design. Effective vaccination within the pig population would decrease the likelihood of the generation of reassortment viruses with pandemic potential. The pandemic risk is particularly high in areas where pigs live in close proximity to humans and poultry, increasing the likelihood for pigs to serve as mixing vessels for antigenic shift in IAV.

The knowledge of cytotoxic T-cell epitopes in pigs lags far behind that currently achieved in humans and mouse models. Few studies have identified and validated *ex vivo* IAV-specific porcine T-cell epitopes (Pedersen et al. 2014; Baratelli et al. 2017). Therefore, the identification in this thesis of four new IAV epitopes in pigs, and the development of tools to study them in greater detail than previously attainable, has enhanced our knowledge in this field of research. Further work will be required to ascertain whether the IAV-specific cytotoxic T-cell populations identified in this thesis are protective and whether they confer heterotypic immunity. However these IAV-specific porcine CD8β T-cells were detected at such high magnitude in the lungs of vaccinated pigs within this study, that it is highly probably they are a key immune response.

Clearly, there are many challenges facing universal influenza vaccine design (reviewed in Sridhar 2016). Although cytotoxic T-cells are considered the primary effectors of heterotypic immunity, it will be important to consider cytotoxic T-cells within the breath of an effective cross-protective immune response. For instance CD4 T-cells are capable of recognising conserved IAV epitopes and may help CD8 T-cell and B-cell immune responses to reduce disease severity, or can themselves directly confer cytotoxic activity (Wilkinson et al. 2012; Sridhar 2016). The development of T-cell based vaccine candidates is a promising way to limit disease severity and a handful of clinical trials aimed at inducing T-cell responses to conserved internal IAV proteins are currently ongoing (Sridhar 2016).

*8.2.6  Super-agonist peptides*

In this thesis, super-agonist peptides were identified for two MHC-I restricted IAV epitopes identified in pigs. The potential to design ligands that can induce stronger T-cell responses than the cognate peptide sequence holds promise for optimal vaccine formulations. Furthermore, there is also the possibility to investigate non-peptide ligands which may confer advantages in stability, removing the need for cold-chain storage of vaccines and enabling oral administration, as is the case for D-amino acids (Pentier et al. 2013). L-amino acids comprise the majority of naturally occurring proteins, whereas D-amino acids are much less prevalent and only found rarely. D-amino acids are mirror image stereoisomers of L-amino acids, but both still exhibit the same physical and chemical properties (Zhao and Lu 2014). The development of "non-natural" D-amino acid ligands capable of inducing strong immune responses is therefore highly desirable. Unpublished data produced by my colleagues has demonstrated the ability for a D-amino acid peptide, derived from CPL data from influenza-specific human T-cells, to prime influenza-specific human cytotoxic T-cells *in vitro*. Additionally, and remarkably, this D-amino acid ligand was shown to confer protection from lethal influenza challenge in a humanised mouse model when administered orally (Miles & Tan *et al*., unpublished). The possibility of "edible vaccines" of this kind is relatively unexplored and in its infancy but could revolutionise vaccine design in the future. Vaccines delivered by this route would be highly desirable in livestock as well as humans. Additionally, the pig represents a good animal model in which to test any such advancements.

## 8.3  Future directions

The work completed in this thesis has opened the possibility to pursue numerous avenues of research into porcine T-cells both in the context of IAV and to other important swine diseases, as well as utilising pigs as an animal model for human diseases. The techniques developed for the long-term culture of cytotoxic porcine T-cells could also be applied to the study of other cell subsets including CD4 T-cells and γδ T-cells. Indeed, in the preliminary stages of this study an IAV-specific CD4 T-cell clone was isolated and cultured successfully *in vitro*.

The epitope identification pursued in this study was performed on samples from vaccinated pigs and focused on responses to viral proteins NP and M1. This work could be expanded to explore other conserved IAV proteins and could be investigated following live IAV infection and across different vaccine candidates. It would be interesting to use the peptide binding motifs defined for the Babraham pig SLA-I molecules to predict epitopes across different IAV viral proteins in

Babraham pigs. These could then be validated by pMHC multimer staining or T-cell activation assays. Epitope predictions can be tested using a peptide matrix allowing many peptides to be tested at once even when sample availability is limited.

The pMHC tetramers produced in this thesis could be used to isolate IAV-specific T-cells from vaccinated pig samples. The pMHC tetramer positive cell populations could be TCR clonotyped to reveal the diversity of the T-cell response and determine whether any 'public' TCRs exist. Further porcine cytotoxic T-cell clones could also be isolated and used to explore the possibility of super-agonists for all four of the IAV epitopes identified in this study. IAV-specific porcine T-cells could also be phenotyped and their cytotoxic effects investigated. It will be interesting to investigate whether these IAV-specific cytotoxic T-cells can confer protection in the Babraham pig model to IAV infection. This could be investigated in vaccination and challenge studies. Heterotypic immunity can be investigated by heterologous challenge experiments. As the Babraham pig line is inbred and MHC identical, there is the possibility to perform adoptive cell transfer to see if the IAV-specific T-cell clones can confer protection in an IAV-naive animal.

The super-agonist peptides identified in this study for two MHC-I restricted IAV epitopes require further investigation. Initially, it will need to be established whether these super-agonist peptides are in fact able to induce stronger cytotoxic T-cell responses *in vitro* than the cognate peptides. The possibility of non-natural ligands could also be explored using D-amino acid formulated CPLs. Any D-amino acid sequence identified in this way would require extensive *in vitro* characterisation and would need to induce good cytotoxic T-cell immune responses. The "non-natural" ligand could then be tested within the Babraham pig model to determine if it can confer protective efficacy to IAV infection.

## 8.4 Concluding remarks

I hope that the techniques developed during this PhD for porcine T-cell culture can be utilised to enhance numerous porcine immunology studies across different research groups. In addition, my studies should position the Babraham pig model as an attractive option for porcine studies particularly applying the Babraham pig SLA-I peptide binding motifs for epitope identification. It has been rewarding to achieve these primary aims and I hope that porcine T-cell studies will continue to improve to the level of that currently attainable in human T-cells and mouse models. This study has also broadened our knowledge of cytotoxic T-cell epitopes to IAV in pigs and

contributed to efforts to investigate the universal vaccine candidate S-FLU. The techniques could be implemented to validate different IAV vaccines and to further explore virus-host dynamics. The generation of novel IAV viruses within the global pig population that could have pandemic potential is an ever-present possibility, and highlights the need for increasing our understanding of porcine IAV immune responses and epidemiology in the global pig population. Human and veterinary immunologists and disease surveillance networks need to work together in order to understand IAV on a global and all-encompassing scale.  A universal IAV vaccine design that could confer heterotypic protection across different species is an interesting concept for the future in combating the pandemic risk.

# 9  <u>References</u>

Aleksic, M., Liddy, N., Molloy, P.E., Pumphrey, N., Vuidepot, A., Chang, K.-M. and Jakobsen, B.K. 2012. Different affinity windows for virus and cancer-specific T-cell receptors: implications for therapeutic strategies. *European journal of immunology* 42(12), pp. 3174–9. doi: 10.1002/eji.201242606.

Allen, H., McCauley, J., Waterfield, M. and Gething, M.J. 1980. Influenza virus RNA segment 7 has the coding capacity for two polypeptides. *Virology* 107(2), pp. 548–551. doi: 10.1016/0042-6822(80)90324-4.

Altman, J.D., Moss, P.A., Goulder, P.J., Barouch, D.H., McHeyzer-Williams, M.G., Bell, J.I., McMichael, A.J. and Davis, M.M. 1996. Phenotypic analysis of antigen-specific T lymphocytes. *Science (New York, N.Y.)* 274(5284), pp. 94–6.

Andersen, M.H., Schrama, D., Thor Straten, P. and Becker, J.C. 2006. Cytotoxic T cells. *J Invest Dermatol* 126(1), pp. 32–41. doi: 10.1038/sj.jid5700001.

Arstila, T.P., Casrouge, A., Baron, V., Even, J., Kanellopoulos, J. and Kourilsky, P. 1999. A Direct Estimate of the Human T Cell Receptor Diversity. *Science* 286(5441), pp. 958–961. doi: 10.1126/science.286.5441.958.

Attaf, M., Huseby, E. and Sewell, A.K. 2015. αβ T cell receptors as predictors of health and disease. *Cellular & molecular immunology* 12(4), pp. 391–9. doi: 10.1038/cmi.2014.134.

Attaf, M., Legut, M., Cole, D.K. and Sewell, A.K. 2015. The T cell antigen receptor: The Swiss army knife of the immune system. *Clinical and Experimental Immunology* 181(1), pp. 1–18. doi: 10.1111/cei.12622.

Baratelli, M., Pedersen, L.E., Trebbien, R., Larsen, L.E., Jungersen, G., Blanco, E., Nielsen, J. and Montoya, M. 2017. Identification of cross-reacting T-cell epitopes in structural and non-structural proteins of swine and pandemic H1N1 influenza A virus strains in pigs. *Journal of General Virology* . doi: 10.1099/jgv.0.000748.

Baz, M., Boonnak, K., Paskel, M., Santos, C., Powell, T., Townsend, A. and Subbarao, K. 2015. Nonreplicating influenza A virus vaccines confer broad protection against lethal challenge. *mBio* 6(5), pp. e01487-15. doi: 10.1128/mBio.01487-15.

Bjorkman, P.J., Saper, M.A., Samraoui, B., Bennett, W.S., Strominger, J.L. and Wiley, D.C. 1987. Structure of the human class I histocompatibility antigen, HLA-A2. *Nature* 329(6139), pp. 506–12. doi: 10.1038/329506a0.

von Boehmer, H., Teh, H.S. and Kisielow, P. 1989. The thymus selects the useful, neglects the useless and destroys the harmful. *Immunology Today* 10(2), pp. 57–61. doi: 10.1016/0167-5699(89)90307-1.

Bot, A., Bot, S. and Bona, C.A. 1998. Protective role of gamma interferon during the recall response to influenza virus. *Journal of virology* 72(8), pp. 6637–45.

Bouvier, N.M. and Palese, P. 2008. The biology of influenza viruses. *Vaccine* 26 Suppl 4, pp. D49-53.

Bridgeman, J.S., Sewell, A.K., Miles, J.J., Price, D.A. and Cole, D.K. 2012. Structural and biophysical determinants of αβ T-cell antigen recognition. *Immunology* 135(1), pp. 9–18. doi: 10.1111/j.1365-2567.2011.03515.x.

Brincks, E.L., Katewa, A., Kucaba, T.A., Griffith, T.S. and Legge, K.L. 2008. CD8 T Cells Utilize TRAIL to Control Influenza Virus Infection. *The Journal of Immunology* 181(7)

Brown, I.H. 2000. The epidemiology and evolution of influenza viruses in pigs. *Veterinary Microbiology* 74(1–2), pp. 29–46. doi: 10.1016/S0378-1135(00)00164-4.

Bulek, A.M., Cole, D.K., Skowera, A., Dolton, G., Gras, S., Madura, F., Fuller, A., Miles, J.J., Gostick, E., Price, D.A., Drijfhout, J.W., Knight, R.R., Huang, G.C., Lissin, N., Molloy, P.E., Wooldridge, L., Jakobsen, B.K., Rossjohn, J., Peakman, M., Rizkallah, P.J. and Sewell, A.K. 2012. Structural basis for the killing of human beta cells by CD8(+) T cells in type 1 diabetes. *Nature immunology* 13(3), pp. 283–9. doi: 10.1038/ni.2206.

Bulek, A.M., Madura, F., Fuller, A., Holland, C.J., Schauenburg, A.J.A., Sewell, A.K., Rizkallah, P.J. and Cole, D.K. 2012. TCR/pMHC Optimized Protein crystallization Screen. *Journal of immunological methods* 382(1–2), pp. 203–10. doi: 10.1016/j.jim.2012.06.007.

Burrows, S.R., Kienzle, N., Winterhalter, A., Bharadwaj, M., Altman, J.D. and Brooks, A. 2000. Peptide-MHC Class I Tetrameric Complexes Display Exquisite Ligand Specificity. *The Journal of Immunology* 165(11)

Carugo, O. and Pongor, S. 2001. A normalized root-mean-square distance for comparing protein three-dimensional structures. *Protein science : a publication of the Protein Society* 10(7), pp. 1470–3. doi: 10.1110/ps.690101.

CCP4 1994. The CCP4 suite: programs for protein crystallography. *Acta Crystallographica Section D Biological Crystallography* 50(5), pp. 760–763. doi: 10.1107/S0907444994003112.

Cerundolo, V., Alexander, J., Anderson, K., Lamb, C., Cresswell, P., McMichael, A., Gotch, F. and Townsend, A. 1990. Presentation of viral antigen controlled by a gene in the major histocompatibility complex. *Nature* 345(6274), pp. 449–452. doi: 10.1038/345449a0.

Chen, Q., Madson, D., Miller, C.L. and Harris, D.L.H. 2012. Vaccine development for protecting swine against influenza virus. *Animal Health Research Reviews* 13(2), pp. 181–195. doi: 10.1017/S1466252312000175.

Choi, E.M.-L., Chen, J.-L., Wooldridge, L., Salio, M., Lissina, A., Lissin, N., Hermans, I.F., Silk, J.D., Mirza, F., Palmowski, M.J., Dunbar, P.R., Jakobsen, B.K., Sewell, A.K. and Cerundolo, V. 2003. High avidity antigen-specific CTL identified by CD8-independent tetramer staining. *Journal of immunology (Baltimore, Md. : 1950)* 171(10), pp. 5116–23.

Chothia, C., Boswell, D.R. and Lesk, A.M. 1988. The outline structure of the T-cell alpha beta receptor. *The EMBO journal* 7(12), pp. 3745–55.

Clement, M., Ladell, K., Ekeruche-Makinde, J., Miles, J.J., Edwards, E.S.J., Dolton, G., Williams, T., Schauenburg, A.J.A., Cole, D.K., Lauder, S.N., Gallimore, A.M., Godkin, A.J., Burrows, S.R., Price, D.A., Sewell, A.K. and Wooldridge, L. 2011. Anti-CD8 Antibodies Can Trigger CD8+ T Cell Effector Function in the Absence of TCR Engagement and Improve Peptide–MHCI Tetramer Staining. *The Journal of Immunology* 187(2)

Cole, D.K., Pumphrey, N.J., Boulter, J.M., Sami, M., Bell, J.I., Gostick, E., Price, D.A., Gao, G.F., Sewell, A.K. and Jakobsen, B.K. 2007. Human TCR-Binding Affinity is Governed by MHC Class Restriction. *The Journal of Immunology* 178(9), pp. 5727–5734. doi: 10.4049/jimmunol.178.9.5727.

Collins, E.J., Garboczi, D.N. and Wiley, D.C. 1994. Three-dimensional structure of a peptide extending from one end of a class I MHC binding site. *Nature* 371(6498), pp. 626–629. doi: 10.1038/371626a0.

Cooper, M.D., Peterson, R.D. and Good, R.A. 1965. DELINEATION OF THE THYMIC AND BURSAL LYMPHOID SYSTEMS IN THE CHICKEN. *Nature* 205, pp. 143–6.

Cox, R.J., Brokstad, K.A. and Ogra, P. 2004. Influenza Virus: Immunity and Vaccination Strategies. Comparison of the Immune Response to Inactivated and Live, Attenuated Influenza Vaccines. *Scandinavian Journal of Immunology* 59(1), pp. 1–15. doi: 10.1111/j.0300-9475.2004.01382.x.

Crawford, F., Kozono, H., White, J., Marrack, P., Kappler, J., Gold, D.., Born, W., White, J., Johnson, J.., Jenkins, M.. and Banerji, J. 1998. Detection of antigen-specific T cells with multivalent soluble class II MHC covalent peptide complexes. *Immunity* 8(6), pp. 675–82. doi: 10.1016/S1074-7613(00)80572-5.

Dela Cruz, C.S. and Wunderlink, R.G. 2017. *Viral and Atypical Pneumonia in Adults, An Issue of Clinics in Chest Medicine,*. Elsevier Health Sciences.

Daniels, M.A. and Jameson, S.C. 2000. Critical role for CD8 in T cell receptor binding and activation by peptide/major histocompatibility complex multimers. *The Journal of experimental medicine* 191(2), pp. 335–46.

Davis, M.M. and Bjorkman, P.J. 1988. T-cell antigen receptor genes and T-cell recognition. *Nature* 334(6181), pp. 395–402. doi: 10.1038/334395a0.

Dawood, F.S., Iuliano, A.D., Reed, C., Meltzer, M.I., Shay, D.K., Cheng, P.-Y., Bandaranayake, D., Breiman, R.F., Brooks, W.A., Buchy, P., Feikin, D.R., Fowler, K.B., Gordon, A., Hien, N.T., Horby, P., Huang, Q.S., Katz, M.A., Krishnan, A., Lal, R., Montgomery, J.M., Mølbak, K., Pebody, R., Presanis, A.M., Razuri, H., Steens, A., Tinoco, Y.O., Wallinga, J., Yu, H., Vong, S., Bresee, J. and Widdowson, M.-A. 2012. Estimated global mortality associated with the first 12 months of 2009 pandemic influenza A H1N1 virus circulation: a modelling study. *The Lancet Infectious Diseases* 12(9), pp. 687–695. doi: 10.1016/S1473-3099(12)70121-4.

Dawson, H. 2011. *A comparative analysis of the porcine, murine, and human immune systems. Chapter*

*22*. McAnulty, P.A., Dayan, A.D., Ganderup, N.-C., Hastings, K. L. ed. CRC Press.

Dawson, H.D., Loveland, J.E., Pascal, G., Gilbert, J.G.R., Uenishi, H., Mann, K.M., Sang, Y., Zhang, J., Carvalho-Silva, D., Hunt, T., Hardy, M., Hu, Z., Zhao, S.-H., Anselmo, A., Shinkai, H., Chen, C., Badaoui, B., Berman, D., Amid, C., Kay, M., Lloyd, D., Snow, C., Morozumi, T., Cheng, R.P.-Y., Bystrom, M., Kapetanovic, R., Schwartz, J.C., Kataria, R., Astley, M., Fritz, E., Steward, C., Thomas, M., Wilming, L., Toki, D., Archibald, A.L., Bed'Hom, B., Beraldi, D., Huang, T.-H., Ait-Ali, T., Blecha, F., Botti, S., Freeman, T.C., Giuffra, E., Hume, D.A., Lunney, J.K., Murtaugh, M.P., Reecy, J.M., Harrow, J.L., Rogel-Gaillard, C. and Tuggle, C.K. 2013. Structural and functional annotation of the porcine immunome. *BMC genomics* 14(1), p. 332. doi: 10.1186/1471-2164-14-332.

Dieckmann, N.M.G., Frazer, G.L., Asano, Y., Stinchcombe, J.C. and Griffiths, G.M. 2016. The cytotoxic T lymphocyte immune synapse at a glance. *Journal of cell science* 129(15), pp. 2881–6. doi: 10.1242/jcs.186205.

DiPiazza, A., Richards, K.A., Knowlden, Z.A.G., Nayak, J.L. and Sant, A.J. 2016. The Role of CD4 T Cell Memory in Generating Protective Immunity to Novel and Potentially Pandemic Strains of Influenza. *Frontiers in immunology* 7, p. 10. doi: 10.3389/fimmu.2016.00010.

Dolton, G., Lissina, A., Skowera, A., Ladell, K., Tungatt, K., Jones, E., Kronenberg-Versteeg, D., Akpovwa, H., Pentier, J.M., Holland, C.J., Godkin, A.J., Cole, D.K., Neller, M.A., Miles, J.J., Price, D.A., Peakman, M. and Sewell, A.K. 2014. Comparison of peptide-major histocompatibility complex tetramers and dextramers for the identification of antigen-specific T-cells. *Clinical and experimental immunology* . doi: 10.1111/cei.12339.

Dolton, G., Tungatt, K., Lloyd, A., Bianchi, V., Theaker, S.M., Trimby, A., Holland, C.J., Donia, M., Godkin, A.J., Cole, D.K., Thor Straten, P., Peakman, M., Svane, I.M. and Sewell, A.K. 2015. More tricks with tetramers: a practical guide to staining T cells with peptide-MHC multimers. *Immunology* 146(1), pp. 11–22. doi: 10.1111/imm.12499.

Draenert, R., Altfeld, M., Brander, C., Basgoz, N., Corcoran, C., Wurcel, A.G., Stone, D.R., Kalams, S.A., Trocha, A., Addo, M.M., Goulder, P.J.R. and Walker, B.D. 2003. Comparison of overlapping peptide sets for detection of antiviral CD8 and CD4 T cell responses. *Journal of immunological methods* 275(1–2), pp. 19–29.

Dustin, M.L., Olszowy, M.W., Holdorf, A.D., Li, J., Bromley, S., Desai, N., Widder, P., Rosenberger, F., van der Merwe, P.A., Allen, P.M. and Shaw, A.S. 1998. A Novel Adaptor Protein Orchestrates Receptor Patterning and Cytoskeletal Polarity in T-Cell Contacts. *Cell* 94(5), pp. 667–677. doi: 10.1016/S0092-8674(00)81608-6.

Effrod, R. and Pawelec, G. 1997. Replicative senescence of T cells: does the Hayflick Limit lead to immune exhaustion? *Immunology Today* 18(9), pp. 450–454. doi: 10.1016/S0167-5699(97)01079-7.

Ekeruche-Makinde, J., Clement, M., Cole, D.K., Edwards, E.S.J., Ladell, K., Miles, J.J., Matthews, K.K., Fuller, A., Lloyd, K.A., Madura, F., Dolton, G.M., Pentier, J., Lissina, A., Gostick, E., Baxter, T.K., Baker, B.M., Rizkallah, P.J., Price, D.A., Wooldridge, L. and Sewell, A.K. 2012. T-cell receptor-optimized peptide skewing of the T-cell repertoire can enhance antigen targeting. *The Journal of biological chemistry* 287(44), pp. 37269–81. doi: 10.1074/jbc.M112.386409.

Ekeruche-Makinde, J., Miles, J.J., van den Berg, H.A., Skowera, A., Cole, D.K., Dolton, G., Schauenburg, A.J.A., Tan, M.P., Pentier, J.M., Llewellyn-Lacey, S., Miles, K.M., Bulek, A.M., Clement, M., Williams, T., Trimby, A., Bailey, M., Rizkallah, P., Rossjohn, J., Peakman, M., Price, D.A., Burrows, S.R., Sewell, A.K. and Wooldridge, L. 2013. Peptide length determines the outcome of TCR/peptide-MHCI engagement. *Blood* 121(7), pp. 1112–1123. doi: 10.1182/blood-2012-06-437202.

ElHefnawi, M., Alaidi, O., Mohamed, N., Kamar, M., El-Azab, I., Zada, S. and Siam, R. 2011. Identification of novel conserved functional motifs across most Influenza A viral strains. *Virology journal* 8, p. 44. doi: 10.1186/1743-422X-8-44.

Ellebaek, E., Iversen, T.Z., Junker, N., Donia, M., Engell-Noerregaard, L., Met, Ö., Hölmich, L.R., Andersen, R.S., Hadrup, S.R., Andersen, M.H., thor Straten, P. and Svane, I.M. 2012. Adoptive cell therapy with autologous tumor infiltrating lymphocytes and low-dose Interleukin-2 in metastatic melanoma patients. *Journal of translational medicine* 10(1), p. 169. doi: 10.1186/1479-5876-10-169.

Emsley, P. and Cowtan, K. 2004. *Coot* : model-building tools for molecular graphics. *Acta Crystallographica*

*Section D Biological Crystallography* 60(12), pp. 2126–2132. doi: 10.1107/S0907444904019158.

Falk, K., Rötzschke, O., Stevanović, S., Jung, G. and Rammensee, H.G. 1991. Allele-specific motifs revealed by sequencing of self-peptides eluted from MHC molecules. *Nature* 351(6324), pp. 290–296. doi: 10.1038/351290a0.

Fan, S., Wu, Y., Wang, S., Wang, Z., Jiang, B., Liu, Y., Liang, R., Zhou, W., Zhang, N. and Xia, C. 2016. Structural and Biochemical Analyses of Swine Major Histocompatibility Complex Class I Complexes and Prediction of the Epitope Map of Important Influenza A Virus Strains. *Journal of virology* 90(15), pp. 6625–41. doi: 10.1128/JVI.00119-16.

FAO 2014. FAOSTAT. Available at: http://www.fao.org/faostat/en/#data/QA [Accessed: 28 March 2017].

Fiore-Gartland, A., Manso, B.A., Friedrich, D.P., Gabriel, E.E., Finak, G., Moodie, Z., Hertz, T., De Rosa, S.C., Frahm, N., Gilbert, P.B. and McElrath, M.J. 2016. Pooled-Peptide Epitope Mapping Strategies Are Efficient and Highly Sensitive: An Evaluation of Methods for Identifying Human T Cell Epitope Specificities in Large-Scale HIV Vaccine Efficacy Trials. Lu, S. ed. *PLOS ONE* 11(2), p. e0147812. doi: 10.1371/journal.pone.0147812.

Freidl, G., Meijer, A., de Bruin, E., de Nardi, M., Munoz, O., Capua, I., Breed, A., Harris, K., Hill, A., Hill, A., Kosmider, R., Banks, J., von Dobschuetz, S., Stark, K., Wieland, B., Stevens, K., van der Werf, S., Enouf, V., van der Meulen, K., Van Reeth, K., Dauphin, G., Koopmans, M. and FLURISK Consortium, C. 2014. Influenza at the animal–human interface: a review of the literature for virological evidence of human infection with swine or avian influenza viruses other than A(H5N1). *Eurosurveillance* 19(18), p. 20793. doi: 10.2807/1560-7917.ES2014.19.18.20793.

Fulton, K.M. and Twine, S.M. 2013. Immunoproteomics: Current Technology and Applications. Humana Press, Totowa, NJ, pp. 21–57. doi: 10.1007/978-1-62703-589-7_2.

Garboczi, D.N., Ghosh, P., Utz, U., Fan, Q.R., Biddison, W.E. and Wiley, D.C. 1996. Structure of the complex between human T-cell receptor, viral peptide and HLA-A2. *Nature* 384, pp. 134–141. doi: 10.1038/384134a0.

Garboczi, D.N., Hung, D.T. and Wiley, D.C. 1992. HLA-A2-peptide complexes: refolding and crystallization of molecules expressed in Escherichia coli and complexed with single antigenic peptides. *Proceedings of the National Academy of Sciences of the United States of America* 89(8), pp. 3429–33.

Gerner, W., Käser, T. and Saalmüller, A. 2009. Porcine T lymphocytes and NK cells--an update. *Developmental and comparative immunology* 33(3), pp. 310–20. doi: 10.1016/j.dci.2008.06.003.

Gerner, W., Talker, S.C., Koinig, H.C., Sedlak, C., Mair, K.H. and Saalmüller, A. 2015. Phenotypic and functional differentiation of porcine αβ T cells: current knowledge and available tools. *Molecular immunology* 66(1), pp. 3–13. doi: 10.1016/j.molimm.2014.10.025.

Godfrey, D.I., Uldrich, A.P., McCluskey, J., Rossjohn, J. and Moody, D.B. 2015. The burgeoning family of unconventional T cells. *Nature Immunology* 16(11), pp. 1114–1123. doi: 10.1038/ni.3298.

Gotch, F., Rothbard, J., Howland, K., Townsend, A. and McMichael, A. 1987. Cytotoxic T lymphocytes recognize a fragment of influenza virus matrix protein in association with HLA-A2. *Nature* 326(6116), pp. 881–882. doi: 10.1038/326881a0.

Grant, E., Wu, C., Chan, K.-F., Eckle, S., Bharadwaj, M., Zou, Q.M., Kedzierska, K. and Chen, W. 2013. Nucleoprotein of influenza A virus is a major target of immunodominant CD8+ T-cell responses. *Immunology and cell biology* 91(2), pp. 184–94. doi: 10.1038/icb.2012.78.

La Gruta, N.L. and Turner, S.J. 2014. T cell mediated immunity to influenza: mechanisms of viral control. *Trends in Immunology* 35(8), pp. 396–402. doi: 10.1016/j.it.2014.06.004.

Gutiérrez, A.H., Loving, C., Moise, L., Terry, F.E., Brockmeier, S.L., Hughes, H.R., Martin, W.D. and De Groot, A.S. 2016. In Vivo Validation of Predicted and Conserved T Cell Epitopes in a Swine Influenza Model. Krammer, F. ed. *PLOS ONE* 11(7), p. e0159237. doi: 10.1371/journal.pone.0159237.

Haney, D., Quigley, M.F., Asher, T.E., Ambrozak, D.R., Gostick, E., Price, D.A., Douek, D.C. and Betts, M.R. 2011. Isolation of viable antigen-specific CD8+ T cells based on membrane-bound tumor necrosis factor (TNF)-α expression. *Journal of immunological methods* 369(1–2), pp. 33–41. doi: 10.1016/j.jim.2011.04.003.

Harley, C.B., Futcher, A.B. and Greider, C.W. 1990. Telomeres shorten during ageing of human fibroblasts. *Nature* 345(6274), pp. 458–460. doi: 10.1038/345458a0.

Hayflick, L. and Moorhead, P.S. 1961. The serial cultivation of human diploid cell strains. *Experimental cell research* 25, pp. 585–621.

Heath, W.R. and Carbone, F.R. 2001. Cross-presentation in viral immunity and self-tolerance. *Nature Reviews Immunology* 1(2), pp. 126–134. doi: 10.1038/35100512.

Heinen, P.P., A., de B.-L.E. and Bianchi, A.T.J. 2001. Respiratory and systemic humoral and cellular immune responses of pigs to a heterosubtypic influenza A virus infection. *Journal of General Virology* 82(11), pp. 2697–2707. doi: 10.1099/0022-1317-82-11-2697.

Heiny, A.T., Miotto, O., Srinivasan, K.N., Khan, A.M., Zhang, G.L., Brusic, V., Tan, T.W. and August, J.T. 2007. Evolutionarily Conserved Protein Sequences of Influenza A Viruses, Avian and Human, as Vaccine Targets. Snel, B. ed. *PLoS ONE* 2(11), p. e1190. doi: 10.1371/journal.pone.0001190.

Hemmink, J.D., Morgan, S.B., Aramouni, M., Everett, H., Salguero, F.J., Canini, L., Porter, E., Chase-Topping, M., Beck, K., Loughlin, R. Mac, Carr, B.V., Brown, I.H., Bailey, M., Woolhouse, M., Brookes, S.M., Charleston, B. and Tchilian, E. 2016. Distinct immune responses and virus shedding in pigs following aerosol, intra-nasal and contact infection with pandemic swine influenza A virus, A(H1N1)09. *Veterinary research* 47(1), p. 103. doi: 10.1186/s13567-016-0390-5.

Ho, C.S., Franzo-Romain, M.H., Lee, Y.J., Lee, J.H. and Smith, D.M. 2009. Sequence-based characterization of swine leucocyte antigen alleles in commercially available porcine cell lines. *International Journal of Immunogenetics* 36(4), pp. 231–234. doi: 10.1111/j.1744-313X.2009.00853.x.

Hodes, R.J., Hathcock, K.S. and Weng, N. 2002. Telomeres in T and B cells. *Nature Reviews Immunology* 2(9), pp. 699–706. doi: 10.1038/nri890.

Hoft, D.F., Babusis, E., Worku, S., Spencer, C.T., Lottenbach, K., Truscott, S.M., Abate, G., Sakala, I.G., Edwards, K.M., Creech, C.B., Gerber, M.A., Bernstein, D.I., Newman, F., Graham, I., Anderson, E.L. and Belshe, R.B. 2011. Live and inactivated influenza vaccines induce similar humoral responses, but only live vaccines induce diverse T-cell responses in young children. *The Journal of infectious diseases* 204(6), pp. 845–53. doi: 10.1093/infdis/jir436.

Hoppes, R., Ekkebus, R., Schumacher, T.N.M. and Ovaa, H. 2010. Technologies for MHC class I immunoproteomics. *Journal of Proteomics* 73(10), pp. 1945–1953. doi: 10.1016/j.jprot.2010.05.009.

Howard, W. 2011. Reassortant Pandemic (H1N1) 2009 Virus in Pigs, United Kingdom. *Emerging Infectious Diseases* 17(6), pp. 1049–1052. doi: 10.3201/eid1706.101886.

Hughes, A.L., Ota, T. and Nei, M. 1990. Positive Darwinian selection promotes charge profile diversity in the antigen-binding cleft of class I major-histocompatibility-complex molecules. *Molecular biology and evolution* 7(6), pp. 515–24.

Hutchinson, E. and Fodor, E. 2013. Transport of the Influenza Virus Genome from Nucleus to Nucleus. *Viruses* 5(10), pp. 2424–2446. doi: 10.3390/v5102424.

Hutchinson, E.C., Charles, P.D., Hester, S.S., Thomas, B., Trudgian, D., Martínez-Alonso, M. and Fodor, E. 2014. Conserved and host-specific features of influenza virion architecture. *Nature Communications* 5, p. 4816. doi: 10.1038/ncomms5816.

*Immune function in healthy and African Swine Fever virus (ASFV) infected pigs. DEFRA final project report: SE 1509.* 2003.

Ito, T., Couceiro, J.N., Kelm, S., Baum, L.G., Krauss, S., Castrucci, M.R., Donatelli, I., Kida, H., Paulson, J.C., Webster, R.G. and Kawaoka, Y. 1998. Molecular basis for the generation in pigs of influenza A viruses with pandemic potential. *Journal of virology* 72(9), pp. 7367–73.

Johnson, N.P.A.S. and Mueller, J. 2002. Updating the accounts: global mortality of the 1918-1920 &quot;Spanish&quot; influenza pandemic. *Bulletin of the history of medicine* 76(1), pp. 105–15.

Kabsch, W. 2010. XDS. *Acta crystallographica. Section D, Biological crystallography* 66(Pt 2), pp. 125–32. doi: 10.1107/S0907444909047337.

Kersh, G.J. and Allen, P.M. 1996. Structural basis for T cell recognition of altered peptide ligands: a single

T cell receptor can productively recognize a large continuum of related ligands. *The Journal of experimental medicine* 184(4), pp. 1259–68.

Kidd, M. 2014. Influenza viruses: update on epidemiology, clinical features, treatment and vaccination. *Current Opinion in Pulmonary Medicine* 20(3), pp. 242–246. doi: 10.1097/MCP.0000000000000049.

Killingley, B. and Nguyen-Van-Tam, J. 2013. Routes of influenza transmission. *Influenza and Other Respiratory Viruses* 7(s2), pp. 42–51. doi: 10.1111/irv.12080.

Kruisbeek, A.M., Kruisbeek and M., A. 2001. Production of Mouse T Cell Hybridomas. In: *Current Protocols in Immunology*. Hoboken, NJ, USA: John Wiley & Sons, Inc., p. 3.14.1-3.14.11. doi: 10.1002/0471142735.im0314s24.

Kuhns, M.S., Davis, M.M. and Garcia, K.C. 2006. Deconstructing the Form and Function of the TCR/CD3 Complex. *Immunity* 24(2), pp. 133–139. doi: 10.1016/j.immuni.2006.01.006.

Kyriakis, C.S., Rose, N., Foni, E., Maldonado, J., Loeffen, W.L.A., Madec, F., Simon, G. and Van Reeth, K. 2013. Influenza A virus infection dynamics in swine farms in Belgium, France, Italy and Spain, 2006–2008. *Veterinary Microbiology* 162(2), pp. 543–550. doi: 10.1016/j.vetmic.2012.11.014.

Lanier, L.L. 2013. Shades of grey — the blurring view of innate and adaptive immunity. *Nature Reviews Immunology* 13. doi: 10.1038/nri3389.

Laugel, B., van den Berg, H.A., Gostick, E., Cole, D.K., Wooldridge, L., Boulter, J., Milicic, A., Price, D.A. and Sewell, A.K. 2007. Different T cell receptor affinity thresholds and CD8 coreceptor dependence govern cytotoxic T lymphocyte activation and tetramer binding properties. *The Journal of biological chemistry* 282(33), pp. 23799–810. doi: 10.1074/jbc.M700976200.

Laugel, B., Price, D.A., Milicic, A. and Sewell, A.K. 2007. CD8 exerts differential effects on the deployment of cytotoxic T lymphocyte effector functions. *European journal of immunology* 37(4), pp. 905–13. doi: 10.1002/eji.200636718.

Lebien, T.W. and Tedder, T.F. 2008. B lymphocytes : how they develop and function. *Blood* 112(5), pp. 1570–1580. doi: 10.1182/blood-2008-02-078071.

Lederberg, J. 2001. H1N1-influenza as Lazarus: genomic resurrection from the tomb of an unknown. *Proceedings of the National Academy of Sciences of the United States of America* 98(5), pp. 2115–6. doi: 10.1073/pnas.051000798.

Lee, L.Y.-H., Ha, D.L.A., Simmons, C., de Jong, M.D., Chau, N.V.V., Schumacher, R., Peng, Y.C., McMichael, A.J., Farrar, J.J., Smith, G.L., Townsend, A.R.M., Askonas, B. a, Rowland-Jones, S. and Dong, T. 2008. Memory T cells established by seasonal human influenza A infection cross-react with avian influenza A (H5N1) in healthy individuals. *The Journal of clinical investigation* 118(10), pp. 3478–3490. doi: 10.1172/JCI32460DS1.

Lefevre, E. a., Carr, B.V., Inman, C.F., Prentice, H., Brown, I.H., Brookes, S.M., Garcon, F., Hill, M.L., Iqbal, M., Elderfield, R. a., Barclay, W., Gubbins, S., Bailey, M. and Charleston, B. 2012. Immune responses in pigs vaccinated with adjuvanted and non-adjuvanted a(H1N1)pdm/09 influenza vaccines used in human immunization programmes. *PLoS ONE* 7(3), p. e32400. doi: 10.1371/journal.pone.0032400.

Leisner, C., Loeth, N., Lamberth, K., Justesen, S., Sylvester-Hvid, C., Schmidt, E.G., Claesson, M., Buus, S. and Stryhn, A. 2008. One-Pot, Mix-and-Read Peptide-MHC Tetramers. Zimmer, J. ed. *PLoS ONE* 3(2), p. e1678. doi: 10.1371/journal.pone.0001678.

Li, Y., Zhi, W., Wareski, P. and Weng, N. 2005. IL-15 Activates Telomerase and Minimizes Telomere Loss and May Preserve the Replicative Life Span of Memory CD8+ T Cells In Vitro. *The Journal of Immunology* 174(7)

Lissina, A., Ladell, K., Skowera, A., Clement, M., Edwards, E., Seggewiss, R., van den Berg, H.A., Gostick, E., Gallagher, K., Jones, E., Melenhorst, J.J., Godkin, A.J., Peakman, M., Price, D.A., Sewell, A.K. and Wooldridge, L. 2009. Protein kinase inhibitors substantially improve the physical detection of T-cells with peptide-MHC tetramers. *Journal of Immunological Methods* 340(1), pp. 11–24. doi: 10.1016/j.jim.2008.09.014.

Liu, J., Wu, B., Zhang, S., Tan, S., Sun, Y., Chen, Z., Qin, Y., Sun, M., Shi, G., Wu, Y., Sun, M., Liu, N., Ning, K., Ma, Y., Gao, B., Yan, J., Zhu, F., Wang, H. and Gao, G.F. 2013. Conserved epitopes dominate cross-CD8 [+] T-

cell responses against influenza A H1N1 virus among Asian populations. *European Journal of Immunology* 43(8), pp. 2055–2069. doi: 10.1002/eji.201343417.

Lodolce, J., Burkett, P., Koka, R., Boone, D., Chien, M., Chan, F., Madonia, M., Chai, S. and Ma, A. 2002. Interleukin-15 and the regulation of lymphoid homeostasis. *Molecular immunology* 39(9), pp. 537–44.

Lyons, A.B. and Parish, C.R. 1994. Determination of lymphocyte division by flow cytometry. *Journal of Immunological Methods* 171(1), pp. 131–137. doi: 10.1016/0022-1759(94)90236-4.

Ma, W., Lager, K.M., Lekcharoensuk, P., Ulery, E.S., Janke, B.H., Solórzano, A., Webby, R.J., García-Sastre, A. and Richt, J.A. 2010. Viral reassortment and transmission after co-infection of pigs with classical H1N1 and triple-reassortant H3N2 swine influenza viruses. *The Journal of general virology* 91(Pt 9), pp. 2314–21. doi: 10.1099/vir.0.021402-0.

Ma, W., Lager, K.M., Vincent, A.L., Janke, B.H., Gramer, M.R. and Richt, J.A. 2009. The role of swine in the generation of novel influenza viruses. *Zoonoses and public health* 56(6–7), pp. 326–37. doi: 10.1111/j.1863-2378.2008.01217.x.

Mao, L., Yang, Y., Qiu, Y. and Yang, Y. 2012. Annual economic impacts of seasonal influenza on US counties: Spatial heterogeneity and patterns. *International Journal of Health Geographics* 11(1), p. 16. doi: 10.1186/1476-072X-11-16.

Mason, D. 1998. A very high level of crossreactivity is an essential feature of the T-cell receptor. *Immunology today* 19(9), pp. 395–404.

Matsumura, M., Fremont, D.H., Peterson, P.A. and Wilson, I.A. 1992. Emerging principles for the recognition of peptide antigens by MHC class I molecules. *Science (New York, N.Y.)* 257(5072), pp. 927–34. doi: 10.1126/science.1323878.

McCoy, A.J., Grosse-Kunstleve, R.W., Adams, P.D., Winn, M.D., Storoni, L.C. and Read, R.J. 2007. *Phaser* crystallographic software. *Journal of Applied Crystallography* 40(4), pp. 658–674. doi: 10.1107/S0021889807021206.

McMichael, A.J., Gotch, F.M., Noble, G.R. and Beare, P.A.S. 1983. Cytotoxic T-Cell Immunity to Influenza. *New England Journal of Medicine* 309(1), pp. 13–17. doi: 10.1056/NEJM198307073090103.

Meurens, F., Summerfield, A., Nauwynck, H., Saif, L. and Gerdts, V. 2012. The pig: a model for human infectious diseases. *Trends in microbiology* 20(1), pp. 50–7. doi: 10.1016/j.tim.2011.11.002.

Mokhtar, H., Pedrera, M., Frossard, J.-P., Biffar, L., Hammer, S.E., Kvisgaard, L.K., Larsen, L.E., Stewart, G.R., Somavarapu, S., Steinbach, F. and Graham, S.P. 2016. The Non-structural Protein 5 and Matrix Protein Are Antigenic Targets of T Cell Immunity to Genotype 1 Porcine Reproductive and Respiratory Syndrome Viruses. *Frontiers in immunology* 7, p. 40. doi: 10.3389/fimmu.2016.00040.

Molinari, N.-A.M., Ortega-Sanchez, I.R., Messonnier, M.L., Thompson, W.W., Wortley, P.M., Weintraub, E. and Bridges, C.B. 2007. The annual impact of seasonal influenza in the US: Measuring disease burden and costs. *Vaccine* 25(27), pp. 5086–5096. doi: 10.1016/j.vaccine.2007.03.046.

Morgan, C.S., Holton, J.M., Olafson, B.D., Bjorkman, P.J. and Mayo, S.L. 1997. Circular dichroism determination of class I MHC-peptide equilibrium dissociation constants. *Protein science : a publication of the Protein Society* 6(8), pp. 1771–3. doi: 10.1002/pro.5560060819.

Morgan, S.B., Hemmink, J.D., Porter, E., Harley, R., Shelton, H., Aramouni, M., Everett, H.E., Brookes, S.M., Bailey, M., Townsend, A.M., Charleston, B. and Tchilian, E. 2016. Aerosol Delivery of a Candidate Universal Influenza Vaccine Reduces Viral Load in Pigs Challenged with Pandemic H1N1 Virus. *Journal of immunology (Baltimore, Md. : 1950)* 196(12), pp. 5014–23. doi: 10.4049/jimmunol.1502632.

Morin, G.B. 1989. The human telomere terminal transferase enzyme is a ribonucleoprotein that synthesizes TTAGGG repeats. *Cell* 59(3), pp. 521–9.

Morrison, J., Elvin, J., Latron, F., Gotch, F., Moots, R., Strominger, J.L. and McMichael, A. 1992. Identification of the nonamer peptide from influenza A matrix protein and the role of pockets of HLA-A2 in its recognition by cytotoxic T lymphocytes. *European Journal of Immunology* 22(4), pp. 903–907. doi: 10.1002/eji.1830220404.

Murphy, K. & Weaver, C. 2016. *Janeway's Immunobiology*. 9th ed. Garland Science.

Murshudov, G.N., Vagin, A.A. and Dodson, E.J. 1997. Refinement of Macromolecular Structures by the Maximum-Likelihood Method. *Acta Crystallographica Section D Biological Crystallography* 53(3), pp. 240–255. doi: 10.1107/S0907444996012255.

Neefjes, J., Jongsma, M.L.M., Paul, P. and Bakke, O. 2011. Towards a systems understanding of MHC class I and MHC class II antigen presentation. *Nature Reviews Immunology* 11(12), p. 823. doi: 10.1038/nri3084.

Nelli, R.K., Kuchipudi, S. V, White, G.A., Perez, B., Dunham, S.P. and Chang, K.-C. 2010. Comparative distribution of human and avian type sialic acid influenza receptors in the pig. *BMC Veterinary Research* 6(1), p. 4. doi: 10.1186/1746-6148-6-4.

Nelson, M.I., Gramer, M.R., Vincent, A.L. and Holmes, E.C. 2012. Global transmission of influenza viruses from humans to swine. *The Journal of general virology* 93(Pt 10), pp. 2195–203. doi: 10.1099/vir.0.044974-0.

Nicholson, K.G., Wood, J.M. and Zambon, M. 2003. Influenza. *Lancet (London, England)* 362(9397), pp. 1733–45. doi: 10.1016/S0140-6736(03)14854-4.

Nielsen, M., Lundegaard, C., Blicher, T., Lamberth, K., Harndahl, M., Justesen, S., Røder, G., Peters, B., Sette, A., Lund, O. and Buus, S. 2007. NetMHCpan, a method for quantitative predictions of peptide binding to any HLA-A and -B locus protein of known sequence. *PloS one* 2(8), p. e796. doi: 10.1371/journal.pone.0000796.

O'Neill, R.E., Talon, J. and Palese, P. 1998. The influenza virus NEP (NS2 protein) mediates the nuclear export of viral ribonucleoproteins. *The EMBO journal* 17(1), pp. 288–96. doi: 10.1093/emboj/17.1.288.

Palese, P. and Schulman, J.L. 1976. Mapping of the influenza virus genome: identification of the hemagglutinin and the neuraminidase genes. *Proceedings of the National Academy of Sciences of the United States of America* 73(6), pp. 2142–6. doi: 10.1073/pnas.73.6.2142.

Parham, P. and Ohta, T. 1996. Population biology of antigen presentation by MHC class I molecules. *Science (New York, N.Y.)* 272(5258), pp. 67–74.

Parker, K.C., Silver, M.L. and Wiley, D.C. 1992. An HLA-A2/β2-microglobulin/peptide complex assembled from subunits expressed separately in Escherichia coli. *Molecular Immunology* 29(3), pp. 371–378. doi: 10.1016/0161-5890(92)90024-R.

Patch, J.R., Pedersen, L.E., Toka, F.N., Moraes, M., Grubman, M.J., Nielsen, M., Jungersen, G., Buus, S. and Golde, W.T. 2011. Induction of foot-and-mouth disease virus-specific cytotoxic T cell killing by vaccination. *Clinical and vaccine immunology : CVI* 18(2), pp. 280–8. doi: 10.1128/CVI.00417-10.

Pedersen, L.E., Breum, S.Ø., Riber, U., Larsen, L.E. and Jungersen, G. 2014. Identification of swine influenza virus epitopes and analysis of multiple specificities expressed by cytotoxic T cell subsets. *Virology journal* 11(1), p. 163. doi: 10.1186/1743-422X-11-163.

Pedersen, L.E., Harndahl, M., Nielsen, M., Patch, J.R., Jungersen, G., Buus, S. and Golde, W.T. 2013. Identification of peptides from foot-and-mouth disease virus structural proteins bound by class i swine leukocyte antigen (SLA) alleles, SLA-1*0401 and SLA-2*0401. *Animal Genetics* 44(3), pp. 251–258. doi: 10.1111/j.1365-2052.2012.02400.x.

Pedersen, L.E., Harndahl, M., Rasmussen, M., Lamberth, K., Golde, W.T., Lund, O., Nielsen, M. and Buus, S. 2011. Porcine major histocompatibility complex (MHC) class I molecules and analysis of their peptide-binding specificities. *Immunogenetics* 63(12), pp. 821–34. doi: 10.1007/s00251-011-0555-3.

Pedersen, L.E., Patch, J.R., Kenney, M., Glabman, R.A., Nielsen, M., Jungersen, G., Buus, S. and Golde, W.T. 2016. Expanding specificity of class I restricted CD8+ T cells for viral epitopes following multiple inoculations of swine with a human adenovirus vectored foot-and-mouth disease virus (FMDV) vaccine. *Veterinary Immunology and Immunopathology* . doi: 10.1016/j.vetimm.2016.07.012.

Pentier, J.M., Sewell, A.K. and Miles, J.J. 2013. Advances in T-cell epitope engineering. *Frontiers in immunology* 4, p. 133. doi: 10.3389/fimmu.2013.00133.

Van Poucke, S.G.M., Nicholls, J.M., Nauwynck, H.J. and Van Reeth, K. 2010. Replication of avian, human and swine influenza viruses in porcine respiratory explants and association with sialic acid distribution. *Virology journal* 7, p. 38. doi: 10.1186/1743-422X-7-38.

Powell, T.J., Silk, J.D., Sharps, J., Fodor, E. and Townsend, A.R.M. 2012. Pseudotyped influenza A virus as a

vaccine for the induction of heterotypic immunity. *Journal of virology* 86(24), pp. 13397–406. doi: 10.1128/JVI.01820-12.

Price, D.A., Sewell, A.K., Dong, T., Tan, R., Goulder, P.J., Rowland-Jones, S.L. and Phillips, R.E. 1998. Antigen-specific release of beta-chemokines by anti-HIV-1 cytotoxic T lymphocytes. *Current biology : CB* 8(6), pp. 355–8.

Purbhoo, M.A., Boulter, J.M., Price, D.A., Vuidepot, A.-L., Hourigan, C.S., Dunbar, P.R., Olson, K., Dawson, S.J., Phillips, R.E., Jakobsen, B.K., Bell, J.I. and Sewell, A.K. 2001. The Human CD8 Coreceptor Effects Cytotoxic T Cell Activation and Antigen Sensitivity Primarily by Mediating Complete Phosphorylation of the T Cell Receptor Chain. *Journal of Biological Chemistry* 276(35), pp. 32786–32792. doi: 10.1074/jbc.M102498200.

Purbhoo, M.A., Li, Y., Sutton, D.H., Brewer, J.E., Gostick, E., Bossi, G., Laugel, B., Moysey, R., Baston, E., Liddy, N., Cameron, B., Bennett, A.D., Ashfield, R., Milicic, A., Price, D.A., Classon, B.J., Sewell, A.K. and Jakobsen, B.K. 2007. The HLA A*0201-restricted hTERT(540-548) peptide is not detected on tumor cells by a CTL clone or a high-affinity T-cell receptor. *Molecular cancer therapeutics* 6(7), pp. 2081–91. doi: 10.1158/1535-7163.MCT-07-0092.

Pymm, P., Illing, P.T., Ramarathinam, S.H., O'Connor, G.M., Hughes, V.A., Hitchen, C., Price, D.A., Ho, B.K., McVicar, D.W., Brooks, A.G., Purcell, A.W., Rossjohn, J. and Vivian, J.P. 2017. MHC-I peptides get out of the groove and enable a novel mechanism of HIV-1 escape. *Nature Structural & Molecular Biology* 24(4), pp. 387–394. doi: 10.1038/nsmb.3381.

Rahn, J., Hoffmann, D., Harder, T.C. and Beer, M. 2015. Vaccines against influenza A viruses in poultry and swine: Status and future developments. *Vaccine* 33(21), pp. 2414–2424. doi: 10.1016/j.vaccine.2015.03.052.

Rajao, D.S. and Vincent, A.L. 2015. Swine as a Model for Influenza A Virus Infection and Immunity. *ILAR Journal* 56(1), pp. 44–52. doi: 10.1093/ilar/ilv002.

Raulf-Heimsoth, M. 2008. T Cell — Primary Culture from Peripheral Blood. Humana Press, pp. 17–30. doi: 10.1007/978-1-59745-366-0_2.

Reid, R.A., Redman, J.E., Rizkallah, P., Fegan, C., Pepper, C. and Man, S. 2014. CD8(+) T-cell recognition of a synthetic epitope formed by t-butyl modification. *Immunology* 144(3), p. 495. doi: 10.1111/imm.12398.

Reimann, J. and Kaufmann, S.H. 1997. Alternative antigen processing pathways in anti-infective immunity. *Current Opinion in Immunology* 9(4), pp. 462–469. doi: 10.1016/S0952-7915(97)80096-9.

Rist, M.J., Theodossis, A., Croft, N.P., Neller, M.A., Welland, A., Chen, Z., Sullivan, L.C., Burrows, J.M., Miles, J.J., Brennan, R.M., Gras, S., Khanna, R., Brooks, A.G., McCluskey, J., Purcell, A.W., Rossjohn, J. and Burrows, S.R. 2013. HLA peptide length preferences control CD8+ T cell responses. *Journal of immunology (Baltimore, Md. : 1950)* 191(2), pp. 561–71. doi: 10.4049/jimmunol.1300292.

Ritchey, M.B., Palese, P. and Schulman, J.L. 1976. Mapping of the influenza virus genome. III. Identification of genes coding for nucleoprotein, membrane protein, and nonstructural protein. *Journal of virology* 20(1), pp. 307–13.

Ritter, A.T., Asano, Y., Stinchcombe, J.C., Dieckmann, N.M.G., Chen, B.-C., Gawden-Bone, C., van Engelenburg, S., Legant, W., Gao, L., Davidson, M.W., Betzig, E., Lippincott-Schwartz, J. and Griffiths, G.M. 2015. Actin Depletion Initiates Events Leading to Granule Secretion at the Immunological Synapse. *Immunity* 42(5), pp. 864–876. doi: 10.1016/j.immuni.2015.04.013.

Rogers, G.N. and D'Souza, B.L. 1989. Receptor binding properties of human and animal H1 influenza virus isolates. *Virology* 173(1), pp. 317–22.

Rosa, C. La, Krishnan, R., Markel, S., Schneck, J.P., Houghten, R., Pinilla, C. and Diamond, D.J. 2001. Enhanced immune activity of cytotoxic T-lymphocyte epitope analogs derived from positional scanning synthetic combinatorial libraries. *Blood* 97(6)

Rose, N., Hervé, S., Eveno, E., Barbier, N., Eono, F., Dorenlor, V., Andraud, M., Camsusou, C., Madec, F. and Simon, G. 2013. Dynamics of influenza A virus infections in permanently infected pig farms: evidence of recurrent infections, circulation of several swine influenza viruses and reassortment events. *Veterinary research* 44(1), p. 72. doi: 10.1186/1297-9716-44-72.

Saper, M.A., Bjorkman, P.J. and Wiley, D.C. 1991. Refined structure of the human histocompatibility antigen HLA-A2 at 2.6 Å resolution. *Journal of Molecular Biology* 219(2), pp. 277–319. doi: 10.1016/0022-2836(91)90567-P.

Sarma, J.V. and Ward, P.A. 2011. Sarma, J. V. and Ward, P. A. (2011) 'The complement system', Cell and Tissue Research. Springer-Verlag, 343(1), pp. 227–235. doi: 10.1007/s00441-010-1034-0.The complement system. *Cell and Tissue Research* 343(1), pp. 227–235. doi: 10.1007/s00441-010-1034-0.

Scholtissek, C. 1990. Pigs as 'Mixing Vessels' for the Creation of New Pandemic Influenza A Viruses. *Medical Principles and Practice* 2(2), pp. 65–71. doi: 10.1159/000157337.

Scholtissek, C., Bürger, H., Kistner, O. and Shortridge, K.F. 1985. The nucleoprotein as a possible major factor in determining host specificity of influenza H3N2 viruses. *Virology* 147(2), pp. 287–294. doi: 10.1016/0042-6822(85)90131-X.

Schulman, J.L. and Kilbourne, E.D. 1965. Induction of Partial Specific Heterotypic immunity in Mice by a Single Infection with Influenza A virus. *Journal of bacteriology* 89(1), pp. 170–4.

Schumacher, T.N., Heemels, M.T., Neefjes, J.J., Kast, W.M., Melief, C.J. and Ploegh, H.L. 1990. Direct binding of peptide to empty MHC class I molecules on intact cells and in vitro. *Cell* 62(3), pp. 563–7.

Schumacher, T.N.M., De Bruijn, M.L.H., Vernie, L.N., Kast, W.M., Melief, C.J.M., Neefjes, J.J. and Ploegh, H.L. 1991. Peptide selection by MHC class I molecules. *Nature* 350(6320), pp. 703–706. doi: 10.1038/350703a0.

Scriba, T.J., Purbhoo, M., Day, C.L., Robinson, N., Fidler, S., Fox, J., Weber, J.N., Klenerman, P., Sewell, A.K. and Phillips, R.E. 2005. Ultrasensitive detection and phenotyping of CD4+ T cells with optimized HLA class II tetramer staining. *Journal of immunology (Baltimore, Md. : 1950)* 175(10), pp. 6334–43.

Serwold, T., Gonzalez, F., Kim, J., Jacob, R. and Shastri, N. 2002. ERAAP customizes peptides for MHC class I molecules in the endoplasmic reticulum. *Nature* 419(6906), pp. 480–483. doi: 10.1038/nature01074.

Sette, A. and Sidney, J. 1998. HLA supertypes and supermotifs: a functional perspective on HLA polymorphism. *Current opinion in immunology* 10(4), pp. 478–82.

Sewell, A.K. 2012a. Why must T cells be cross-reactive? *Nature reviews. Immunology* 12(9), pp. 669–77. doi: 10.1038/nri3279.

Sewell, A.K. 2012b. Why must T cells be cross-reactive? *Nature Reviews Immunology* 12(9), pp. 669–677. doi: 10.1038/nri3279.

Shinya, K., Ebina, M., Yamada, S., Ono, M., Kasai, N. and Kawaoka, Y. 2006. Avian flu: Influenza virus receptors in the human airway. *Nature* 440(7083), pp. 435–436. doi: 10.1038/440435a.

Sidney, J., Peters, B., Frahm, N., Brander, C., Sette, A., Schatz, M., Kloetzel, P., Rammensee, H., Schild, H. and Holzhutter, H. 2008. HLA class I supertypes: a revised and updated classification. *BMC Immunology* 9(1), p. 1. doi: 10.1186/1471-2172-9-1.

Skowera, A., Ellis, R.J., Varela-calviño, R., Arif, S., Huang, G.C., Van-Krinks, C., Zaremba, A., Rackham, C., Allen, J.S., Tree, T.I.M., Zhao, M., Dayan, C.M., Sewell, A.K., Unger, W.W., Drijfhout, J.W., Ossendorp, F., Roep, B.O. and Peakman, M. 2008. CTLs are targeted to kill β cells in patients with type 1 diabetes through recognition of a glucose-regulated preproinsulin epitope. *The Journal of clinical investigation* 118(10), pp. 3390–402. doi: 10.1172/JCI35449DS1.

Sloan-Lancaster, J. and Allen, P.M. 1995. Significance of T-cell stimulation by altered peptide ligands in T cell biology. *Current opinion in immunology* 7(1), pp. 103–9.

Slomka, M.J., Densham, A.L.E., Coward, V.J., Essen, S., Brookes, S.M., Irvine, R.M., Spackman, E., Ridgeon, J., Gardner, R., Hanna, A., Suarez, D.L. and Brown, I.H. 2010. Real time reverse transcription (RRT)-polymerase chain reaction (PCR) methods for detection of pandemic (H1N1) 2009 influenza virus and European swine influenza A virus infections in pigs. *Influenza and Other Respiratory Viruses* 4(5), pp. 277–293. doi: 10.1111/j.1750-2659.2010.00149.x.

Smith, G.J.D., Vijaykrishna, D., Bahl, J., Lycett, S.J., Worobey, M., Pybus, O.G., Ma, S.K., Cheung, C.L., Raghwani, J., Bhatt, S., Peiris, J.S.M., Guan, Y. and Rambaut, A. 2009. Origins and evolutionary genomics of the 2009 swine-origin H1N1 influenza A epidemic. *Nature* 459(7250), pp. 1122–1125. doi: 10.1038/nature08182.

Smith, K.A. 1988. Interleukin-2: inception, impact, and implications. *Science (New York, N.Y.)* 240(4856), pp. 1169–76.

Sridhar, S. 2016. Heterosubtypic T-Cell Immunity to Influenza in Humans: Challenges for Universal T-Cell Influenza Vaccines. *Frontiers in Immunology* 7, p. 195. doi: 10.3389/fimmu.2016.00195.

Sridhar, S., Begom, S., Bermingham, A., Hoschler, K., Adamson, W., Carman, W., Bean, T., Barclay, W., Deeks, J.J. and Lalvani, A. 2013. Cellular immune correlates of protection against symptomatic pandemic influenza. *Nature medicine* 19(10), pp. 1305–12. doi: 10.1038/nm.3350.

Szomolay, B., Liu, J., Brown, P.E., Miles, J.J., Clement, M., Llewellyn-Lacey, S., Dolton, G., Ekeruche-Makinde, J., Lissina, A., Schauenburg, A.J., Sewell, A.K., Burrows, S.R., Roederer, M., Price, D.A., Wooldridge, L. and van den Berg, H.A. 2016. Identification of human viral protein-derived ligands recognized by individual MHCI-restricted T-cell receptors. *Immunology and cell biology* 94(6), pp. 573–82. doi: 10.1038/icb.2016.12.

Talker, S.C., Koinig, H.C., Stadler, M., Graage, R., Klingler, E., Ladinig, A., Mair, K.H., Hammer, S.E., Weissenböck, H., Dürrwald, R., Ritzmann, M., Saalmüller, A. and Gerner, W. 2015. Magnitude and kinetics of multifunctional CD4(+) and CD8β(+) T cells in pigs infected with swine influenza A virus. *Veterinary research* 46(1), p. 52. doi: 10.1186/s13567-015-0182-3.

Talker, S.C., Stadler, M., Koinig, H.C., Mair, K.H., Rodríguez-Gómez, I.M., Graage, R., Zell, R., Dürrwald, R., Starick, E., Harder, T., Weissenböck, H., Lamp, B., Hammer, S.E., Ladinig, A., Saalmüller, A. and Gerner, W. 2016. Influenza A Virus Infection in Pigs Attracts Multifunctional and Cross-Reactive T Cells to the Lung. *Journal of virology* 90(20), pp. 9364–82. doi: 10.1128/JVI.01211-16.

Tan, M.P., Dolton, G.M., Gerry, A.B., Brewer, J.E., Bennett, A.D., Pumphrey, N.J., Jakobsen, B.K. and Sewell, A.K. 2017. Human leucocyte antigen class I-redirected anti-tumour CD4(+) T cells require a higher T cell receptor binding affinity for optimal activity than CD8(+) T cells. *Clinical and experimental immunology* 187(1), pp. 124–137. doi: 10.1111/cei.12828.

Taubenberger, J.K., Reid, A.H., Krafft, A.E., Bijwaard, K.E. and Fanning, T.G. 1997. Initial Genetic Characterization of the 1918 'Spanish' Influenza Virus. *Science* 275(5307)

Theaker, S.M., Rius, C., Greenshields-Watson, A., Lloyd, A., Trimby, A., Fuller, A., Miles, J.J., Cole, D.K., Peakman, M., Sewell, A.K. and Dolton, G. 2016. T-cell libraries allow simple parallel generation of multiple peptide-specific human T-cell clones. *Journal of Immunological Methods* 430, pp. 43–50. doi: 10.1016/j.jim.2016.01.014.

Thomas, P.G., Brown, S.A., Keating, R., Yue, W., Morris, M.Y., So, J., Webby, R.J. and Doherty, P.C. 2007. Hidden Epitopes Emerge in Secondary Influenza Virus-Specific CD8+ T Cell Reponses. *The Journal of Immunology* 178(5)

Topham, D.J., Tripp, R.A. and Doherty, P.C. 1997. CD8+ T cells clear influenza virus by perforin or Fas-dependent processes. *The Journal of Immunology* 159(11)

Townsend, A.R. and Skehel, J.J. 1984. The influenza A virus nucleoprotein gene controls the induction of both subtype specific and cross-reactive cytotoxic T cells. *The Journal of experimental medicine* 160(2), pp. 552–63.

Trebbien, R., Bragstad, K., Larsen, L.E., Nielsen, J., Bøtner, A., Heegaard, P.M.H., Fomsgaard, A., Viuff, B. and Hjulsager, C.K. 2013. Genetic and biological characterisation of an avian-like H1N2 swine influenza virus generated by reassortment of circulating avian-like H1N1 and H3N2 subtypes in Denmark. *Virology journal* 10, p. 290. doi: 10.1186/1743-422X-10-290.

Trolle, T., McMurtrey, C.P., Sidney, J., Bardet, W., Osborn, S.C., Kaever, T., Sette, A., Hildebrand, W.H., Nielsen, M. and Peters, B. 2016. The Length Distribution of Class I-Restricted T Cell Epitopes Is Determined by Both Peptide Supply and MHC Allele-Specific Binding Preference. *Journal of immunology (Baltimore, Md. : 1950)* 196(4), pp. 1480–7. doi: 10.4049/jimmunol.1501721.

Tungatt, K., Bianchi, V., Crowther, M.D., Powell, W.E., Schauenburg, A.J., Trimby, A., Donia, M., Miles, J.J., Holland, C.J., Cole, D.K., Godkin, A.J., Peakman, M., Straten, P.T., Svane, I.M., Sewell, A.K. and Dolton, G. 2015. Antibody stabilization of peptide-MHC multimers reveals functional T cells bearing extremely low-affinity TCRs. *Journal of immunology (Baltimore, Md. : 1950)* 194(1), pp. 463–74. doi: 10.4049/jimmunol.1401785.

Valitutti, S., Müller, S., Cella, M., Padovan, E. and Lanzavecchia, A. *Serial triggering of many T-cell receptors by a few peptide-MHC complexes*. Nature Publishing Group. 375. doi: 10.1038/375148a0.

Vasin, A.V., Temkina, O.A., Egorov, V.V., Klotchenko, S.A., Plotnikova, M.A. and Kiselev, O.I. 2014. Molecular mechanisms enhancing the proteome of influenza A viruses: An overview of recently discovered proteins. *Virus Research* 185, pp. 53–63. doi: 10.1016/j.virusres.2014.03.015.

Wang, Z., Wan, Y., Qiu, C., Quiñones-Parra, S., Zhu, Z., Loh, L., Tian, D., Ren, Y., Hu, Y., Zhang, X., Thomas, P.G., Inouye, M., Doherty, P.C., Kedzierska, K. and Xu, J. 2015. Recovery from severe H7N9 disease is associated with diverse response mechanisms dominated by CD8+ T cells. *Nature Communications* 6, p. 6833. doi: 10.1038/ncomms7833.

Watson, S.J., Langat, P., Reid, S.M., Lam, T.T.-Y., Cotten, M., Kelly, M., Van Reeth, K., Qiu, Y., Simon, G., Bonin, E., Foni, E., Chiapponi, C., Larsen, L., Hjulsager, C., Markowska-Daniel, I., Urbaniak, K., Dürrwald, R., Schlegel, M., Huovilainen, A., Davidson, I., Dán, Á., Loeffen, W., Edwards, S., Bublot, M., Vila, T., Maldonado, J., Valls, L., Brown, I.H., Pybus, O.G. and Kellam, P. 2015. Molecular Epidemiology and Evolution of Influenza Viruses Circulating within European Swine between 2009 and 2013. *Journal of virology* , p. JVI.00840-15-. doi: 10.1128/JVI.00840-15.

Whelan, J.A., Dunbar, P.R., Price, D.A., Purbhoo, M.A., Lechner, F., Ogg, G.S., Griffiths, G., Phillips, R.E., Cerundolo, V. and Sewell, A.K. 1999. Specificity of CTL interactions with peptide-MHC class I tetrameric complexes is temperature dependent. *Journal of immunology (Baltimore, Md. : 1950)* 163(8), pp. 4342–8.

WHO 1980. A revision of the system of nomenclature for influenza viruses: a WHO Memorandum*. *Bulletin of the World Health Organization* 58(4), pp. 585–591.

Wilkinson, T.M., Li, C.K.F., Chui, C.S.C., Huang, A.K.Y., Perkins, M., Liebner, J.C., Lambkin-Williams, R., Gilbert, A., Oxford, J., Nicholas, B., Staples, K.J., Dong, T., Douek, D.C., McMichael, A.J. and Xu, X.-N. 2012. Preexisting influenza-specific CD4+ T cells correlate with disease protection against influenza challenge in humans. *Nature Medicine* 18(2), pp. 274–280. doi: 10.1038/nm.2612.

Winn, M.D., Ballard, C.C., Cowtan, K.D., Dodson, E.J., Emsley, P., Evans, P.R., Keegan, R.M., Krissinel, E.B., Leslie, A.G.W., McCoy, A., McNicholas, S.J., Murshudov, G.N., Pannu, N.S., Potterton, E.A., Powell, H.R., Read, R.J., Vagin, A. and Wilson, K.S. 2011. Overview of the CCP4 suite and current developments. *Acta crystallographica. Section D, Biological crystallography* 67(Pt 4), pp. 235–42. doi: 10.1107/S0907444910045749.

Winter, G. 2010. xia2 : an expert system for macromolecular crystallography data reduction. *Journal of Applied Crystallography* 43(1), pp. 186–190. doi: 10.1107/S0021889809045701.

Wooldridge, L., van den Berg, H.A., Glick, M., Gostick, E., Laugel, B., Hutchinson, S.L., Milicic, A., Brenchley, J.M., Douek, D.C., Price, D.A. and Sewell, A.K. 2005. Interaction between the CD8 Coreceptor and Major Histocompatibility Complex Class I Stabilizes T Cell Receptor-Antigen Complexes at the Cell Surface. *Journal of Biological Chemistry* 280(30), pp. 27491–27501. doi: 10.1074/jbc.M500555200.

Wooldridge, L., Ekeruche-Makinde, J., van den Berg, H.A., Skowera, A., Miles, J.J., Tan, M.P., Dolton, G., Clement, M., Llewellyn-Lacey, S., Price, D.A., Peakman, M. and Sewell, A.K. 2012. A single autoimmune T cell receptor recognizes more than a million different peptides. *The Journal of biological chemistry* 287(2), pp. 1168–77. doi: 10.1074/jbc.M111.289488.

Wooldridge, L., Lissina, A., Cole, D.K., van den Berg, H.A., Price, D.A. and Sewell, A.K. 2009. Tricks with tetramers: how to get the most from multimeric peptide-MHC. *Immunology* 126(2), pp. 147–64. doi: 10.1111/j.1365-2567.2008.02848.x.

Wooldridge, L., Scriba, T.J., Milicic, A., Laugel, B., Gostick, E., Price, D.A., Phillips, R.E. and Sewell, A.K. 2006. Anti-coreceptor antibodies profoundly affect staining with peptide-MHC class I and class II tetramers. *European Journal of Immunology* 36(7), pp. 1847–1855. doi: 10.1002/eji.200635886.

Wu, C., Zanker, D., Valkenburg, S., Tan, B., Kedzierska, K. and Ming, Q. 2011. Systematic identification of immunodominant CD8 + T-cell responses to influenza A virus in HLA-A2 individuals., pp. 1–6. doi: 10.1073/pnas.1105624108/-/DCSupplemental.www.pnas.org/cgi/doi/10.1073/pnas.1105624108.

Yang, H., Oura, C.A., Kirkham, P.A. and Parkhouse, R.M. 1996. Preparation of monoclonal anti-porcine CD3 antibodies and preliminary characterization of porcine T lymphocytes. *Immunology* 88(4), pp. 577–85.

Yang, H. and Parkhouse, R.M. 1997. Differential expression of CD8 epitopes amongst porcine CD8-positive functional lymphocyte subsets. *Immunology* 92(1), pp. 45–52.

Yang, H., Parkhouse, R.M.E. and Wileman, T. 2005. Monoclonal antibodies that identify the CD3 molecules expressed specifically at the surface of porcine gammadelta-T cells. *Immunology* 115(2), pp. 189–96. doi: 10.1111/j.1365-2567.2005.02137.x.

Yewdell, J.W., Bennink, J.R., Smith, G.L. and Moss, B. 1985. Influenza A virus nucleoprotein is a major target antigen for cross-reactive anti-influenza A virus cytotoxic T lymphocytes. *Proceedings of the National Academy of Sciences of the United States of America* 82(6), pp. 1785–9.

Zell, R., Motzke, S., Krumbholz, A., Wutzler, P., Herwig, V. and Durrwald, R. 2008. Novel reassortant of swine influenza H1N2 virus in Germany. *Journal of General Virology* 89(1), pp. 271–276. doi: 10.1099/vir.0.83338-0.

Zhang, N., Qi, J., Feng, S., Gao, F., Liu, J., Pan, X., Chen, R., Li, Q., Chen, Z., Li, X., Xia, C. and Gao, G.F. 2011. Crystal structure of swine major histocompatibility complex class I SLA-1 0401 and identification of 2009 pandemic swine-origin influenza A H1N1 virus cytotoxic T lymphocyte epitope peptides. *Journal of virology* 85(22), pp. 11709–24. doi: 10.1128/JVI.05040-11.

Zhao, L. and Lu, W. 2014. Mirror image proteins. *Current Opinion in Chemical Biology* 22, pp. 56–61. doi: 10.1016/j.cbpa.2014.09.019.

Zheng, W. and Tao, Y.J. 2013. Structure and assembly of the influenza A virus ribonucleoprotein complex. *FEBS Letters* 587(8), pp. 1206–1214. doi: 10.1016/j.febslet.2013.02.048.

Zuckermann, F.A. and Husmann, R.J. 1996. Functional and phenotypic analysis of porcine peripheral blood CD4/CD8 double-positive T cells. *Immunology* 87(3), pp. 500–12.

# 10 Appendix

**Table 10.1. List of overlapping peptides of nucleoprotein**

| Pool | Designation | Aa length | Peptide Sequence |
|------|-------------|-----------|------------------|
| A | NP1 | 18 | MASQGTKRSYEQMETDGE |
| A | NP2 | 18 | KRSYEQMETDGERQNATE |
| A | NP3 | 18 | METDGERQNATEIRASVG |
| A | NP4 | 18 | RQNATEIRASVGKMIGGI |
| A | NP5 | 18 | IRASVGKMIGGIGRFYIQ |
| A | NP6 | 18 | KMIGGIGRFYIQMCTELK |
| A | NP7 | 18 | GRFYIQMCTELKLSDYEG |
| A | NP8 | 18 | MCTELKLSDYEGRLIQNS |
| A | NP9 | 18 | LSDYEGRLIQNSLTIERM |
| A | NP10 | 19 | RLIQNSLTIERMVLSAFDE |
| A | NP11 | 18 | LTIERMVLSAFDERRNKY |
| A | NP12 | 18 | VLSAFDERRNKYLEEHPS |
| A | NP13 | 18 | ERRNKYLEEHPSAGKDPK |
| A | NP14 | 18 | LEEHPSAGKDPKKTGGPI |
| A | NP15 | 18 | AGKDPKKTGGPIYRRVNG |
| A | NP16 | 18 | KTGGPIYRRVNGKWMREL |
| A | NP17 | 18 | YRRVNGKWMRELILYDKE |
| A | NP18 | 18 | KWMRELILYDKEEIRRIW |
| A | NP19 | 18 | ILYDKEEIRRIWRQANNG |
| A | NP20 | 18 | EIRRIWRQANNGDDATAG |
| B | NP21 | 15 | RQANNGDDATAGLTH |
| B | NP22 | 19 | DDATAGLTHMMIWHSNLND |
| B | NP23 | 18 | LTHMMIWHSNLNDATYQR |
| B | NP24 | 18 | WHSNLNDATYQRTRALVR |
| B | NP25 | 18 | DATYQRTRALVRTGMDPR |
| B | NP26 | 18 | TRALVRTGMDPRMCSLMQ |
| B | NP27 | 19 | RTGMDPRMCSLMQGSTLPR |
| B | NP28 | 19 | RMCSLMQGSTLPRRSGAAG |
| B | NP29 | 18 | GSTLPRRSGAAGAAVKGV |
| B | NP30 | 19 | RRSGAAGAAVKGVGTMVME |
| B | NP31 | 18 | VKGVGTMVMELVRMIKRG |
| B | NP32 | 18 | GTMVMELVRMIKRGINDR |
| B | NP33 | 18 | LVRMIKRGINDRNFWRGE |
| B | NP34 | 19 | GINDRNFWRGENGRKTRIA |
| B | NP35 | 17 | FWRGENGRKTRIAYERM |
| B | NP36 | 17 | GRKTRIAYERMCNILKG |
| B | NP37 | 18 | IAYERMCNILKGKFQTAA |
| B | NP38 | 18 | CNILKGKFQTAAQKAMMD |

| | | | |
|---|---|---|---|
| **B** | NP39 | 18 | KFQTAAQKAMMDQVRESR |
| **B** | NP40 | 17 | KAMMDQVRESRNPGNAE |
| **C** | NP41 | 17 | VRESRNPGNAEFEDLTF |
| **C** | NP42 | 17 | PGNAEFEDLTFLARSAL |
| **C** | NP43 | 18 | EFEDLTFLARSALILRGS |
| **C** | NP44 | 18 | LARSALILRGSVAHKSCL |
| **C** | NP45 | 18 | ILRGSVAHKSCLPACVYG |
| **C** | NP46 | 19 | HKSCLPACVYGPAVASGYD |
| **C** | NP47 | 18 | PACVYGPAVASGYDFERE |
| **C** | NP48 | 18 | PAVASGYDFEREGYSLVG |
| **C** | NP49 | 18 | YDFEREGYSLVGIDPFRL |
| **C** | NP50 | 20 | EREGYSLVGIDPFRLLQNSQ |
| **C** | NP51 | 16 | DPFRLLQNSQVYSLIR |
| **C** | NP52 | 19 | LQNSQVYSLIRPNENPAHK |
| **C** | NP53 | 18 | YSLIRPNENPAHKSQLVW |
| **C** | NP54 | 17 | ENPAHKSQLVWMACHSA |
| **C** | NP55 | 18 | KSQLVWMACHSAAFEDLR |
| **C** | NP56 | 18 | CHSAAFEDLRVLSFIKGT |
| **C** | NP57 | 18 | AFEDLRVLSFIKGTKVVP |
| **C** | NP58 | 18 | VLSFIKGTKVVPRGKLST |
| **C** | NP59 | 18 | GTKVVPRGKLSTRGVQIA |
| **C** | NP60 | 18 | RGKLSTRGVQIASNENME |
| **D** | NP61 | 18 | RGVQIASNENMETMESST |
| **D** | NP62 | 19 | ASNENMETMESSTLELRSR |
| **D** | NP63 | 18 | TMESSTLELRSRYWAIRT |
| **D** | NP64 | 18 | LELRSRYWAIRTRSGGNT |
| **D** | NP65 | 18 | YWAIRTRSGGNTNQQRAS |
| **D** | NP66 | 18 | RSGGNTNQQRASAGQISI |
| **D** | NP67 | 18 | TNQQRASAGQISIQPTFS |
| **D** | NP68 | 20 | AGQISIQPTFSVQRNLPFDR |
| **D** | NP69 | 17 | PTFSVQRNLPFDRTTVM |
| **D** | NP70 | 17 | RNLPFDRTTVMAAFTGN |
| **D** | NP71 | 19 | DRTTVMAAFTGNTEGRTSD |
| **D** | NP72 | 18 | AAFTGNTEGRTSDMRTEI |
| **D** | NP73 | 18 | TEGRTSDMRTEIIRMMES |
| **D** | NP74 | 18 | DMRTEIIRMMESARPEDV |
| **D** | NP75 | 18 | IRMMESARPEDVSFQGRG |
| **D** | NP76 | 18 | ARPEDVSFQGRGVFELSD |
| **D** | NP77 | 18 | SFQGRGVFELSDEKAASP |
| **D** | NP78 | 18 | VFELSDEKAASPIVPSFD |
| **D** | NP79 | 18 | EKAASPIVPSFDMSNEGS |
| **D** | NP80 | 18 | IVPSFDMSNEGSYFFGDN |
| **D** | NP81 | 18 | MSNEGSYFFGDNAEEYDN |

150

**Table 10.2: List of overlapping peptides of Matrix 1 protein**

| Pool | Designation | Aa length | Peptide Sequence |
|------|-------------|-----------|------------------|
| E | M82 | 18 | MSLLTEVETYVLSIIPSG |
| E | M83 | 19 | EVETYVLSIIPSGPLKAEI |
| E | M84 | 18 | SIIPSGPLKAEIAQRLED |
| E | M85 | 18 | PLKAEIAQRLEDVFAGKN |
| E | M86 | 18 | AQRLEDVFAGKNTDLEVL |
| E | M87 | 18 | VFAGKNTDLEVLMEWLKT |
| E | M88 | 18 | TDLEVLMEWLKTRPILSP |
| E | M89 | 18 | MEWLKTRPILSPLTKGIL |
| E | M90 | 17 | RPILSPLTKGILGFVFT |
| E | M91 | 17 | TKGILGFVFTLTVPSER |
| E | M92 | 18 | GFVFTLTVPSERGLQRRR |
| E | M93 | 18 | TVPSERGLQRRRFVQNAL |
| E | M94 | 18 | GLQRRRFVQNALNGNGDP |
| E | M95 | 18 | FVQNALNGNGDPNNMDKA |
| E | M96 | 17 | GNGDPNNMDKAVKLYRK |
| E | M97 | 19 | PNNMDKAVKLYRKLKREIT |
| E | M98 | 18 | VKLYRKLKREITFHGAKE |
| E | M99 | 18 | LKREITFHGAKEISLSYS |
| E | M100 | 17 | HGAKEISLSYSAGALAS |
| E | M101 | 19 | SLSYSAGALASCMGLIYNR |
| F | M102 | 15 | GALASCMGLIYNRMG |
| F | M103 | 15 | MGLIYNRMGAVTTEV |
| F | M104 | 19 | RMGAVTTEVAFGLVCATCE |
| F | M105 | 18 | TTEVAFGLVCATCEQIAD |
| F | M106 | 18 | GLVCATCEQIADSQHRSH |
| F | M107 | 18 | CEQIADSQHRSHRQMVTT |
| F | M108 | 18 | SQHRSHRQMVTTTNPLIR |
| F | M109 | 18 | RQMVTTTNPLIRHENRMV |
| F | M110 | 18 | TNPLIRHENRMVLASTTA |
| F | M111 | 18 | HENRMVLASTTAKAMEQM |
| F | M112 | 18 | LASTTAKAMEQMAGSSEQ |
| F | M113 | 18 | KAMEQMAGSSEQAAEAME |
| F | M114 | 18 | AGSSEQAAEAMEVASQAR |
| F | M115 | 15 | EAMEVASQARQMVQA |
| F | M116 | 18 | VASQARQMVQAMRTIGTH |
| F | M117 | 19 | RQMVQAMRTIGTHPSSSAG |
| F | M118 | 18 | RTIGTHPSSSAGLKNDLL |
| F | M119 | 18 | PSSSAGLKNDLLENLQAY |
| F | M120 | 18 | LKNDLLENLQAYQKRMGV |
| F | M121 | 18 | ENLQAYQKRMGVQMQRFK |
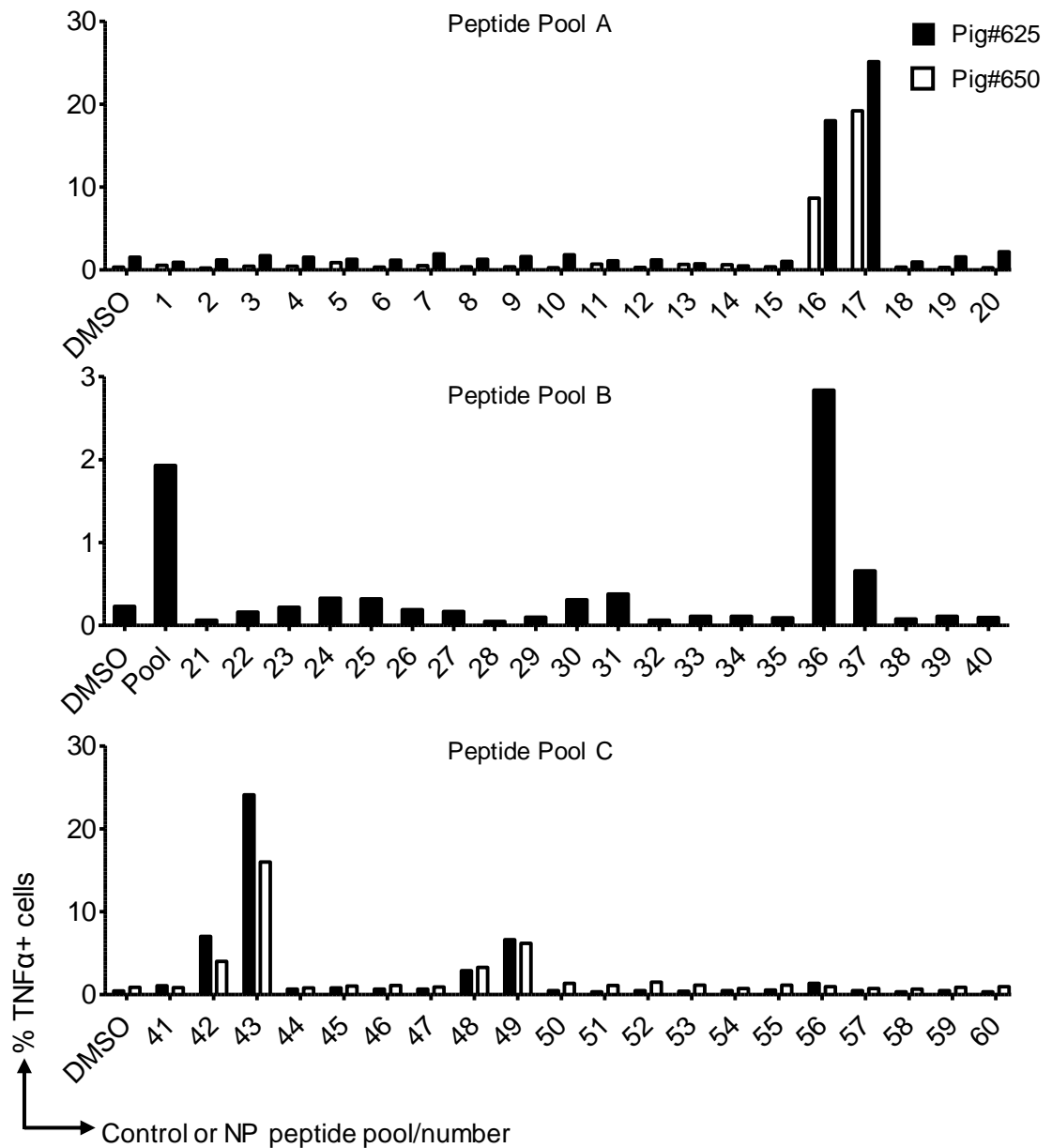
**Figure 10.1. Influenza-specific CD8β T-cell line procurement**
Summarised flow cytometry data of Influenza-specific CD8β T-cell lines from pigs #625 and #650 raised against NP peptide pools A, B and C. All CD8β sorted T-cell lines displayed were raised for two weeks against their respective peptide pool. T-cell lines were incubated with DMSO or 2 μM peptide pool/peptide for 5 h then stained for CD8β and intracellular TNFα. Cells were gated for size and viability and the percentage of TNFα+ cells is plotted on the *y* axes.

**Table 10.3. Peptide truncations of the overlapping sequence between peptides NP48 and NP49.**

| Truncation | Aa length | Peptide Sequence |
|---|---|---|
| **12aa overlap** | 12 | YDFEREGYSLVG |
| **N-1** | 11 | DFEREGYSLVG |
| **N-1 C-1** | 10 | DFEREGYSLV |
| **N-1 C-2** | 9 | DFEREGYSL |
| **N-1 C-3** | 8 | DFEREGYS |
| **N-2** | 10 | FEREGYSLVG |
| **N-2 C-1** | 9 | FEREGYSLV |
| **N-2 C-2** | 8 | FEREGYSL |
| **N-3** | 9 | EREGYSLVG |
| **N-3 C-1** | 8 | EREGYSLV |
| **N-4** | 8 | REGYSLVG |
| **C-1** | 11 | YDFEREGYSLV |
| **C-2** | 10 | YDFEREGYSL |
| **C-3** | 9 | YDFEREGYS |
| **C-4** | 8 | YDFEREGY |

*N: N-terminus. C: Carboxyl-terminus.*


**Table 10.4. Peptide truncations of the overlapping sequence between peptides NP42 and NP43.**

| Truncation | Aa length | Peptide Sequence |
|---|---|---|
| **13aa overlap** | 13 | EFEDLTFLARSAL |
| **N-1** | 12 | FEDLTFLARSAL |
| **N-1 C-1** | 11 | FEDLTFLARSA |
| **N-1 C-2** | 10 | FEDLTFLARS |
| **N-1 C-3** | 9 | FEDLTFLAR |
| **N-1 C-4** | 8 | FEDLTFLA |
| **N-2** | 11 | EDLTFLARSAL |
| **N-2 C-1** | 10 | EDLTFLARSA |
| **N-2 C-2** | 9 | EDLTFLARS |
| **N-2 C-3** | 8 | EDLTFLAR |
| **N-3** | 10 | DLTFLARSAL |
| **N-3 C-1** | 9 | DLTFLARSA |
| **N-3 C-2** | 8 | DLTFLARS |
| **N-4** | 9 | LTFLARSAL |
| **N-4 C-1** | 8 | LTFLARSA |
| **N-5** | 8 | TFLARSAL |
| **C-1** | 12 | EFEDLTFLARSA |
| **C-2** | 11 | EFEDLTFLARS |
| **C-3** | 10 | EFEDLTFLAR |
| **C-4** | 9 | EFEDLTFLA |
| **C-5** | 8 | EFEDLTFL |

*N: N-terminus. C: Carboxyl-terminus.*

**Table 10.5. Peptide truncations of the overlapping sequence between peptides NP16 and NP17.**

| Truncation | Aa length | Peptide Sequence |
|---|---|---|
| **12aa overlap** | 12 | YRRVNGKWMREL |
| **N-1** | 11 | RRVNGKWMREL |
| **N-1 C-1** | 10 | RRVNGKWMRE |
| **N-1 C-2** | 9 | RRVNGKWMR |
| **N-1 C-3** | 8 | RRVNGKWM |
| **N-2** | 10 | RVNGKWMREL |
| **N-2 C-1** | 9 | RVNGKWMRE |
| **N-2 C-2** | 8 | RVNGKWMR |
| **N-3** | 9 | VNGKWMREL |
| **N-3 C-1** | 8 | VNGKWMRE |
| **N-4** | 8 | NGKWMREL |
| **C-1** | 11 | YRRVNGKWMRE |
| **C-2** | 10 | YRRVNGKWMR |
| **C-3** | 9 | YRRVNGKWM |
| **C-4** | 8 | YRRVNGKW |
| **Additional peptide truncations:** | | |
| **N-3 C+1** | 10 | VNGKWMRELI |
| **N-3 C+2** | 11 | VNGKWMRELIL |
| **N-4 C+1** | 9 | NGKWMRELI |
| **N-4 C+2** | 10 | NGKWMRELIL |
| **N-4 C+3** | 11 | NGKWMRELILY |
| **N-5** | 7 | GKWMREL |
| **N-5 C+1** | 8 | GKWMRELI |
| **N-5 C+2** | 9 | GKWMRELIL |
| **N-5 C+3** | 10 | GKWMRELILY |
| **N-5 C+4** | 11 | GKWMRELILYD |

*N: N-terminus. C: Carboxyl-terminus.*

**Table 10.6. Peptide truncations of the overlapping sequence between peptides NP36 and NP37.**

| Truncation | Aa length | Peptide Sequence |
|---|---|---|
| **12aa overlap** | 12 | IAYERMCNILKG |
| **C-1** | 11 | AYERMCNILKG |
| **C-1 N-1** | 10 | AYERMCNILK |
| **C-1 N-2** | 9 | AYERMCNIL |
| **C-1 N-3** | 8 | AYERMCNI |
| **C-2** | 10 | YERMCNILKG |
| **C-2 N-1** | 9 | YERMCNILK |
| **C-2 N-2** | 8 | YERMCNIL |
| **C-3** | 9 | ERMCNILKG |
| **C-3 N-1** | 8 | ERMCNILK |
| **C-4** | 8 | RMCNILKG |
| **N-1** | 11 | IAYERMCNILK |
| **N-2** | 10 | IAYERMCNIL |
| **N-3** | 9 | IAYERMCNI |
| **N-4** | 8 | IAYERMCN |

*N: N-terminus. C: Carboxyl-terminus.*


**Table 10.7. SLA-2*11:04 predicted epitopes for Influenza viral protein PB2.**

| Peptide Sequence |
|---|
| MSQSRTREI |
| KTTVDHMAI |
| TTVDHMAII |
| MNDAGSDRV |
| DAGSDRVMV |
| RVMVSPLAV |
| RNGPMTNTV |
| TNTVHYPKI |
| LKHGTFGPV |
| VKIRRRVDI |
| LSAKEAQDV |
| SAKEAQDVI |
| EAQDVIMEV |
| PNEVGARIL |
| LTSESQLTI |
| ITKEKKEEL |
| VAYMLEREL |
| PVAGGTSSV |
| AGGTSSVYI |
| GTSSVYIEV |
| TSSVYIEVL |
| SVYIEVLHL |
| GGEVKNDDV |
| KNDDVDQSL |
| RNIVRRAAV |
| RAAVSADPL |
| VSADPLASL |
| SADPLASLL |
| IGGIRMVDI |

| |
|---|
| GGIRMVDIL |
| QNPTEEQAV |
| PTEEQAVDI |
| CKAAMGLRI |
| FKRTSGSSV |
| SSVKREEEV |
| SVKREEEVL |
| TGNLQTLKI |
| EGSEEFTMV |
| MVGRRATAI |
| VGRRATAIL |
| KATRRLIQL |
| ATRRLIQLI |
| VSGRDEQSI |
| QSIAEAIIV |
| AVRGDLNFV |
| FVNRANQRL |
| KVLFQNWGV |
| WGVEPIDNV |
| DNVMGMIGI |
| NVMGMIGIL |
| GVRISKMGV |
| YSSTERVVV |
| STERVVVSI |
| VVVSIDRFL |
| VSIDRFLRV |
| RVRDQRGNV |
| NVLLSPEEV |
| YSSSMMWEI |
| INGPESVLV |
| LVNTYQWII |
| LGTFDTAQI |
| GTFDTAQII |
| DTAQIIKLL |
| NVRGSGMRI |
| RGSGMRILV |
| NKATKRLTV |
| KATKRLTVL |
| GTAGVESAV |
| TAGVESAVL |
| ESAVLRGFL |
| SAVLRGFLI |
| AVLRGFLIL |
| LSINELSNL |
| LAKGEKANV |
| AKGEKANVL |
| KGEKANVLI |
| NVLIGQGDV |
| IGQGDVVLV |
| MKRKRDSSI |
| DSQTATKRI |
| ATKRIRMAI |

156

# Antibody Stabilization of Peptide–MHC Multimers Reveals Functional T Cells Bearing Extremely Low-Affinity TCRs

Katie Tungatt,* Valentina Bianchi,* Michael D. Crowther,* Wendy E. Powell,*
Andrea J. Schauenburg,* Andrew Trimby,* Marco Donia,[†] John J. Miles,*,[‡]
Christopher J. Holland,* David K. Cole,* Andrew J. Godkin,* Mark Peakman,[§]
Per Thor Straten,[†] Inge Marie Svane,[†] Andrew K. Sewell,*,[1] and Garry Dolton*,[1]

Fluorochrome-conjugated peptide–MHC (pMHC) multimers are commonly used in combination with flow cytometry for direct ex vivo visualization and characterization of Ag-specific T cells, but these reagents can fail to stain cells when TCR affinity and/or TCR cell-surface density are low. pMHC multimer staining of tumor-specific, autoimmune, or MHC class II–restricted T cells can be particularly challenging, as these T cells tend to express relatively low-affinity TCRs. In this study, we attempted to improve staining using anti-fluorochrome unconjugated primary Abs followed by secondary staining with anti-Ab fluorochrome-conjugated Abs to amplify fluorescence intensity. Unexpectedly, we found that the simple addition of an anti-fluorochrome unconjugated Ab during staining resulted in considerably improved fluorescence intensity with both pMHC tetramers and dextramers and with PE-, allophycocyanin-, or FITC-based reagents. Importantly, when combined with protein kinase inhibitor treatment, Ab stabilization allowed pMHC tetramer staining of T cells even when the cognate TCR–pMHC affinity was extremely low ($K_D$ >1 mM) and produced the best results that we have observed to date. We find that this inexpensive addition to pMHC multimer staining protocols also allows improved recovery of cells that have recently been exposed to Ag, improvements in the recovery of self-specific T cells from PBMCs or whole-blood samples, and the use of less reagent during staining. In summary, Ab stabilization of pMHC multimers during T cell staining extends the range of TCR affinities that can be detected, yields considerably enhanced staining intensities, and is compatible with using reduced amounts of these expensive reagents. *The Journal of Immunology*, 2015, 194: 463–474.

F luorochrome-conjugated peptide–MHC (pMHC) multimers are now widely used in conjunction with flow cytometry for identifying Ag-specific T cell populations in direct ex vivo samples (1). The staining of T cells with multimerized pMHC circumvents the need for cellular activation required by other T cell detection methodologies and thereby allows detection

*Institute of Infection and Immunity, Cardiff University School of Medicine, University Hospital, Cardiff CF14 4XN, Wales, United Kingdom; [†]Center for Cancer Immune Therapy, Herlev University Hospital, DK-2730 Herlev, Denmark; [‡]QIMR Berghofer Medical Research Institute, Brisbane, Queensland 4029, Australia; and [§]Department of Immunobiology, King's College London School of Medicine, Guy's Hospital, London SE1 9RT, United Kingdom

[1]A.K.S. and G.D. contributed equally to this work.

Address correspondence and reprint requests to Dr. Andrew K. Sewell, Cardiff University School of Medicine, Henry Wellcome Building, Heath Park, Cardiff CF14 4XN, Wales, U.K. E-mail address: sewellak@cardiff.ac.uk

The online version of this article contains supplemental material.

Abbreviations used in this article: 1°, primary; 2°, secondary; APL, altered peptide ligand; hTERT, human telomerase reverse transcriptase; ICS, intracellular cytokine staining; MFI, mean fluorescence intensity; PFA, paraformaldehyde; PKI, protein kinase inhibitor; pMHC, peptide–MHC; pMHC I, pMHC class I; pMHC II, pMHC class II; PPI, preproinsulin; P/S, penicillin and streptomycin; RT, room temperature; TIL, tumor-infiltrating lymphocyte.

of cells that fail to activate or that do not respond with the effector function(s) used for function-based profiling. pMHC multimer staining is also compatible with T cell phenotyping directly ex vivo by using a spectrum of fluorochrome-conjugated Abs specific for other T cell markers. Our previous studies have demonstrated that the binding affinity threshold for staining with pMHC class I (pMHC I) tetramers is significantly higher than that required for T cell activation (2). Thus, pMHC tetramers fail to stain all T cell subsets that are capable of responding to any given pMHC Ag. The disparity between the TCR affinity required for pMHC multimer staining and that required for T cell activation is highlighted when attempting to identify T cells specific for self-derived peptides (antitumor and autoimmune T cells), which generally bear TCRs that bind relatively weakly ($K_D$ 10–300 μM) (3–5). This issue is further compounded when staining pMHC class II (pMHC II)-restricted T cells as, unlike the CD8 molecule, the CD4 co-receptor does not cooperate to aid TCR–pMHC binding (1, 6–12). The importance of this issue was highlighted by Sabatino and colleagues (13), who demonstrated that staining with pMHC II tetramers ex vivo underestimated the lymphocyte choriomeningitis virus glycoprotein$_{61–80}$ and myelin oligodendrocyte glycoprotein$_{35–55}$ CD4$^+$ T cell populations by 4- and 8-fold, respectively. Demonstrations that pMHC tetramers can fail to detect the majority of responding cells in polyclonal antiviral and autoimmune T cell populations (13) highlight the pressing need to extend pMHC multimer technology to a point where it can be used to stain all T cells capable of responding to a given pMHC Ag (14, 15). Previously, we have described several improvements in pMHC multimer technology that extend the range of TCR–pMHC interactions that can be detected (1). The most promising of these technologies include use of anti-coreceptor Abs that enhance,

rather than inhibit, staining (16, 17), use of protein kinase inhibitor (PKI) during staining (18), and use of ultra-bright high-valency reagents such as pMHC dextramers (15). Importantly, all of these methodologies can be used in combination for synergistic effects. In this study, we examined whether signal amplification via use of Abs to pMHC multimers could be used for improved detection. Our data revealed that simple addition of anti-multimer Ab during pMHC tetramer or dextramer staining can result in substantial improvements in staining intensity even when a log-fold lower concentration of reagent was used. We anticipate that this improved methodology will become widely adopted due to the large potential cost saving and a substantial extension to the range of TCR affinities that can be detected with pMHC multimers.

# Materials and Methods

## Cells

T cell clones/lines and tumor-infiltrating lymphocytes (TILs) were cultured in RPMI 1640 media supplemented with penicillin and streptomycin (P/S), L-glutamine, 10% FBS, 0.01 M HEPES buffer, nonessential amino acids, sodium pyruvate (Life Technologies, Paisley, U.K.), 25 ng/ml IL-15 (PeproTech, Rocky Hill, NJ) (T cell clones and TILs only), and either 20 or 200 IU/ml IL-2 (aldesleukin, brand name Proleukin; Prometheus, San Diego, CA), depending on the stage of culture. Tumor cells and surrogate pancreatic β cells (19) were cultured in RPMI 1640 media supplemented with P/S, L-glutamine, and 10% FBS (R10). Adherent cells were detached from tissue culture flasks by gently rinsing the cells with calcium and magnesium chloride–free Dulbecco's PBS (Life Technologies), followed by incubation with Dulbecco's PBS and 2 mM EDTA at 37°C, until the cells detached.

We made use of the following HLA-A*0201 (HLA-A2)–restricted CD8+ T cell clones: 1) ILA1, which is specific for the human telomerase reverse transcriptase (hTERT)–derived peptide ILAKFLHWL (residues 540–548) (20) as well as four altered peptide ligands (APL), referred to as 8E, 4L, 5Y, and 3G, which bind to the ILA-1 TCR with varying affinities (2, 21); 2) 1E6 and 3F2, which recognize the ALWGPDPAAA epitope from preproinsulin (PPI: residues 15–24) and originate from the same patient with type 1 diabetes (19); and 3) VB6G4.24, which recognizes the heteroclitic peptide E**L**AGIGILTV (heteroclitic residue in boldface) from Melan A (residues 26–35) and was derived from TILs of a patient with malignant melanoma [patient MM909.24 (22)]. We also made use of the HLA-DRB1*0101 (HLA-DR1)–restricted CD4+ clone DCD10, which recognizes the PKYVKQNTLKLAT epitope from influenza A hemagglutinin (residues 307–319) (23). T cell clones were routinely expanded by restimulation with allogeneic PBMCs and PHA as previously described (24), then cultured for at least 14 d before being used for staining, unless stated otherwise.

Fresh blood samples were obtained by venipuncture from volunteers (heparinized) or buffy coats (EDTA treated) from the Welsh Blood Service in accordance with the appropriate ethical approval. PBMCs were isolated by density centrifugation over an equal volume of Lymphoprep (Axis Shields, Oslo, Norway). PBMCs were either used immediately or from cryopreserved samples, with the latter being treated with 10–50 μg/ml DNase-I (Roche, Burgess Hill, U.K.) for at least 20 min after thawing at 37°C. We find that it is preferable to use fresh samples, as previously frozen samples can exhibit higher background levels of staining with some pMHC multimers. Cells were frozen in FBS with 10% DMSO using a controlled-rate freezing device (CoolCell; Biocision, Larkspur, CA) as per the manufacturer's instructions and viable cell numbers enumerated by trypan blue exclusion. Spiked samples were created by mixing clonal T cells ($10^4$) with defrosted PBMCs ($10^6$), with the latter being cultured (24-well plates at a density of 3 to 4 × $10^6$/well in 2 ml R10) for 1 d prior to staining. The spiked PBMCs were minimally HLA matched for the restricting HLA of the spiking clone and treated as PBMC.

## pMHC multimer assembly

Soluble biotinylated pMHC I and pMHC II were produced as previously described (12, 25). Tetramers were assembled over five separate 20-min steps with the successive addition of streptavidin-allophycocyanin or –R-PE conjugates (Life Technologies) to monomeric pMHC at a molar streptavidin:pMHC ratio of 1:4. Dextramer (Immudex, Copenhagen, Denmark) PE, allophycocyanin, and FITC conjugates are assembled with monomeric pMHC as previously described (15). Protease inhibitors (set 1; Merck, London, U.K.) and PBS (tetramers) or dextramer buffer (15) were

added to give a final pMHC multimer concentration of 0.1 μg/μl (with regards to the pMHC component), stored in the dark at 4°C, and used within 3 d of assembly. The same monomeric pMHC were used when tetramers and dextramers were assembled for use within the same experiment.

## PKI treatment

Cells were treated with the PKI dasatinib (Axon Medchem, Reston, VA) at a final concentration of 50 nM (18) for 30 min at 37°C and then stained with tetramer or dextramer without washing or prechilling to 4°C. It is important to note that PKI is unstable when stored at 4°C, so 1 mM DMSO aliquots of PKI were stored at −20°C. Then for each experiment, working aliquots of 100 nM were prepared in PBS.

## Primary and secondary Abs

Mouse anti-PE (clones PE001, BioLegend, London, U.K.; and eBioPE-DLF, eBioscience, San Diego, CA), -allophycocyanin (clones APC003, BioLegend; and eBioAPC-6A2, eBioscience), and -FITC (clone FIT-22; BioLegend) primary (1°) unconjugated mAbs were used at a concentration of 10 μg/ml (0.5 μg/test). Unless otherwise stated, the 1° Abs sourced from BioLegend were used throughout this study. The goat anti-mouse conjugated secondary (2°) Abs (multiple adsorbed PE-, allophycocyanin-, or FITC-conjugated Ig polyclonal; BD Biosciences, Oxford, U.K.) were used at 2 μg/ml (0.1 μg/test). The fluorochrome conjugated to the 2° Abs were matched to the fluorochrome used for the initial pMHC multimer staining. Both anti-fluorochrome and anti-Ab Abs were spun at maximum speed in a microcentrifuge for 1 min to remove any aggregates before staining cells. The optimal amounts of 1° and 2° Abs were established during this study using an Ab matrix on the 1E6 T cell clone. The matrix covered a range of 1° and 2° Ab concentrations (0.25–2 μg and 0.025–0.2 μg, respectively), tested individually and in combination. The concentration used for this study was based upon the highest signal (1° and 2° Abs in combination) to noise (2° alone) ratio of fluorescent intensity.

## Cell staining and flow cytometry

The desired number of cells, which was typically 0.5–1 × $10^5$ of a T cell clone and 1–3 × $10^6$ TILs, PBMCs, T cell line, or spiked samples, was transferred to flow cytometry tubes. Cells were washed with buffer (PBS with 2% FBS) before proceeding to PKI treatment or tetramer/dextramer staining as required. Tetramer concentrations ranged from 0.02 to 2.4 μg (0.4–48 μg/ml with respect to the monomeric pMHC concentration) per stain in 50 μl buffer, and typically 0.3 or 0.5 μg (6 or 10 μg/ml) was used unless stated otherwise. Dextramer was used at 0.3 μg (6 μg/ml) per stain. Following tetramer/dextramer addition, cells were placed on ice and in the dark for 30 min. All subsequent Ab staining of the cells was performed for 20 min on ice and in the dark. Post–pMHC multimer staining, the cells were washed in buffer and labeled with anti-fluorochrome unconjugated 1° Ab, followed by two washes with buffer before the anti-Ab conjugated 2° Ab was added. Cells were washed with buffer then PBS and the violet LIVE/DEAD Fixable Dead Cell Stain, Vivid (Life Technologies) added and placed in the dark at room temperature (RT) for 5 min, and then Abs against cell-surface markers were added directly without washing. Samples were prepared for flow cytometry by washing once in buffer and resuspended in PBS or 2% paraformaldehyde (PFA). For whole-blood samples, 0.1–0.125 ml heparinized blood was added to prealiquoted tetramer in flow cytometry tubes and incubated for 10 min at RT, with 0.375–0.5 ml blood being used per condition. A one-step staining approach was adopted in which the anti-fluorochrome 1° Ab was added directly to the tetramer staining for 15 min at 4°C, followed by a mixture of Abs against cell-surface markers and incubated for a further 15 min at 4°C. RBCs were lysed by incubating for 10 min at 37°C with 2.5 ml lysis buffer (155 mM NH$_4$Cl, 10 mM KHCO$_3$, and 0.01 mM EDTA [pH 7.2]) and then washed by the addition of 2 ml of PBS. Lysis was repeated where necessary and samples were combined for the same condition and run immediately on the flow cytometer or fixed with 2% PFA for 20 min on ice before two washes with PBS. A dead stain was not used for the whole-blood samples, although DNA binding reagents could easily be incorporated during the staining protocol and may give tetramer stains with less background. The following mAbs were used depending on each experiment: anti–CD8-PE and anti–CD8-allophycocyanin/PE-vio770 (clone BW135/80; Miltenyi Biotec, Bergisch Gladbach, Germany); anti–CD3-PerCP (clone BW264/56; Miltenyi Biotec); anti–CD19-Pacific blue (clone HIB19; BioLegend); and anti–CD14-Pacific blue (clone M5E2; BioLegend). Typically, PBMC, spiked, and whole-blood samples were gated on single, viable (not for whole blood), CD19−CD14−CD3+ lymphocytes and displayed in bivariate CD8 versus tetramer/dextramer plots. T cell clones were typically gated on single, viable, CD8+ or CD4+ lymphocytes

displayed as histograms of tetramer fluorescence. Data were acquired on an FACSCanto II (BD Biosciences) and analyzed with FlowJo software (Tree Star, Ashland, OR).

### Intracellular cytokine staining assay

Cells were washed from culture medium and incubated in resting media (RPMI 1640 supplemented with P/S, L-glutamine, and 5% FBS) for 24 h prior to activation. Subsequently, cells were incubated at 37°C for 4 h, with and without (±) APCs, at a 1:1 ratio, in 2 ml resting media (24-well culture plate with a total cell density of $3–6 \times 10^6$/ml) containing GolgiStop and GolgiPlug (both from BD Biosciences), according to the manufacturer's instructions. Cells were then stained as above with cognate or irrelevant tetramer, 1° and 2° Ab(s), viability dye, and Abs against desired cell-surface markers. Cells were prepared for intracellular cytokine staining (ICS) by incubation with Cytofix/Cytoperm (BD Biosciences) according to the manufacturer's instructions (including wash steps), before staining for 20 min on ice with mouse anti-human IFN-γ–allophycocyanin Ab (clone 45-15; Miltenyi Biotec). Cells were stored overnight (4°C in the dark) in 2% PFA before flow cytometry and data analysis.

### $[^{51}Cr]$ release cytotoxicity assay

Target cells were labeled for 1 h at 37°C with 30 μCi chromium (sodium chromate in normal saline; PerkinElmer, Waltham, MA) per $1 \times 10^6$ cells, washed with R10, and allowed to leach for a further hour at 37°C in R10 to remove any excess chromium from the cells. After chromium labeling, target cells were washed and plated at 2000 cells/well in 96-well tissue culture plates. T cells were added to give the desired T cell to target cell ratio and a final volume of 150 μl R10. Target cells were also incubated alone or with 1% Triton X-100 detergent to give the spontaneous and total chromium released from the target cells, respectively. After 4 h of incubation, at 37°C and 5% CO$_2$, the supernatants were harvested (10% of total volume), mixed with 150 μl Optipahse supermix scintillation mixture (PerkinElmer) 96-well polyethylene terephthalate plates (PerkinElmer), sealed, and the amount of released chromium measured indirectly on a 1450 Microbeta counter (PerkinElmer). The percentage of specific target cell lysis by T cells was calculated according to the following formula: (experimental release [with T cells and target cells] − spontaneous release from target cells)/(total release from target cells − spontaneous release from target cells) × 100.

### Tetramer decay assays

T cell clone ($5 \times 10^5$) was pretreated with PKI then stained with cognate tetramer ± an anti-fluorochrome unconjugated 1° Ab ± a conjugated 2° Ab. Cells were washed with staining buffer, supernatant aspirated, and incubated with 10 μg anti–HLA-A2 Ab (clone BB7.2, allophycocyanin conjugated; eBioscience) or diluted in 3 ml buffer and incubated at RT in the dark. PKI was present throughout some of the decay assays. Cells were sampled at the times indicated in the results section, washed with excess buffer, and fixed with 2% PFA.

## Results

### Addition of an anti-fluorochrome Ab substantially improves the staining and detection of T cells with tetramer

We have previously described an important disparity between the TCR–pMHC affinity required for T cell activation and that required for effective capture of pMHC tetramers from solution (2). This difference means that pMHC tetramers do not stain all Ag-specific T cell populations (2) and represents a particular problem when pMHC multimers are used to stain self-specific or pMHC II–restricted T cells with weaker affinity TCRs (1, 3–5, 13). We made use of the ILA1 T cell clone that recognizes the HLA-A2–restricted hTERT-derived peptide ILAKFLHWL. This hTERT peptide is not naturally presented at the tumor cell surface (20) and therefore provides a model system that is uncomplicated by the possibility of a natural ligand. We have previously characterized a wide range of APL that act as agonists of the ILA1 T cell and that range in affinity for the ILA1 TCR from $K_D$ ~3 μM to $K_D$ ~2 mM by surface plasmon resonance while binding to HLA-A2 equally well (2, 21). The ILA1 T cell system therefore enables the TCR–pMHC affinity to be varied, whereas other variables such as surface density of TCR and CD8 remain identical. Two of the weaker APL in this system, 4L and 5Y, bind with a $K_D$ of 117 and ~250 μM, respectively, and provide a good model for weakly binding autoimmune TCRs. A further APL, 8E, still acts as a good agonist of ILA1 T cells when supplied exogenously at a concentration of 1 μM (2, 21) yet binds to the TCR with a $K_D$ ~2 mM by extrapolation of response units from surface plasmon resonance experiments. Previously, we have devised a number of novel techniques that lower the detection limit of pMHC multimer staining. These include CD8-enhanced tetramers (10) and the use of a PKI to prevent the internalization of TCRs from the cell surface that have not productively captured pMHC multimer from solution (18). The use of PKI considerably enhanced the range of TCR affinities amenable to detection with pMHC tetramers (18). When pMHC multimers are used in conjunction with PKI, the multimers remain at the cell surface (15, 18). We reasoned that, in the presence of PKI, pMHC multimers would be available for further signal amplification using fluorochrome-conjugated Abs. We therefore set up a staining protocol as shown in Fig. 1 that included combinations of an anti-PE unconjugated 1° and anti-Ab PE-conjugated 2° Abs as indicated. Initial experiments were conducted using the weak ILA1 ligand HLA-A2–ILA**L**FLHWL
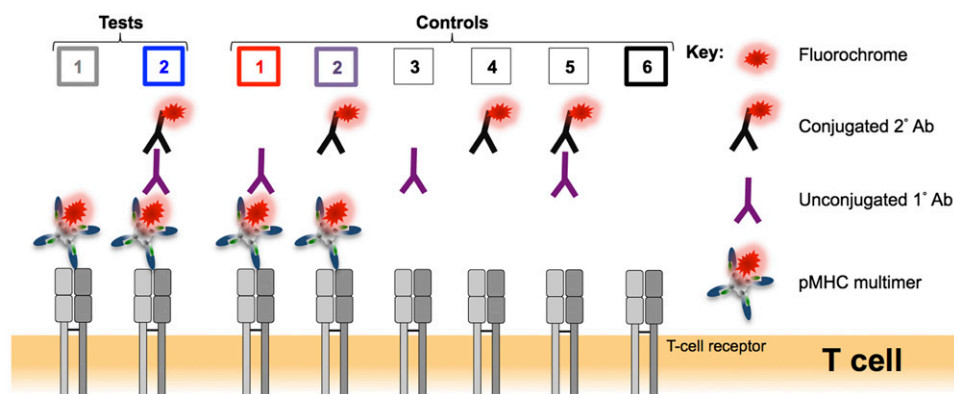
**FIGURE 1.** Schematic representation of the test and control conditions used in this study. Alongside a standard pMHC multimer (tetramer or dextramer) staining protocol (test 1), the binding of a mouse anti-fluorochrome unconjugated 1° Ab to the pMHC multimer associated fluorochrome followed by a goat anti-mouse conjugated 2° Ab (test 2) was tested to see whether the fluorescence intensity of pMHC multimer staining could be improved. A number of controls were performed: control 1: pMHC multimer with 1° Ab; control 2: pMHC multimer with 2° Ab; control 3: 1° Ab alone; control 4: 2° Ab alone; control 5: 1° and 2° Abs in combination; and control 6: unstained. The color coding for tests 1 + 2 and controls 1 + 2 + 6 is used throughout this study.

(4L; $K_D$ = 117 μM). Tetramers of the weak 4L ligand barely stained the ILA1 T cell clone in the absence of 50 nM PKI (Fig. 2A). Addition of PKI enhanced staining by >6-fold. Further inclusion of 1° and 2° Abs enhanced staining by ~20-fold in the absence of PKI and by ~6-fold in the presence of PKI (Fig. 2A). These results show that inclusion of Ab stabilization can have marked effects on staining even when PKI is not included to preclude TCR internalization. The additional increase in mean fluorescence intensity (MFI) observed using anti-pMHC multimer Ab in the presence of PKI confirmed that these two techniques could be used in combination. Moreover, there was a 10-fold enhancement in staining with tetramer and 1° Ab compared with staining with tetramer alone (conditions: control 1 and test 1 in Fig. 1, respectively). pMHC tetramer staining in the presence of the 1° Ab was also almost four times brighter in the presence of PKI. This substantial increase in pMHC tetramer staining in the presence of a 1° Ab, but in the absence of any further fluoro-

chrome provided by a 2° Ab staining, was highly unexpected. We next studied this unanticipated large increase in MFI afforded by simple addition of anti-fluorochrome Ab during pMHC tetramer staining by examining recovery of the ILA1 clone spiked into an HLA-A2⁺ PBMC sample using tetrameric forms of a number of different APL (Fig. 2B). Complete recovery of spiked ILA1 T cells was achieved in all cases when the 3G ligand ($K_D$ ~3 μM) was used (considered as 100% recovery). Only 71% of the cells were recovered with pMHC tetramers of the cognate, hTERT-derived HLA-A2–ILAKFLHWL ligand ($K_D$ ~35 μM) in the absence of PKI treatment. This was increased to full recovery when either PKI or 1° Ab were included. The greatest fluorescence intensity was seen when both PKI and 1° Ab were included. The effects of including 1° Ab during pMHC tetramer staining became even more exaggerated with the 4L ligand ($K_D$ = 117 μM) in which recovery with normal tetramer staining in the absence of PKI treatment or Ab stabilization was extremely poor (6%). With
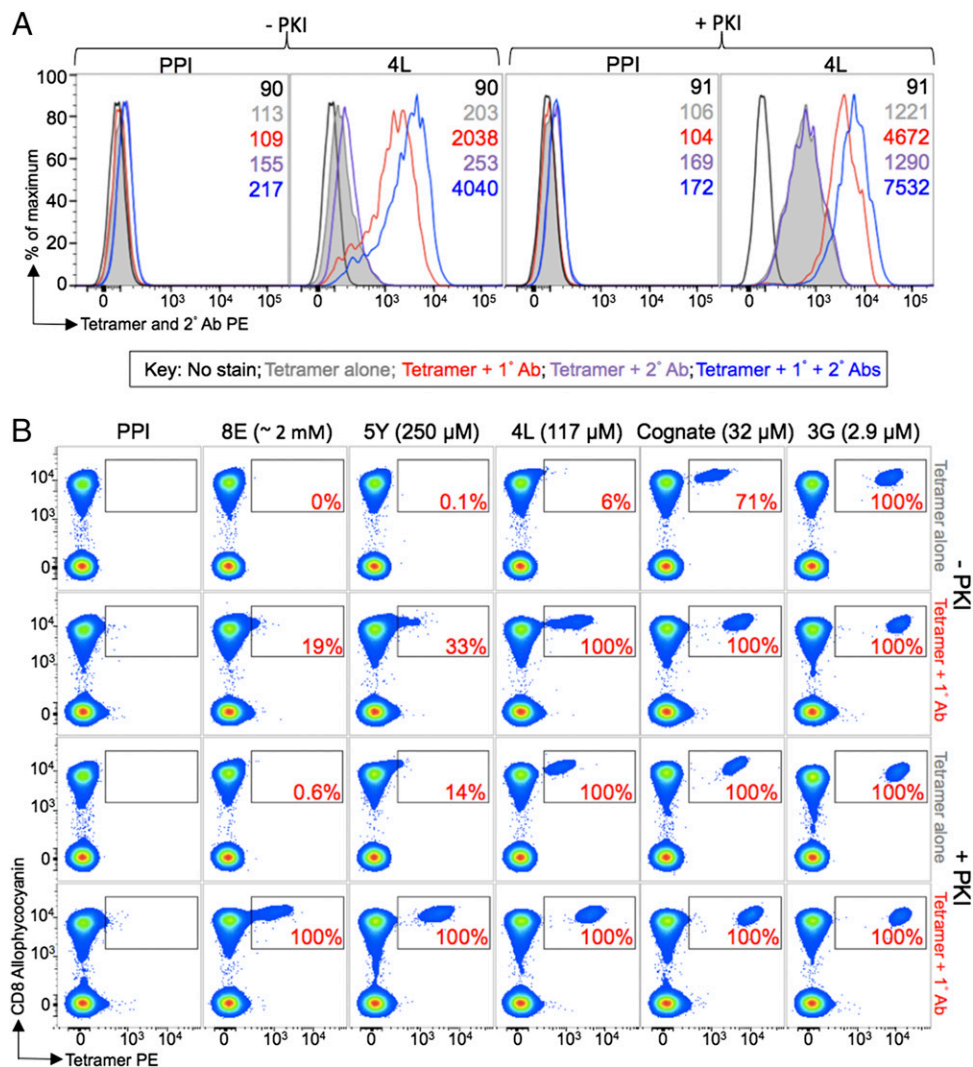


**FIGURE 2.** An anti-fluorochrome unconjugated Ab greatly enhanced the staining of T cells with tetramers when TCR–pMHC affinity is weak. (**A**) ILA1 hTERT-specific CD8⁺ T cells ± 50 nM PKI were stained with HLA-A2 PE-conjugated tetramers, assembled with the 4L peptide ($K_D$ = 117 μM) or irrelevant (HLA-A2–ALWGPDPAAA, PPI) tetramers. Cells were stained with tetramers alone or with an anti-PE unconjugated 1° Ab, a 2° PE-conjugated Ab, or 1° + 2° Abs together. The MFI is shown for each histogram. (**B**) In a separate experiment, the ILA1 CD8⁺ clone was spiked in to PBMCs from an HLA-A2⁺ donor (used from frozen), treated ± PKI, and stained with PE-conjugated tetramers folded with cognate and APL agonists of the ILA1 clone ($K_D$ [μM] shown in parentheses) or irrelevant epitope (as in A). Tetramers were used alone or in combination with anti-PE unconjugated 1° Ab. 2° Ab was not used in this experiment to highlight the unexpected effect of 1° anti-fluorochrome Ab. The percentage recovery of gated cells is displayed in the *inset* and was determined relative to the proportion of cells that stained with the 3G variant (considered 100%) after subtracting any background seen with the PPI tetramer. Display is based on viable CD3⁺CD14⁻CD19⁻ cells.

the 5Y ligand ($K_D$ ~250 μM), full recovery was *only* achieved when tetramer was used with PKI and 1° Ab in combination (Fig. 2B). Remarkably, full recovery of ILA1 clone was still possible when tetramers of the 8E ligand ($K_D$ ~2 mM) were used in conjunction with PKI and 1° Ab. In the past, we have failed to recover cells using the 8E ligand using even our best technology to date of PKI treatment in conjunction with higher valency, ultra-bright, pMHC dextramers (15). Thus, the simple technology described in this study extends the range of TCR–pMHC interactions that are amenable to detection using pMHC multimers beyond the current limit possible for these reagents.

*Anti-fluorochrome Abs alone or in combination with conjugated secondary Abs substantially improve staining of autoimmune T cells with pMHC tetramers*

We next looked at whether the increase in the MFI of staining with pMHC tetramers observed with the ILA1 model system was applicable with other T cells and with pMHC multimers conjugated to other fluorochrome molecules. For these experiments, we used the 1E6 T cell clone that exhibits glucose-dependent killing of HLA-A2[+] human pancreatic β-cells and was derived from a patient with type 1 diabetes (19). 1E6-mediated killing occurs via the PPI-derived peptide ALWGPDPAAA presented by the disease risk allele HLA-A2 (19). The 1E6 TCR binds to its cognate HLA-A2–ALWGPDPAAA with a $K_D$ of >250 μM (26, 27). Fig. 3A shows results with both PE and allophycocyanin reagents using anti-fluorochrome unconjugated 1° Ab clones PE001 and APC003, respectively. Inclusion of a 1° Ab and further fluorescence enhancement with anti-Ab conjugated 2° Ab increased the MFI of staining by ~4-fold and >5-fold for the PE and allophycocyanin staining, respectively. In both cases, and as seen in the ILA1 system (Fig. 2A), the majority of this increase in fluorescence intensity was apparent in the absence of a 2° Ab. Thus, inclusion of a 1° Ab during pMHC tetramer staining can substantially increase the intensity of staining of an autoimmune T cell clone with pMHC tetramer. We also tested another anti-PE 1° Ab (eBioPE-DL; BioLegend) and an anti-allophycocyanin 1° Ab (eBioAPC-6A2; BioLegend), which gave increases of 3.5- and 2.4-fold, respectively in the absence of a 2° Ab (data not shown). Similar levels of enhancement were also observed with FITC-conjugated reagents (dextramer FITC with corresponding reagents, data not shown), showing that the substantial benefits afforded by addition of anti-fluorochrome and anti-Ab Abs when staining cognate autoimmune T cells are generally applicable and evident regardless of which fluorochrome is used.

*Anti-fluorochrome Abs alone or in combination with conjugated secondary Abs enhance staining of CD4 T cells with pMHC II tetramers*

The weaker average affinity of TCRs derived from MHC II–restricted T cells (3) and lack of coreceptor help from CD4 (1) means that it is generally more difficult to stain cognate T cells with pMHC II tetramer than pMHC I tetramers (28), and pMHC II tetramers have been shown to miss the majority of Ag-specific T cells in polyclonal antiviral and autoimmune populations (13). Given this limit in visualization, we next examined whether inclusion of anti-fluorochrome and anti-Ab Abs could be beneficial in the pMHC II tetramer setting. For these experiments, we made use of the HLA-DR1–restricted, influenza-specific T cell clone DCD10. This antiviral T cell clone stains reasonably well with cognate tetramer, with MFIs of 528 and 199 for the PE and allophycocyanin reagents, respectively (Fig. 3B). Addition of an anti-PE or -allophycocyanin unconjugated 1° Ab, used alone or in combination with an anti-Ab conjugated 2° Ab enhanced the
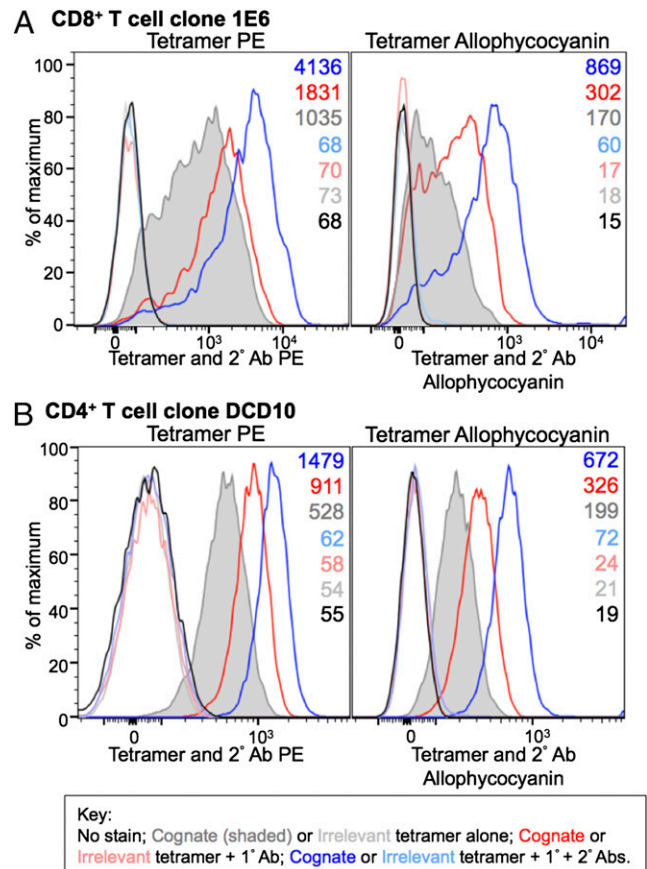


**FIGURE 3.** Enhanced tetramer staining of an autoimmune T cell and an MHC II–restricted T cell with anti-fluorochrome unconjugated and secondary conjugated Abs. (**A**) PKI-treated CD8^{+} T cell clone 1E6 was left unstained or stained with PE and allophycocyanin-conjugated cognate HLA-A2–ALWGPDPAAA (PPI) cognate and HLA-A2–ELAGIGILTV (Melan-A) irrelevant tetramers, alone or with an anti-fluorochrome unconjugated 1° Ab ± PE- or allophycocyanin-conjugated 2° Ab. (**B**) The CD4^{+} T cell clone, DCD10, was left unstained or stained from culture with cognate HLA-DR1–PKYVKQNTLKLAT (hemagglutinin of influenza) or irrelevant HLA-DR1–DRFYKTLRAEQASQ (p24 Gag of HIV) PE- and allophycocyanin-conjugated tetramer as described in (A). MFIs are shown at the *right* of each graph.

staining of this T cell clone by 1.7- and 2.8-fold for PE reagents and 1.6- and 3.3-fold for allophycocyanin reagents, respectively. Thus, stabilization of pMHC II tetramers can improve the intensity of cell staining with these reagents.

*Ab stabilization illuminates low-affinity T cells otherwise undetected by conventional tetramer staining and with lower concentrations of tetramer*

We next examined the effect of 1° and 2° Abs on pMHC tetramer staining of the tumor-specific CTL clone VB6G4.24 that was grown from the TILs derived from a patient with stage IV malignant melanoma (22). This clone efficiently kills the patient's autologous tumor even at low E:T ratios but does not stain by conventional pMHC tetramer staining even when high amounts of reagent were used (Fig. 4A). Tetramer staining of this clone was negligible even with 2.4 μg of tetramer (with respect to the pMHC component). Addition of an anti-PE unconjugated 1° Ab enabled staining of this clone with most of the cognate pMHC tetramer amounts tested and as low as 0.6 μg (with respect to the pMHC I component) of tetramer. Further inclusion of an anti-Ab PE-conjugated 2° Ab doubled the staining observed with the 1° Ab, but as before, the majority of the enhancement in MFI was provided by inclusion of the 1° Ab alone.

**FIGURE 4.** Anti-fluorochrome and secondary Abs enable staining of weak-avidity T cells at lower concentrations of tetramer. (**A**) The CD8⁺ VB6G4.24 T cell clone, grown from TILs from a malignant melanoma patient, kills autologous tumor (*top left panel*). The clone was stained with various amounts of PE-conjugated cognate HLA-A2–ELAGIGILTV (Melan-A) and irrelevant HLA-A2–ALWGPDPAAA (PPI) tetramers. Fresh cells were left unstained or stained with tetramer alone or with an anti-PE unconjugated 1° Ab ± PE conjugated 2° Ab. The *bottom left panel* shows the MFI of tetramer staining, which is shown in the histograms (*right panel*). (**B**) Fresh HLA-A2⁺ PBMC was stained with HLA-A2–NLVPMVTAV (pp65 of CMV, *top panel*) or PPI (*bottom panel*) PE-conjugated tetramers. Cells stained with 0.003 μg were either stained with tetramer alone or tetramer with a combination of 1° and 2° Abs, as described in (A). The proportion of cells that stained with 0.003 μg of tetramer is expressed as a percentage (*inset*) of the cells that stained with 1 μg of tetramer after subtraction of any background seen with the PPI tetramer (*bottom panel*). PBMC were stained for viability and Abs against CD8, CD3, CD14, and CD19. No pretreatment with PKI was used throughout.
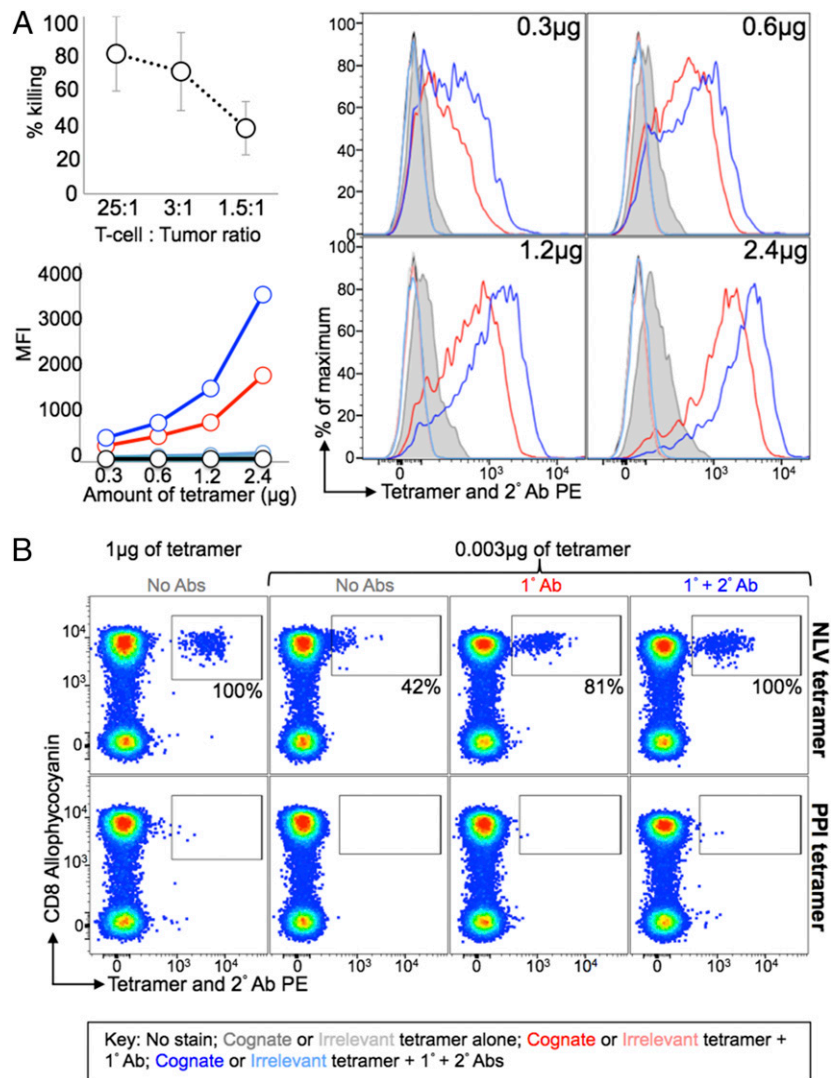
Tetramers are most commonly used to stain antipathogen CD8⁺ T cells and have excelled for such applications (1, 29, 30). The TCRs of CD8⁺ T cells raised against non–self-peptides tend to bind with relatively strong affinity to their cognate pMHC Ag ($K_D$ 0.1–10 μM) (3, 5, 31). We used tetramers to stain CMV-specific T cell populations directly ex vivo and showed that inclusion of Ab allowed full recovery of CMV-specific T cells from PMBC samples even when >300-fold lower concentrations of pMHC tetramer were used (just 3 ng with respect to pMHC). CMV-specific T cells could not be detected as a separate distinct population of cells in the absence of Ab when this amount of pMHC tetramer was used for staining (Fig. 4B). Thus, the methodology described in this study allows recovery of T cells with dramatically lower amounts of pMHC multimer regardless of the TCR–pMHC affinity and is compatible with ex vivo staining of PBMC. Lower concentrations of tetramer could also be used when recovering the 1E6 PPI-specific clone from spiked HLA-A2⁺ PBMC samples. Addition of a 1° Ab resulted in recovery of >80% of the 1E6 cells even when 25-fold less pMHC tetramer was used. Inclusion of a 2° Ab allowed full recovery of cells, even when 25-fold less tetramer was used (data not shown).

*Ab stabilization of pMHC tetramer and dextramers gives superior recovery of T cells from multiple sources*

We next compared pMHC multimer staining of a T cell line, TILs, and PBMC samples using the following conditions: 1) pMHC

multimer alone (test 1, Fig. 1); 2) pMHC multimer + anti-PE unconjugated 1° Ab (control 1, Fig. 1); and 3) pMHC multimer + the 1° Ab + anti-Ab PE-conjugated 2° Ab (test 2, Fig. 1) (Fig. 5). Fig. 5A shows classic tetramer staining of an HLA-A2–restricted influenza matrix-specific T cell line. As expected, the cognate CD8⁺ T cells in this antiviral line stain well with tetramer. Nevertheless, inclusion of a 1° Ab during staining almost doubled the MFI and resulted in recovery of a ∼25% greater population of cells. Further inclusion of a 2° Ab resulted in a further minor increase in both MFI and percent population recovered. We next applied the same conditions in the presence of PKI for staining of HLA-A2–ELAGIGILTV-specific cells in TILs expanded from a melanoma lesion (Fig. 5B). A total of 2.3% of the cells in these TILs stained with Melan-A–specific pMHC tetramer. The size of this population almost doubled when 1° Ab was included in the protocol. The population recovered increased from 3.9 to 4.9% when a 2° Ab was also included. In an independent assay using the same TILs, the Melan-A specific T cell population segregated into two clean populations when 1° and 2° Abs were included with tetramer (Supplemental Fig. 1A). The VB6G4.24 T cell clone shown in Fig. 4A was cloned from these TILs and is effective at killing patient autologous tumors. This clone does not stain with pMHC tetramer (Fig. 4A), so we assume that this clone is one of the T cell clonotypes that fails to stain using tetramer alone in the presence of PKI in Fig. 5B. Importantly, staining can be recovered
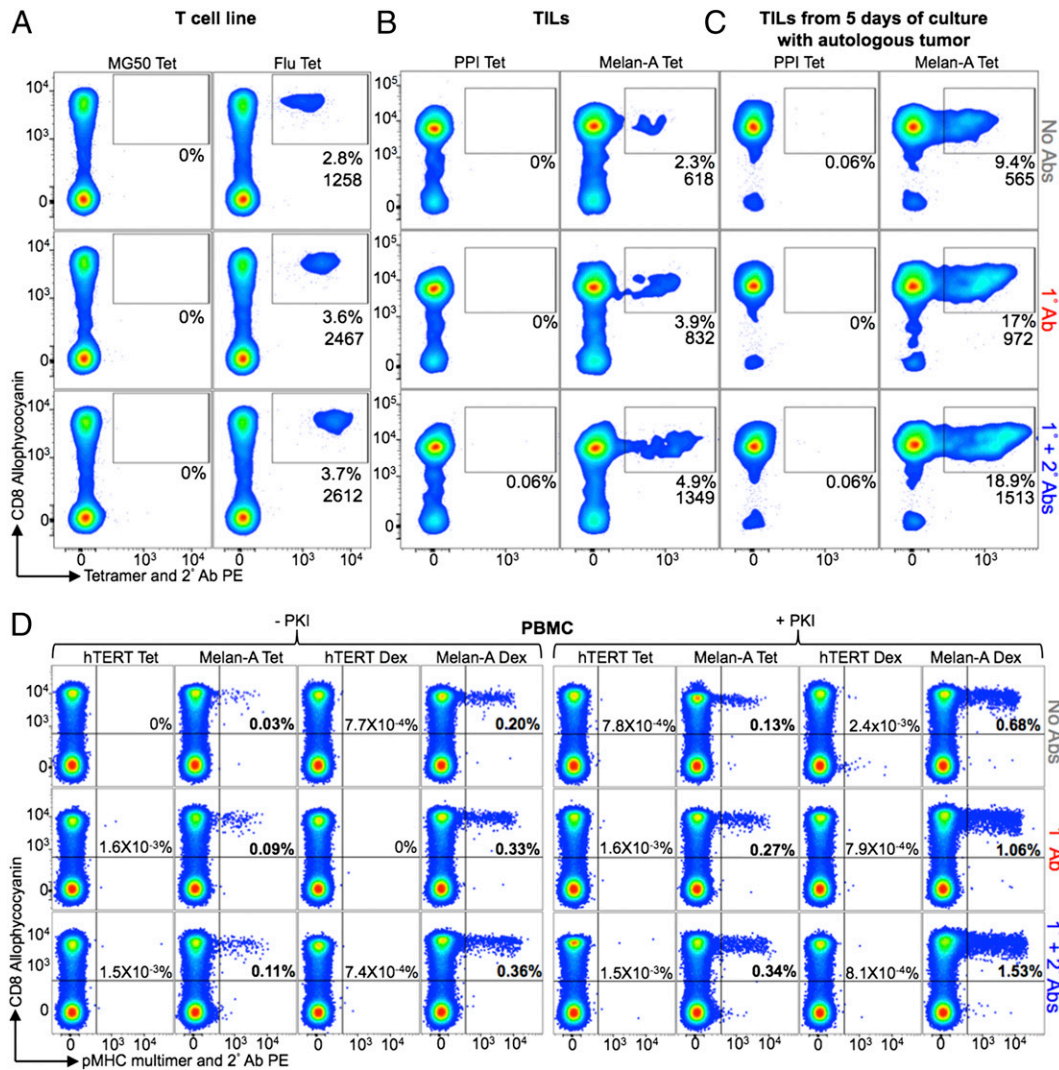
**FIGURE 5.** Ex vivo staining and detection of T cells is improved by the addition of an anti-fluorochrome and conjugated secondary Ab to standard pMHC multimer staining protocols. (**A**) A T cell line primed with GILGFVFTL peptide from the influenza virus (flu) was treated with PKI and stained with cognate HLA-A2 PE-conjugated cognate and control (HLA-A2-RLGPTLMCL from MG50 protein) tetramers (Tet), alone or in combination with anti-PE unconjugated 1° Ab ± a PE-conjugated 2° Ab. (**B**) TILs from an HLA-A2[+] metastatic melanoma patient were treated with PKI and stained with HLA-A2– ELAGIGILTV (Melan-A) or HLA-A2–ALWGPDPAAA (PPI) PE-conjugated tetramers and Abs as in (A). (**C**) The staining described in (B) was performed on TILs that had been cultured with autologous tumor for 5 d. (**D**) HLA-A2[+] PBMCs taken directly ex vivo were incubated ± PKI and stained with HLA-A2–ELAGIGILTV or HLA-A2–ILAKFLHWL (hTERT) PE-conjugated tetramers or dextramers (Dex) and Abs as described in (A). Samples were minimally stained for viability, CD3, and CD8, with CD14 and CD19 also being stained in (C). The tetramer^{+} cells are expressed as a percentage of total cells (A and B) or CD8^{+} cells (C) and the MFIs are shown (*inset*).

when 1° Ab and 1° + 2° Abs were included in the staining protocol. Enhanced tetramer staining was also seen when tumor-specific T cells were relatively abundant. The aforementioned TILs were enriched for Melan-A–specific cells by coculture with autologous tumor for 5 d. Twice as many cells were stained with Melan-A tetramers when 1° and 2° Abs (9.4% versus 18.9%) were included, which represents a considerable increase in the number of T cells being detected (Fig. 5C). Thus, pMHC tetramer staining in the absence of Ab stabilization can fail to recover effective cognate CD8^{+} T cells resulting in a large underestimation of the size of an Ag-specific T cell population. This large underestimation of effective, Ag-specific CD8^{+} T cells with pMHC I tetramer is in accordance with a previous study that showed that most Ag-specific CD4^{+} T cells could not be detected by pMHC II tetramer staining of ex vivo samples (13).

pMHC multimers are most commonly used for detecting Ag-specific T cell populations directly ex vivo. To compare various methodologies available in this context, we took advantage of the fact that there is a relatively large population of naive T cells in HLA-A2[+] individuals that recognize a commonly used variant of a self-peptide from the Melan-A protein (sequence ELAGIGILTV) due to a hardwired germline-encoded recognition motif (32, 33). Some of these self-specific CD8^{+} T cells can be detected by regular tetramer staining (Fig. 5D). The size of this population increases from 0.03% of CD3^{+}CD8^{+} cells to 0.09 and 0.11% of cells when 1° Ab and 1° + 2° Abs were included, respectively. We recently used this system to show that pMHC dextramers were better at recovering low-avidity T cells when compared with pMHC tetramers, with the best recoveries seen when dextramers were used in the presence of PKI (15). The same effect was also observed in this study in which use of pMHC dextramer gave 6.6-fold more cells being recovered than with the equivalent pMHC tetramer alone in the absence of PKI and 5.2-fold in the presence of PKI (Fig. 5D). We also tested the effect of Ab with pMHC

dextramers, which increased recovery from 0.20% for dextramer alone, to 0.33 and 0.36% when 1° Ab and 1° + 2° Abs were included, respectively. In the presence of PKI, the recovery of cells increased from 0.68% (dextramer alone) to 1.06 and 1.53% when 1° Ab and 1° + 2° Abs were included. In accordance with our earlier results, higher numbers of CD8^{+} T cells stained with pMHC dextramer than with pMHC tetramer, reflecting the ability of these higher valency reagents to stain T cells bearing lower-affinity TCRs. Optimal recovery was seen with PKI + pMHC dextramer + 1° + 2° Abs. The population recovered using this combination was 50-fold greater than could be recovered with pMHC tetramer alone, with no PKI, and 11-fold greater when pMHC tetramer was used with PKI. Staining of PKI-treated PBMCs from a second donor with Melan-A dextramers + 1° + 2° Abs recovered 11-fold more cells than Melan-A tetramers alone (Supplemental Fig. 1B). Overall, in terms of cellular recovery and regardless of PKI treatment, pMHC dextramer + 1° + 2° Ab > pMHC dextramer + 1° Ab > pMHC dextramer > pMHC tetramer + 1° + 2° Abs > pMHC tetramer + 1° Ab > pMHC tetramer.

*Ab stabilization is compatible with whole-blood staining with pMHC tetramers*

We next tested the compatibility of Ab stabilization when staining whole blood with pMHC tetramers. Blood samples from two HLA-A2^{+} healthy donors were stained with four different pMHC tetramers as described in the *Materials and Methods*. Donor 1 had populations of CD8^{+} T cells that stained with HLA-A2-GILGFVFTL (influenza) and HLA-A2–ELAGIGILTV (Melan-A) tetramers with MFIs of 2334 and 1032, respectively, for the gates shown in Fig. 6. These MFIs increased to 7276 and 4095 when a 1° anti-PE Ab was included, and the number of cells staining with the ELAGIGILTV Melan-A–specific reagent dou-

bled. Donor 2 had populations of T cells that stained with HLA-A2–CLGGLLTMV (EBV) and HLA-A2-NLVPMVTAV (CMV) tetramers, with the 1° Ab increasing the MFI of tetramer staining from 613 to 2115 and 674 to 5774, respectively. We conclude that Ab stabilization of pMHC multimers is compatible with whole-blood staining protocols.

*Ab stabilization of pMHC tetramers improves recovery of T cells that have recently been exposed to Ag*

Ag engagement is known to trigger and downregulate TCR from the T cell surface (34) and makes pMHC multimer staining more difficult due to low TCR density (15). This aspect could be problematic if staining pathogen-specific T cells during acute or chronic infections. It is also likely that self-specific T cells, be they antitumor T cells in TILs or of autoimmune origins, will have recently encountered their cognate Ag in vivo prior to staining. We mimicked this situation by exposing TIL to autologous tumor or autoimmune T cells to target cells endogenously producing cognate self-Ag prior to examining cellular recovery with pMHC multimers. TILs from an HLA-A2[+] metastatic melanoma patient were incubated with brefeldin A and monensin ± autologous tumor for 4 h prior to staining with Melan A tetramer and intracellularly with anti–IFN-γ Ab (Fig. 7A). After exposure to tumor, tetramer alone, tetramer with an anti-PE unconjugated 1° Ab ± anti-Ab PE-conjugated 2° Ab recovered 29, 62, and 80% of the ELAGIGILTV-specific T cells that could be recovered without prior exposure to tumor, respectively. We also examined staining of the 1E6 PPI-specific T cell clone after incubation with K526 cells expressing HLA-A2 or K526 cells expressing HLA-A2 and PPI, with the latter termed "surrogate pancreatic β cells." Staining of 1E6 cells was very poor with tetramer alone postexposure to K526 cells expressing the cognate Ag compared with when



**FIGURE 6.** Ab stabilization is compatible with whole-blood staining with pMHC multimers. Fresh heparinized whole blood from two HLA-A2[+] donors was treated with PKI then added to prealiquoted PE- (donor 1) or allophycocyanin-conjugated (donor 2) tetramers. Both donors were stained with HLA-A2–ALWGPDPAAA (PPI) tetramer. Donor 1 was stained with HLA-A2–GILGFVFTL (influenza [Flu]) and HLA-A2–ELAGIGILTV (Melan-A) tetramers and donor 2 with HLA-A2–CLGGLLTMV (EBV) and HLA-A2–NLVPMVTAV (CMV) tetramers. Anti-PE or allophycocyanin unconjugated 1° Ab was added directly to the cells, followed by a mixture of Abs against cell-surface markers (CD19, CD14, CD3, and CD8) before lysis of RBCs. A total number of $3 \times 10^5$ and $1 \times 10^5$ CD3^{+}CD19^{−}CD14^{−} cells were acquired from 0.5 ml and 0.375 ml of whole blood for donors 1 and 2, respectively. The percentage of cells residing within the gate and the MFI of this population are shown for each plot.
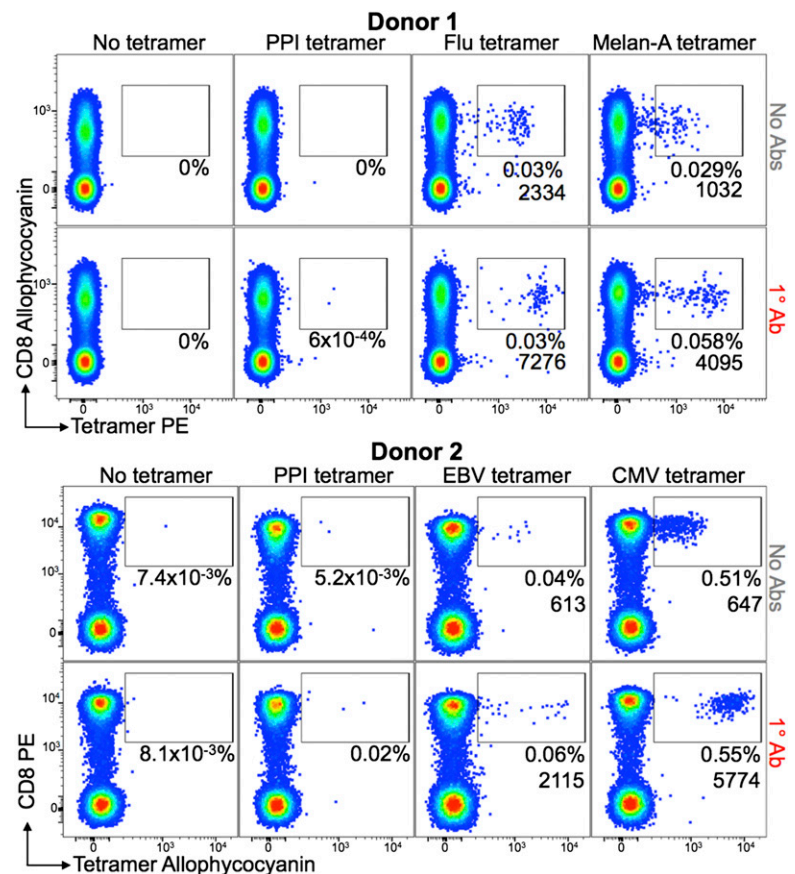
**FIGURE 7.** Activated T cells can be detected when tetramers were used with anti-fluorochrome and secondary Abs. (**A**) TILs from a HLA-A2$^+$ metastatic melanoma patient were incubated with brefeldin A and monensin, ± autologous tumor. Cells were stained with cognate HLA-A2–ELAGIGILTV (Melan A) or HLA-A2–ALWGPDPAAA, PPI) PE-conjugated tetramers (Tet) alone or further labeled with an anti-PE unconjugated 1° Ab ± PE conjugated 2° Ab. Cells were also stained intracellularly for IFN-γ. Tetramer$^+$ cells (red box) from the TILs with autologous tumor are expressed as a percentage (*inset*, *top panel*) of tetramer$^+$ cells (Tet + 1° + 2° Abs) from the TILs alone after subtracting the number of gated cells seen with the PPI tetramer (*bottom panel*). (**B**) The CD8$^+$ T cell clone 1E6, specific for ALWGPDPAAA from PPI, was incubated with K562-A2$^+$ or K562-A2$^+$ that express PPI (the latter process and present the cognate epitope). At 24 h postincubation, the cells were treated with 50 nM PKI and stained with cognate or irrelevant (HLA-A2–ILAKFLHWL, hTERT) tetramer alone or further labeled with an anti-PE 1° Ab ± a PE-conjugated 2° Ab. The percentages of 1E6 detected above the staining with an irrelevant tetramer are displayed for each histogram. (**C**) From the same experiment in (**B**), the 1E6 clone that had been cocultured with K562 or K562-PPI was spiked in to CD3/CD28-amplified PBMCs (HLA-A2$^+$) and then PKI treated and stained as described in (**B**). The proportion of HLA-A2–ALWGPDPAAA tetramer$^+$ cells (gated) from 1E6 activated with K562-PPI is expressed as a percentage of HLA-A2–ALWGPDPAAA tetramer$^+$ cells (stained with Tet + 1° + 2° Abs) from 1E6 cultured with K562 (*top panel*). The gates are based on staining with an irrelevant tetramer (*bottom panel*). All cells were stained for viability and expression of CD3 and CD8.
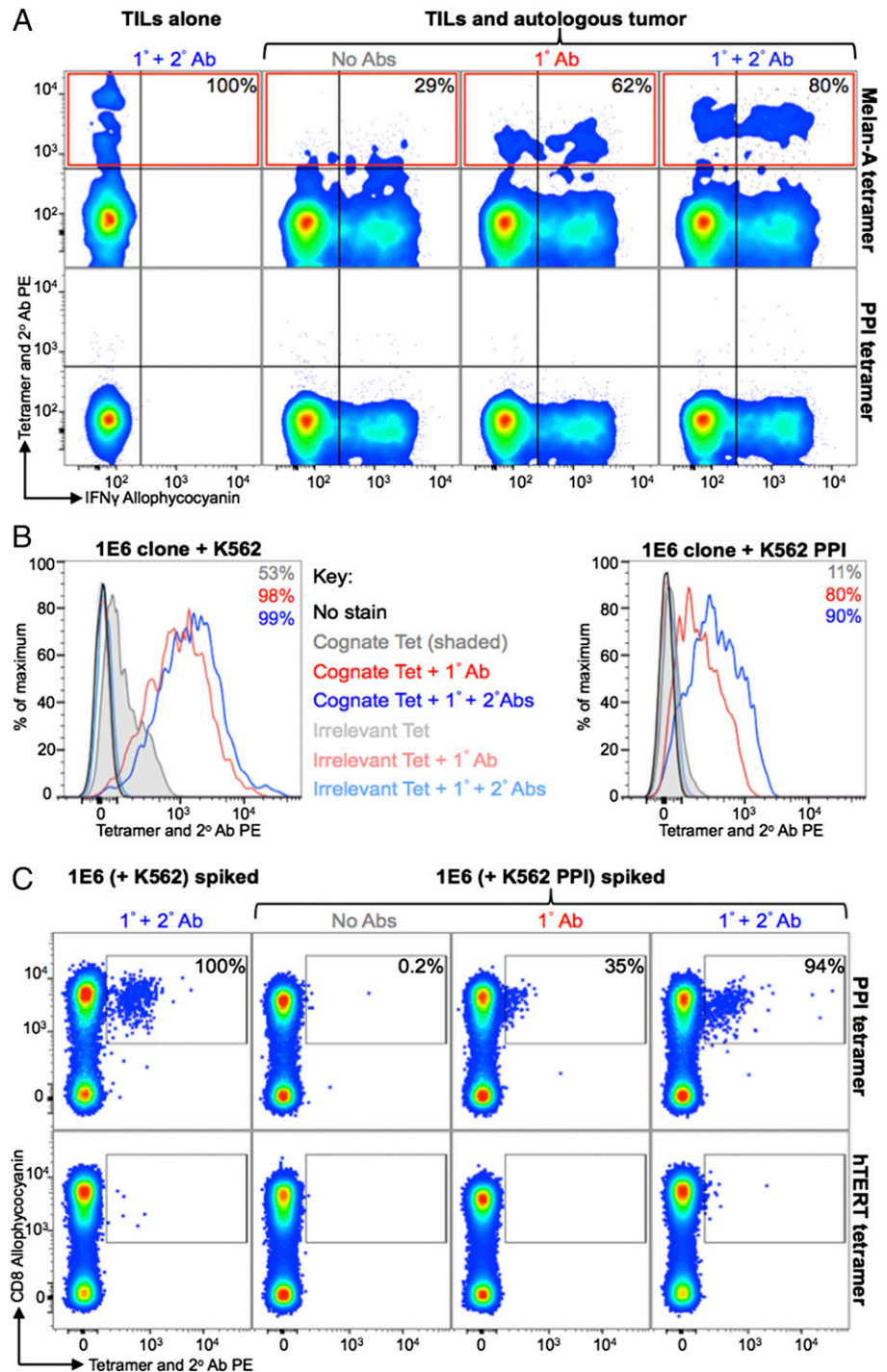
1° Ab ± 2° Ab, were used (11, 80, and 90% of the cells stained with each condition, respectively; Fig. 7B). This staining pattern was reflected when 1E6 cells that had been incubated with K526 cells ± cognate Ag were spiked into HLA-A2$^+$ PBMC. Tetramer + 1° + 2° Abs was able to recover 94% of the cells that had been exposed to K526 surrogate β cells, whereas recovery with tetramer + 1° Ab or tetramer alone was 35 and 0.2%, respectively (Fig. 7C). These results confirm our previous findings that tetramers are poor at recovering T cells following exposure to cognate Ag (15) but show that the inclusion of 1° or 1° + 2° Abs against tetramer as described in Fig. 1 can reverse most of this effect and enable effective T cell staining (Fig. 7B, 7C).

### Ab stabilizes pMHC tetramer at the T cell surface

When we initially saw that inclusion of an unconjugated anti-fluorochrome Ab dramatically improved the MFI of staining during pMHC tetramer staining, we considered the possibility that the 1° Ab might function by somehow stabilizing the fluorochrome and/or enhancing its ability to emit detectable fluorescence. Subsequent experiments showed the same affect with different Ab clones and MFI enhancements with anti-allophycocyanin or anti-FITC Abs and appropriate fluorochrome-conjugated pMHC multimers (Fig. 3 for allophycocyanin data, FITC not shown). We further tested the stabilization of fluorochrome hypothesis by using an unconjugated 1° Ab against the streptavidin component of

the tetramer. Anti-streptavidin 1° Ab enhanced the MFI of tetramer staining, although not as impressively as the anti-fluorochrome Ab tested alongside (data not shown). The reduced effect of an anti-streptavidin Ab compared with anti-PE Ab may reflect steric difficulties in Ab binding to streptavidin in a PE-conjugated pMHC tetramer. Overall, there was fluorochrome-independent 1° Ab-induced enhancement of tetramer staining regardless of which anti-pMHC tetramer Ab was used. This made it more likely that the Ab was functioning by stabilizing pMHC multimer at the T cell surface during the staining protocol. We formally tested this hypothesis using the PPI-specific 3F2 CD8+ T cell clone that bears an identical TCR to the 1E6 T cell clone. T cells were stained ± PKI with cognate and control pMHC tetramer. Samples were fixed with PFA immediately after staining and washed or taken through subsequent incubations and washing steps. Surprisingly, almost half of the staining with pMHC tetramer was lost (Fig. 8A); this loss was greatest in the absence of PKI. In contrast, the intensity of the initial staining was maintained in the presence of PKI and 1° Ab (Fig. 8). Tetramer staining was completely stable when 1° Ab or 1° + 2° Ab was included and cells were diluted (Fig. 8B). In contrast, almost half of the staining was lost in just 30 min under the same conditions without inclusion of anti-pMHC tetramer Ab (Fig. 8B). We also performed pMHC tetramer off rate experiments in the presence of anti–HLA-A2 Ab to prevent rebinding of TCRs (Fig. 8C) (12). These conditions exaggerate the dissociation of pMHC multimer from the cell surface and showed that addition of 2° Ab with the 1° Ab did not further alter the decay rate (Fig. 8C). The MFIs of staining in the presence of competing pMHC Ab highlighted the differences in staining intensities over time with the different conditions (Fig. 8D). We conclude that cross-linking of pMHC multimer substantially reduces its dissociation from the cell surface after staining. Presumably, this effect is also at play during regular staining and washing protocols. Such losses could be very substantial given that our own standard ICS protocol involves 12 washes and 3 incubation steps, thereby providing ample opportunity for pMHC multimer staining to decrease due to dissociation from the T cell surface. Overall, it appears that there is a large loss of tetramer from the cell surface over time when stained cells are incubated on ice as during most pMHC multimer, ICS, and Ab phenotyping experiments. This loss can be largely prevented by stabilizing pMHC multimer at the cell surface using anti-fluorochrome 1° Ab.

## Discussion

Fluorescent pMHC multimers are now part of the standard toolset for the study of Ag-specific T cells (1), but the binding affinity threshold for staining with these tools can be significantly higher than that required for T cell activation (2, 13). Thus, pMHC tetramers fail to stain all T cells that are capable of responding to the pMHC used in the multimer, and there is a pressing need for reagents that can stain T cells with relatively weak affinity TCRs such as those that predominate in cancer-specific, autoimmune, or MHC II–restricted T cell populations. In this study, we examined whether a combination of anti-fluorochrome unconjugated 1° Ab followed by anti-Ab conjugated 2° Ab could be used to boost the fluorescence signal during pMHC multimer staining and detection by flow cytometry. Our initial experiments with the ILA1 T cell clone and the weak 4L ligand showed that a combination of 1° and 2° Abs could boost the MFI by ~20-fold compared with regular tetramer staining. A 6-fold boost in fluorescence was still observed when the staining was performed in the presence of the PKI dasatinib that we have previously shown affords considerable advantages during T cell staining with multimerized pMHC (1, 15, 18). Signal amplification by including a combination of 1° and 2°

Abs was not wholly unexpected, although the 20-fold increase observed was higher than expected based on calculations of how much extra fluorochrome this procedure was expected to deliver.

We were also very surprised to observe that the majority of the signal boost apparent with a combination of 1° and 2° Ab was still present when only the unconjugated 1° Ab was used. The substantial increase in MFI observed in the presence of anti-pMHC tetramer Ab might represent an inexpensive and easy way to increase the utility of pMHC multimers and warranted further investigation. Recovery of ILA1 T cells spiked into HLA-A2+ PBMC using pMHC tetramers of the 4L, 5Y, and 8E variant that bind with $K_{D}$s of 117, ~250, and ~2000 μM was 6, 0.1, and 0%, respectively, with regular tetramer staining. These levels increased to 100, 33, and 19%, respectively, when a 1° Ab was included during staining. Remarkably, all of the clone could be recovered with pMHC tetramers of all these ligands when 1° Ab was included with PKI and we were able to see effective staining of the ILA1 T cell with the 8E variant agonist. We conclude that the inclusion of anti-fluorochrome 1° Ab during pMHC tetramer staining substantially increases both the intensity of staining and the range of TCR–pMHC interactions that can be used to detect T cells using these reagents. The increase in staining we observed when an anti-pMHC multimer Ab is included is a general effect that was also seen with other Ab clones against PE and when allophycocyanin- or FITC-based pMHC multimers were used in combination with Abs against the relevant fluorochrome. Inclusion of 1° Ab during pMHC tetramer staining also enabled good detection of T cells even when substantially less pMHC reagent was used. The benefits of including Ab were evident when staining T cells specific for viral, tumor, and autoimmune Ags and with both pMHC tetramers and pMHC dextramers. There was a distinct hierarchy of cellular recovery of antitumor T cells from a PMBC sample that ran dextramer + 1° + 2° Abs > dextramer + 1° Ab > dextramer > tetramer + 1° + 2° Abs > tetramer + 1° Ab > tetramer. Thus, addition of Abs against pMHC multimers during staining improves MFI and cellular recovery with both pMHC tetramers and pMHC dextramers. The most sensitive staining protocol used a combination of: 1) pMHC dextramer; 2) PKI; 3) anti-fluorochrome unconjugated Ab; and 4) anti-Ab conjugated 2° Ab.

It is well documented that TCRs downregulate from the T cell surface once they are triggered (34). Thus, T cells that have recently engaged cognate Ag exhibit a lower surface density of TCR and are more difficult to stain with pMHC multimers (15). This issue becomes particularly problematic when attempting to identify self-specific T cells (anticancer or autoimmune) that tend to bear lower affinity TCRs (3) and might be expected to have had a reasonable chance of recent Ag encounter in vivo. When pMHC tetramer staining ELAGIGILTV-specific T cells in the TILs expanded from an HLA-A2+ patient with stage IV melanoma after exposure to autologous tumor, 80% of the original population could be recovered after pMHC tetramer staining with 1° and 2° Abs. This compared with just 29% with tetramer alone. Similarly, almost all of the 1E6 PPI-specific T cells spiked into HLA-A2+ PBMC after incubation with HLA-A2+ cells expressing PPI could be recovered using pMHC tetramer + 1° and 2° Abs, whereas none of the cells could be recovered when stained with pMHC tetramer alone. Thus, addition of Ab against pMHC multimers during cellular staining can considerably improve detection of self-specific T cells that have recently encountered Ag.

We finally examined the mechanism by which staining was enhanced. The rational of using an unconjugated 1° Ab in combination with a conjugated 2° Ab was to boost the amount of fluorochrome that could be loaded onto Ag-specific T cells using pMHC multimers. In some cases, this methodology increased the
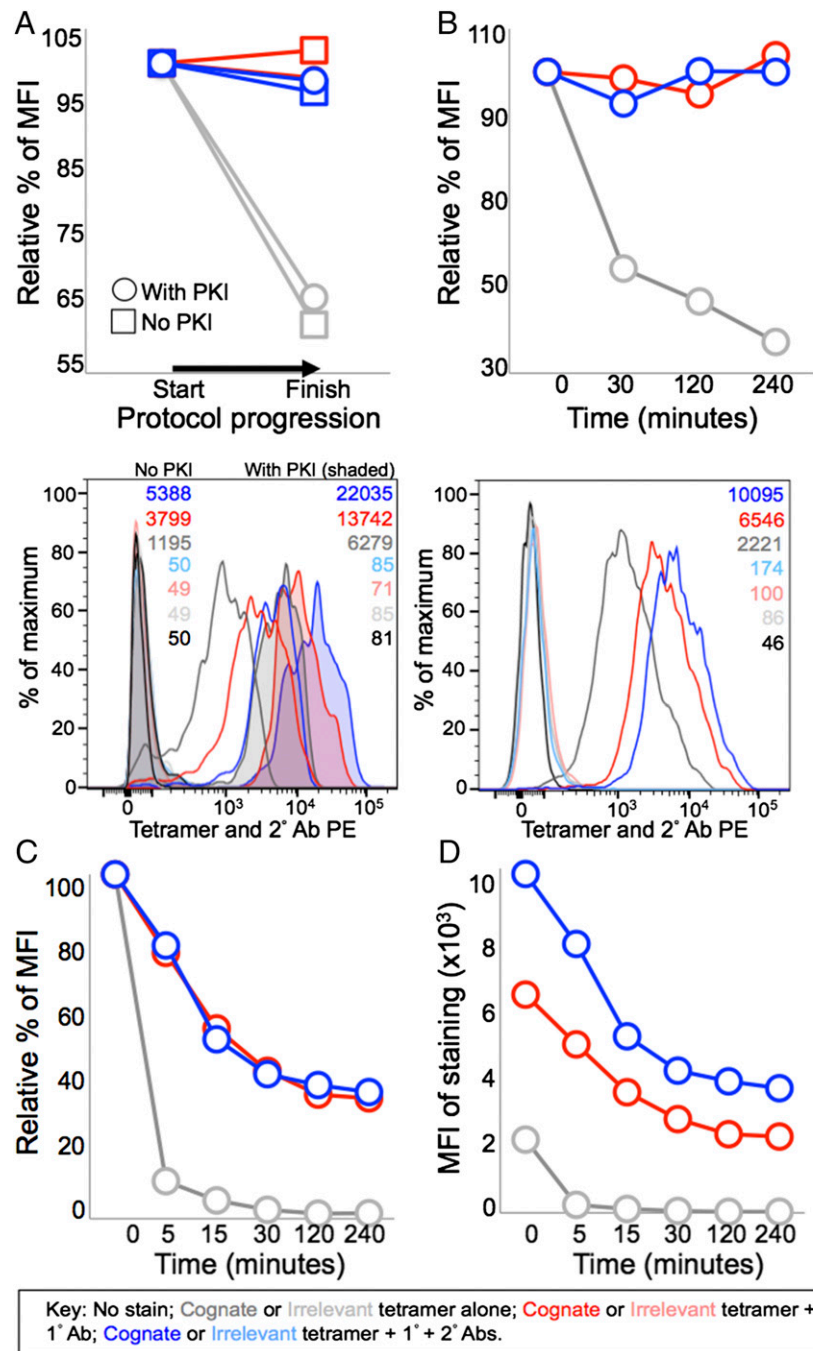
**FIGURE 8.** Stabilization with an anti-fluorochrome Ab preserves tetramer staining at the surface of T cells. (**A**) The CD8^{+} T cell clone 3F2 was treated with 50 nM PKI, or left untreated, and stained with cognate HLA-A2–ALWGPDPAAA (from preproinsulin) PE-conjugated tetramers or irrelevant HLA-A2–NLVPMVTAV (from CMV) tetramers. Cells were stained with tetramer alone (gray) or tetramer with anti-PE unconjugated 1° Ab (red) ± a PE-conjugated secondary 2° Ab (blue). Once stained with tetramer ± 1° Ab ± 2° Ab (Start), the cells were taken through three incubations (20 min on ice) and associated wash steps (two times) before being analyzed (Finish). The histogram shows the staining at the start of the assay. (**B**) 3F2 was treated with PKI and stained as in (A), then diluted in an excess volume of buffer (3 ml), and incubated at RT for the times shown. The histogram shows the staining at the start of the assay. (**C** and **D**) From the same experiment in (B), cells were incubated at RT with an anti–HLA-A2 Ab (BB7.2) in 0.1 ml of buffer and samples taken at the times shown. Graphs display the percentage of tetramer staining relative to the start of the experiment for each condition (A–C) or the MFI (C). PKI was present throughout the assay for (B)–(D).

staining intensity of cognate T cells by ∼20-fold. Simple arithmetic suggested that the additional fluorochrome added with a combination of 1° and 2° Ab could not explain the majority of the increase in MFI we observed. Experiments confirmed that the majority of the increase in MFI observed with 1° and 2° Abs during staining as described could be induced by addition of just 1° Ab. Further experiments showed that the enhancement afforded by addition of Ab against pMHC tetramers extended to reagents manufactured with allophycocyanin and FITC specificities in addition to PE and could be induced with all Ab clones tested. These experiments, and enhancement observed when using anti-streptavidin Ab, rule out the possibility that our original observation was due to an Ab-induced effect on fluorochrome emission. Instead, it seemed more likely that the major effect observed was due to an increase in stabilization via a substantially reduced off rate. Experiments designed to look at tetramer off rates during

standard staining incubations showed that there was a large loss of tetramer staining during the course of experiments in the absence of anti-pMHC tetramer Abs. Addition of an Ab against pMHC tetramer reversed the majority of this loss.

Although the inclusion of both unconjugated 1° and conjugated 2° Abs gave the best results, our laboratory now routinely stains using only the former Ab. Use of just 1° Ab provides the vast majority of the enhancement at very little cost (<$0.25 per stain). Addition of unconjugated 1° Ab does not introduce any risk of increased background staining that is possible with the further addition of fluorochrome-conjugated 2° Abs. Importantly, the procedures described in this study have been compatible with all of the polychromatic T cell phenotyping we have attempted to date, providing the tetramer + 1° ± 2° Abs are applied prior to other Abs. Nevertheless, it should be noted that anti-fluorochrome Abs are bivalent, resulting in the potential that if one binding site

were not occupied by cross-linking pMHC multimer, then it could be available to bind Abs coupled to tandem dyes, leading to potential artifacts in phenotypic measurements. Although our own preferred staining protocol includes PKI staining and only 1° Ab, all of the methodologies used in this study show additive benefits for both the MFI of staining and the range of TCR interactions that are amenable to detection, thereby allowing researchers to adjust protocols to suit their own individual needs and circumstances.

In summary, we show that including Abs against pMHC tetramers or dextramers during cell staining can result in substantial improvements in both the MFI of staining and the range of TCR interactions amenable to detection, thereby revealing important cell populations that could not be identified otherwise. The best results were observed with a combination of pMHC multimer, PKI, anti-fluorochrome 1° Ab, and anti-Ab conjugated 2° Ab. Surprisingly, the majority of the benefits observed with this protocol were still evident when only the 1° Ab was included. In addition to increased MFI and a weaker TCR affinity threshold required for staining, inclusion of Ab also allowed use of log-fold lower pMHC multimer reagent concentrations. The mechanism for these unanticipated affects appears to involve stabilization of reagent capture at the T cell surface during the staining protocol. We anticipate that this improved methodology will become routinely adopted during pMHC multimer staining, as it represents a considerable improvement in the brightness of staining, an extension in the scope of interactions that can be detected, and large potential cost savings compared with existing technology.

## Disclosures

The authors have no financial conflicts of interest.

## References

1. Wooldridge, L., A. Lissina, D. K. Cole, H. A. van den Berg, D. A. Price, and A. K. Sewell. 2009. Tricks with tetramers: how to get the most from multimeric peptide-MHC. *Immunology* 126: 147–164.
2. Laugel, B., H. A. van den Berg, E. Gostick, D. K. Cole, L. Wooldridge, J. Boulter, A. Milicic, D. A. Price, and A. K. Sewell. 2007. Different T cell receptor affinity thresholds and CD8 coreceptor dependence govern cytotoxic T lymphocyte activation and tetramer binding properties. *J. Biol. Chem.* 282: 23799–23810.
3. Cole, D. K., N. J. Pumphrey, J. M. Boulter, M. Sami, J. I. Bell, E. Gostick, D. A. Price, G. F. Gao, A. K. Sewell, and B. K. Jakobsen. 2007. Human TCR-binding affinity is governed by MHC class restriction. *J. Immunol.* 178: 5727–5734.
4. Aleksic, M., N. Liddy, P. E. Molloy, N. Pumphrey, A. Vuidepot, K. M. Chang, and B. K. Jakobsen. 2012. Different affinity windows for virus and cancer-specific T-cell receptors: implications for therapeutic strategies. *Eur. J. Immunol.* 42: 3174–3179.
5. Bridgeman, J. S., A. K. Sewell, J. J. Miles, D. A. Price, and D. K. Cole. 2012. Structural and biophysical determinants of αβ T-cell antigen recognition. *Immunology* 135: 9–18.
6. Choi, E. M., J. L. Chen, L. Wooldridge, M. Salio, A. Lissina, N. Lissin, I. F. Hermans, J. D. Silk, F. Mirza, M. J. Palmowski, et al. 2003. High avidity antigen-specific CTL identified by CD8-independent tetramer staining. *J. Immunol.* 171: 5116–5123.
7. Choi, E. M., M. Palmowski, J. Chen, and V. Cerundolo. 2002. The use of chimeric A2K(b) tetramers to monitor HLA A2 immune responses in HLA A2 transgenic mice. *J. Immunol. Methods* 268: 35–41.
8. Wooldridge, L., S. L. Hutchinson, E. M. Choi, A. Lissina, E. Jones, F. Mirza, P. R. Dunbar, D. A. Price, V. Cerundolo, and A. K. Sewell. 2003. Anti-CD8 antibodies can inhibit or enhance peptide-MHC class I (pMHCI) multimer binding: this is paralleled by their effects on CTL activation and occurs in the absence of an interaction between pMHCI and CD8 on the cell surface. *J. Immunol.* 171: 6650–6660.
9. Wooldridge, L., B. Laugel, J. Ekeruche, M. Clement, H. A. van den Berg, D. A. Price, and A. K. Sewell. 2010. CD8 controls T cell cross-reactivity. *J. Immunol.* 185: 4625–4632.
10. Wooldridge, L., A. Lissina, J. Vernazza, E. Gostick, B. Laugel, S. L. Hutchinson, F. Mirza, P. R. Dunbar, J. M. Boulter, M. Glick, et al. 2007. Enhanced immunogenicity of CTL antigens through mutation of the CD8 binding MHC class I invariant region. *Eur. J. Immunol.* 37: 1323–1333.
11. Wooldridge, L., T. J. Scriba, A. Milicic, B. Laugel, E. Gostick, D. A. Price, R. E. Phillips, and A. K. Sewell. 2006. Anti-coreceptor antibodies profoundly

12. affect staining with peptide-MHC class I and class II tetramers. *Eur. J. Immunol.* 36: 1847–1855.
13. Wooldridge, L., H. A. van den Berg, M. Glick, E. Gostick, B. Laugel, S. L. Hutchinson, A. Milicic, J. M. Brenchley, D. C. Douek, D. A. Price, and A. K. Sewell. 2005. Interaction between the CD8 coreceptor and major histocompatibility complex class I stabilizes T cell receptor-antigen complexes at the cell surface. *J. Biol. Chem.* 280: 27491–27501.
14. Sabatino, J. J., Jr., J. Huang, C. Zhu, and B. D. Evavold. 2011. High prevalence of low affinity peptide-MHC II tetramer-negative effectors during polyclonal CD4+ T cell responses. *J. Exp. Med.* 208: 81–90.
15. Massilamany, C., B. Upadhyaya, A. Gangaplara, C. Kuszynski, and J. Reddy. 2011. Detection of autoreactive CD4 T cells using major histocompatibility complex class II dextramers. *BMC Immunol.* 12: 40.
16. Dolton, G., A. Lissina, A. Skowera, K. Ladell, K. Tungatt, E. Jones, D. Kronenberg-Versteeg, H. Akpovwa, J. M. Pentier, C. J. Holland, et al. 2014. Comparison of peptide-major histocompatibility complex tetramers and dextramers for the identification of antigen-specific T cells. *Clin. Exp. Immunol.* 177: 47–63.
17. Daniels, M. A., and S. C. Jameson. 2000. Critical role for CD8 in T cell receptor binding and activation by peptide/major histocompatibility complex multimers. *J. Exp. Med.* 191: 335–346.
18. Clement, M., K. Ladell, J. Ekeruche-Makinde, J. J. Miles, E. S. Edwards, G. Dolton, T. Williams, A. J. Schauenburg, D. K. Cole, S. N. Lauder, et al. 2011. Anti-CD8 antibodies can trigger CD8+ T cell effector function in the absence of TCR engagement and improve peptide-MHCI tetramer staining. *J. Immunol.* 187: 654–663.
19. Lissina, A., K. Ladell, A. Skowera, M. Clement, E. Edwards, R. Seggewiss, H. A. van den Berg, E. Gostick, K. Gallagher, E. Jones, et al. 2009. Protein kinase inhibitors substantially improve the physical detection of T-cells with peptide-MHC tetramers. *J. Immunol. Methods* 340: 11–24.
20. Skowera, A., R. J. Ellis, R. Varela-Calviño, S. Arif, G. C. Huang, C. Van-Krinks, A. Zaremba, C. Rackham, J. S. Allen, T. I. Tree, et al. 2008. CTLs are targeted to kill beta cells in patients with type 1 diabetes through recognition of a glucose-regulated preproinsulin epitope. [Published erratum appears in 2009 *J. Clin. Invest.* 119: 2844.] *J. Clin. Invest.* 118: 3390–3402.
21. Purbhoo, M. A., Y. Li, D. H. Sutton, J. E. Brewer, E. Gostick, G. Bossi, B. Laugel, R. Moysey, E. Baston, N. Liddy, et al. 2007. The HLA A*0201-restricted hTERT(540-548) peptide is not detected on tumor cells by a CTL clone or a high-affinity T-cell receptor. *Mol. Cancer Ther.* 6: 2081–2091.
22. Laugel, B., D. A. Price, A. Milicic, and A. K. Sewell. 2007. CD8 exerts differential effects on the deployment of cytotoxic T lymphocyte effector functions. *Eur. J. Immunol.* 37: 905–913.
23. Donia, M., R. Anderson, E. Ellebaek, T. Z. Iversen, M. H. Andersen, P. T. Straten, and I. M. Svane. 2013. Adoptive T-cell therapy (ACT) with TILs for metastatic melanoma: Clinical responses and durable persistence of anti-cancer responses in peripheral blood. *J. Clin. Oncol.* 31(Suppl): 1028.
24. Stern, L. J., J. H. Brown, T. S. Jardetzky, J. C. Gorga, R. G. Urban, J. L. Strominger, and D. C. Wiley. 1994. Crystal structure of the human class II MHC protein HLA-DR1 complexed with an influenza virus peptide. *Nature* 368: 215–221.
25. Nunes, C. T., K. L. Miners, D. Colton, C. Pepper, C. Fegan, M. D. Mason, and S. Man. 2011. A novel tumor antigen derived from enhanced degradation of bax protein in human cancers. *Cancer Res.* 71: 5435–5444.
26. Holland, C. J., P. J. Rizkallah, S. Vollers, J. M. Calvo-Calle, F. Madura, A. Fuller, A. K. Sewell, L. J. Stern, A. Godkin, and D. K. Cole. 2012. Minimal conformational plasticity enables TCR cross-reactivity to different MHC class II heterodimers. *Sci. Reports* 2: 629.
27. Bulek, A. M., D. K. Cole, A. Skowera, G. Dolton, S. Gras, F. Madura, A. Fuller, J. J. Miles, E. Gostick, D. A. Price, et al. 2012. Structural basis for the killing of human beta cells by CD8(+) T cells in type 1 diabetes. *Nat. Immunol.* 13: 283–289.
28. Wooldridge, L., J. Ekeruche-Makinde, H. A. van den Berg, A. Skowera, J. J. Miles, M. P. Tan, G. Dolton, M. Clement, S. Llewellyn-Lacey, D. A. Price, et al. 2012. A single autoimmune T cell receptor recognizes more than a million different peptides. *J. Biol. Chem.* 287: 1168–1177.
29. Vollers, S. S., and L. J. Stern. 2008. Class II major histocompatibility complex tetramer staining: progress, problems, and prospects. *Immunology* 123: 305–313.
30. Altman, J. D., P. A. Moss, P. J. Goulder, D. H. Barouch, M. G. McHeyzer-Williams, J. I. Bell, A. J. McMichael, and M. M. Davis. 1996. Phenotypic analysis of antigen-specific T lymphocytes. *Science* 274: 94–96.
31. Klenerman, P., V. Cerundolo, and P. R. Dunbar. 2002. Tracking T cells with tetramers: new tales from new tools. *Nat. Rev. Immunol.* 2: 263–272.
32. Varela-Rohena, A., P. E. Molloy, S. M. Dunn, Y. Li, M. M. Suhoski, R. G. Carroll, A. Milicic, T. Mahon, D. H. Sutton, B. Laugel, et al. 2008. Control of HIV-1 immune escape by CD8 T cells expressing enhanced T-cell receptor. *Nat. Med.* 14: 1390–1395.
33. Cole, D. K., F. Yuan, P. J. Rizkallah, J. J. Miles, E. Gostick, D. A. Price, G. F. Gao, B. K. Jakobsen, and A. K. Sewell. 2009. Germ line-governed recognition of a cancer epitope by an immunodominant human T-cell receptor. *J. Biol. Chem.* 284: 27281–27289.
34. Pittet, M. J., D. Valmori, P. R. Dunbar, D. E. Speiser, D. Liénard, F. Lejeune, K. Fleischhauer, V. Cerundolo, J. C. Cerottini, and P. Romero. 1999. High frequencies of naive Melan-A/MART-1-specific CD8(+) T cells in a large proportion of human histocompatibility leukocyte antigen (HLA)-A2 individuals. *J. Exp. Med.* 190: 705–715.
35. Valitutti, S., S. Müller, M. Cella, E. Padovan, and A. Lanzavecchia. 1995. Serial triggering of many T-cell receptors by a few peptide-MHC complexes. *Nature* 375: 148–151.

## Supplementary Figure 1. Tungatt et al.
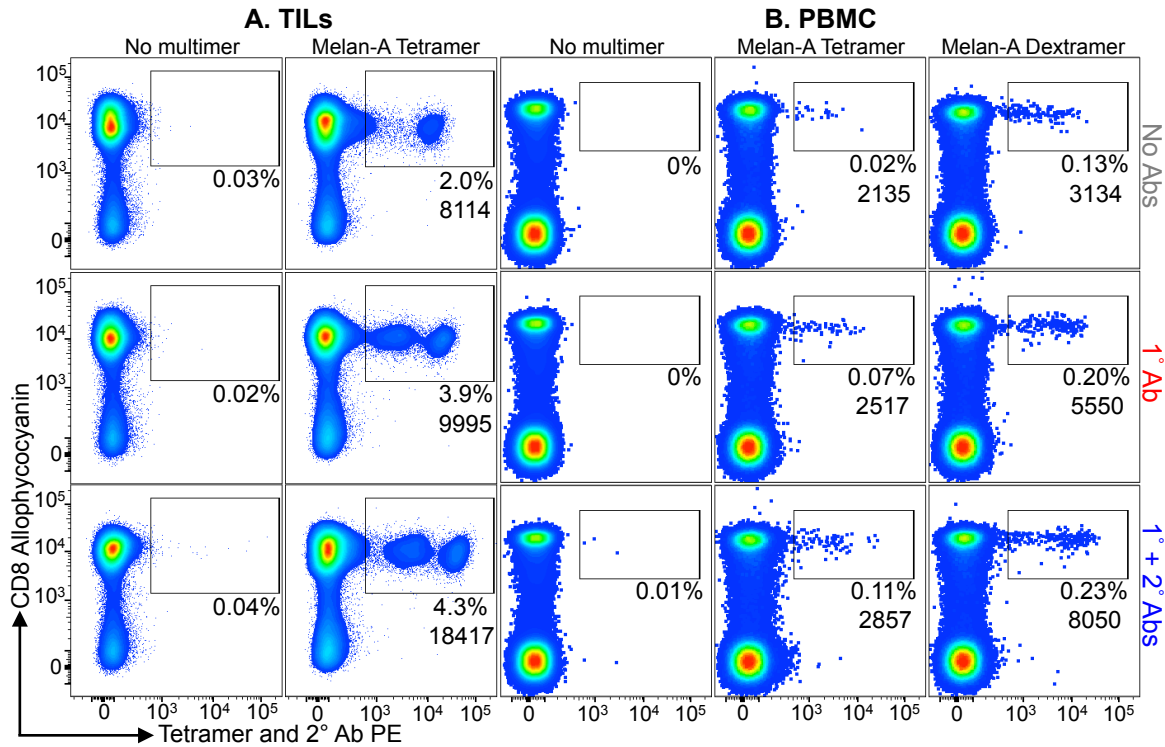


**Supplementary Figure 1: Ex vivo staining and detection of T-cells is improved by the addition of an anti-fluorochrome and conjugated secondary antibody to standard pMHC multimer staining protocols. (A)** TILs from a HLA-A2$^+$ metastatic melanoma patient were left unstained or stained with HLA-A2-ELAGIGILTV (from Melan-A) PE conjugated tetramers ± an anti-PE unconjugated 1° Ab ± a PE conjugated 2° Ab. These TILs did not stain with irrelevant tetramer (e.g. Figure 5). **(B)** Peripheral blood mononuclear cells (PBMCs) from a healthy donor were stained ex vivo with tetramers or dextramers (HLA-A2-ELAGIGILTV) and Abs as in A. Samples were minimally stained for viability, CD3 and CD8, with CD14 and CD19 also being stained in B. The tetramer$^+$ cells are expressed as a percentage of total cells (A) or CD8$^+$ cells (B) and the mean fluorescence intensity shown inset. Cells were pre-treated with PKI throughout.

## IMMUNOLOGY REVIEW ARTICLE

# More tricks with tetramers: a practical guide to staining T cells with peptide–MHC multimers

Garry Dolton,[1,*] Katie Tungatt,[1,*] Angharad Lloyd,[1] Valentina Bianchi,[1] Sarah M. Theaker,[1] Andrew Trimby,[1] Christopher J. Holland,[1] Marco Donia,[2] Andrew J. Godkin,[1] David K. Cole,[1] Per Thor Straten,[2] Mark Peakman,[3] Inge Marie Svane[2] and Andrew K. Sewell[1]

[1]*Division of Infection and Immunity, Cardiff University School of Medicine, Cardiff, UK,* [2]*Centre for Cancer Immune Therapy, Herlev University Hospital, Herlev, Denmark and* [3]*Peter Gorer Department of Immunobiology, King's College London, Guy's Hospital, London, UK*

Correspondence: Andrew K. Sewell, Division of Infection and Immunity, Henry Wellcome Building Cardiff University School of Medicine, University Hospital, Cardiff, Wales CF14 4XN, UK.
Email: sewellak@cf.ac.uk
Senior author: Andrew Sewell

## Summary

Analysis of antigen-specific T-cell populations by flow cytometry with peptide–MHC (pMHC) multimers is now commonplace. These reagents allow the tracking and phenotyping of T cells during infection, autoimmunity and cancer, and can be particularly revealing when used for monitoring therapeutic interventions. In 2009, we reviewed a number of 'tricks' that could be used to improve this powerful technology. More recent advances have demonstrated the potential benefits of using higher order multimers and of 'boosting' staining by inclusion of an antibody against the pMHC multimer. These developments now allow staining of T cells where the interaction between the pMHC and the T-cell receptor is over 20-fold weaker ($K_D > 1$ mM) than could previously be achieved. Such improvements are particularly relevant when using pMHC multimers to stain anti-cancer or autoimmune T-cell populations, which tend to bear lower affinity T-cell receptors. Here, we update our previous work to include discussion of newer tricks that can produce substantially brighter staining even when using log-fold lower concentrations of pMHC multimer. We further provide a practical guide to using pMHC multimers that includes a description of several common pitfalls and how to circumvent them.

**Keywords:** peptide–MHC dextramer; peptide–MHC tetramer; T-cell receptor; T cell.

## Introduction

The $\alpha\beta$ T-cell antigen receptor (TCR) allows T cells to inspect the proteome for anomalies by sampling peptide antigens cradled in either MHC class I or II molecules at the cell surface.[1,2] The interaction between TCR and peptide–MHC (pMHC) is weak, and typically only lasts a few seconds. Multimerization of soluble pMHC can considerably extend the half-life of this interaction due to the avidity effect,[3] and can thereby produce reagents that stably adhere to the cell surface of T cells bearing a cognate TCR. Peptide-MHC multimers in the form of avidin–biotin-based pMHC tetramers were first used to stain T cells by Altman *et al.* in 1996[4] and have gone on to transform the analysis of antigen-specific T-cell populations. Peptide-MHC multimers have been used in many thousands of studies and spawned the generation of several commercial companies that sell various forms of these reagents.[3] Moreover, pMHC multimers can be used in conjunction with a cocktail of antibodies raised against other cell surface proteins. This enables co-staining of antigen-specific T cells and segregation into various phenotypic populations without the distortion associated with function-based profiling.[5–9] Such phenotyping can be informative on antigen-experience, effector function, and also location of original antigen encounter, thereby allowing researchers to begin to deconvolute the complexities of T-cell immunity.

Peptide–MHC multimers are most commonly linked to fluorochromes, and used to detect T cells by conventional flow cytometry,[10] although next-generation technology uses pMHC multimers and antibodies that are linked to rare metal ions (typically lanthanides), which are then detected via mass spectrometry (MS).[6,7,11] This cytometry by time of flight, or 'mass cytometry', offers several advantages over conventional fluorescent cell sorting, but also comes with some major disadvantages. One advantage of MS-based detection is that heavy metal ion-based detection is not limited to the ~ 20 parameters possible

with conventional flow cytometers; metal-ion-conjugated antibodies and pMHC multimers could, in theory, be used to separate cells in over 100 dimensions. MS detection of heavy metal ions also allows greater sensitivity, and does not suffer from the spectral overlap or spreading error that is associated with detection of emission from fluorochromes. One major drawback of mass cytometry is that it does not yet allow cell sorting on the light-based properties of forward and side scatter. Furthermore, it incinerates cells, so making it impossible to collect them. These shortcomings mean that mass cytometry is unlikely to fully supplant conventional, fluorochrome-based cytometry for the analysis of antigen-specific T-cell populations.[11]

### Limitations of pMHC multimer staining

Peptide–MHC multimers have excelled for analyses of pathogen-specific CD8^{+} T-cell responses, but their use for dissection of autoimmune or anti-cancer T cells or CD4^{+} T cells is less widespread.[3] We have demonstrated that the TCR–pMHC affinity required for pMHC tetramer binding exceeds that required for T-cell activation.[12] This difference in affinity threshold means that conventional pMHC tetramer staining can fail to detect functional T cells.[12–15] Failure to stain cognate T cells that have a low affinity TCR is likely to be a more serious problem when pMHC multimers are used to stain self-specific (anti-cancer and autoimmune) T-cell populations, which tend to express lower affinity TCRs.[3,16–19] This issue is even greater when staining pMHCII-restricted T cells because the CD4 co-receptor, unlike the CD8 molecule, does not cooperate to aid TCR–pMHC binding.[3,20–26] Evavold and colleagues recently highlighted the potential level of under-estimation of antigen-specific CD4^{+} T-cell populations when staining with pMHCII tetramers *ex vivo*.[19] This study found a high prevalence of low-affinity pMHCII tetramer-negative effectors during polyclonal CD4^{+} T-cell responses, and demonstrated that myelin oligodendrocyte glycoprotein (35–55) and lymphocyte choriomeningitis virus glycoprotein (61–80) CD4^{+} T-cell populations were under-estimated by eightfold and fourfold, respectively by pMHCII tetramer staining. We have further demonstrated that the majority of the Melan A-specific CD8^{+} T cells in tumour-infiltrating lymphocyte (TIL) populations derived from malignant melanoma samples were not detected by conventional pMHC tetramer staining.[13] T-cell clones derived from these TILs that failed to stain by conventional pMHC tetramer staining were efficient killers of autologous tumour, indicating that pMHC tetramers missed fully functional cognate T cells.[13] These demonstrations highlight the pressing need to extend pMHC multimer technology to a point where it can be used to stain all T cells capable of responding to a given pMHC antigen.[13,27] Fortunately, new develop-

ments in the last 12 months considerably lower the TCR–pMHC affinity threshold required for efficient pMHC multimer staining. These, and other 'tricks' for improving staining with pMHC multimers are described below.

## Materials and methods

This study aims to provide an appraisal of the tricks that can be used to produce enhanced staining of cognate T cells with pMHC multimers. We review a number of tricks below. The methodologies for these individual techniques have been published elsewhere as indicated. Here we apply these procedures to the staining of a number of different samples in order to demonstrate how they can be of benefit. We also detail the optimized staining protocol that we use in Cardiff within the results, and demonstrate what each step adds to the procedure. We therefore only document the materials used in this section.

### Manufacture of pMHC tetramers and dextramers

The following streptavidin conjugates were used: streptavidin-allophycocyanin (APC) and -R-phycoerythrin (PE) (Life Technologies, Paisley, UK); streptavidin-brilliant violet (BV) 421 and -FITC. (Biolegend, London, UK). Peptide-MHC tetramer and dextramer were assembled as previously described.[13] Depending on experiment, either 0·3 μg or 0·5 μg (6 or 10 μg/ml) of tetramer or dextramer were used per stain, and equivalent amounts were used when tetramer and dextramer were being compared.

### T-cell clones

The following HLA-A*0201 (HLA A2) -restricted CD8^{+} T-cell clones were used: ST8.24 and VB25D12.24, which recognize the peptide EAAGIGILTV, in addition to the heteroclitic version of the peptide, ELAGIGILTV, from Melan A (residues 26–35)[28,29] and were derived from TILs of a patient with stage IV malignant melanoma (patient MM909.24); GD.GIL influenza-specific clone which recognizes GILGFVFTL from the matrix protein (residues 58–66); 1E6, which was grown from a patient with type 1 diabetes[30] and recognizes the preproinsulin (PPI) epitope, ALWGPDPAAA (residues 15–24).[31] The CD4^{+} HLA-DRB*0101 (HLA DR1) clone, DCD10, which recognizes PKYVKQNTLKLAT (residues 307–319) from haemagglutinin of influenza A virus.

### Antibody clones

Mouse anti-PE (clone PE001, BioLegend) and anti-APC (clone APC003, BioLegend) primary (1°) unconjugated monoclonal antibodies were used at a concentration of 10 μg/ml (0·5 μg/test). Goat anti-mouse conjugated secondary (2°) antibodies (multiple adsorbed PE- or

APC-conjugated immunoglobulin polyclonal; BD Biosciences, Oxford, UK) were used at 2 µg/ml (0·1 µg/test). We used the violet LIVE/DEAD Fixable Dead Cell Stain, Vivid (Life Technologies). The following monoclonal antibodies were used as indicated for individual experiments: anti-CD8-PE and anti-CD8-APC (clone BW135/80; Miltenyi Biotec, Bergisch Gladbach, Germany); anti-CD3-peridinin chlorophyll protein (PerCP) (clone BW264/56; Miltenyi Biotec); anti-CD19-Pacific blue (clone HIB19; BioLegend); and anti-CD14-Pacific blue (clone M5E2; BioLegend). Anti-rat CD2-PE (clone OX34; BioLegend) was used to stain lentivirally transduced T cells.

### Dasatinib

The protein kinase inhibitor (PKI), Dasatinib (Axon Medchem, VA), was reconstituted in dimethylsulphoxide (1 mM) and stored frozen in 5 µl one-use aliquots. Each 5 µl aliquot only costs < £0·02 and makes enough reagent to treat 1000 samples (100 µl volume at 50 nM).

### MEL5 TCR transduced CD8 T cells

The HLA A2-restricted Melan A-specific TCR MEL5 recognizes the natural 10-mer peptide, EAAGIGILTV. The TCR $\alpha$ and $\beta$ chains[32] were cloned into the pELN third-generation lentivirus vector (a kind gift from James Riley, University of Pennsylvania). The pELN lentiviral vector contained a rat CD2 marker to determine the frequency of transduction, and the TCR $\alpha$ and $\beta$ chains were separated by a 2A cleavage sequence. Integrase proficient lentivirus stocks were prepared by co-transfecting 293T/17 cells by calcium phosphate precipitation with the transfer vector and packaging plasmids – pRSV.REV (Addgene #12253), pMDLg/p.RRE (Addgene #12251)[33] and pCMV-VSV-G (Addgene #8454).[34] Supernatant was collected after 24-hr and 48-hr incubations, and the lentivirus stocks were concentrated by ultracentrifugation and used to transduce Dynabead (Life Technology) stimulated CD8+ T cells. The efficiency of lentivirus transduction was assessed by flow cytometry staining.

## Results

### Important tricks for improving staining efficiency

Several tricks for improving T-cell staining with pMHC multimers have been described and are reviewed elsewhere.[3] Here we detail the five most important tricks that we currently apply within our laboratory when staining antigen-specific T cells. These techniques are: (i) using a bright fluorochrome, (ii) inclusion of a PKI during staining, (iii) staining with anti-coreceptor antibody after staining with pMHC multimer, (iv) use of higher-order multimers, and (v) signal boosting with an anti-multimer antibody. The benefits of the latter two techniques were published in 2014. We refer the reader to our previous review[3] for a full list of tricks and a detailed explanation of the benefits of PKI and correct anti-coreceptor antibody usage.

### Using bright fluorochromes

It stands to reason that, when high staining intensity with pMHC multimer is required, it is better to use reagents coupled to a bright fluorochrome. This aspect is irrelevant when using MS-based detection methodology, and is less important when using pMHC dextramers that can be constructed to carry multiple fluorochrome molecules and also work well with FITC.[13] Our favourite 'flavours' of pMHC multimers are constructed with PE and APC. We have found wide variations in the quality of these reagents between different manufacturers. We currently use fluorochrome-conjugated streptavidin from Life Technologies for pMHC tetramers. However, researchers should remain mindful of the fact that we have not exhaustively tested all of the various products on the market so there may be better preparations available. Quantum dots (Q-dots) offer a good way of making very bright and robust pMHC multimers.[35] Although we have used Q-dot pMHC multimers, we do not have extensive experience with these reagents. Corry and colleagues directly compared Q-dots and tetramers for staining the same sample, and while Q-dots gave brighter staining in this comparison there was a noticeable staining of the general CD8+ cell population.[36] We have also noticed a similar phenomenon when some pMHC dextramers are used to stain some peripheral blood mononuclear cell (PBMC) populations.[13] Restriction of this non-specific staining to CD8+ T cells suggests that it is due to the avidity of pMHCI–CD8 interactions made possible with higher order multimers like Q-dots and dextramers. However, we remain unsure of why this background staining of CD8+ T-cell populations is only observed with some combinations of pMHC and PBMC. Figure 1(a) shows staining of HLA A2-restricted, influenza-specific CD8+ T-cell clone GD.GIL with pMHC tetramer manufactured with identical biotinylated HLA A2-GILGFVFTL monomer, and streptavidin linked to FITC, PE, APC and BV421 (see Materials and methods for details). These reagents gave mean fluorescence intensities (MFI) of 474, 4545, 3886 and 3684, and staining indices of 5·4, 52·8, 44·2 and 32·3, respectively. The BV421 reagent gave a higher background than the other fluorochromes when staining a T-cell clone (Fig. 1a) and PBMC (see Supplementary material, Fig. S1). Indeed, at the time of writing this review a higher degree of background on PBMC with BV421 cytomegalovirus (CMV) tetramers, compared with PE tetramers, is displayed on the manufacturer's website. We do not know the reason for the increase of non-specific staining with the BV421-containing reagents, but with optimization its use may offer an

## The benefits of protein kinase inhibitors

Staining with pMHC multimers is critically dependent on the TCR density at the T-cell surface as effective capture of a pMHC multimer from solution requires that a second TCR engages further pMHC in the multimer during the duration of the first TCR–pMHC engagement, to establish an initial avidity effect.[3] TCRs are known to trigger and internalize after engaging cognate antigen,[37] and we have shown that pMHC tetramers can fail to stain anti-cancer and anti-human pancreatic $\beta$-cell T cells after these cells have been exposed to cognate antigen.[13,14] Fortunately, TCR internalization can be inhibited by inclusion of a PKI, such as dasatinib for as little as 30 seconds before pMHC multimer staining, resulting in substantially enhanced staining intensities.[15] This increase in staining can be > 50-fold when TCR affinity is extremely low.[15] Incubation of T cells in 50 nM dasatinib for 60 min increases surface concentrations of both TCR and co-receptor at the cell surface.[15] We assume that this increase is due to inhibition of normal turnover of these molecules because of inhibited down-regulation. We recommend researchers to avoid repeated freeze–thawing of dasatinib by storing it as frozen one-use aliquots for use within 1 week of being defrosted. PKI treatment also enhances staining with higher-order multimers such as pMHC dextramers,[13] and has been used in conjunction with pMHC multimer detection by MS.[6] We now include dasatinib during pMHC multimer staining as a matter of routine. Inclusion of PKI prevents cellular activation, and so it is incompatible with function-based profiling techniques such as intracellular cytokine staining. Figure 1(b) shows that a fully functional T-cell clone, VB25D12.24, isolated from the TILs of a patient with Stage IV melanoma, recognizes Melan A peptide (left panel), and responds to autologous tumour (middle panel). However, the clone fails to stain with HLA A2-Melan A tetramer in the absence of PKI treatment (right panel). Nevertheless, the clone stains well with cognate tetramer after pre-treatment with 50 nM dasatinib for 30 min. These data serve to highlight what could be missed during regular pMHC tetramer staining without added 'tricks'. Figure 1(c) demonstrates the benefits of dasatinib when staining antigen-specific T cells in PBMC, the situation where they are most commonly used. Inclusion of 50 nM dasatinib increases by fourfold the number of cells detected when staining with HLA A2-Melan A tetramer.

## The importance of anti-coreceptor antibody

Peptide–MHC multimers are normally used in conjunction with an antibody for the relevant T-cell co-receptor (anti-CD4 for pMHCII multimers, and anti-CD8 for pMHCI multimers). It is well established that some antibody clones can disrupt staining of cognate T cells, while some antibodies can augment the interaction of pMHC multimers with cell surface TCR.[22,24,25,38–40] It is consequently preferable to use an anti-coreceptor antibody that aids pMHC multimer binding, or to stain with pMHC multimer before staining the T-cell co-receptor.[3] Figure 1(c) demonstrates that staining with CD8 antibody clone BW135/80, a clone we like to use in our laboratory, before staining of PBMC with HLA A2 Melan A tetramer, blocks staining in the absence of PKI and also reduces by half the number of cells that stain when PKI is included. The effects are less pronounced for an antiviral (cytomegalovirus) response, but there is still a reduction in the intensity of overall staining if anti-CD8 antibody is added first.

## Higher valency pMHC multimers

We recently compared staining of antiviral, anticancer and autoimmune T cells with pMHC tetramers and pMHC dextramers.[13] Peptide-MHC dextramers are dextran-based multimers that can carry greater numbers of both pMHC and fluorochrome per molecule, due to the larger scaffold. When staining was compared, we found that dextramers stain more brightly than tetramers and outperformed them when TCR–pMHC affinity was low. Dextramers also outperformed tetramers with pMHC class II reagents where there was an absence of co-receptor stabilization. Importantly, we also found that staining with pMHC dextramers was additionally enhanced when PKI was included, demonstrating that the two techniques are compatible.[13] Figure 2 shows pMHC staining of a Melan A-specific T-cell clone, ST8.24, with a full range of conditions. Staining with dextramer + PKI was more than threefold brighter than with tetramer + PKI. Dextramers + PKI uncovered 25-fold more Melan A-specific cells when compared with regular tetramer staining of HLA A2[+] PBMC (Fig. 5).

## Signal boosting with antibodies

We have also recently made use of the ILA1 T-cell clone that recognizes the pseudo HLA A2-restricted hTERT-derived epitope ILAKFLHWL,[41] and for which we have characterized a wide range of altered peptide ligands that act as agonists. These agonist peptides bind to HLA A2 equally well, but exhibit binding affinities for the ILA1 TCR that range from $K_D \sim 3$ μM to $K_D \sim 2$ mM by surface plasmon resonance.[12,42] The weakest ligand, 8E, still acts as a good agonist of ILA1 T cells when supplied exogenously at a concentration of 1 μM,[12,42] yet binds to the TCR with a $K_D \sim 2$ mM by extrapolation of response
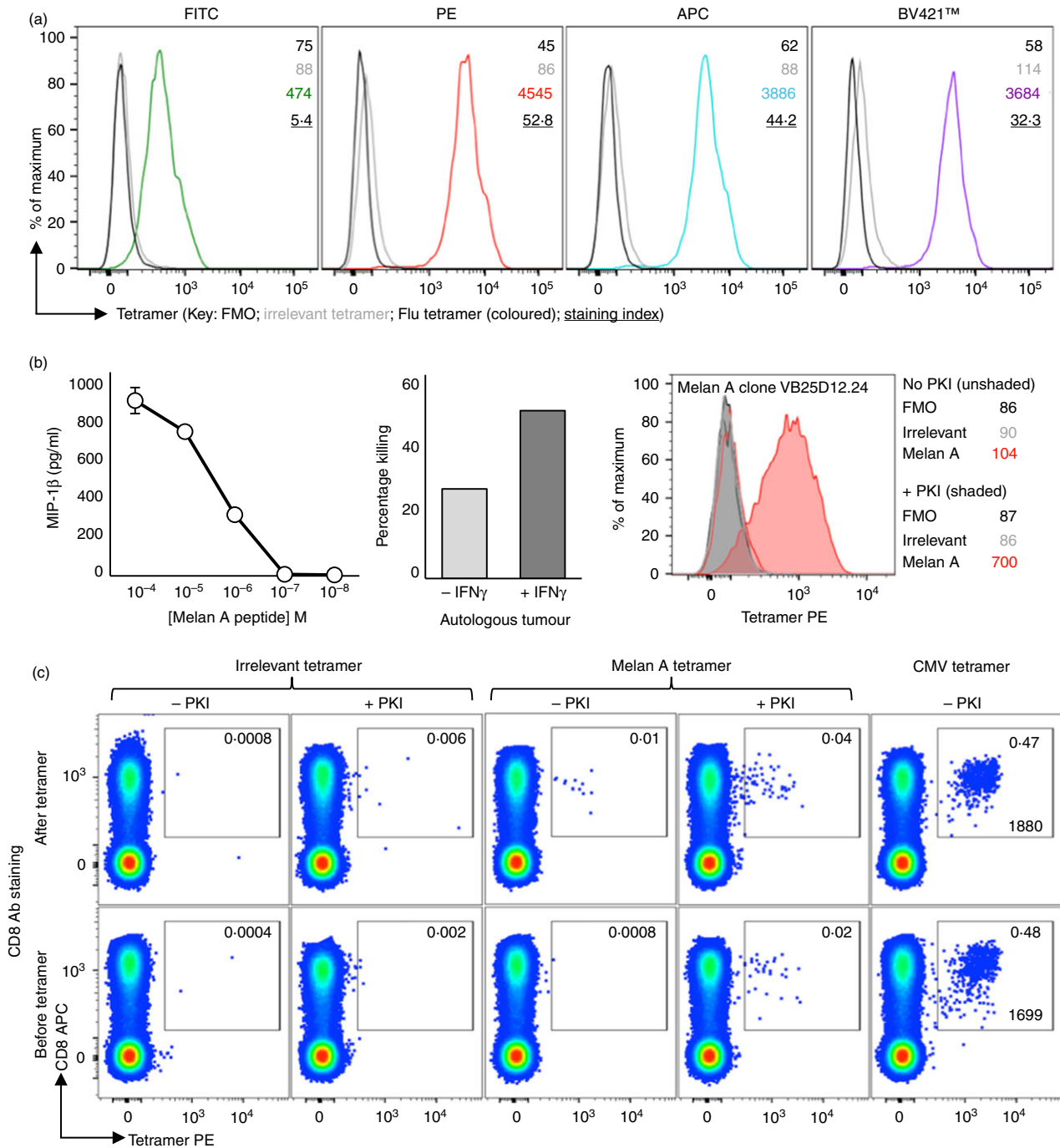
**Figure 1.** Tetramer staining of T cells is improved by using bright fluorochromes, protein kinase inhibitor treatment and addition of anti-CD8 antibody after tetramer staining. (a) HLA A2-restricted, influenza (flu) specific T-cell clone (GD.GIL) was stained with FITC, phycoerythrin (PE), allophycocyanin (APC) and brilliant violet (BV)421-conjugated cognate (matrix protein, GILGFVFTL) or irrelevant (preproinsulin; PPI; AL-WGPDPAAA) tetramers. The staining index [mean fluorescence intensity (MFI) of flu stain/MFI of PPI stain] is shown underlined. (b) T-cell clone (VB25D12.24) that recognizes a peptide from Melan A (left) and kills autologous tumour [± pre-treatment with interferon-γ (IFNγ)], at a T-cell to tumour ratio of 10:1 (middle), was stained with PE-conjugated Melan A (ELAGIGILTV) and PPI tetramers ± protein kinase inhibitor (PKI) pre-treatment (right). (c) HLA A2⁺ PBMC used from frozen ± PKI were stained with PE-conjugated PPI, Melan A and cytomegalovirus (CMV) (pp65, NLVPMVATV) tetramers (no PKI for the latter), with anti-CD8 APC antibody added before (lower panel) or after (upper panel) tetramer staining. The percentage of CD8⁺ cells that were also tetramer⁺ is shown inset for each gate and MFI displayed for the CMV tetramer stain.
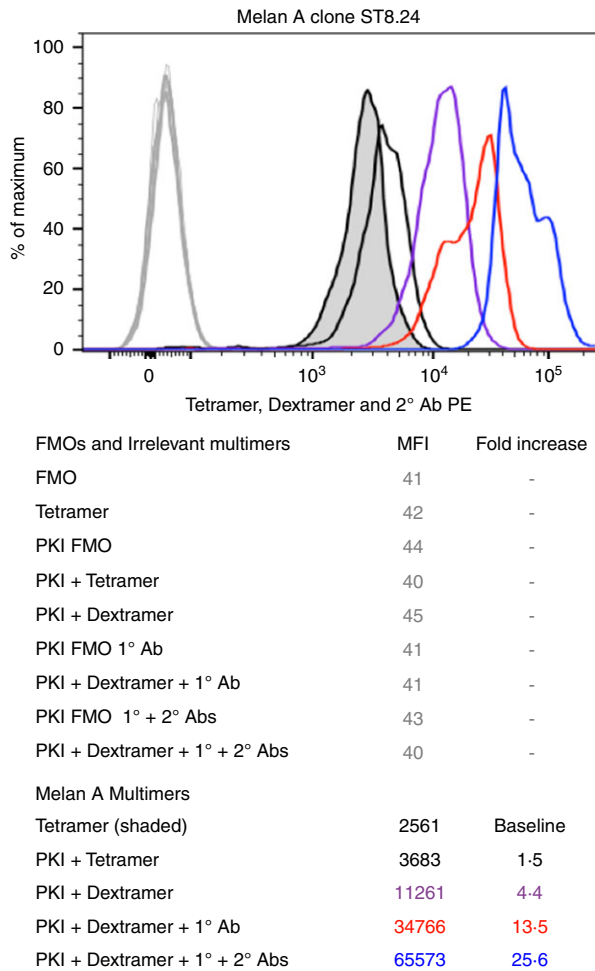
Melan A clone ST8.24

| FMOs and Irrelevant multimers | MFI | Fold increase |
|---|---|---|
| FMO | 41 | - |
| Tetramer | 42 | - |
| PKI FMO | 44 | - |
| PKI + Tetramer | 40 | - |
| PKI + Dextramer | 45 | - |
| PKI FMO 1° Ab | 41 | - |
| PKI + Dextramer + 1° Ab | 41 | - |
| PKI FMO 1° + 2° Abs | 43 | - |
| PKI + Dextramer + 1° + 2° Abs | 40 | - |
| **Melan A Multimers** | | |
| Tetramer (shaded) | 2561 | Baseline |
| PKI + Tetramer | 3683 | 1·5 |
| PKI + Dextramer | 11261 | 4·4 |
| PKI + Dextramer + 1° Ab | 34766 | 13·5 |
| PKI + Dextramer + 1° + 2° Abs | 65573 | 25·6 |

**Figure 2.** Chronological improvements to staining T cells with peptide–MHC (pMHC) multimers. 'Tricks' shown by our group to improve the staining of T cells with pMHC multimers were compared with tetramer alone (baseline) when staining a Melan A-specific CD8^{+} clone (ST8.24). ST8.24 was pretreated with protein kinase inhibitor (PKI) and stained with Melan A (ELAGIGILTV) or irrelevant [preproinsulin (PPI); ALWGPDPAAA] multimers (tetramer and dextramer) followed by the addition of 1° antibody (Ab) ± phycoerythrin (PE)-conjugated 2° Ab as indicated. Mean fluorescence intensity (MFI). Fluorescence Minus One (FMO).

units from surface plasmon resonance experiments. Until recently, we had failed to stain the ILA1 T-cell well with pMHC multimers made with HLA A2-ILAKFLHEL (8E), suggesting that even a combination of the techniques described above does not allow pMHC multimer staining with the very weakest TCR ligands.

It has long been known that T cells rapidly internalize pMHC multimers when stained at room temperature or physiological temperatures.[43] Some internalization is also observed during regular staining protocols on ice when cells are not pre-chilled.[13] Treatment with a PKI, like dasatinib, prevents TCR triggering and internalization of the TCR and any pMHC multimer bound to

it.[13,15] We reasoned that this would leave pMHC multimers available at the T-cell surface for further signal boosting with anti-pMHC multimer antibody. In testing this hypothesis we discovered that just adding anti-multimer antibody during stains with pMHC dextramers or pMHC tetramers boosted the MFI of staining, and lowered the TCR–pMHC affinity that was amenable to detection with these reagents. Indeed, adding anti-PE antibody to staining with PE-conjugated tetramer in the presence of PKI boosted staining to a point where the ILA1 T-cell clone could be recovered from HLA A2[+] PBMC using tetramer made with HLA A2-ILAKFLHEL, a ligand that binds to the cognate TCR with extremely low affinity ($K_D \sim 2$ mM).[14] This unexpected enhancement was shown to be the result of a substantial reduction in the off-rate of pMHC tetramer during the process of staining and washing before flow cytometric analysis.[14] This boost in staining is so powerful that it enabled brighter staining of cognate T cells, even when log-fold lower concentrations of pMHC multimer were used; thereby allowing for a considerable reduction in costs.[14] Further enhancements were observed when a fluorochrome-conjugated antibody against the original anti-pMHC multimer antibody was also included, or when pMHC dextramers were used. However, this extra level of enhancement is unlikely to be necessary during the vast majority of pMHC multimer stains. Staining of Melan A clone, ST8.24, with PE-conjugated pMHC dextramer in the presence of a 1° antibody increased the MFI of staining from 11261 to 34766 (Fig. 2). Further inclusion of a PE-conjugated 2° antibody additionally increased staining to 65573, while the intensity of background staining with an irrelevant HLA A2 multimer remained unchanged at an MFI of ~ 40. The benefits of signal boosting with antibody are also evident in Fig. 3(a), where HLA A2 Melan A tetramer was used to stain cells that were lentivirally transduced with Melan-specific TCR MEL5, as described in the Materials and methods. The lentivirus also expressed rat CD2, allowing identification of transduced cells with PE-conjugated anti-rat CD2 antibody (Fig. 3a). Transduced TCRs have to compete with the natural endogenous TCR for expression at the T-cell surface, such that the introduced TCR may be present at a low surface density. Low TCR density is also a problem during pMHC multimer staining of autoimmune or cancer-specific T cells that may have recently encountered their cognate antigen *in vivo*.[13,14] Seventeen per cent of the transduced cells stained with APC-conjugated HLA A2-ELAGIGILTV tetramer (Fig. 3a); this increased to 39% when PKI was included. Further addition of 1°, anti-APC antibody, or 1° anti-APC antibody + APC-conjugated 2° antibody increased this percentage to 53% and 65% of lentivirally transduced cells, respectively, and demonstrated the benefits of antibody boosting when surface

TCR density is low. Furthermore, we recently showed that signal boosting with antibody can enhance the ability of tetramers to stain, and detect both autoimmune and CD4^{+} HLA class II restricted T cells.[14] Figure 3(b) shows tetramer staining of PBMC spiked with the HLA A2 restricted CD8^{+} T-cell clone, 1E6. This clone was derived from a patient with type I diabetes,[30] and has a TCR that binds weakly to a PPI-derived peptide (ALWGPDPAAA) with a $K_D$ of >200 $\mu$M.[31] This is a feature that often precludes the effective staining of autoimmune T cells when tetramers are used without 'tricks'. Tetramer in combination with PKI recovered 6% of 1E6 from the spiked PBMC, and addition of 1° anti-PE antibody, alone or in combination with a PE-conjugated 2° antibody, gave 100% recovery with clear 1E6 T-cell discrimination from non-specific CD8^{+} T cells (Fig. 3b). The complete recovery of 1E6 with tetramer + 1° + 2° antibodies was achievable with eightfold less tetramer compared with tetramer alone, an observation we had previously shown with even less tetramer (25-fold).[14] CD4^{+} HLA class II restricted T cells also present a challenge when staining with tetramers, due to a lack of co-receptor help from CD4[3] and possession of TCRs with weaker average affinities.[16] Figure 3c demonstrates that the addition of a 1° antibody, with or without a 2° antibody, enhances the staining of the HLA DR1 restricted influenza-specific clone, DCD10, with 1·8-fold and 2·8-fold increases in staining, respectively.
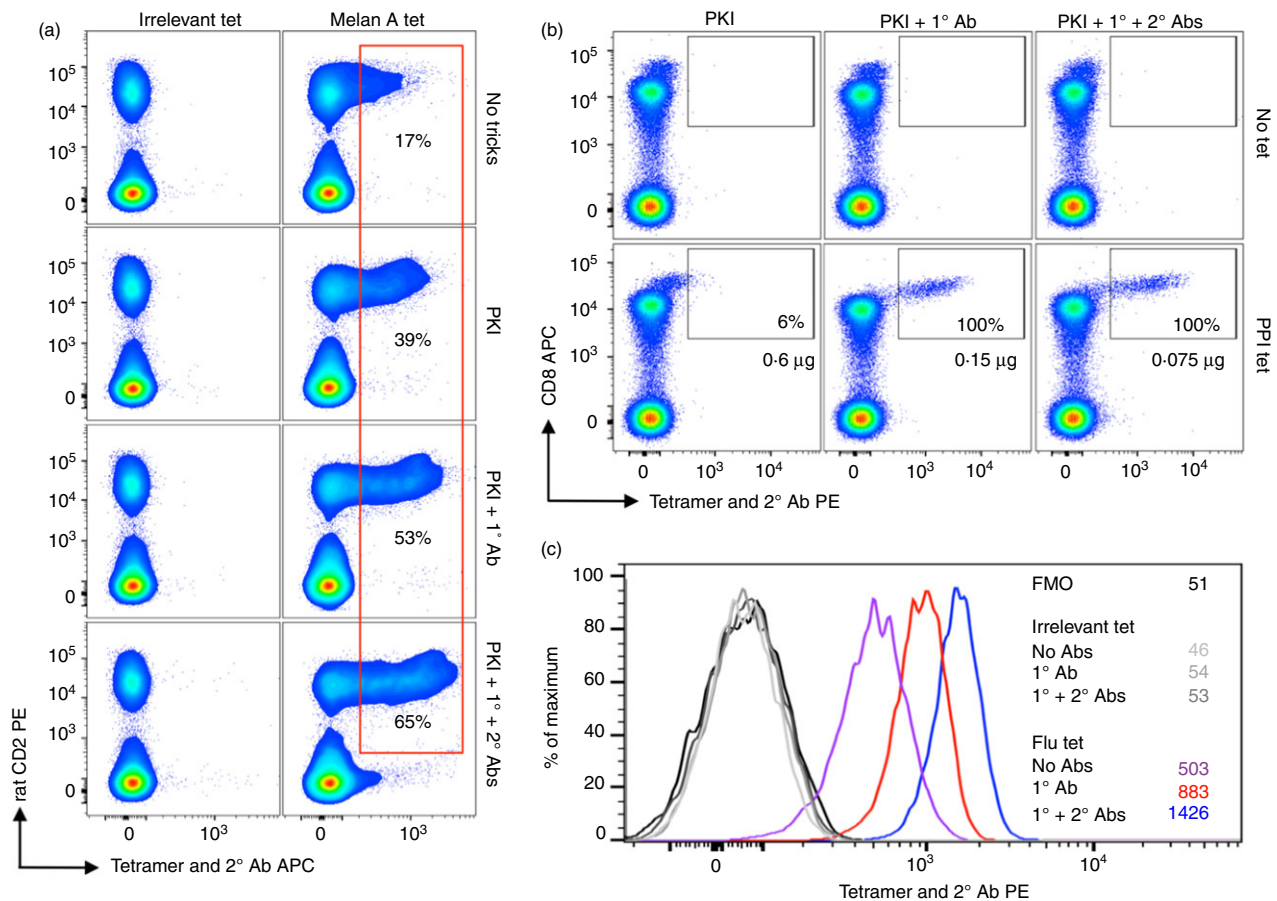


Figure 3. Improved staining of T-cell receptor (TCR)-transduced, autoimmune and MHC class II restricted T cells with tetramers by applying various tricks. (a) CD8^{+} T cells lentivirally co-transduced with a Melan A-specific TCR and rat CD2 ± protein kinase inhibitor (PKI) were stained with allophycocyanin (APC)-conjugated Melan A or irrelevant [preproinsulin (PPI); ALWGPDPAAA] tetramers. In addition to tetramer, PKI-treated cells were also labelled with unconjugated 1° antibody (Ab) ± APC-conjugated 2° Ab, as indicated. The percentage of Melan A tetramer^{+} cells of rat CD2^{+} cells is displayed. (b) The PPI-specific CD8^{+} T-cell clone, 1E6, which was grown from a patient with type I diabetes, was spiked into HLA A2^{+} peripheral blood mononuclear cells (PBMC), PKI treated and stained with PPI tetramer (amounts shown for each plot) ± 1° Ab ± phycoerythrin (PE)-conjugated 2° Ab. The 1E6 clone is CD8^{high} allowing it to be seen within the PBMC population based on CD8 staining alone. The percentage recovery of 1E6 with PPI tetramer is shown for each condition. (c) An influenza-specific HLA DR restricted CD4^{+} T-cell clone was stained with cognate (PKYVKQNTLKLAT from haemagglutinin) or irrelevant (DRFYKTLRAEQASQ from p24 Gag of HIV) PE-conjugated tetramer ± 1° Ab ± PE-conjugated 2° Ab.
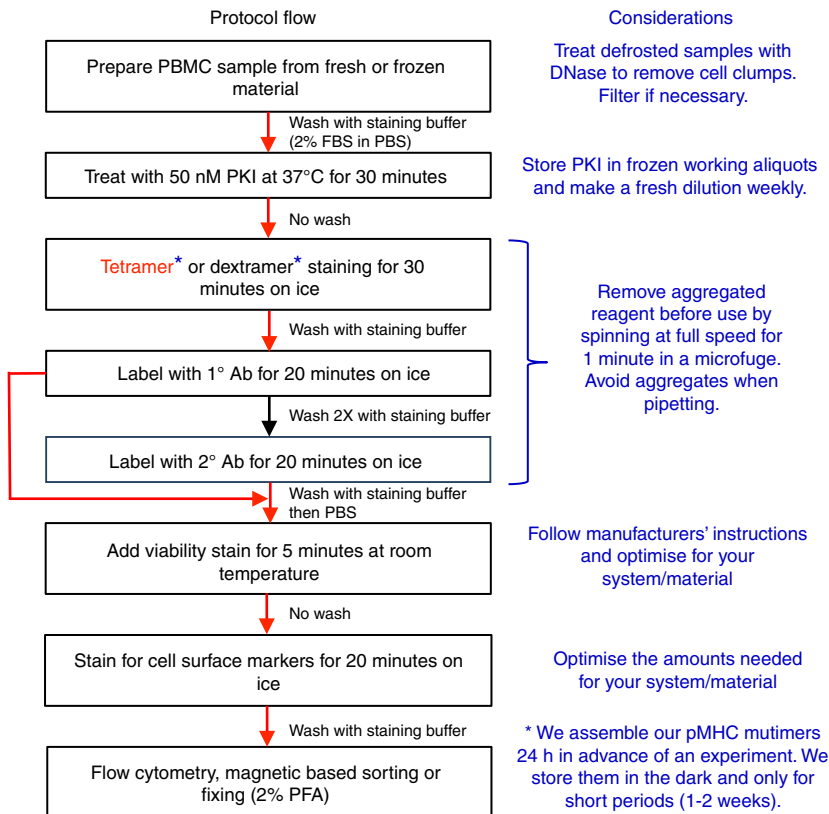
We are currently exploring the advantages of using boosted MHC class II tetramers on anti-tumour CD4^{+} T-cell clones and *ex vivo* PBMC samples.

## An optimized staining protocol

The techniques described above provide multiple ways to enhance staining with pMHC multimers. The most sensitive staining we have seen to date included use of: (i) bright fluorochrome, (ii) PKI, (iii) addition of anti-coreceptor antibody after pMHC multimer staining, (iv) higher order multimers (pMHC dextramers), (v) 1° anti-pMHC dextramer antibody, and (vi) fluorochrome-conjugated 2° antibody[14] as summarized in Fig. 2. However, use of all these tricks together is well beyond what is necessary for most pMHC multimer stains. Since publishing the above tricks, we have been asked many times by other researchers to provide an optimal pMHC staining protocol. We provide our own optimized protocol in Fig. 4, but in doing so we advise that researchers adjust their staining method using the above tricks so as to produce the best results in their own individual experimental systems.

The optimal pMHC multimer protocol will vary depending on the particular assay, the nature of the T cells and pMHC multimers being used. The tricks described above work well in conjunction, allowing researchers to tailor pMHC multimer staining to their own individual requirements. The most sensitive staining technique of using a bright fluorochrome using PKI and pMHC dextramers in conjunction with an anti-multimer 1° antibody and fluorochrome-conjugated 2° antibody (Fig. 2) is well beyond the requirements of most experiments. Inclusion of fluorochrome-conjugated 2° antibody adds expense, and the possibility of off-target staining due to the addition of fluorochrome that is not conjugated to pMHC; whereas pMHC dextramers are difficult to assemble in-house. Hence our own preferred standard protocol uses pMHC tetramers, PKI and anti-tetramer 1° antibody, as described in Fig. 4 (shown by the red arrows and text). This combination is sufficient for staining T cells with very-low TCR affinity ($K_D > 1$ mM), and so is more than adequate for staining the vast majority of antigen-specific T cells.[14] Figure 5 demonstrates the improvements possible by applying the various tricks above to the staining of HLA A2[+] PBMC with HLA A2 Melan A tetramer. Addition of PKI and 1° antibody to the stain increases the number of cells recovered by sixfold compared with no tricks (baseline). Use of PKI and 1° antibody with pMHC dextramer instead of pMHC tetramer recovers 25-fold more Melan A-specific cells than regular pMHC tetramer staining. Further addition of 2° antibody increases staining with tetramer and dextramer to 7·5-
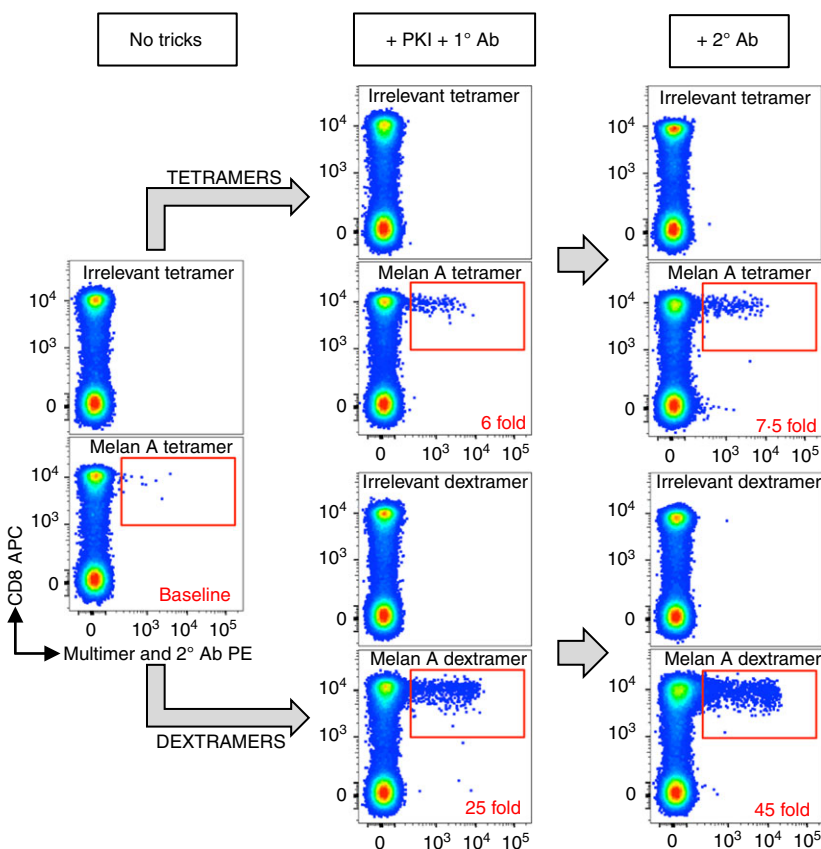


**Figure 4.** Our protocol for staining peripheral blood mononuclear cells (PBMC) with peptide–MHC (pMHC) multimers including the 'tricks' discussed in this review. Staining is performed in 5 ml 'FACS' tubes. Our default protocol flow is shown by red arrows/text and involves using tetramer, protein kinase inhibitor (PKI) and 1° antibody (Ab). PKI is sometimes used without other tricks. Dextramers and/or 2° Ab are used when T cells are particularly challenging to stain. The same protocol can be used for staining T cell clones and lines.

**Figure 5.** The combination of tricks greatly improves the recovery of T cells from peripheral blood mononuclear cells (PBMC) with pMHC multimers. HLA A2[+] PBMC were stained with Melan A (ELAGIGILTV) and irrelevant [preproinsulin (PPI); AL-WGPDPAAA] phycoerythrin (PE) -conjugated tetramers or dextramers ± protein kinase inhibitor (PKI) and unconjugated 1° antibody (Ab) ± PE-conjugated 2° Ab, as indicated. The recovery of Melan A tetramer or dextramer^{+} cells (red box) is compared to the staining with tetramer alone (baseline).

fold and 45-fold above standard pMHC tetramer staining without tricks, respectively. These data demonstrate the additive nature of these tricks when applied to pMHC multimer staining of PBMC.

## Troubleshooting

Various issues can arise when staining with pMHC multimers and we are occasionally asked to try and troubleshoot issues for other laboratories. One of the commonest problems seems to arise due to aggregation of the pMHC multimer preparation. This problem can be quickly eliminated if pMHC multimer is spun in a microfuge at top speed for 1 min before use to precipitate any aggregates present. Figure 6(a) shows a clean staining of HLA A2[+] PBMC with spun HLA A2 Melan A tetramer adjacent to the identical stain with this reagent before spinning. In the absence of centrifugation there is considerable background in the CD8-negative cell population, in addition to some high intensity staining in the CD8^{+} population. Similar issues are also apparent, although to a lesser degree, when the same PBMC are stained with HLA A2-GILGFVFTL influenza-specific reagents. It is also important to include a 'dump channel' during pMHC multimer analyses that eliminates dead/dying cells, B cells and CD14^{+} cells that can

take up pMHC multimers non-specifically without the need for cognate TCR expression. Figure 6(b) shows the staining of HLA A2^{+} PBMC with HLA A2-PPI and HLA A2-CMV tetramers (peptide sequences ALWGPDPAAA and NLVPMVATV, respectively) ± a viability stain, to demonstrate how dumping of dead and dying cells, as well as those capable of non-specific pMHC multimer uptake via macropinocytosis and other mechanisms, can substantially improve staining with pMHC multimers.

## Detection of non-classical T cells

Recent advances have described how T cells are able to recognize lipid antigens in the context of CD1a, CD1b, CD1c and CD1d molecules, or bacterial metabolites in the context of MHC-related protein (MR)1.[1,2] Multimeric forms of CD1-lipid and MR1-metabolite can also be used to identify and phenotype the T cells that respond to these antigens.[44–52] TCR interactions with these non-classical ligands tend to be relatively robust, such that regular tetrameric versions of these molecules appear to stain cognate cells well. Nevertheless, it is likely that the application of higher-order multimers, PKI and signal boosting with antibodies (as described for conventional pMHC multimers) will enhance the intensity of staining, with concomitant poten-
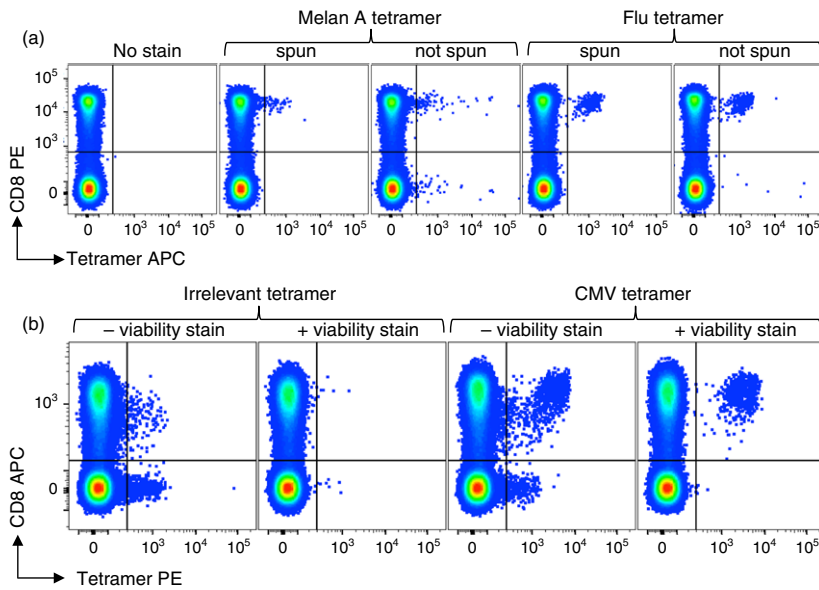
**Figure 6.** Removal of aggregated tetramer and including a viability stain improves the clarity of tetramer staining. (a) HLA A2[+] peripheral blood mononuclear cells (PBMC) from frozen were stained with allophycocyanin (APC) -conjugated Melan A (ELAGIGILTV) and influenza (flu) (matrix protein; GILGFVFTL) tetramers that were either spun (microfuge at full speed for 1 min) before use to remove aggregates or left unspun. (b) HLA A2[+] PBMC from frozen were stained with phycoerythrin (PE)-conjugated cytomegalocirus (pp65, NLVPMVATV) and irrelevant (preproinsulin (PPI), AL-WGPDPAAA) tetramers and co-stained for CD3, CD8, CD19 and CD14 ± a viability stain and the plots shown gated on CD3[+](viable when viability stain was present)/CD19^{−}/CD14^{−} cells.

tial for also using less multimerized non-classical ligand during staining. It remains to be seen whether the application of more sensitive techniques to the staining of non-classical T cells with multimeric ligands will lead to the discovery of new subsets of T cells.

## Conclusions

Fluorochrome-conjugated pMHC multimers have already revolutionized the study of antigen-specific T cells. Until recently, the major problem with these reagents has been that the TCR affinity threshold required for pMHC multimer staining exceeded that required for T-cell activation, resulting in a failure to detect all T cells capable of responding to a particular pMHC.[12–15] This problem is far more likely when staining anti-cancer T cells, autoimmune T cells, or MHC class II-restricted T cells, as such populations tend to bear TCRs with lower affinity for cognate antigen.[16,17] There is a further issue caused by low TCR surface densities when staining T cells that have been recently exposed to antigen.[13,14] Recent antigen exposure can occur naturally *in vivo*, or artificially during functional profiling following antigen exposure *in vitro* (e.g. intracellular cytokine staining).[13,14] Newer developments including staining in the presence of PKI,[15] using higher order pMHC multimers,[13] and boosting staining by including anti-multimer antibody,[14] have lowered the TCR affinity required for effective pMHC multimer staining by > 20-fold, while increasing staining intensity. These advances enhance pMHC multimer technology to a point where it can be used to stain T cells where the affinity between the TCR and antigen exceeds a $K_D$ of 1 mM.[13] It remains to be determined whether this improvement takes pMHC multimer staining to a point where it stains all functional T cells and thereby allows these reagents to realize their

full potential for immune monitoring. Recent addition of MS-based detection to pMHC multimer staining increases the number of cell surface molecules that can be studied simultaneously, and also circumvents the requirement for spectral overlap compensation during antibody phenotyping so increasing the power of this influential technology further still.[6,11] Contemporary developments using pyrosequencing of TCRs to quantify T cells or inform on their function[53] are still far from routine, so we anticipate that pMHC multimers will continue to remain prominent for T-cell detection for many years to come.

## Disclosures

AKS is inventor on patent application numbers EP 09737105.8 and US 13/119,795 which has been

licensed to a company by University College Cardiff Consultants Limited. He has not benefitted personally from the exploitation of the technology at the current time.

# References

1 Rossjohn J, Gras S, Miles JJ, Turner SJ, Godfrey DI, McCluskey J. T Cell antigen receptor recognition of antigen-presenting molecules. *Annu Rev Immunol* 2014; **33**:169–200.

2 Attaf M, Legut M, Cole DK, Sewell AK. The T cell antigen receptor: the Swiss Army knife of the immune system. *Clin Exp Immunol* 2015; **181**:1–18.

3 Wooldridge L, Lissina A, Cole DK, van den Berg HA, Price DA, Sewell AK. Tricks with tetramers: how to get the most from multimeric peptide-MHC. *Immunology* 2009; **126**:147–64.

4 Altman JD, Moss PA, Goulder PJ, Barouch DH, McHeyzer-Williams MG, Bell JI, McMichael AJ, Davis MM. Phenotypic analysis of antigen-specific T lymphocytes. *Science* 1996; **274**:94–6.

5 Fergusson JR, Smith KE, Fleming VM *et al.* CD161 defines a transcriptional and functional phenotype across distinct human T cell lineages. *Cell Rep* 2014; **9**:1075–88.

6 Newell EW, Sigal N, Bendall SC, Nolan GP, Davis MM. Cytometry by time-of-flight shows combinatorial cytokine expression and virus-specific cell niches within a continuum of CD8+ T cell phenotypes. *Immunity* 2012; **36**:142–52.

7 Newell EW, Sigal N, Nair N, Kidd BA, Greenberg HB, Davis MM. Combinatorial tetramer staining and mass cytometry analysis facilitate T-cell epitope mapping and characterization. *Nat Biotechnol* 2013; **31**:623–9.

8 Appay V, van Lier RA, Sallusto F, Roederer M. Phenotype and function of human T lymphocyte subsets: consensus and issues. *Cytometry A* 2008; **73**:975–83.

9 Appay V, Dunbar PR, Callan M *et al.* Memory CD8+ T cells vary in differentiation phenotype in different persistent virus infections. *Nat Med* 2002; **8**:379–85.

10 Klenerman P, Cerundolo V, Dunbar PR. Tracking T cells with tetramers: new tales from new tools. *Nat Rev Immunol* 2002; **2**:263–72.

11 Bendall SC, Nolan GP, Roederer M, Chattopadhyay PK. A deep profiler's guide to cytometry. *Trends Immunol* 2012; **33**:323–32.

12 Laugel B, van den Berg HA, Gostick E *et al.* Different T cell receptor affinity thresholds and CD8 coreceptor dependence govern cytotoxic T lymphocyte activation and tetramer binding properties. *J Biol Chem* 2007; **282**:23799–810.

13 Dolton G, Lissina A, Skowera A *et al.* Comparison of peptide-major histocompatibility complex tetramers and dextramers for the identification of antigen-specific T cells. *Clin Exp Immunol* 2014; **177**:47–63.

14 Tungatt K, Bianchi V, Crowther MD *et al.* Antibody stabilization of peptide-MHC multimers reveals functional T cells bearing extremely low-affinity TCRs. *J Immunol* 2015; **194**:463–74.

15 Lissina A, Ladell K, Skowera A *et al.* Protein kinase inhibitors substantially improve the physical detection of T-cells with peptide-MHC tetramers. *J Immunol Methods* 2009; **340**:11–24.

16 Cole DK, Pumphrey NJ, Boulter JM *et al.* Human TCR-binding affinity is governed by MHC class restriction. *J Immunol* 2007; **178**:5727–34.

17 Aleksic M, Liddy N, Molloy PE, Pumphrey N, Vuidepot A, Chang KM, Jakobsen BK. Different affinity windows for virus and cancer-specific T-cell receptors: implications for therapeutic strategies. *Eur J Immunol* 2012; **42**:3174–9.

18 Bridgeman JS, Sewell AK, Miles JJ, Price DA, Cole DK. Structural and biophysical determinants of alphabeta T-cell antigen recognition. *Immunology* 2012; **135**:9–18.

19 Sabatino JJ Jr, Huang J, Zhu C, Evavold BD. High prevalence of low affinity peptide-MHC II tetramer-negative effectors during polyclonal CD4+ T cell responses. *J Exp Med* 2011; **208**:81–90.

20 Choi EM, Chen JL, Wooldridge L *et al.* High avidity antigen-specific CTL identified by CD8-independent tetramer staining. *J Immunol* 2003; **171**:5116–23.

21 Choi EM, Palmowski M, Chen J, Cerundolo V. The use of chimeric A2K(b) tetramers to monitor HLA A2 immune responses in HLA A2 transgenic mice. *J Immunol Methods* 2002; **268**:35–41.

22 Wooldridge L, Hutchinson SL, Choi EM *et al.* Anti-CD8 antibodies can inhibit or enhance peptide-MHC class I (pMHCI) multimer binding: this is paralleled by their effects on CTL activation and occurs in the absence of an interaction between pMHCI and CD8 on the cell surface. *J Immunol* 2003; **171**:6650–60.

23 Wooldridge L, Laugel B, Ekeruche J, Clement M, van den Berg HA, Price DA, Sewell AK. CD8 controls T cell cross-reactivity. *J Immunol* 2010; **185**:4625–32.

24 Wooldridge L, Lissina A, Vernazza J *et al.* Enhanced immunogenicity of CTL antigens through mutation of the CD8 binding MHC class I invariant region. *Eur J Immunol* 2007; **37**:1323–33.

25 Wooldridge L, Scriba TJ, Milicic A, Laugel B, Gostick E, Price DA, Phillips RE, Sewell AK. Anti-coreceptor antibodies profoundly affect staining with peptide-MHC class I and class II tetramers. *Eur J Immunol* 2006; **36**:1847–55.

26 Wooldridge L, van den Berg HA, Glick M *et al.* Interaction between the CD8 coreceptor and major histocompatibility complex class I stabilizes T cell receptor-antigen complexes at the cell surface. *J Biol Chem* 2005; **280**:27491–501.

27 Massilamany C, Upadhyaya B, Gangaplara A, Kuszynski C, Reddy J. Detection of autoreactive CD4 T cells using major histocompatibility complex class II dextramers. *BMC Immunol* 2011; **12**:40.

28 Cole DK, Edwards ES, Wynn KK *et al.* Modification of MHC anchor residues generates heteroclitic peptides that alter TCR binding and T cell recognition. *J Immunol* 2010; **185**:2600–10.

29 Madura F, Rizkallah PJ, Holland CJ *et al.* Structural basis for ineffective T-cell responses to MHC anchor residue-improved "heteroclitic" peptides. *Eur J Immunol* 2015; **45**:584–91.

30 Skowera A, Ellis RJ, Varela-Calvino R *et al.* CTLs are targeted to kill beta cells in patients with type 1 diabetes through recognition of a glucose-regulated preproinsulin epitope. *J Clin Invest* 2008; **118**:3390–402.

31 Bulek AM, Cole DK, Skowera A *et al.* Structural basis for the killing of human beta cells by CD8(+) T cells in type 1 diabetes. *Nat Immunol* 2012; **13**:283–9.

32 Cole DK, Yuan F, Rizkallah PJ *et al.* Germ line-governed recognition of a cancer epitope by an immunodominant human T-cell receptor. *J Biol Chem* 2009; **284**:27281–9.

33 Dull T, Zufferey R, Kelly M, Mandel RJ, Nguyen M, Trono D, Naldini L. A third-generation lentivirus vector with a conditional packaging system. *J Virol* 1998; **72**:8463–71.

34 Stewart SA, Dykxhoorn DM, Palliser D *et al.* Lentivirus-delivered stable gene silencing by RNAi in primary cells. *RNA* 2003; **9**:493–501.

35 Hadrup SR, Bakker AH, Shu CJ *et al.* Parallel detection of antigen-specific T-cell responses by multidimensional encoding of MHC multimers. *Nat Methods* 2009; **6**:520–6.

36 Zhu J, Koelle DM, Cao J, Vazquez J, Huang ML, Hladik F, Wald A, Corey L. Virus-specific CD8+ T cells accumulate near sensory nerve endings in genital skin during subclinical HSV-2 reactivation. *J Exp Med* 2007; **204**:595–603.

37 Valitutti S, Muller S, Cella M, Padovan E, Lanzavecchia A. Serial triggering of many T-cell receptors by a few peptide-MHC complexes. *Nature* 1995; **375**:148–51.

38 Clement M, Ladell K, Ekeruche-Makinde J *et al.* Anti-CD8 antibodies can trigger CD8+ T cell effector function in the absence of TCR engagement and improve peptide-MHCI tetramer staining. *J Immunol* 2011; **187**:654–63.

39 Daniels MA, Jameson SC. Critical role for CD8 in T cell receptor binding and activation by peptide/major histocompatibility complex multimers. *J Exp Med* 2000; **191**:335–46.

40 Holman PO, Walsh ER, Jameson SC. Characterizing the impact of CD8 antibodies on class I MHC multimer binding. *J Immunol* 2005; **174**:3986–91.

41 Purbhoo MA, Li Y, Sutton DH *et al.* The HLA A*0201-restricted hTERT(540-548) peptide is not detected on tumor cells by a CTL clone or a high-affinity T-cell receptor. *Mol Cancer Ther* 2007; **6**:2081–91.

42 Laugel B, Price DA, Milicic A, Sewell AK. CD8 exerts differential effects on the deployment of cytotoxic T lymphocyte effector functions. *Eur J Immunol* 2007; **37**:905–13.

43 Whelan JA, Dunbar PR, Price DA *et al.* Specificity of CTL interactions with peptide-MHC class I tetrameric complexes is temperature dependent. *J Immunol* 1999; **163**:4342–8.

44 de Jong A, Cheng TY, Huang S *et al.* CD1a-autoreactive T cells recognize natural skin oils that function as headless antigens. *Nat Immunol* 2014; **15**:177–85.

45 Kasmar AG, Van Rhijn I, Magalhaes KG *et al.* Cutting Edge: CD1a tetramers and dextramers identify human lipopeptide-specific T cells ex vivo. *J Immunol* 2013; **191**:4499–503.

46 Kasmar AG, van Rhijn I, Cheng TY *et al.* CD1b tetramers bind alphabeta T cell receptors to identify a mycobacterial glycolipid-reactive T cell repertoire in humans. *J Exp Med* 2011; **208**:1741–7.

47 Van Rhijn I, Kasmar A, de Jong A *et al.* A conserved human T cell population targets mycobacterial antigens presented by CD1b. *Nat Immunol* 2013; **14**:706–13.

48 Ly D, Kasmar AG, Cheng TY *et al.* CD1c tetramers detect ex vivo T cell responses to processed phosphomycoketide antigens. *J Exp Med* 2013; **210**:729–41.

49 Sidobre S, Kronenberg M. CD1 tetramers: a powerful tool for the analysis of glycolipid-reactive T cells. *J Immunol Methods* 2002; **268**:107–21.

50 Gadola SD, Karadimitris A, Zaccai NR, Salio M, Dulphy N, Shepherd D, Jones EY, Cerundolo V. Generation of CD1 tetramers as a tool to monitor glycolipid-specific T cells. *Philos Trans R Soc Lond B Biol Sci* 2003; **358**:875–7.

51 Karadimitris A, Gadola S, Altamirano M *et al.* Human CD1d-glycolipid tetramers generated by in vitro oxidative refolding chromatography. *Proc Natl Acad Sci U S A* 2001; **98**:3294–8.

52 Corbett AJ, Eckle SB, Birkinshaw RW *et al.* T-cell activation by transitory neo-antigens derived from distinct microbial pathways. *Nature* 2014; **509**:361–5.

53 Attaf M, Huseby E, Sewell AK. alphabeta T cell receptors as predictors of health and disease. *Cell Mol Immunol* 2015;. doi:10.1038/cmi.2014.134.

## Supporting Information

Additional Supporting Information may be found in the online version of this article:

**Figure S1** Comparison of phycoerythrin (PE) and brilliant violet (BV)-conjugated tetramers on peripheral blood mononuclear cells (PBMC). HLA A2$^+$ PBMC + PKI were stained with Melan A (ELAGIGILTV) and influenza (flu) (matrix protein; GILGFVFTL) PE-conjugated and BV-conjugated tetramers. More background staining was evident on the CD8$^-$ cells with the BV tetramer (red arrows) as observed in Fig. 1.
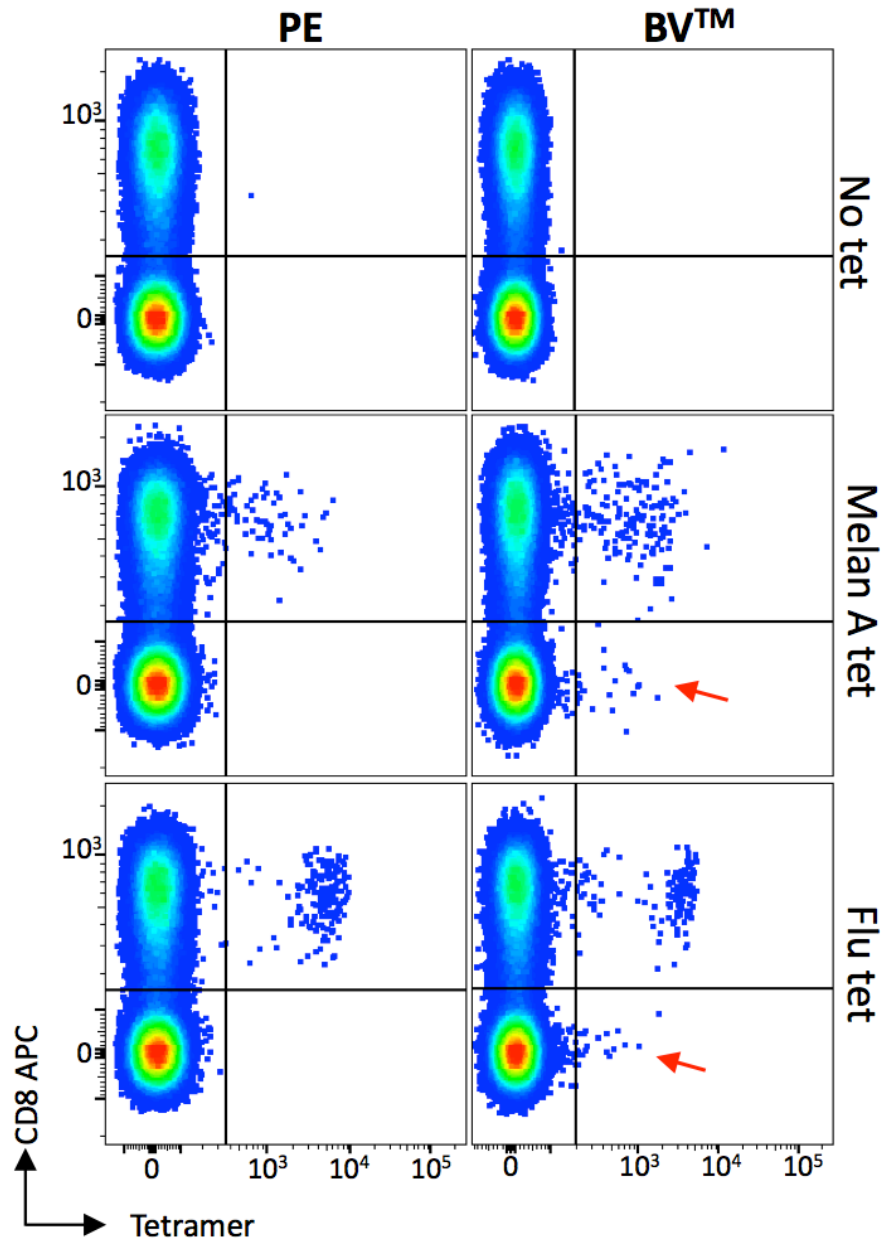
**Supplementary figure 1: Comparison of phycoerythrin and brilliant violet conjugated tetramers on PBMC.** HLA A2[+] PBMC +PKI were stained with Melan A (ELAGIGILTV) and influenza (flu) (matrix protein, GILGFVFTL) PE and BV conjugated tetramers. More background staining was evident on the CD8^{-} cells with the BV tetramer (red arrow).